

## **INFORMATION TO USERS**

**This manuscript has been reproduced from the microfilm master. UMI films the text directly from the original or copy submitted. Thus, some thesis and dissertation copies are in typewriter face, while others may be from any type of computer printer.**

**The quality of this reproduction is dependent upon the quality of the copy submitted. Broken or indistinct print, colored or poor quality illustrations and photographs, print bleedthrough, substandard margins, and improper alignment can adversely affect reproduction.**

**In the unlikely event that the author did not send UMI a complete manuscript and there are missing pages, these will be noted. Also, if unauthorized copyright material had to be removed, a note will indicate the deletion.**

**Oversize materials (e.g., maps, drawings, charts) are reproduced by sectioning the original, beginning at the upper left-hand corner and continuing from left to right in equal sections with small overlaps.**

**Photographs included in the original manuscript have been reproduced xerographically in this copy. Higher quality 6" x 9" black and white photographic prints are available for any photographs or illustrations appearing in this copy for an additional charge. Contact UMI directly to order.**

**ProQuest Information and Learning  
300 North Zeeb Road, Ann Arbor, MI 48106-1346 USA  
800-521-0600**

**UMI<sup>®</sup>**



**University of Alberta**

**Controlling Hydrogen-Bonding Receptors Using Allosteric Modulators**

by

**Mohammad Hussein Al-Sayah**



A thesis submitted to the Faculty of Graduate Studies and Research in partial fulfillment  
of the requirements for the degree of  
Doctor of Philosophy

Department of Chemistry

Edmonton, Alberta

Spring 2002



**National Library  
of Canada**

**Acquisitions and  
Bibliographic Services**

**395 Wellington Street  
Ottawa ON K1A 0N4  
Canada**

**Bibliothèque nationale  
du Canada**

**Acquisitions et  
services bibliographiques**

**395, rue Wellington  
Ottawa ON K1A 0N4  
Canada**

*Your file Votre référence*

*Our file Notre référence*

**The author has granted a non-exclusive licence allowing the National Library of Canada to reproduce, loan, distribute or sell copies of this thesis in microform, paper or electronic formats.**

**The author retains ownership of the copyright in this thesis. Neither the thesis nor substantial extracts from it may be printed or otherwise reproduced without the author's permission.**

**L'auteur a accordé une licence non exclusive permettant à la Bibliothèque nationale du Canada de reproduire, prêter, distribuer ou vendre des copies de cette thèse sous la forme de microfiche/film, de reproduction sur papier ou sur format électronique.**

**L'auteur conserve la propriété du droit d'auteur qui protège cette thèse. Ni la thèse ni des extraits substantiels de celle-ci ne doivent être imprimés ou autrement reproduits sans son autorisation.**

0-612-68536-5

**Canada**



# University of Alberta

## Library Release Form

**Name of Author:** Mohammad Hussein Al-Sayah


**Title of Thesis:** Controlling Hydrogen-Bonding Receptors Using Allosteric Modulators

**Degree:** Doctor of Philosophy

**Year this Degree Granted:** 2002

Permission is hereby granted to the University of Alberta Library to reproduce single copies of this thesis and to lend or sell such copies for private, scholarly or scientific research purposes only.

The author reserves all other publication and other rights in association with the copyright in the thesis, and excepts as herein before provided, neither the thesis nor any substantial portion thereof may be printed or otherwise reproduced in any material form whatever without the author's prior written permission



Kefraya  
West Bekka  
Lebanon

Dated: April 15, 2002

**Faculty of Graduate Studies and Research**

The undersigned certify that they have read, and recommend to the Faculty of Graduate Studies and Research for acceptance, a thesis entitled Controlling Hydrogen-Bonding Receptors Using Allosteric Modulators by Mohammad Hussein Al-Sayah in partial fulfillment of the requirements for the degree of Doctor of Philosophy.



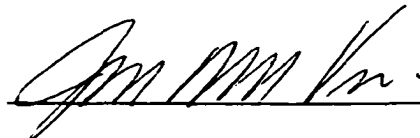
---

Dr. Neil R. Branda



---

Dr. David Bundle



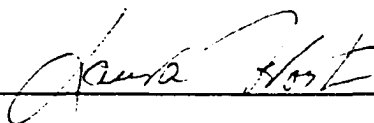
---

Dr. John C. Vederas




---

Dr. John Klassen



---

Dr. Laura S. Frost



---

Dr. Vincent Rotello

Dated: April 02, 2002

*To my parents, Hussein and Souraya,  
and my sisters, Nisserin, Soha and Fatima*

## ABSTRACT

A series of artificial receptors were prepared such that their hydrogen bonding surfaces are tethered to allosteric binding sites. The binding of a cofactor to an allosteric site induced conformational changes in the receptor rendering the hydrogen bonding surface unsuitable to accommodate the substrate. The activity of the receptor was regenerated by removing the allosteric cofactor or by regulating its binding properties.

In the first approach, the binding of the cofactor to the receptor induced conformational changes that led to distortion of the active site rendering it unsuitable for binding the substrate. 2,2'-Bipyridine ligands were incorporated into triaminotriazine and urea receptors for uracils and carboxylates, respectively. When Cu(I) ion was added, it bound to the bipyridine ligands. This chelation resulted in the distortion of the active sites and inhibited the binding of the substrates.

The triazine receptor was modified by incorporating a terpyridine ligand. In the presence, of Cu(I) ion, the receptor chelated the metal by two bipyridine ligands destroying the hydrogen bonding site and rendering the receptor inactive. When the Cu(I) was oxidized to Cu(II), the receptor rearranged its conformation to coordinate the metal by one bipyridine ligand and the terpyridine. This reactivated the receptor.

**Toggling between the active and the inactive states of the receptor was possible through redox switching from copper (II) to copper (I) and vice versa.**

**In the second approach, the binding of the cofactor did not perturb the hydrogen bonding site but it blocked the entrance of the binding pocket. Receptors based on *N,N*-bis(6-aminopyridin-2-yl)-isophthalamide scaffold were prepared appended with two 2,2'-bipyridine ligands. These ligands chelated the Zn(II) ion and prevented the binding of the barbiturate substrates.**

**Urea and triaminotriazine receptors were prepared such the allosteric sites consist of ethylamine and crown-ether moieties. The binding of these receptors to their carboxylate and uracil guests was inhibited by the addition of a proton cofactor. When the amino group was protonated, it formed an intramolecular hydrogen-bonded complex with the crown ether. The induced conformational changes upon this complexation distorted the active site of the receptors inhibiting its recognition of the substrate.**

## **ACKNOWLEDGMENTS**

**I gratefully acknowledge my supervisor, Dr. Neil Branda, for his continual encouragement, support and guidance throughout this research experience. I would like to thank all the members of Branda's research group for their help and friendship. Also, I would like to extend my gratitude to Dr. Rik Tykwinski and his group members for accommodating me for the last six months in their lab. I am grateful to Mike Pollard and Andrew Myles for proof reading this manuscript. The staff members in the spectral and analytical services at the Department of Chemistry, especially Dr. Tom Nakashima, are sincerely acknowledged for their technical expertise and aid in identification and characterization of compounds. I would like also to gratefully thank my family including my grandparents, parents, sisters, uncles, aunts and cousins for their endless support and encouragement. In particular, I would like to thank my cousin Kaled and my friends for all the fun time during the last five years. The Natural Sciences and Engineering Research Council, Research Corporation (Research Innovation Award) and University of Alberta are gratefully acknowledged for financial support.**

## Table of Contents

	Page
<b>Chapter 1- An Overview of Molecular Recognition Events and How They Apply to Supramolecular Chemistry</b>	1
1.1 Introduction	1
1.2 The Design of a Synthetic Receptor	3
1.3 An Overview of Hydrogen Bonding	4
1.4 Solvent Effects and the Hydrogen Bond	5
1.5 Experimental Characterization of Hydrogen-Bonding Complexes	6
1.6 Summary	11
1.7 References	13
<b>Chapter 2- Copper(I) Ions as Allosteric Inhibitors of Hydrogen-Bonding Receptors. Approach 1: Binding Site Deformation</b>	15
2.1 Introduction to Allostery	15
2.2 Metal Ions As Allosteric Cofactors in Artificial Systems	17
2.3 The Design of Allosteric Receptors for Carboxylate and Imide Derivatives	18
2.4 Synthesis and Characterization	20
2.4.1 Synthesis and Characterization of a Triaminotriazine Receptor for Imide Derivatives	20
2.4.2 Synthesis and Characterization of the Cu(I) Complex of Triaminotriazine Receptor 6	21

	<b>2.4.3 Synthesis and Characterization of the Carboxylate Receptors and Their Cu(I) Complexes</b>	<b>23</b>
<b>2.5</b>	<b>Binding Studies</b>	<b>26</b>
	<b>2.5.1 Binding Activity of Triaminotriazine Receptor 6 Toward <i>N</i>- Butyluracil</b>	<b>26</b>
	<b>2.5.2 The Effect of Cu(I) Ions on the Binding Efficacy of Triaminotriazine Receptor 6</b>	<b>29</b>
	<b>2.5.3 The Binding Activity of Urea Receptor 7 Toward Acetate</b>	<b>31</b>
	<b>2.5.4 The Effect of Cu(I) Ions on the Binding Efficacy of Urea Receptor 7</b>	<b>32</b>
	<b>2.5.5 The Binding Activity of Thiourea Receptor 8 Toward Acetate</b>	<b>40</b>
	<b>2.5.6 The Binding Activity of Squarate Receptor 10 Toward Acetate</b>	<b>44</b>
<b>2.6</b>	<b>Conclusions</b>	<b>48</b>
<b>2.7</b>	<b>Experimental</b>	<b>51</b>
<b>2.8</b>	<b>References</b>	<b>64</b>
	<b>Chapter 3- Controlling Copper Allosteric Effects Through Redox Chemistry</b>	<b>67</b>
<b>3.1</b>	<b>Molecular Machines</b>	<b>67</b>
<b>3.2</b>	<b>Receptor Design</b>	<b>70</b>
<b>3.3</b>	<b>Synthesis and Characterization of Diaminotriazine Receptor 17</b>	<b>73</b>
<b>3.4</b>	<b>Synthesis and Characterization of the Metal Complexes</b>	<b>75</b>
	<b>3.4.1 UV-Vis Spectra</b>	<b>75</b>
	<b>3.4.2 <sup>1</sup>H NMR and X-Ray Crystallography</b>	<b>76</b>



	3.4.3 Cyclic Voltammetry	79
3.5	Redox Switching Studies of the Copper Complexes	82
	3.5.1 Chemical Redox Switching Between Cu(17) <sup>+</sup> and Cu(17) <sup>2+</sup>	82
	3.5.2 Electrochemical Redox Switching Between Cu(17) <sup>+</sup> and Cu(17) <sup>2+</sup>	83
3.6	Binding Studies of the Complexes	85
3.7	Redox Effect on Binding of the Complexes	89
3.8	Conclusions	92
3.9	Experimental	95
3.10	References	103
<b>Chapter 4- Metal Ions as Allosteric Inhibitors of Hydrogen Bonding</b>		
	<b>Receptors. Approach 2: Cavity Size Alteration</b>	105
4.1	Introduction to the Cavity Size Alteration Approach	105
4.2	Designing A Specific Allosteric Receptor for Barbiturate Guests	106
4.3	Synthesis of the Bipyridyl Receptor <b>26</b>	108
4.4	Binding Studies	111
	4.4.1 Studies on the Binding of the Bipyridyl Receptor <b>26</b> to Barbiturate Guests	111
	4.4.2 Binding Studies on the Model Receptors for the Bipyridyl Receptor <b>26</b>	114
	4.4.2.1 Design, Synthesis and Binding Studies of the Di- <i>tert</i> - butyl Receptor <b>27</b>	114
	4.4.2.2 Design, Synthesis and Binding Studies of 2-Pyridyl Receptor <b>28</b>	116

4.4.2.3	<b>Design, Synthesis and Binding Studies of the 3-Pyridyl Receptors (29, 30 and 31)</b>	121
4.4.2.4	<b>Conclusions of the Binding Studies on the Control Receptors</b>	127
4.5	<b>New Bipyridyl Receptors for Barbiturate Guests</b>	130
4.5.1	<b>Design, Synthesis and Binding Studies of Bipyridyl Receptor 32</b>	130
4.5.2	<b>Synthesis and Binding Studies of the Bipyridyl Receptor 34</b>	131
4.5.3	<b>The Effect of Metal Ions on the Activity of the Bipyridyl Receptor 34</b>	134
4.6	<b>Conclusions</b>	137
4.7	<b>Experimental</b>	141
4.8	<b>References</b>	159
<b>Chapter 5- Protons As Allosteric Modulators for H-Bonding Receptors</b>		160
5.1	<b>Introduction</b>	160
5.2	<b>Design of Receptors</b>	162
5.3	<b>Synthesis of Receptors and Their Protonated Complexes</b>	164
5.4	<b>Characterization of Receptors and Their Protonated Complexes</b>	166
5.5	<b>Binding Studies</b>	170
5.5.1	<b>The Binding of Receptor 38 to Tetrabutylammonium (TBA) Acetate</b>	170
5.5.2	<b>Effect of Protons on Binding of Receptor 38</b>	171
5.5.3	<b>Binding of Triaminotriazine Receptor 40 to <i>N</i>-Butyluracil</b>	173
5.5.4	<b>Effect of Protons on Binding of Triaminotriazine Receptor 40</b>	176

<b>5.6</b>	<b>Conclusions</b>	<b>178</b>
<b>5.7</b>	<b>Experimental</b>	<b>180</b>
<b>5.8</b>	<b>References</b>	<b>189</b>
<b>Chapter 6- Conclusion</b>		<b>190</b>
<b>Appendix I- Crystallography Experimental Data</b>		<b>192</b>
<b>Appendix II-Selected <sup>1</sup>H NMR Data</b>		<b>212</b>

## List of Tables

	Page
<b>Chapter 2</b>	
Table 2.1	Changes in $^1\text{H}$ NMR chemical shifts of the N—H protons of the urea receptor <b>7</b> and <i>N,N</i> -dimethyl urea
	34
Table 2.2	The results of the isothermal titration calorimetry
	48
<b>Chapter 4</b>	
Table 4.1	Changes in $^1\text{H}$ NMR chemical shifts of the N—H protons of the barbiturate-specific receptors upon the addition of the substrate
	121
<b>Appendix I</b>	
Table 1	Crystallographic Experimental Details for <b>6•Cu</b>
	192
Table 2	Atomic Coordinates and Equivalent Isotropic Displacement Parameters for <b>6•Cu</b>
	195
Table 3	Crystallographic Experimental Details for <b>7•Cu</b>
	199
Table 4	Crystallographic Experimental Details for <b>Cu(17)<sup>+</sup></b>
	201
Table 5	Atomic Coordinates and Equivalent Isotropic Displacement Parameters for <b>Cu(17)<sup>+</sup></b>
	204
Table 6	Crystallographic Experimental Details for receptor <b>28</b>
	208
Table 7	Atomic Coordinates and Equivalent Isotropic Displacement Parameters for <b>28</b>
	210

## List of Figures

	Page
<b>Chapter 1</b>	
Figure 1.1	The DNA duplex showing the complementary hydrogen bonding between G-C and A-T pairs. 3
Figure 1.2	Schematic representation of the <i>lock-and-key</i> approach of a host-guest system 4
Figure 1.3	A typical titration curve in which the binding of a host to a guest is <i>fast</i> . 7
Figure 1.4	A typical van't Hoff plot. 8
Figure 1.5	A series of <sup>1</sup> H NMR spectra in which a capped axle of a rotaxane is treated with aliquots of dibenzo[24]crown-8 9
Figure 1.6	An example of the output of a calorimetric titration. 10
<b>Chapter 2</b>	
Figure 2.1	A schematic illustration of positive and negative allosteric receptors 16
Figure 2.2	The crystal structure of <b>6•Cu</b> 23
Figure 2.3	The titration curve of <i>N</i> -butyluracil with triaminotriazine receptor <b>6</b> 27
Figure 2.4	The titration curves of <i>N</i> -butyluracil with receptor <b>6</b> and its Cu(I) complex <b>6•Cu</b> 28
Figure 2.5	The binding of uracil derivatives to the two less effective sites of <b>6•Cu</b> 29

Figure 2.6	Changes in the $^1\text{H}$ NMR spectra of <i>N</i> -butyluracil	31
Figure 2.7	Titration curves of urea receptors <b>7</b> and <b>7•Cu</b>	32
Figure 2.8	$^1\text{H}$ NMR spectrum of <b>7•Cu</b> after 1.6 equivalents of TBAOAc were added	36
Figure 2.9	X-ray structure of <b>7•Cu</b>	37
Figure 2.10	Electrospray mass spectrum of <b>7•Cu</b>	38
Figure 2.11	The change in the peak intensity of the dimer relative to its initial intensity in the mass spectrum	38
Figure 2.12	Calorimetric titration of thiourea receptor <b>8</b> with TBAOAc	41
Figure 2.13	Titration curves of receptor <b>8</b> with TBAOAc	43
Figure 2.14	Calorimetric titration of thiourea receptor <b>10</b> with TBAOAc	46
Figure 2.15	Titration curves of squarate receptor <b>10</b> with TBAOAc	47
 <b>Chapter 3</b>		
Figure 3.1	The UV-Vis absorption spectra of $\text{Cu}(\mathbf{17})^+$ and $\text{Cu}(\mathbf{17})^{2+}$	75
Figure 3.2	The diastereoisomers of $\text{Cu}(\mathbf{17})^+$	77
Figure 3.3	Molecular structure of $\text{Cu}(\mathbf{17})^+$ in the crystal	78
Figure 3.4	Cyclic voltammograms of $\text{Cu}(\mathbf{17})^+$ and $\text{Cu}(\mathbf{17})^{2+}$	81
Figure 3.5	Changes in the UV-Vis absorption spectra of (A) $\text{Cu}(\mathbf{17})^+$ and (B) $\text{Cu}(\mathbf{17})^{2+}$ upon electrolysis	85
Figure 3.6	The modulated absorption spectra during alternating electrolysis of (A) $\text{Cu}(\mathbf{17})^+$ and (B) $\text{Cu}(\mathbf{17})^{2+}$	85
Figure 3.7	Partial $^1\text{H}$ NMR spectra showing the change in the chemical shift of the N—H proton signal of <i>N</i> -butyluracil upon the subsequent addition of <b>17</b> and Cu(I)	87

<b>Figure 3.8</b>	<b>Partial <math>^1\text{H}</math> NMR spectra showing the change in the chemical shift of the N—H proton signal of <i>N</i>-butyluracil upon the subsequent addition of <b>17</b> and Cu(II)</b>	<b>88</b>
 <b>Chapter 4</b>		
<b>Figure 4.1</b>	<b>A schematic representation of the cavity-size alteration approach</b>	<b>105</b>
<b>Figure 4.2</b>	<b>The hydrogen-bonding motif of 5,5-disubstituted barbiturate</b>	<b>106</b>
<b>Figure 4.3</b>	<b>A schematic representation of Hamilton's receptor for barbiturates</b>	<b>107</b>
<b>Figure 4.4</b>	<b>A computer-generated structure of the metal complex of bipyridyl receptor <b>26</b></b>	<b>109</b>
<b>Figure 4.5</b>	<b>Titration curves for receptors <b>26</b>, <b>27</b>, and <b>28</b></b>	<b>112</b>
<b>Figure 4.6</b>	<b>The possible effects of bipyridine substituents on the binding of receptor <b>26</b></b>	<b>113</b>
<b>Figure 4.7</b>	<b>Modification of ring C of the bipyridyl receptor <b>26</b></b>	<b>114</b>
<b>Figure 4.8</b>	<b>Removal of ring D of the bipyridyl receptor <b>26</b></b>	<b>117</b>
<b>Figure 4.9</b>	<b>The crystal structure of receptor <b>28</b></b>	<b>119</b>
<b>Figure 4.10</b>	<b>Removal of ring D and changing the N-atom position of ring C of the bipyridyl receptor <b>26</b></b>	<b>112</b>
<b>Figure 4.11</b>	<b>The effects of bipyridine substituents on the binding of receptor <b>26</b></b>	<b>127</b>
<b>Figure 4.12</b>	<b>The possible conformers of receptor <b>26</b></b>	<b>128</b>
<b>Figure 4.13</b>	<b>Titration curves of <b>34</b> and <b>34•Zn</b></b>	<b>134</b>
<b>Figure 4.14</b>	<b>Partial <math>^1\text{H}</math> NMR spectra of <b>34</b> and <b>34•Zn</b></b>	<b>137</b>

## **Chapter 5**

<b>Figure 5.1</b>	<b>Partial TROESY spectrum of 38•H<sup>+</sup> in CD<sub>3</sub>OD</b>	<b>168</b>
<b>Figure 5.2</b>	<b>Partial TROESY spectrum of 38 in CD<sub>3</sub>OD</b>	<b>168</b>
<b>Figure 5.3</b>	<b>Electrospray mass spectrum of 40•H<sup>+</sup></b>	<b>169</b>
<b>Figure 5.4</b>	<b>Titration curves of 38 and 38•H<sup>+</sup></b>	<b>170</b>
<b>Figure 5.5</b>	<b>Titration curves of 40 and 40•H<sup>+</sup></b>	<b>175</b>
<b>Figure 5.6</b>	<b>The hydrogen bonding complex of diphenyl triazine receptor 42 and <i>N</i>-butyluracil</b>	<b>176</b>
<b>Figure 5.7</b>	<b>The binding of uracil derivatives to the two less effective sites of 40•H<sup>+</sup></b>	<b>177</b>

## **Appendix I**

<b>Figure 1</b>	<b>Crystal structure of 6•Cu</b>	<b>192</b>
<b>Figure 2</b>	<b>Crystal structure of 7•Cu</b>	<b>198</b>
<b>Figure 3</b>	<b>Crystal structure of Cu(17)<sup>+</sup></b>	<b>201</b>
<b>Figure 4</b>	<b>Crystal structure of receptor 28</b>	<b>207</b>



## **List of Schemes**

	<b>Page</b>
<b>Chapter 2</b>	
Scheme 2.1	17
Scheme 2.2	18
Scheme 2.3	19
Scheme 2.4	19
Scheme 2.5	20
Scheme 2.6	21
Scheme 2.7	24
Scheme 2.8	39
<b>Chapter 3</b>	
Scheme 3.1	68
Scheme 3.2	69
Scheme 3.3	71
Scheme 3.4	72
Scheme 3.5	74
Scheme 3.6	82
Scheme 3.7	90
<b>Chapter 4</b>	
Scheme 4.1	108

<b>Scheme 4.2</b>	<b>110</b>
<b>Scheme 4.3</b>	<b>129</b>
<b>Scheme 4.4</b>	<b>132</b>
<b>Scheme 4.5</b>	<b>140</b>
<b>Chapter 5</b>	
<b>Scheme 5.1</b>	<b>161</b>
<b>Scheme 5.2</b>	<b>162</b>
<b>Scheme 5.3</b>	<b>163</b>
<b>Scheme 5.4</b>	<b>164</b>
<b>Scheme 5.5</b>	<b>164</b>
<b>Scheme 5.6</b>	<b>165</b>
<b>Scheme 5.7</b>	<b>166</b>
<b>Scheme 5.8</b>	<b>173</b>

## **List of Equations**

	<b>Page</b>
<b>Chapter 1</b>	
Equation 1.1	6
Equation 1.2	8
Equation 1.3	8
Equation 1.4	8
<b>Chapter 4</b>	
Equation 4.1	115
Equation 4.2	117
Equation 4.3	123
Equation 4.4	124
Equation 4.5	126
Equation 4.6	131

## List of Abbreviations

<b>A</b>	<b>acceptor</b>
<b>AIBN</b>	<b>azobisisobutyronitrile</b>
<b>br</b>	<b>broad</b>
<b><i>n</i>-BuLi</b>	<b><i>n</i>-butyl lithium</b>
<b><i>t</i>-BuOK</b>	<b>potassium <i>tert</i>-butoxide</b>
<b>CV</b>	<b>cyclic voltammetry</b>
<b>D</b>	<b>donor</b>
<b>DMF</b>	<b>dimethylformamide</b>
<b>DMSO</b>	<b>dimethylsulfoxide</b>
<b>dmph</b>	<b>2,9-dimethyl-1,10-phenanthroline</b>
<b>DNA</b>	<b>deoxyribonucleic acid</b>
<b>dpp</b>	<b>2,9-diphenyl-1,10-phenanthroline</b>
<b>EtOAc</b>	<b>ethyl acetate</b>
<b>EtOH</b>	<b>ethanol</b>
<b>G</b>	<b>guest</b>
<b>GCOSY</b>	<b>pulsed field gradient absolute-value correlated spectroscopy</b>
<b>H</b>	<b>host</b>
<b>HMTA</b>	<b>hexamethylenetetraamine</b>
<b>IR</b>	<b>infrared</b>
<b>ITC</b>	<b>isothermal titration calorimetry</b>
<b>M.p.</b>	<b>melting point</b>
<b>MeOH</b>	<b>methanol</b>
<b>MO</b>	<b>molecular orbital</b>

<b>NBS</b>	<b>N-bromosuccinimide</b>
<b>NMR</b>	<b>nuclear magnetic resonance</b>
<b>NOE</b>	<b>nuclear Overhauser effect</b>
<b>OAc</b>	<b>acetate</b>
<b>OTf</b>	<b>triflate</b>
<b>RNA</b>	<b>ribosnucleic acid</b>
<b>TBA</b>	<b>tetrabutyl ammonium</b>
<b>TBAOAc</b>	<b>tetrabutyl ammonium acetate</b>
<b>TEA</b>	<b>triethylamine</b>
<b>terpy</b>	<b>terpyridine</b>
<b>THF</b>	<b>tetrahydrofuran</b>
<b>TROESY</b>	<b>transverse rotating frame Overhauser effect spectroscopy</b>
<b>U</b>	<b>uracil</b>
<b>UV-Vis</b>	<b>ultraviolet - visible</b>

## **Chapter 1 – An Overview of Molecular Recognition Events and How They Apply to Supramolecular Chemistry**

### **1.1 Introduction**

Since its inception, supramolecular chemistry has advanced rapidly and has now reached a high level of sophistication. This is testified by the number of complex chemical systems that have been synthesized to accomplish catalytic functions, binding and transport of substrates, and sensing. These systems not only perform these useful functions, they also serve as models for the study of natural systems.<sup>1</sup> Research in supramolecular chemistry has increased tremendously, especially after the 1987 Nobel Prize was awarded to Cram, Lehn and Pedersen for their role in developing molecular systems that display highly selective structure-specific interactions. Their work has laid the foundations of what is today one of the most active and expanding fields of chemical research, a field for which Cram coined the term "host-guest chemistry".<sup>2</sup> Lehn preferred to call it "supramolecular chemistry".<sup>3</sup>

A more descriptive definition of supramolecular chemistry is "the chemistry beyond the molecule".<sup>3</sup> Just as molecular chemistry is that of the covalent bond, supramolecular chemistry concerns the intermolecular bond. A "supermolecule" is formed when two or more molecules interact with each other through non-covalent interactions based on molecular information stored within the interacting partners. For example, the selective binding of a substrate (guest) by a molecular receptor (host) requires that the receptor possesses steric and electronic features complementary to those of the substrate. Therefore, the process of molecular recognition, which hinges on the reading of structural information programmed within the molecules, is the basis of supramolecular chemistry.<sup>3</sup>

Intermolecular bonds are the forces that hold the different building blocks of a supermolecule together. These include ion pairing, hydrogen bonding,  $\pi$ - $\pi$  stacking, dispersion forces, hydrophobic effects and coordination bonding.<sup>4</sup> The combination of two or more of these interactions increases the selectivity and adaptability of the interacting partners and the stability of the resulting "supermolecule".

DNA and RNA represent examples of natural supramolecular systems where a combination of different interactions is utilized to assemble the secondary structures (Figure 1.1). Hydrogen bonding,  $\pi$ - $\pi$  stacking and the hydrophobic effect are all responsible for holding the two strands of the nucleic acid together. The complementarity in hydrogen-bonding surfaces between the base pairs directs the pattern of assembly of the strands.<sup>5</sup> These and other natural systems such as enzyme–substrate, receptor–substrate, and antibody–antigen complexes have inspired supramolecular chemists to build artificial systems. The goals are the selective recognition of substrates for catalysis, sensing and transport, and the creation of supermolecules that exhibit useful optical and electronic properties.

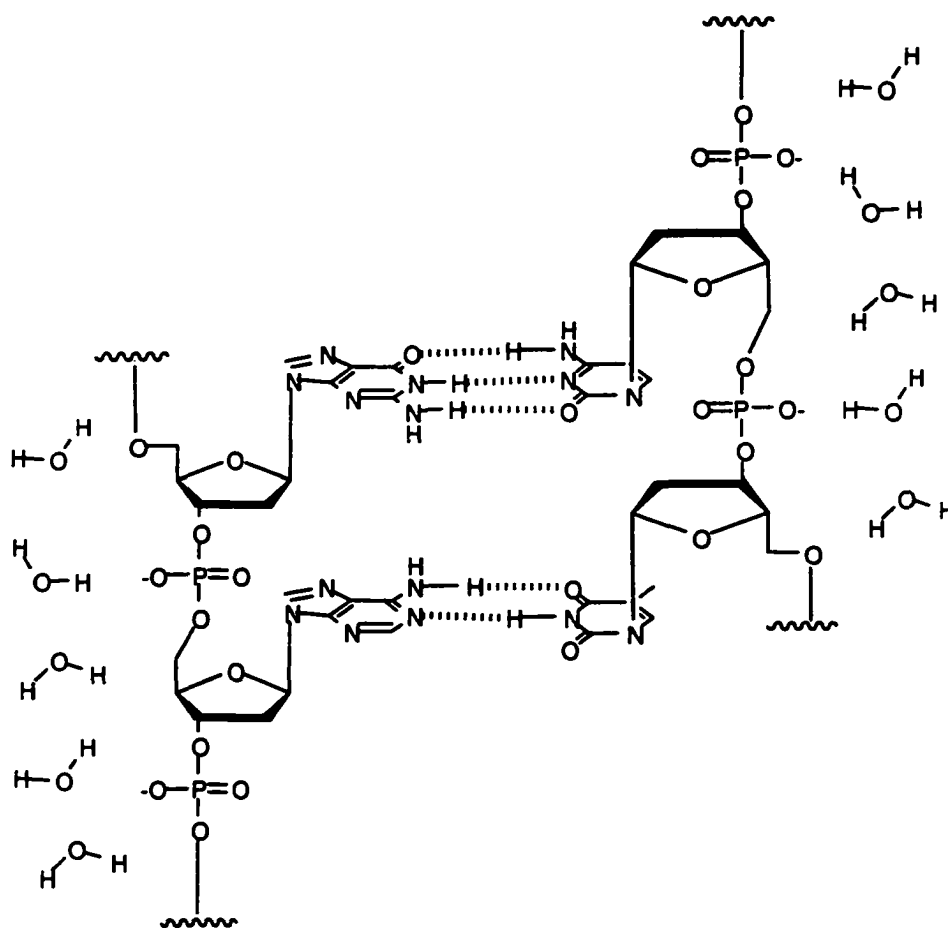


**Figure 1.1** The DNA duplex showing the complementary hydrogen bonding between G-C and A-T pairs. The negatively charged backbone is solvated by water molecules.

## 1.2 The Design of a Synthetic Receptor

The design of an artificial molecular receptor is based on identifying the recognition entities displayed by the target substrate. For effective recognition, the receptor should provide a "hosting" site which is complementary to the guest in size, shape, and electronic makeup. Since non-covalent interactions are weak relative to covalent bonds, multiple interaction sites are vital for strong association and high selectivity. Three-dimensional pre-organization of the interacting sites through the use of proper spacers further enhances the efficiency of the receptor (Figure 1.2).



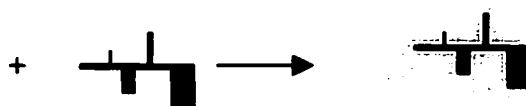


**Figure 1.2** Schematic representation of the *lock-and-key* approach of a host-guest system.

The design of synthetic receptors with similar activities to natural systems, such as regulation, cooperativity, and allostery, requires some degree of flexibility to allow the interacting sites to be arranged in more than one pattern. Different patterns of interacting sites induce different functions of the receptor. The spacers should have the ability to adapt and respond to structural and environmental changes in order to regulate these functions.<sup>1a</sup> The choice of spacers with particular dynamic features is based on rational design and computer modeling and is optimized through trial and error testing.

One of the most versatile natural recognition elements used in supramolecular chemistry is hydrogen bonding. For example, vancomycin, an antibiotic that kills bacteria by binding to a peptide projecting from the bacteria's cell wall, forms a hydrogen-bonded complex with the bacterial peptide.<sup>19</sup> Bacteria resist this powerful antibiotic by replacing an amide group in the peptide with an ester. This removes a single hydrogen bond from the complex and prevents vancomycin from destroying the bacteria.<sup>1c</sup> The use of hydrogen bonds as the basis for the recognition of a guest by its host ensures a high level of selectivity of binding within the active site of the receptor. Since this selectivity depends on the arrangement of hydrogen bonds, modifying this arrangement will alter the affinity and the selectivity of the host for its guest.

### **1.3 An Overview of Hydrogen Bonding**

A hydrogen bond is formed between an acidic hydrogen atom, covalently bonded to a proton donor (D), and the accessible electrons in a basic proton acceptor (A). The

strength of a hydrogen bond increases with an increase in the acidity of the hydrogen in the donor and an increase of the basicity of the acceptor.<sup>6</sup> It is generally accepted that hydrogen bonding is an electrostatic interaction between the donor and acceptor.<sup>7</sup> According to Molecular Orbital (MO) theory, this electrostatic attraction is only significant at appropriate distances between the acceptor and the donor. When the two components are too close, there is repulsion between the electrons in the X–H bond of the donor and the lone pair of electrons of the acceptor. Additional weakening of a hydrogen bond may be caused by delocalization of the lone pair electrons on the acceptor to a  $\sigma^*$  antibonding orbital on the proton donor.<sup>8</sup> In general, the electrostatic theory is widely accepted as a simple and accurate model for hydrogen bonding .

#### **1.4 Solvent Effects and the Hydrogen Bond**

The strength of a hydrogen bond is greatly affected by the solvent. The stability of a hydrogen bonded complex is usually highest in apolar aprotic solvents, such as alkanes, and lower in solvents that can act either as a hydrogen bond donor or acceptor. This is because of competitive hydrogen bonding with the solvent.<sup>6</sup> The energy of a hydrogen bond in the gas phase is typically in the range of 2-20 kcal mol<sup>-1</sup>, while in chloroform it is 1.5-5 kcal mol<sup>-1</sup>.<sup>1c</sup>

If the donor is positively charged and/or the acceptor is negatively charged, electrostatic attraction will be amplified, making hydrogen bonds much stronger. In this case, the effect of the solvent is more significant since the stability of the complex depends on the dielectric constant and the electron donor/acceptor ability of the solvent. Solvents with high dipole moments interact more effectively with charged species, shielding them from one another and diminishing the strength of their interactions with each other. For example, a good electron-donor solvent solvates cationic species

efficiently, competing for receptor recognition of cationic guests. A good electron-acceptor solvent solvates anions very effectively and weakens anion binding by receptors.<sup>9</sup>



**S = solvent**

**Equation 1.1**

In general, if the solvent strongly solvates either host, guest or host-guest complex, or if the solvent interacts strongly with itself, there can be a dramatic effect on the host-guest equilibrium. In order for the host and guest to form an intermolecular complex, desolvation of each of the reacting species is necessary (Equation 1.1). A delicate balance between enthalpy ( $\Delta H$ ) and entropy ( $\Delta S$ ) is needed to ensure a stable host-guest complex. Enthalpy will be favorable if the energy produced by the formation of the intermolecular complex and its subsequent solvation is greater than energy required to break the bonds between the host and guest and the solvent molecules. Entropy will be favorable if the disorder created as solvent molecules are released during the molecular recognition event is enough to overcome the order created when the guest is complexed by the host.<sup>1c</sup>

### 1.5 Experimental Characterization of Hydrogen-Bonding Complexes

<sup>1</sup>H NMR is a sensitive and valuable technique for monitoring the formation of hydrogen-bonding complexes and the overall kinetics and thermodynamics of the molecular recognition process. Since complexation involves a dynamic exchange between the bound and the unbound forms of the host and guest, the rate of complex

formation is reflected by the NMR spectrum. The formation of a hydrogen bond results in a decrease in electron density around the proton involved, because it is shared by the donor and the acceptor. Consequently, the NMR signal of this proton shifts downfield.<sup>6</sup> To measure the stability of the hydrogen-bonded complex, an *NMR titration* experiment can be performed in which <sup>1</sup>H NMR shifts of one of the interacting species (typically assigned as the "host") are monitored as aliquot amounts of the other species (typically assigned as the "guest") are added. If the binding between the components is kinetically fast compared to the NMR time scale ( $10^{-2}$ - $10^{-3}$  s), the host's NMR resonances will be observed as an average signal. As the concentration of the guest increases, these time-averaged peaks will shift continuously until the receptor is saturated at which point the position of the signals in the NMR spectrum will be constant.<sup>1c</sup>

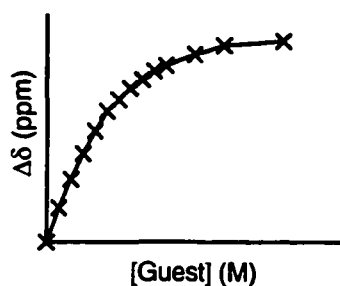


**Figure 1.3** A typical titration curve in which the binding of a host to a guest is *fast*. The concentration of guest is plotted against the change in the chemical shift of the protons on the host. The addition of the guest causes the time-averaged signals in the spectrum to shift until the host is saturated.

In a typical titration curve (Figure 1.3) the changes in the chemical shift of the signals corresponding to the host (H) are plotted as a function of the concentration of the guest (G). The change in the slope of the curve reflects the thermodynamic stability of the host-guest complex (H•G). Computer programs are used to estimate the binding constant ( $K_b$  in Equation 1.2) using a non-linear least squares procedure to fit a theoretical model of complexation to the experimental data.



$$\text{where } K_a = \frac{[\text{H}\cdot\text{G}]}{[\text{H}][\text{G}]} \quad \text{Equation 1.3}$$

Other thermodynamic parameters ( $\Delta H$  and  $\Delta S$ ) can be obtained through the van't Hoff equation (Equation 1.4) by performing the titration experiments at different temperatures to produce different values of  $K_a$ .<sup>10</sup> In this case  $\ln K_a$  is plotted against  $1/T$  (Figure 1.4).

$$\ln K_a = (\Delta S/R) - (\Delta H/R)(1/T) \quad \text{Equation 1.4}$$

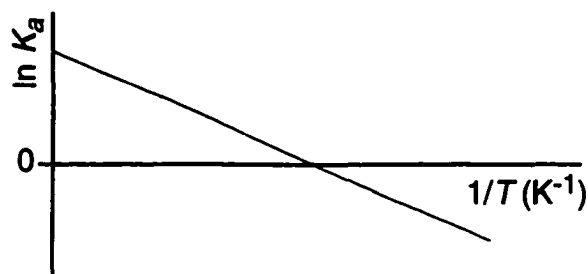


**Figure 1.4** A typical van't Hoff plot for an endothermic reaction. The slope of the line provides a measure of  $\Delta H$ . Where the line intercepts the y-axis provides a measure of  $\Delta S$ .

If binding is slow on the  $^1\text{H}$  NMR time scale, the intensity of signals corresponding to the free host diminish while those corresponding to the host-guest complex grow as the concentration of guest increases. A representative example is shown in Figure 1.5. By directly measuring the relative integrations of individual  $^1\text{H}$  NMR signals that corresponds to free and bound forms, relative concentrations of all

three species (H, G, and H•G) can be obtained. The association constant is then calculated directly from these concentrations (Equation 1.3).

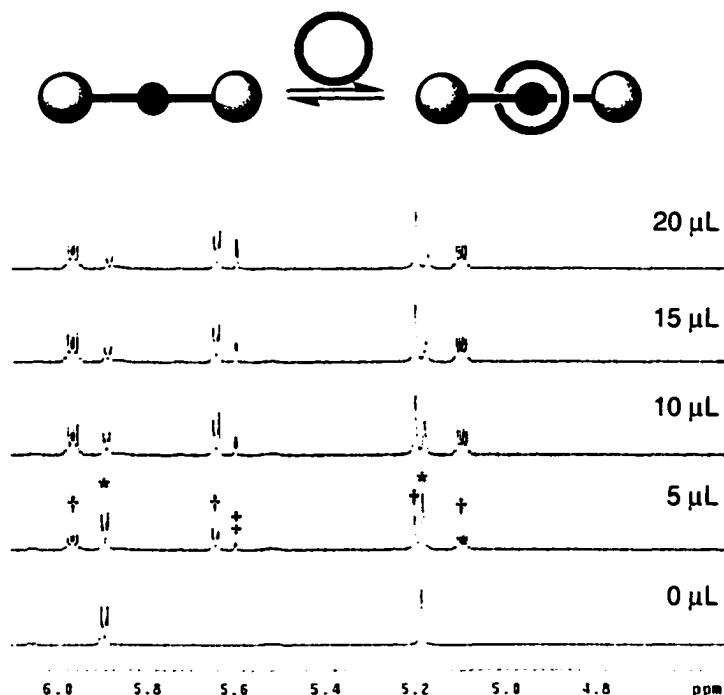


**Figure 1.5** A series of  $^1\text{H}$  NMR spectra in which a capped axle of a rotaxane is treated with aliquots of dibenzo[24]crown-8 (the “wheel”). Since the assembly is *slow*, the resonances signals for both the free axle (\*) and the assembled rotaxane (†) are clearly visible (residual  $\text{CD}_2\text{Cl}_2$  is denoted by ‡). (Reprinted from the Ph.D. Dissertation of Kelly Chichak, University of Alberta, 2002, with the permission of the author).

Another method for determining thermodynamic parameters for molecular recognition processes is microcalorimetry. In a typical experiment, the quantity of heat evolved or absorbed on complex formation is measured.<sup>11</sup> The temperature of the solution of the host is monitored as the guest is added to the calorimeter cell. Thermodynamic values are directly related to the heat change upon binding. The change in heat produced or absorbed is plotted as a function of time. Integration of the peaks

provides the amount of heat produced or absorbed upon each addition. A typical plot of heat versus molar ratio of the titrant is shown in Figure 1.6. This curve is compared to a theoretical binding curve using computer-aided programs.

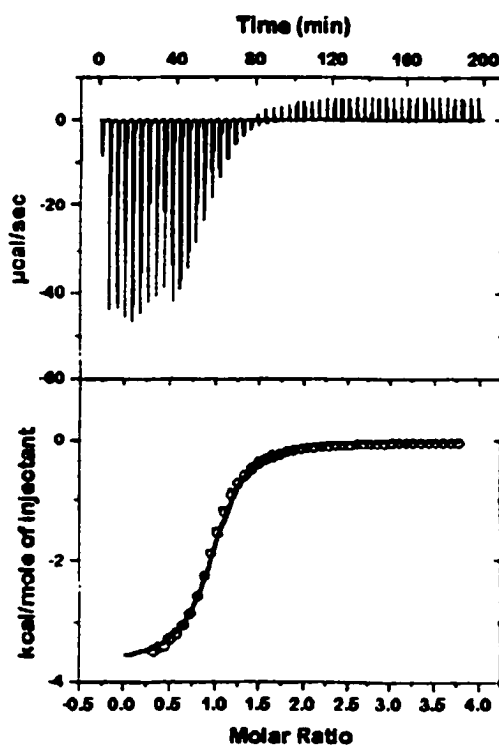


**Figure 1.6** An example of the output of a calorimetric titration. Top panel: raw data showing heat evolved with each injection of guest. Bottom panel: integrated curve of the raw titration (O) and a non-linear least squares fit (—).

Other techniques frequently used to monitor hydrogen bonding are infra-red (IR) spectroscopy, mass spectrometry (MS) and crystallography. The stretching vibration of the donor X–H bond can be detected in the IR region of the electromagnetic spectrum. The formation of a hydrogen bond lengthens the X–H bond, causing a shift of the vibration to a lower frequency. Also, the hydrogen-bonded X–H absorption is stronger and broader than that of non-hydrogen-bonded X–H bond. The magnitude of the shift in the spectrum correlates linearly with hydrogen bond strength and, therefore, provides

an assessment of the stability of the host-guest complex.<sup>12</sup> Mass spectrometry usually detects hydrogen-bonded complexes which are not destroyed during the ionization process. Soft ionization methods such as electrospray techniques have been used successfully to detect hydrogen-bonded assemblies that have relatively high stability in solution.<sup>13</sup> Crystallography provides strong evidence for complex formation and the type of interactions that are holding the guest in place. A crystal structure is valid for the solid state where factors such as crystal packing may alter the properties of the complex as it exists in solution.

## 1.6 Summary

Inspired by the examples of non-covalently linked biological systems, supramolecular chemists have constructed fascinating assemblies by exploiting a wide range of intermolecular non-covalent interactions. A vast number of molecular arrangements have been prepared including host-guest systems (artificial receptors, capsules, ionophores) and self assembled architectures (catenanes, rotaxanes, racks, ladders). A large number of these systems have specific applications in areas such as drug delivery,<sup>14</sup> sensors,<sup>15</sup> information and communication technology,<sup>16</sup> catalysis<sup>17</sup> and separation.<sup>18</sup>

The remaining chapters of this thesis will describe the design of synthetic receptors with hydrogen bonding surfaces that have affinity for neutral and charged guests. The focus will be on the ability to control the activity of these receptors through allosteric modulators. Chapter Two explores the utility of metal ions as allosteric cofactors for inhibiting the binding of guests. In Chapter Three, the modulation of the allosteric effect of the metal is exploited to build a functional "molecular machine". Chapter Four introduces a different approach of allosteric mechanism of metals for



**inhibiting the binding of guests. Finally, Chapter Five presents the proton as a trigger for regulating binding.**

## 1.7 References

1. For an overview of *Supramolecular Chemistry* see: (a) J. –M. Lehn, *Supramolecular Chemistry: Concepts and Perspectives*, VCH, Weinheim, 1995; (b) F. Vögtle, *Supramolecular Chemistry*, John Wiley and Sons, New York, 1991; (c) P. D. Beer, P. A. Gale, D. K. Smith, *Supramolecular Chemistry*, Oxford University Press Inc., New York, 1999; (d) For a comprehensive survey of *supramolecular* technology see: *Comprehensive Supramolecular Chemistry*, Vol. 10, Ed. J. L. Atwood, J. E. D. Davies, D. D. MacNicol; F. Vögtle, Elsevier, Oxford, 1996; (e) For a comprehensive overview on methodology see: H. –J. Schneider, A. Yatsimirsky, *Principles and Methods in Supramolecular Chemistry*, John Wiley and Sons, New York, 2000 and references cited therein.
2. D. J. Cram, *Angew. Chem. Int. Ed. Engl.* **1986**, *25*, 1039.
3. J. –M. Lehn, *Angew. Chem. Int. Ed. Engl.* **1990**, *29*, 1304.
4. J. March, *Advanced Organic Chemistry*, John Wiley and Sons, New York, **1992**.
5. P. Schuster, P. Wolschann, *Monat. Chem.* **1999**, *130*, 947.
6. G. A. Jeffrey, *An Introduction to Hydrogen Bonding*, Oxford University Press Inc., New York, 1997.
7. L. J. Prins, D. N. Reinhoudt, P. Timmerman; *Angew. Chem. Int. Ed.* **2001**, *40*, 2382.
8. C. Fonseca Guerra, F. M. Bickelhaupt, J. G. Snijders, E. J. Baerends, *Chem. Eur. J.* **1999**, *5*, 3581
9. P. Beer, P. Gale, *Angew. Chem. Int. Ed.* **2001**, *40*, 486.
10. K. A. Connors, *Binding Constants, The Measurement of Molecular Complex Stability*, John Wiley and Sons, New York, 1987.

11. For an overview of using isothermal microcalorimetry to determine binding interactions see: (a) M. L. Doyle, *Curr. Opin. Biotech.* **1997**, *8*,; (b) M. Stodeman, I. Waso, *Pure Appl. Chem.* **1995**, *67*, 1059; (c) T. Wiseman, S. Williston, J. F. Brandts, L.-N. Lin, *Anal. Biochem.* **1989**, *179*, 131.
12. S. Scheiner, *Hydrogen Bonding: A Theoretical Perspective*, Oxford University Press, New York, **1997**.
13. (a) C. A. Schalley, *Int. J. Mass Spectrom.* **2000**, *194*, 11. (b) K. Wang, G. W. Gokel, *Pure Appl. Chem.*, **1996**, *68*, 1267; (c) R. D. Smith, J. E. Bruce, L. Wu, Q. P. Lei, *Chem Soc. Rev.* **1997**, *26*, 191; (d) M. Przybylski, M. O. Glocker, *Angew. Chem. Int. Ed. Engl.* **1996**, *35*, 807.
14. J. M. Rivera, T. Martin, J. Rebek, *Science* **1998**, *279*, 1021.
15. (a) A. P. DeSilva, *Chem. Rev.* **1997**, *97*, 1515; (b) P. D. Beers, *Acc. Chem. Res.* **1998**, *31*, 71.
16. (a) D. Philp, J. F. Stoddart, *Angew. Chem. Int. Ed. Engl.* **1996**, *35*, 1155; (b) Y. -Z. Hu, D. V. Loyen, O. Schwarz, S. Bossman, H. Dürr, V. Huch, M. Veith, *J. Am. Chem. Soc.* **1998**, *120*, 5822.
17. (a) L. E. Orgel, *Acc. Chem. Res.* **1995**, *28*, 109; (b) M. M. Conn, E. A. Wintner, J. Rebek, *J. Am. Chem. Soc.* **1994**, *116*, 8823; (c) L. G. Mackay, R. S. Wylie, J. K. M. Sanders, *J. Am. Chem. Soc.* **1994**, *116*, 3141.
18. (a) G. R. Desiraju, *Angew. Chem. Int. Ed. Engl.* **1995**, *34*, 2311; (b) A. Müller, H. Reuter, S. Dillinger, *Angew. Chem. Int. Ed. Engl.* **1995**, *34*, 2328; (c) T. Webb, C. S. Wilcox, *Chem. Soc. Rev.* **1993**, 383 (d) W. H. Pirkle, T. C. Pochapsky, *Chem. Rev.* **1989**, *89*, 347.
19. J. R. Kalman, D. H. Williams, *J. Am. Chem. Soc.* **1980**, *102*, 906.

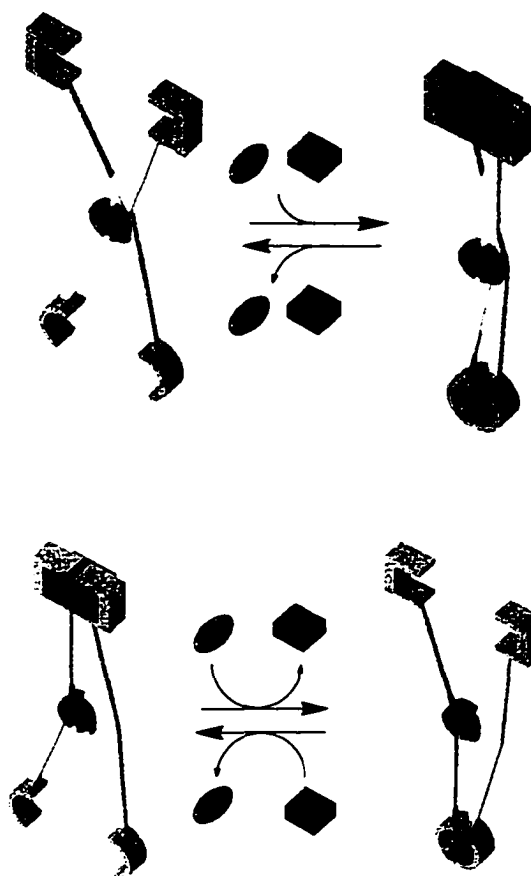
## Chapter 2 – Copper(I) Ions as Allosteric Inhibitors of Hydrogen-Bonding Receptors



### Approach 1: Binding Site Deformation

#### 2.1 Introduction to Allostery

Regulation of the activity of an artificial receptor requires incorporating into its design a mechanism by which the receptor can adapt and respond to changes in its environment. The activity and regulation of receptors are based on the reversible intermolecular non-covalent interactions with substrates and cofactors. Ideally, the receptor should have the ability to recognize the presence or absence of specific stimuli and respond by changing its structure and, ultimately, function. The stimuli may be chemical (changes in concentration of a certain chemical species, for example) or physical (changes in temperature, pressure or light, for example). The resulting response may be conformational or electronic alterations in the receptor's structure which regulates the binding of the substrate to its host.<sup>1</sup>

The regulation of the catalytic activity of an enzyme by the binding of a cofactor at a position other than the active site is frequently observed in biological systems. This process, known as allostery, occurs when the cofactor is structurally and chemically different from the substrate and the binding is at a location far removed from the active site. The binding of the cofactor to the enzyme causes a reversible alteration in the conformation of the protein, which changes the binding efficacy of the enzyme for its substrate as schematically illustrated in Figure 2.1. Allosteric effects have been classified as positive, when the induced conformational change increases the enzyme's binding efficacy, or negative, when the initial interaction of the cofactor results in a decrease in the enzyme's affinity for its substrate. In the first case, the cofactor is called an *activator* while in the latter, it is termed as an *inhibitor*.<sup>2</sup>

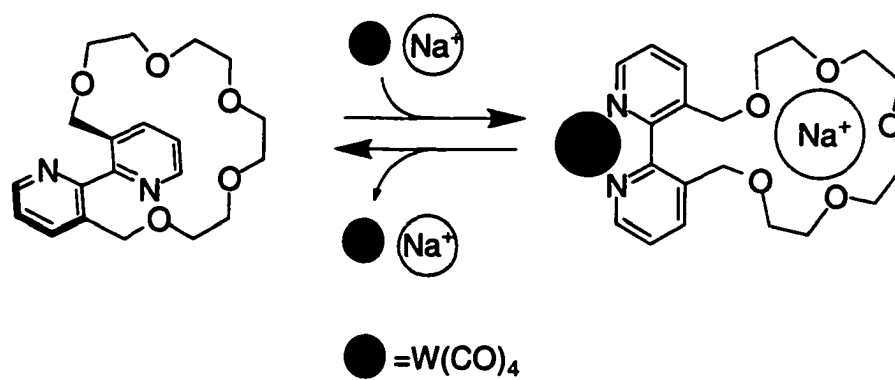


**Figure 2.1** A schematic illustration of positive (top) and negative (bottom) allosteric receptors; cofactor= , substrate= .

Inspired by these natural systems, chemists are building smaller, synthetically accessible molecules that mimic the behavior of natural receptors. The minimum requirements for an artificial receptor to be capable of allosteric behavior are: (1) an active substrate binding site, (2) an allosteric cofactor binding site, and (3) an allosteric transition,<sup>3</sup> (a mechanism by which the binding of the allosteric cofactor is structurally transmitted from the remote site to the active site of the receptor). Several artificial receptors have been reported whose binding ability is regulated through allosteric effects. A complete review<sup>3-7</sup> of these systems is beyond the scope of the thesis, however, a few examples, relevant to this work, will be presented.

## 2.2 Metal Ions As Allosteric Cofactors in Artificial Systems

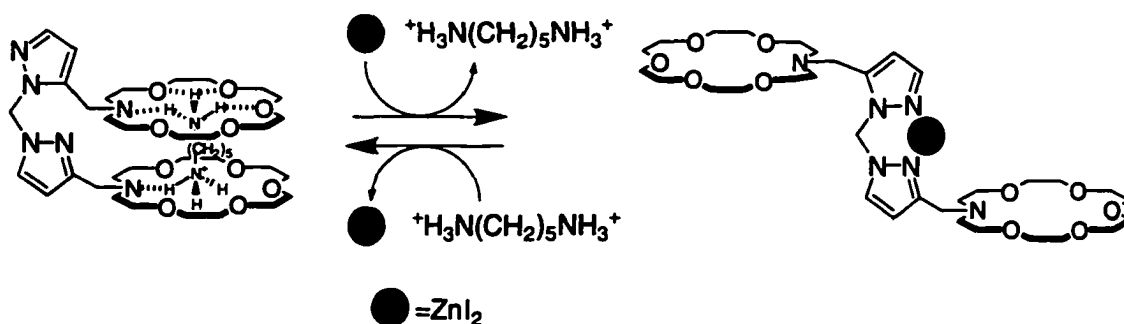
Rebek has reported one of the early examples of an artificial ionophore that exhibits positive allostery.<sup>4,5</sup> The molecule is constructed of a crown ether moiety connected to the 3- and 3'-positions of 2,2'-bipyridine (Scheme 2.1). The crown ether acts as the active site of the receptor while the bipyridine scaffold provides the allosteric site. The chelation of a tungsten ion by the bipyridine ligand forces the aromatic nuclei towards coplanarity bringing the groups in the 3- and 3'-positions closer together (the allosteric transition). The resulting conformational change of the crown ether renders it a more effective binder of sodium ions. The binding of sodium ions and subsequent membrane transport was enhanced by the presence of tungsten ions (the allosteric cofactor) in solution.



Scheme 2.1

Scheme 2.2 illustrates an example of an artificial receptor that shows a negative allosteric response to the presence of Zn(II) ions.<sup>6,7</sup> The binding of pentane-1,5-diammonium dipicrate was decreased by over 30% in the presence of zinc iodide. In absence of the metal, the guest was bound by the receptor through co-operation of the two crown-ether rings. When the metal ion was added, it was coordinated by the pyrazole ligands, forcing the crown-ether moieties to be in divergent non-binding

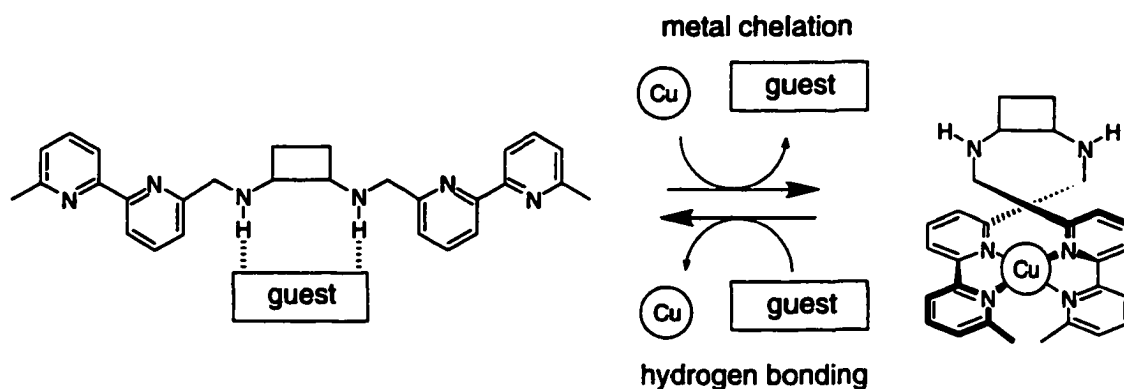
conformation. Therefore, the Zn(II) ion acts as an inhibitor for the binding of the diammonium salt by the receptor.



Scheme 2.2

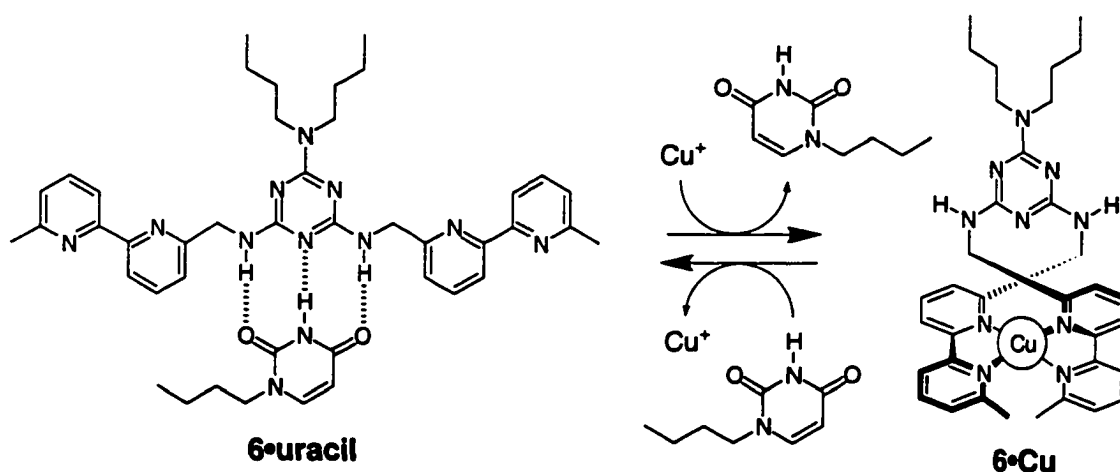
### 2.3 The Design of Allosteric Receptors for Carboxylate and Imide Derivatives

This chapter of the thesis describes the use of copper ions as allosteric inhibitors for receptors with well-ordered hydrogen-bonding surfaces. The general approach is schematically illustrated in Scheme 2.3. The receptors incorporate chelating 2,2'-bipyridine ligands that form metal-ligand coordination compounds with copper ions. This complexation induces conformational changes in the molecules, distorting the hydrogen-bonding surfaces. When the metal ion is extracted from the coordination pockets, the original hydrogen-bonding surfaces are reconstructed and the receptors are reactivated.



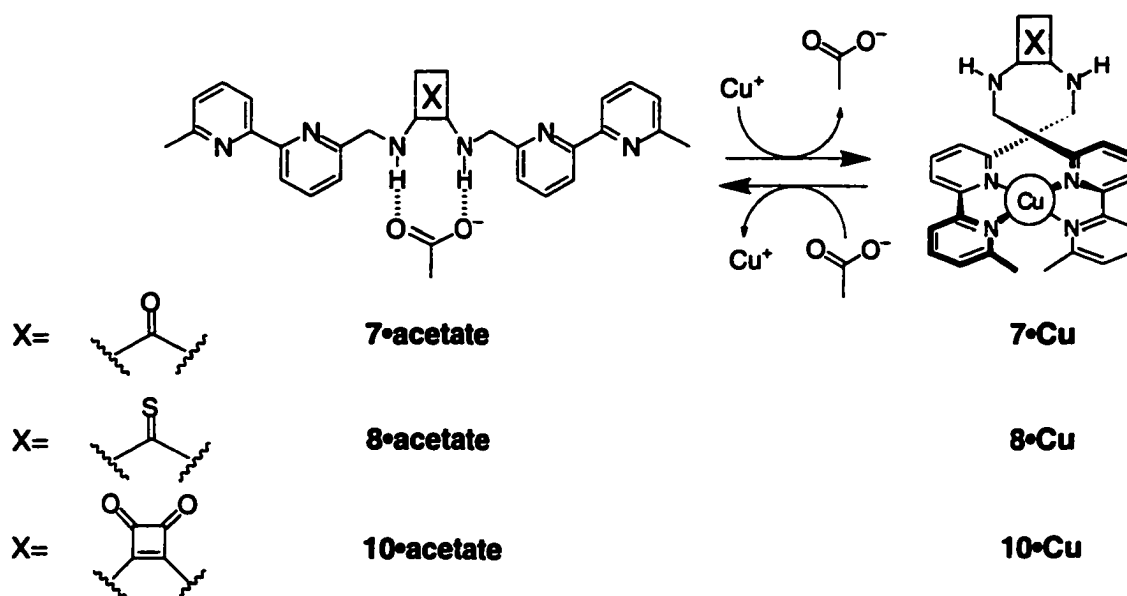
Scheme 2.3

Receptor **6** is based on the triaminotriazine scaffold (Scheme 2.4) which presents a donor-acceptor-donor hydrogen bond surface well suited to act as a host for imide guests such as uracil and thymine.<sup>8</sup> Receptors **7**, **8** and **10** (Scheme 2.5) present donor-donor hydrogen bond recognition sites suitable for binding carboxylate guests using urea,<sup>9,10f</sup> thiourea<sup>10</sup> and squaric amide<sup>11</sup> scaffolds, respectively. Upon complexation with copper ion, the two bipyridine arms on the receptor swing toward each other and forces the exocyclic C—N bonds to rotate, destroying the hydrogen-bonding surfaces.



Scheme 2.4





Scheme 2.5

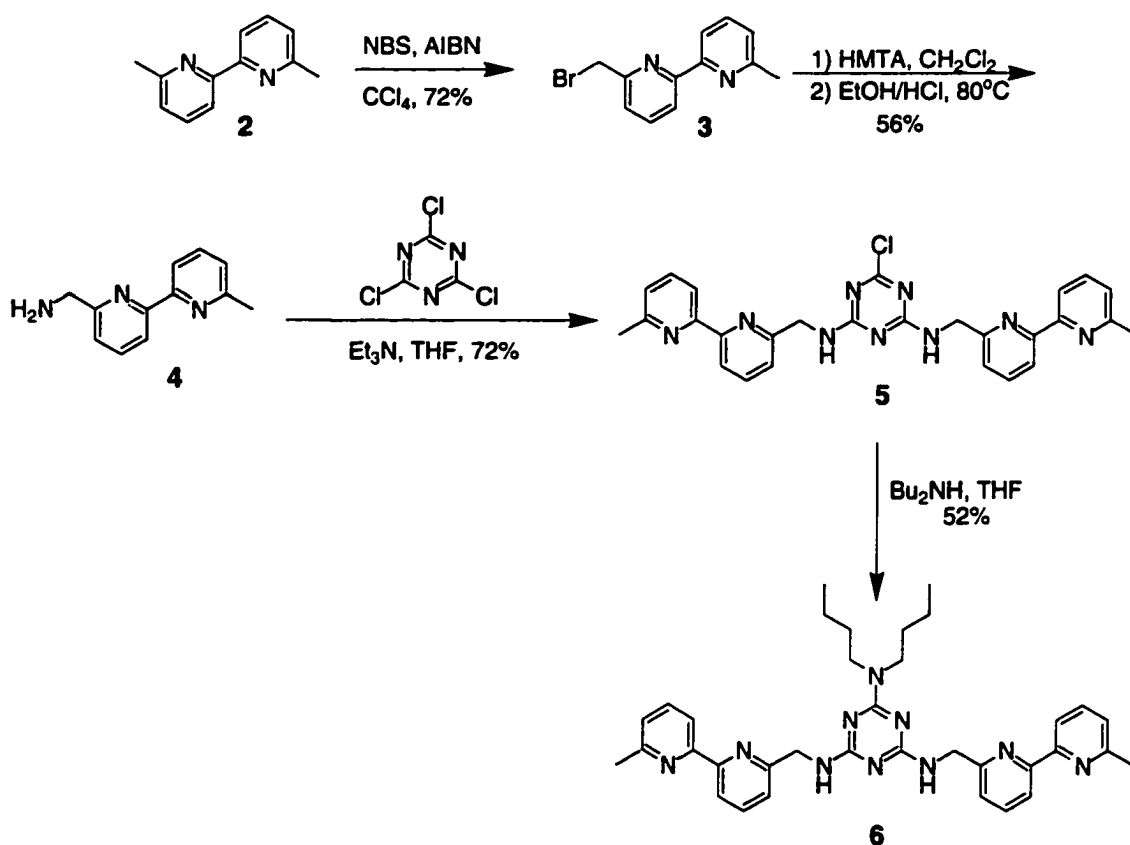
## 2.4 Synthesis and Characterization

### 2.4.1 Synthesis and Characterization of a Triaminotriazine Receptor for Imide Derivatives

As shown in Scheme 2.6, the synthesis of **6** began with the bromination of 6,6'-dimethyl-2,2'-bipyridine followed by the reaction of bromide **3** with HMTA to afford the quaternary ammonium salt. Hydrolysis of the salt at 80 °C with HCl in ethanol led to the formation of 6-aminomethyl-6'-methyl-2,2'-bipyridine **4**. Reaction of cyanuric chloride and amine **4** gave the bis(bipyridyl)triazine **5** which was heated under reflux with dibutylamine in THF in the presence of triethylamine to yield the final receptor **6** in 52 % yield.

Characterization of receptor **6** by  $^1\text{H}$  NMR spectroscopy revealed the presence of a broad peak at 5.99 ppm in  $\text{CDCl}_3$  corresponding to the N—H protons. The signal corresponding to the methylene protons of the bipyridine arms appeared as a broad singlet at 4.74 ppm. The broadness of these peaks as well as the signals corresponding to

the *n*-butyl groups was attributed to the slow rotation around the exocyclic C—N bonds of the triaminotriazine.<sup>8b</sup> The electron-impact mass spectrum of the receptor shows a peak at  $m/z= 602.3593$  which corresponds to the molecular ion of the receptor. The mass spectrum also showed the fragmentation of the molecule. A peak corresponding to the loss of one of the bipyridine groups was detected at  $m/z= 419.2676$  (29%), while a peak that corresponds to the bipyridine group itself appeared at  $m/z= 183.0923$  (58%).



Scheme 2.6

### 2.4.2 Synthesis and Characterization of the Cu(I) Complex of Triaminotriazine Receptor 6

The Cu(I) complex of triaminotriazine receptor 6 was prepared by the addition of 1.0 molar equivalent of  $\text{Cu}(\text{CH}_3\text{CN})_4\text{PF}_6$  to an acetonitrile solution of the receptor. An

immediate change in color from colorless to red-orange was observed due to formation of a tetrahedral complex of Cu(I) ions with the bipyridine ligands.<sup>22</sup> The addition of ether induced the precipitation of a red-orange solid which was collected by filtration. The <sup>1</sup>H NMR spectrum of the complex, **6•Cu**, indicated that the product is a symmetrical molecule with single sets of peaks for the protons of the bipyridines and the alkyl chains. The -CH<sub>2</sub>- linkage of the bipyridines appeared as a doublet of a doublet for each proton at 4.60 and 4.04 ppm. This reveals that these protons are in different magnetic environments due to the tetrahedral geometry around the metal. The bipyridine ligands locks the position of these methylene protons in space. The signals for the methylene CH<sub>2</sub> protons of the *N*-alkyl chains appeared as two doublets of triplets at 3.44 and 3.22 ppm. This is due to diastereotopic environment created by the chelation of the metal and the slow rotation around the C—N triazine bond attached to the chains.

The structure of the Cu(I) complex was further confirmed by X-ray crystal analysis of **6•Cu**. X-ray quality crystals of the complex were obtained through the slow diffusion of the ether into an acetonitrile solution of **6•Cu**. The crystal structure (Figure 2.2) shows the tetrahedral arrangement of the bipyridine ligands around the metal ion. In the Cu(I) complex the C(2)-N(5) and C(3)-N(4) bonds are rotated almost 180° from their original positions in the active hydrogen-bonding receptor. The torsional angles C(4)-N(4)-C(3)-N(1) and C(5)-N(5)-C(2)-N(2) are 175° and 179°, respectively. The N—H bonds at N(4) and N(5) are in a divergent arrangement where the donor-acceptor-donor hydrogen bonding surface (H(N4), N(3), H(N5)) for the imide guest is destroyed. This reduces the recognition elements to two identical, but weakly bonding, donor-acceptor hydrogen bond surfaces (N(1), H(N4) and N(2), H(N5)).

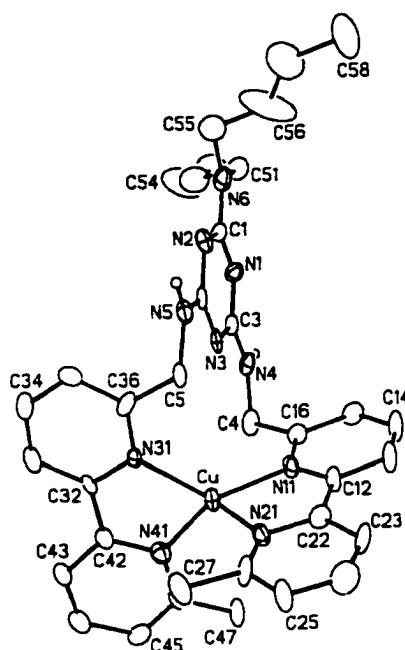
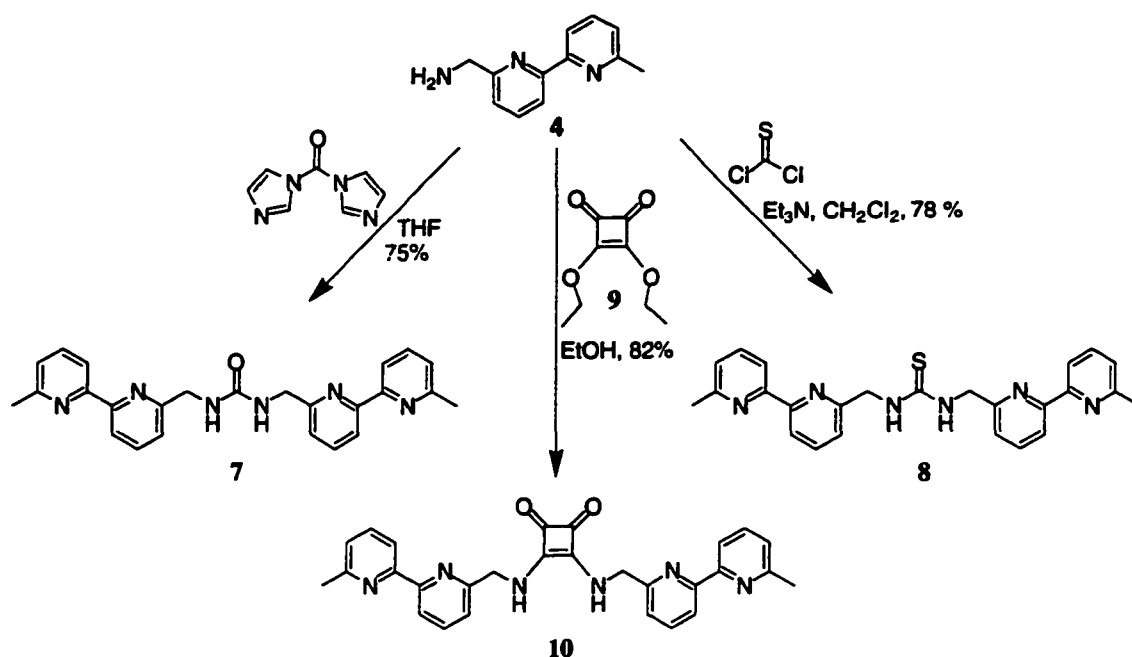


**Figure 2.2** The crystal structure of **6•Cu**. The  $\text{PF}_6^-$  counterion and all the hydrogen atoms, except for those on N4 and N5, have been removed for clarity.

### 2.4.3 Synthesis and Characterization of the Carboxylate Receptors and Their Cu(I) Complexes

Receptors **7**, **8**, and **10** were each prepared in one step from 6-methyl-6'-aminomethyl-2,2'-bipyridine **4** as shown in Scheme 2.7. The reaction of amine **4** with carbonyl diimidazole in THF afforded urea **7** in 75% yield. The receptor was insoluble in organic solvents such as chloroform, dichloromethane, acetone and THF but was soluble in DMSO. In the  $^1\text{H}$  NMR spectrum, taken in  $\text{DMSO}-d_6$ , a triplet peak appeared at 6.89 ppm clearly revealed the formation of the urea N—H protons while a doublet at 4.43 ppm was observed for the  $\text{CH}_2$  protons of the bipyridine arms. The electron-impact mass spectrum showed the molecular ion peak at  $m/z = 424.2012$  (2%). The fragment peak, at  $m/z = 225.0905$  (96%), corresponds to the loss of an aminomethyl bipyridine group.



Scheme 2.7

The Cu(I) complex of urea receptor 7 was prepared by the addition of 1.0 equivalent of the receptor to a solution of  $\text{Cu}(\text{CH}_3\text{CN})_4\text{PF}_6$  in acetonitrile. Upon stirring the solution for 10 minutes, the color changed from colorless to red-brown indicating formation of the 4-coordinate Cu(I) complex,  $7 \cdot \text{Cu}$ . The red-brown solid that precipitated by the addition of diethyl ether was collected and characterized by  $^1\text{H}$  NMR spectroscopy and electrospray mass spectrometry. The  $^1\text{H}$  NMR spectrum revealed the presence of one set of peaks for the protons of the bipyridines consisting of six signals. The urea N—H appeared a broad peak at 6.28 ppm. Two very broad signals for the protons of the  $\text{CH}_2$  groups appeared at 4.31 and 3.87 ppm. The broadness of these peaks suggests that the coordination of the copper ion by the bipyridine is more labile in urea complex  $7 \cdot \text{Cu}$  than was observed for triaminotriazine complex  $6 \cdot \text{Cu}$ . The electrospray mass spectrum of the urea complex  $7 \cdot \text{Cu}$  exhibited the molecular ion ( $M$ ) peak for the complex at  $m/z = 487.1300$  where the isotopic pattern indicated the presence of a minor

amount of a doubly charged species (at  $m/z=487$ ) corresponding to  $[M+M]^{2+}$ . Also, the spectrum revealed the presence of a peak at  $m/z=1121$  corresponding to  $[M+M+PF_6]^+$ . This peak could be due to either the presence of a dimer  $(7\bullet Cu)_2$ , where two molecules of receptor coordinate with two copper ions, or to aggregation taking place during the electrospray process of the complex inside the mass spectrometer.

Thiourea receptor **8** was obtained in 78% yield by the addition of 0.5 equivalents of thiophosgene to amine **4** in  $CH_2Cl_2$ . In order to prepare the Cu(I) complex,  $8\bullet Cu$ ,  $Cu(CH_3CN)_4PF_6$  was added to a solution of the receptor dissolved in a 1:1 mixture of chloroform and acetonitrile. The color of the solution changed immediately from colorless to red-brown and the addition of the diethyl ether to the solution induced the precipitation of a brown solid which was collected. The  $^1H$  NMR spectrum of the solid in  $CD_3CN$  showed peaks that were so broad and poorly resolved it was impossible to characterize the complex. Moreover, the electrospray mass spectrum of an acetonitrile solution of the brown solid did not show the presence of the target copper complex of receptor **8**. Similar results were obtained when an attempt was made to prepare the Fe(II) complex of receptor **8**. These observations suggest that the oxidation state of the metal is affected by the presence of sulfur as similar behavior was previously reported for systems with thiol groups.<sup>15b, 16</sup>

Squarate receptor **10** was prepared in 82% yield by the reaction of amine **4** with diethyl squarate in ethanol. All attempts to prepare the copper complex  $10\bullet Cu$  gave similar results as were already observed for the attempted syntheses of  $8\bullet Cu$ . The color of the solution did change from colorless to red-brown when  $Cu(CH_3CN)_4PF_6$  was added to a solution of squarate **10** in a 1:1 mixture of chloroform and acetonitrile. The  $^1H$  NMR spectrum of the collected brown solid could not be characterized due to broad peaks. However, the electrospray mass spectrum of the complex showed a peak that

corresponds to the  $m/z$  of  $[10+Cu]^+$ . Although this peak indicated the presence of a species where the copper may be coordinated to the ligand, it did not verify that the metal was chelated by the bipyridines in a tetrahedral fashion and it did not rule out the presence of metal-ligand aggregates.

## 2.5 Binding Studies

The binding efficacy of the receptors to their substrates was evaluated by analyzing the  $^1H$  NMR spectral changes that occurred upon treating solutions of the hosts (usually the receptors) with aliquot amounts of the guests (usually the substrates). A solution of a host of known concentration was placed in an NMR-tube and aliquot amounts of the guest, dissolved in the same solvent, were added via a syringe. A  $^1H$  NMR spectrum of the solution was obtained after each addition. The guest was added until no further changes in the chemical shift of the protons of the host that are associated with the molecular recognition process were observed.

### 2.5.1 Binding Activity of Triaminotriazine Receptor 6 Toward *N*-Butyluracil

In the case of the triaminotriazine receptor **6**, the receptor was titrated into a solution of the substrate for the following reason. The signal in the  $^1H$  NMR spectrum that corresponds to the N—H hydrogen-bond-donor protons of the triaminotriazine lies in the region between 6.00 and 7.00 ppm. As the substrate (*N*-butyluracil) was added, this signal shifted into the aromatic region of the spectrum which made it impossible to follow throughout the entire titration experiment. However, the signal corresponding to the imide N—H proton of *N*-butyluracil appeared at 8.50 ppm, an uncluttered region of the spectrum. The downfield shift of this imide signal as receptor **6** was added was monitored.

A solution of *N*-butyluracil in toluene- $d_6$  (2 mM) was treated with a solution of the triaminotriazine receptor **6** (30 mM) in the same solvent. The signal corresponding to the N—H proton of *N*-butyluracil appeared at 7.90 ppm before the addition of the receptor. A significant downfield shift ( $\Delta\delta$  greater than 6 ppm) was observed for the signal as the imide was treated with aliquot amounts of receptor **6** (Figure 2.3). This is an indication of very effective hydrogen bonding between the uracil and the triazine receptor **6** (as already mentioned in Chapter 1). After 3-4 equivalents of the receptor were added, the change in the chemical shift of the imide N—H proton was insignificant. This indicates that the uracil has reached saturation where the signal corresponding to N—H proton reached 14.28 ppm after the addition of ten equivalents of receptor **6**. The data set collected from the experiment correlated well with calculated curves using 1:1 binding models and gave an association constant ( $K_a$ ) value of  $600 \pm 10 \text{ M}^{-1}$ .

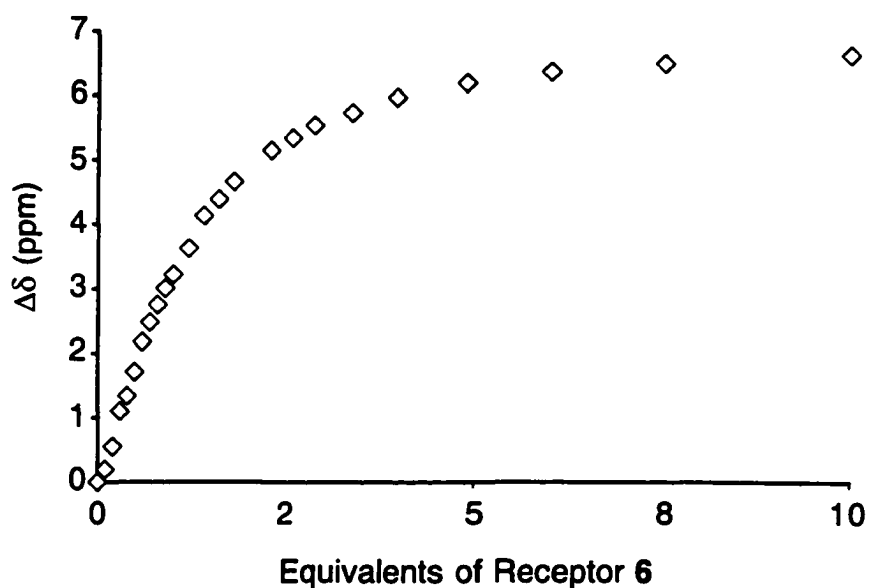


**Figure 2.3** The titration curve of *N*-butyluracil ( $\diamond$ ) (2 mM) with triaminotriazine receptor **6** (30 mM) in toluene- $d_6$ .



In order to compare the association constants of the triaminotriazine receptor **6** and its Cu(I) complex **6•Cu** it was necessary to perform the titration experiments in the same solvent (see Chapter 1). Thus, the titration experiment of metal-free receptor **6** was repeated in 1:1 CD<sub>3</sub>Cl/CD<sub>3</sub>CN since the Cu(I) complex was not soluble in toluene (Figure 2.4). The change in the chemical shift of the uracil N—H proton was followed as aliquot amounts of the receptor were added. The signal corresponding to the uracil N—H proton initially appeared at 8.51 ppm and shifted downfield ( $\Delta\delta$  about 2 ppm) upon the addition of the triazine receptor **6**. The shift was less than the shift observed in toluene but still significant (Figure 2.4). This indicates an association between the receptor and the substrate through hydrogen bonding but this association is weaker than that in toluene due to the competitive nature of the CD<sub>3</sub>Cl/CD<sub>3</sub>CN solvent system used (see Chapter 1). After 10 equivalents of the receptor was added, the signal for the N—H proton of the uracil shifted to 10.38 ppm. The data set collected fit well to a curve calculated for 1:1 binding model giving a  $K_a$  value of  $50 \pm 2 \text{ M}^{-1}$ .

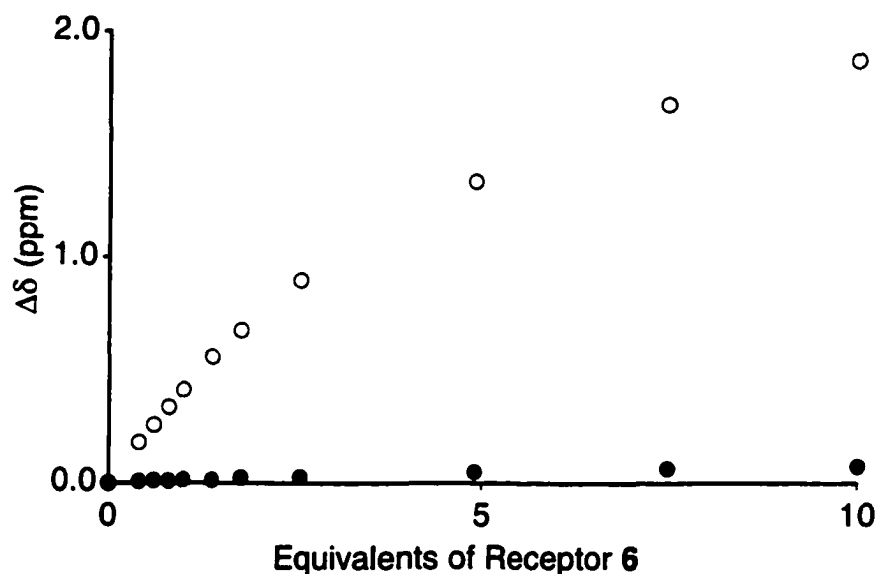


**Figure 2.4** The titration curves of *N*-butyluracil with receptor **6** (O) and its Cu(I) complex **6•Cu** (●) in 1:1 mixture of CDCl<sub>3</sub>/CD<sub>3</sub>CN.

## 2.5.2 The Effect of Cu(I) Ions on the Binding Efficacy of Triaminotriazine Receptor **6**

The ability of the Cu(I) ion to inhibit the recognition process for the triaminotriazine receptor **6** was evaluated by repeating the titration experiment, but replacing the active receptor with the preformed complex **6**•Cu (Figure 2.4). The signal corresponding to the N—H proton of *N*-butyluracil appeared at 8.50 ppm in the <sup>1</sup>H NMR spectrum before the addition of the complex **6**•Cu. A small but observable change ( $\Delta\delta$  less than 0.1 ppm) in the chemical shift of the signal corresponding to the imide N-H proton of uracil was observed upon the addition of a 1:1 CD<sub>3</sub>CN/CDCl<sub>3</sub> solution of **6**•Cu. This signifies the existence of only very weak hydrogen bonds attributed to the association of *N*-butyluracil with the less effective donor-acceptor sites in **6**•Cu as illustrated in Figure 2.5. The non-complementarity of these sites to the imide guest and the steric bulk of the butyl groups reduced the affinity of Cu•**6** for imide derivatives resulting in a significantly less effective receptor.

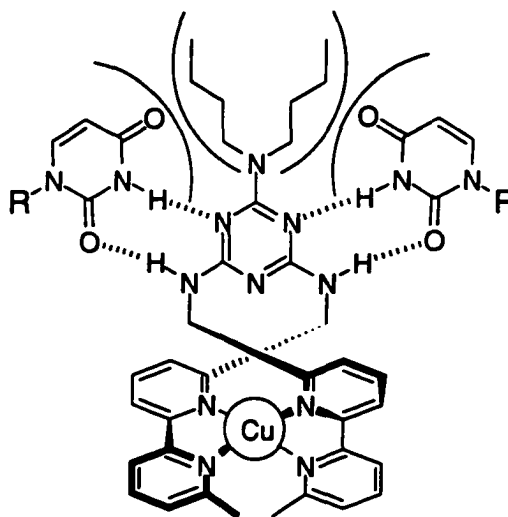


**Figure 2.5** The binding of uracil derivatives to the two less effective sites of **6**•Cu. The presence of only two hydrogen bonds per site and the steric effect of the dibutylamine group reduced the affinity of the sites for the substrate.

The metal-induced allosteric inhibition was also effective when the coordination compound **6•Cu** was prepared *in situ*, in the presence of the imide substrate. This was again diagnosed by the relative position of the imide N-H chemical shift in the  $^1\text{H}$  NMR spectra (Figure 2.6(a)). The addition of one equivalent of the triaminotriazine receptor **6** to a 1:1  $\text{CD}_3\text{CN}/\text{CDCl}_3$  solution of *N*-butyluracil produced an immediate downfield shift of the signal for this hydrogen atom from 8.52 ppm to 8.92 ppm (Figure 2.6(b)) as was observed in the titration experiments described above. This indicates effective hydrogen bonding between the receptor and the substrate and the formation of the hydrogen-bonded **6•uracil** complex. When one molar equivalent of  $\text{Cu}(\text{CH}_3\text{CN})_4\text{PF}_6$  was added directly to the NMR sample, the uracil N—H proton signal returned to its original position at 8.53 ppm (Figure 2.6(c)) and all the signals corresponding to receptor **6** were replaced by those of its Cu(I) complex **6•Cu**. This  $^1\text{H}$  NMR spectrum was identical to the spectrum obtained of an equimolar solution of the pre-formed complex **6•Cu** and *N*-butyluracil. These observations reveal clearly that the copper complex **6•Cu** can be formed in the presence of the imide substrate and that coordination to the metal prevents the hydrogen bond recognition process.

Subsequent addition of an excess of the stronger coordinating ligand,<sup>12</sup> neocuproine (2,9-dimethyl-1,10-phenanthroline, **dmph**), resulted in the immediate disappearance of the signals corresponding to the metal complex **6•Cu**, and the regeneration of those representing the hydrogen-bonded **6•uracil** complex (Figure 2.6(d)). This implies that the metal was removed from the chelation site of the receptor to form the more favorable  $\text{Cu}(\text{dmph})_2$  complex.<sup>5a,12</sup> The uracil N—H proton signal shifted back downfield to 8.92 ppm indicating a strong association with the receptor. The hydrogen-bonding donor-acceptor-donor surface of the triaminotriazine receptor **6** was

thus recreated, by the removal of the metal ion, and the receptor was reactivated to bind its imide substrate.

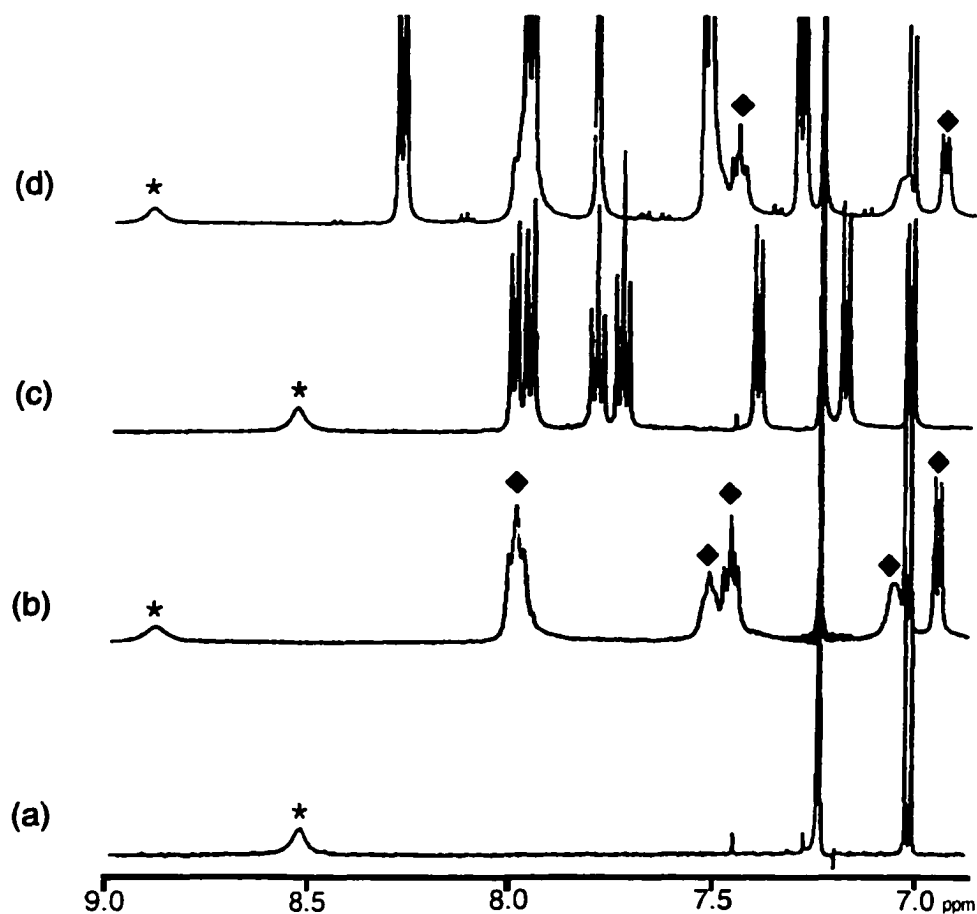


**Figure 2.6** Changes in the <sup>1</sup>H NMR spectra (300 MHz) of (a) *N*-butyluracil (2 mM) in CD<sub>3</sub>Cl/CD<sub>3</sub>CN (1:1) upon subsequent additions of (b) one molar equivalent of **6**, (c) one molar equivalent of Cu(CH<sub>3</sub>CN)<sub>4</sub>PF<sub>6</sub> and (d) four molar equivalents of neocuproine (*dmph*). The signals denoted by (★) corresponds to the N—H proton of *N*-butyluracil while the signals corresponding to the metal-free receptor **6** are denoted by (◆). (The chemical shifts were referenced to the residual peak of CDCl<sub>3</sub> at δ 7.24 ppm).

### 2.5.3 The Binding Activity of Urea Receptor 7 Toward Acetate

The binding efficacy of urea receptor **7** was studied by treating a 5 mM solution of the receptor in DMSO-*d*<sub>6</sub> with a 100 mM solution of tetrabutylammonium acetate

(TBAOAc) in the same solvent. The downfield shift of the signal corresponding to the urea N-H protons of receptor **7** was followed as aliquot amounts of the substrate were added (Figure 2.7). Initially, the signal for the N—H protons appeared at 6.89 ppm. As the acetate substrate was added, a significant downfield shift ( $\Delta\delta$  greater than 1 ppm) of the signal for the urea N—H protons was observed indicating effective hydrogen bonding between the urea receptor **7** and the acetate guest. As the receptor reached saturation (when about 10 equivalents of guest were added), the signal for the urea N—H protons reached 8.81 ppm. The collected data correlate well with calculated curves using 1:1 binding models and gave an association constant value of  $50 \pm 4 \text{ M}^{-1}$ .

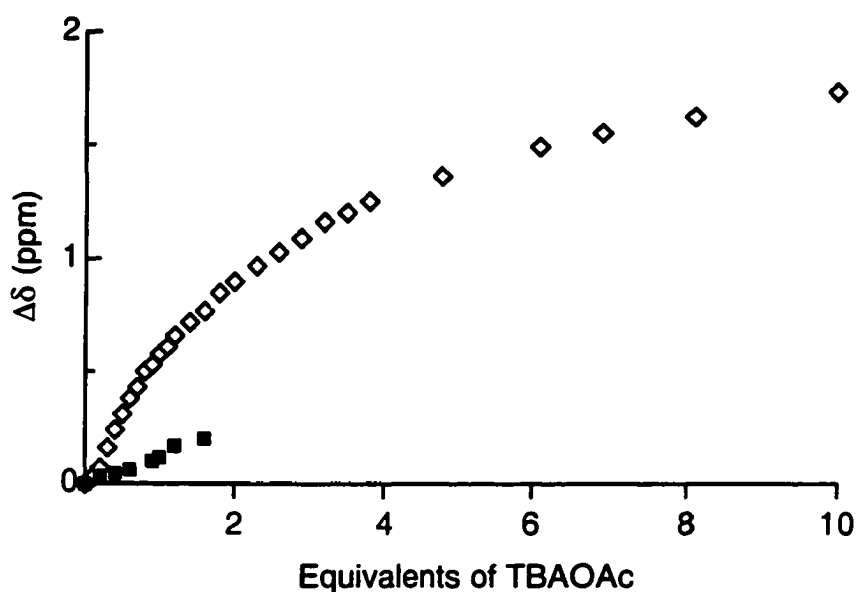


**Figure 2.7** Titration curves of urea receptor **7** (□) (5 mM) and **7**•Cu (■) (5 mM) when treated with TBAOAc (100 mM) in  $\text{DMSO-}d_6$ .

#### 2.5.4 The Effect of Cu(I) Ions on the Binding Efficacy of Urea Receptor **7**

In a similar fashion to the triaminotriazine receptor **6**, the effect of Cu(I) ion on the ability of the urea receptor **7** to act as a receptor was evaluated by titrating the

preformed complex **7•Cu** (5 mM) with TBAOAc (100 mM) in DMSO- $d_6$ . In this case, the signal for the urea N-H protons of the complex **7•Cu** could not be followed throughout the concentration range of the entire titration, as it quickly broadened to become indistinguishable from the baseline. This signal appeared at 7.02 ppm before the addition of the acetate substrate. As the substrate was added (Figure 2.7), an insignificant but observable downfield shift was noticed for the signal corresponding to the urea N-H protons of the complex **7•Cu**. The movement of this signal was monitored up to the addition of 1.6 equivalents of substrate where the observed trend of the insignificant change in the chemical shift supports our claim that the metal is a successful negative allosteric cofactor.

Table 2.1 lists the chemical shifts for the urea N-H proton of complex **7•Cu** prepared *in situ* as previously described for the triaminotriazine receptor **6**. In the case of urea receptor **7**, however, only 0.5 equivalents of the acetate substrate were added because the addition of one equivalent of TBAOAc shifted the N—H peak into the aromatic region of the spectrum. This resulted in overlapping with the other aromatic signals making this signal impossible to follow. The addition of 0.5 equivalents of TBA acetate to a DMSO- $d_6$  solution of urea receptor **7** produced a small, but significant downfield shift ( $\Delta\delta = 0.2$  ppm) of the signal for the N—H protons on the receptor. This suggested the formation of the hydrogen-bonded **7•acetate** complex. When one molar equivalent of  $\text{Cu}(\text{CH}_3\text{CN})_4\text{PF}_6$  was added directly to the NMR sample, the **7•acetate** signals were all replaced with signals for **7•Cu**. The resulting spectrum was similar to that of a mixture of the pre-formed complex **7•Cu** and TBA acetate under similar conditions. Also, the signal for the urea N-H protons returned to the original position at 6.89 ppm, indicating that the presence of Cu(I) ions inhibited the binding of receptor **7** to its substrate. In order to remove the copper metal, four equivalents of neocuproine were

added to the NMR tube. The spectrum showed the disappearance of the signals that correspond to the complex **7**•Cu and the formation of the signals for the free receptor **7**. However, the urea N—H protons signal did not shift significantly downfield as was observed in the spectrum of the **7**•acetate complex. This implies that the hydrogen-bonded **7**•acetate complex did not form despite the fact that the free receptor **7** was regenerated. This was attributed to the acetate ion's preference to act as a counterion for the harder copper cation rather than the softer TBA cation. This favorable ion pairing effectively removes the acetate from acting as a guest for urea receptor **7**.

**Table 2.1**  $^1\text{H}$  NMR chemical shifts of the urea N—H protons of receptor **7** and *N,N'*-dimethylurea upon sequential treatment with additives.<sup>[a]</sup>

Additive	$\delta/\text{ppm}$	
	Urea <b>7</b>	<i>N,N'</i> -Dimethylurea
none	6.89	5.70
$\text{CH}_3\text{CO}_2^-$ <sup>[b]</sup>	7.09	5.84
$\text{CH}_3\text{CO}_2^- + \text{Cu(I)}$ <sup>[c]</sup>	6.89	5.71
$\text{CH}_3\text{CO}_2^- + \text{Cu(I)} + \text{dmph}$ <sup>[d]</sup>	6.91	5.71

[a] run in  $\text{DMSO}-d_6$ ; [b] 0.5 equivalent added as TBA salt; [c] 1 equivalent added as  $\text{Cu}(\text{CH}_3\text{CN})_4\text{PF}_6$ ; [d] 4 equivalents neocuproine (**dmph**) added.

In order to further support the evidence that acetate ions prefer to bind to copper ions rather than to the urea, the above experiment was repeated replacing receptor **7** with *N,N'*-dimethylurea. *N,N'*-Dimethylurea has no coordinating ligands that can chelate to Cu(I) ions and the presence of the metal should not have an allosteric effect on the receptor binding. The addition of 0.5 equivalents of TBA acetate to a solution of *N,N'*-dimethylurea caused a downfield shift of the urea N—H protons from 5.70 to 5.84 ppm (Table 2.1), indicating the formation of a strong hydrogen-bonded complex. Upon the

addition of one equivalent of  $\text{Cu}(\text{CH}_3\text{CN})_4\text{PF}_6$ , the signal for the urea N—H protons shifted back to 5.71 ppm. This chemical shift was not affected by the addition of excess neocuproine to the NMR tube (Table 2.1). This indicates that the addition of the copper ion prevented the association of acetate and *N,N'*-dimethylurea. Since the metal should not form a stable coordination complex with *N,N'*-dimethylurea and, thus, can not act as an allosteric inhibitor for it, it was concluded that Cu(I) ions prevents the acetate from acting as a substrate for *N,N'*-dimethylurea through effective ion pairing between the acetate anion and the Cu(I) cation or between the acetate and the  $\text{Cu}(\text{dmph})_2$  complex.

. During the titration of the pre-formed metal complex  $7\cdot\text{Cu}$  with the acetate substrate, it was observed that when more than one equivalent of carboxylate was added, new signals began to appear (Figure 2.8) becoming significantly more intense as the concentration of TBA acetate increased. These peaks appeared at chemical shifts similar to the aromatic signals of receptor **7** and were initially attributed to a competition between the copper complexation to the bipyridine ligands and the binding of the carboxylate to the hydrogen-bonding surface of the receptor. Perhaps, the increase in the concentration of the acetate favors the hydrogen-bonded  $7\cdot\text{acetate}$  complex over the copper complex  $7\cdot\text{Cu}$ . However, X-ray structure analysis of the copper complex of **7** uncovered the presence of another species (Figure 2.9) that could be the source of the new peaks in the  $^1\text{H}$  NMR spectrum.



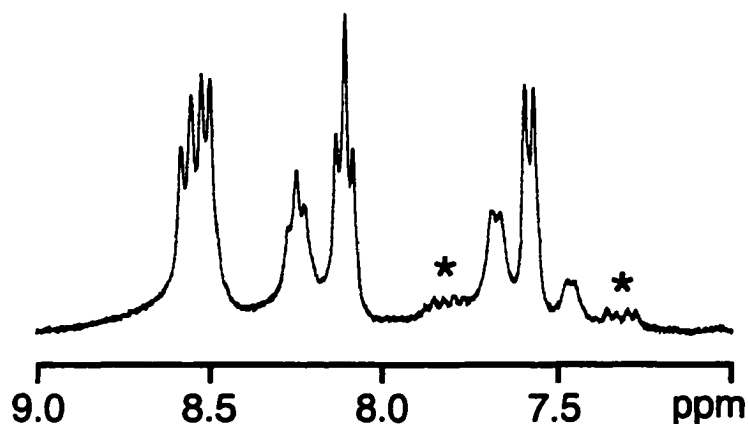


**Figure 2.8**  $^1\text{H}$  NMR spectrum (500 MHz,  $\text{DMSO-}d_6$ ) of  $7\cdot\text{Cu}$  after 1.6 equivalents of TBAOAc were added. The new peaks appearing are denoted by (\*).

The slow evaporation of an acetonitrile solution of complex  $7\cdot\text{Cu}$  afforded low quality crystals that were used to obtain the structure of the copper complex of receptor **7**. The structure (Figure 2.9) shows the presence of two molecules of receptor **7** coordinating to two Cu(I) ions  $(7\cdot\text{Cu})_2$ , instead of just one Cu(I) ion chelated by one receptor molecule  $7\cdot\text{Cu}$ . The structure exhibits the presence of hydrogen bonds between the two urea groups through the N—H donors (H(N3) and H(N4)) of one molecule and the carbonyl acceptor (O1) of the other. This geometry allows the dimer to preserve the donor-donor (H(N1) and H(N2)) hydrogen-bonding surface suitable for binding carboxylates.

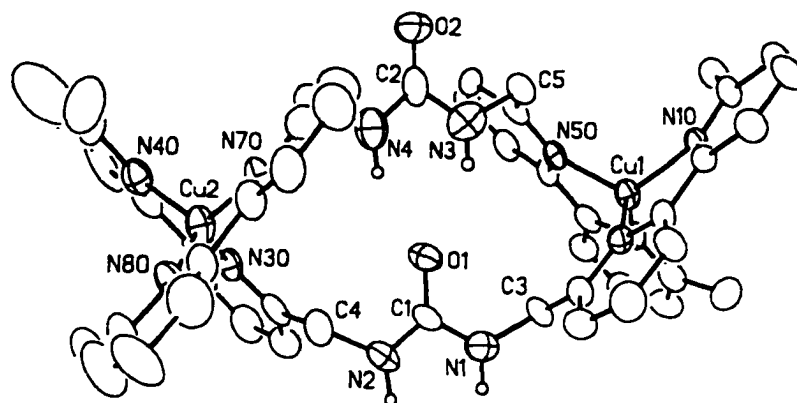


**Figure 2.9** X-ray structure of **7•Cu**. The  $\text{PF}_6^-$  counterion and all the hydrogen atoms, except for those on N1, N2, N3 and N4, have been removed for clarity.

The presence of the dimeric copper complex  $(7\bullet\text{Cu})_2$  was already observed in minor amounts by electrospray mass spectrometry (Figure 2.10). This technique may give an indication of the relative amounts of the ions present in solution. The intensity of a peak in the electrospray mass spectrum is directly related to the concentration of its corresponding ion in the gas phase, which is related to its concentration in solution.<sup>13</sup> Thus, a relative comparison of the intensity of the peaks corresponding to the monomer complex **7•Cu** with that of the dimer complex  $(7\bullet\text{Cu})_2$  in electrospray mass spectrum may give a qualitative indication of the relative concentrations of these ions in solution. The relative intensity of the dimer peak to that of the monomer increased as tetrabutylammonium acetate was added to the copper complex **7•Cu** solution (Figure 2.11). This relative intensity continued to increase as the concentration of acetate increased. This implies that the dimer is favored over the monomer at high concentration of the substrate.

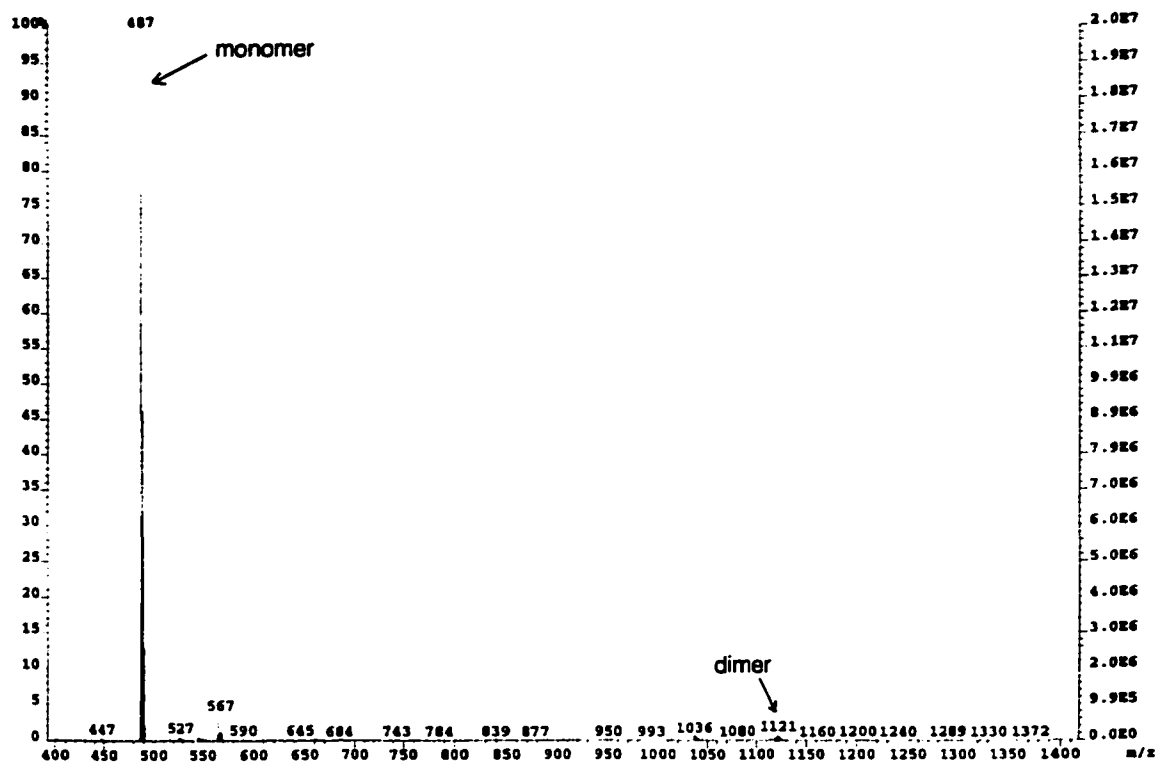


Figure 2.10 Electrospray mass spectrum of  $7\bullet\text{Cu}$

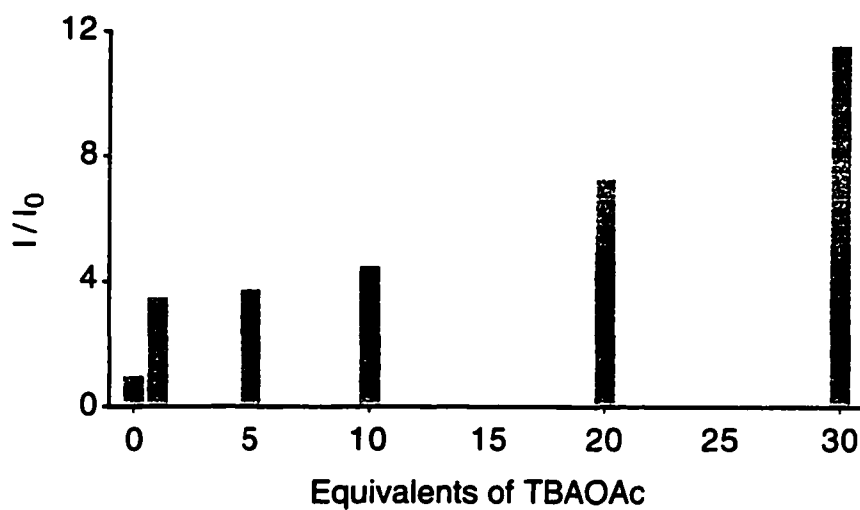
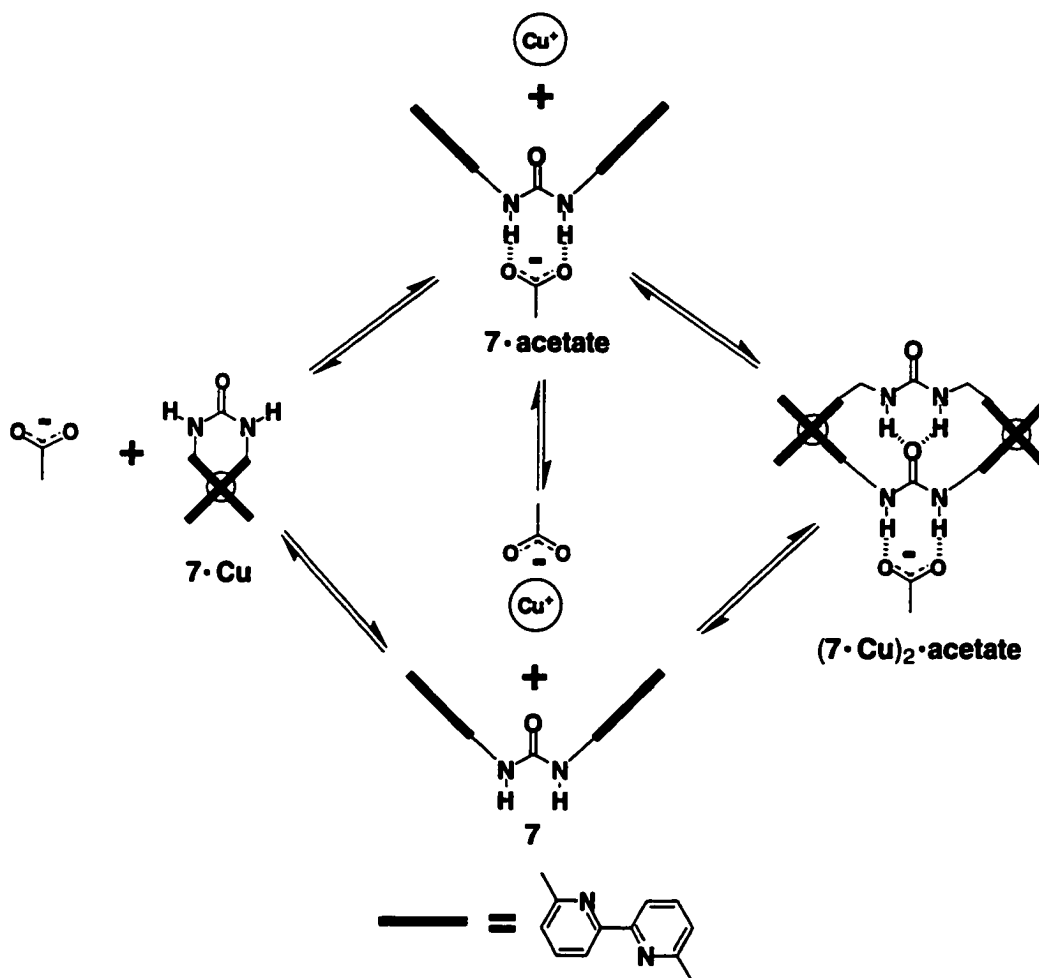


Figure 2.11 The change in the peak intensity ( $I$ ) of the dimer relative to its initial intensity ( $I_0$ ) in the mass spectrum as the concentration of TBAOAc was increased.

The appearance of the new signals in the  $^1\text{H}$  NMR spectrum during the titration of  $7\cdot\text{Cu}$  was, therefore, attributed to the formation of the dimer  $(7\cdot\text{Cu})_2$ . The increase in the concentration of the acetate shifts the equilibrium (illustrated in the Scheme 2.8) toward formation of a dimer-acetate complex  $(7\cdot\text{Cu})_2\cdot\text{acetate}$ . This complex is favored over  $7\cdot\text{Cu}$  because it satisfies the self association of the urea, the coordination of the metal to the bipyridines, and the hydrogen bonding of acetate to urea. Such an equilibrium shift is facilitated by the high association and the strong ion-solvating abilities of DMSO which enable it to dissolve the copper ions making the rearrangement of the metal complexes feasible.<sup>14</sup>



Scheme 2.8

### 2.5.5 The Binding Activity of Thiourea Receptor **8** Towards Acetate

Receptor **8**, the thiourea analog of urea receptor **7**, provides a similar donor-donor hydrogen bonding site for carboxylates. Since thiourea ( $pK_a = 21.0$ ) is more acidic than urea ( $pK_a = 26.9$ ), the N—H protons of the former are expected to be a better hydrogen bonding donors for carboxylate guests.<sup>10f</sup> The thiourea receptor **8** is also more soluble than urea receptor **7** in organic solvents, such as chloroform and dichloromethane, which have lower dielectric constants and lower electron donating abilities than DMSO.<sup>14</sup> The higher solubility of receptor **8** is attributed to the weakness of intermolecular hydrogen bonds between thiourea derivatives as sulfur atoms are weaker hydrogen bonding acceptors than oxygens.<sup>15</sup>

The binding activity of the thiourea receptor **8** was studied by microcalorimetric titration experiments using an isothermal titration calorimeter (ITC). The heat change upon the formation of a hydrogen bonding complex was monitored as the substrate was added to the receptor cell. A 100 mM solution of TBA acetate was injected into a microcalorimetric cell containing a 5 mM solution of receptor **8** at 25 °C. The heat evolved with each injection is displayed versus the time in the top panel in Figure 2.11. The first few injections usually deviate from ideal binding behavior due to the presence of the receptor in large excess compared to the substrate. The heat evolved in the initial injections produced larger signals due to the complete complexation of the added substrate, but as titration experiment proceeded, the signal became smaller due to the saturation of the receptor by the guest. The binding isotherm was generated by integrating each peak and plotting the resulting data versus molar ratio of the acetate substrate (Figure 2.11, bottom panel (■)). The heat evolved due to the dilution of the

injectant substrate was measured by a separate titration where a solution of TBA acetate (100 mM in DMSO) was injected into blank DMSO. The heat evolved from the blank titration was subtracted from the binding isothermal curve for the thiourea receptor before the fitting analysis of the latter. Also, the integrated value of the first few injections were not considered in the fitting analysis because of the reasons mentioned above. The resulting isothermal curve correlated well with a one-site binding model (the solid line in bottom panel, Figure 2.12) giving a  $K_a$  value of  $172.1 \pm 9.5 \text{ M}^{-1}$ , a  $\Delta H$  value of  $-563.2 \pm 14.21 \text{ cal mole}^{-1}$  and a  $\Delta S$  value of  $8.340 \text{ cal mol}^{-1} \text{ K}^{-1}$ . The  $K_a$  value indicates that receptor **8** has a higher affinity to acetate than its urea analogue, receptor **7** ( $K_a = 50 \pm 2 \text{ M}^{-1}$ ). This supports the claim that the thiourea N—H protons are better hydrogen bonding donors than the urea N—H protons. The association of thiourea receptor **8** and the acetate ion is both enthalpy and entropy driven as shown by the values of  $\Delta H$  and  $\Delta S$ .

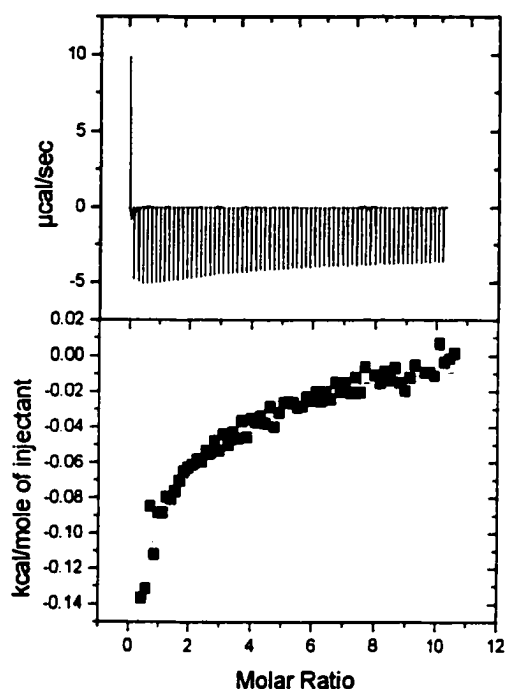


**Figure 2.12** Calorimetric titration of thiourea receptor **8** (5 mM) with TBAOAc (100 mM) in DMSO at 25°C. Top panel: raw data showing heat evolved with each injection of the acetate ion. Bottom panel:

integrated curve of the raw titration (■); the solid line represents a nonlinear least squares fit using 1:1 binding model.

The binding of thiourea receptor **8** was also studied by  $^1\text{H}$  NMR titration experiments in  $\text{DMSO-}d_6$  where the change in the chemical shift of the signal corresponding to the thiourea N—H protons of the receptor (5 mM) was followed as a solution of TBA acetate (100 mM) was added. Before the addition of the acetate, the signal corresponding to the N—H protons appeared at 8.42 ppm. As the acetate was added (Figure 2.13), the signal shifted significantly downfield ( $\Delta\delta$  about 2 ppm) indicating the formation of effective hydrogen bonding between the substrate and the receptor. After the addition of 4-5 equivalents of the acetate ion, the observable shift of the signal corresponding to the N—H protons of the thiourea receptor was insignificant. This observation implies that the receptor has reached saturation. After 10 equivalents of the acetate were added the signal for the N—H protons reached 11.10 ppm. The obtained titration curve was fit to 1:1 binding model giving an association constant  $K_a$  of  $241 \pm 35 \text{ M}^{-1}$ . This value is similar to the value obtained from the ITC experiments indicating a good correlation between the two methods.

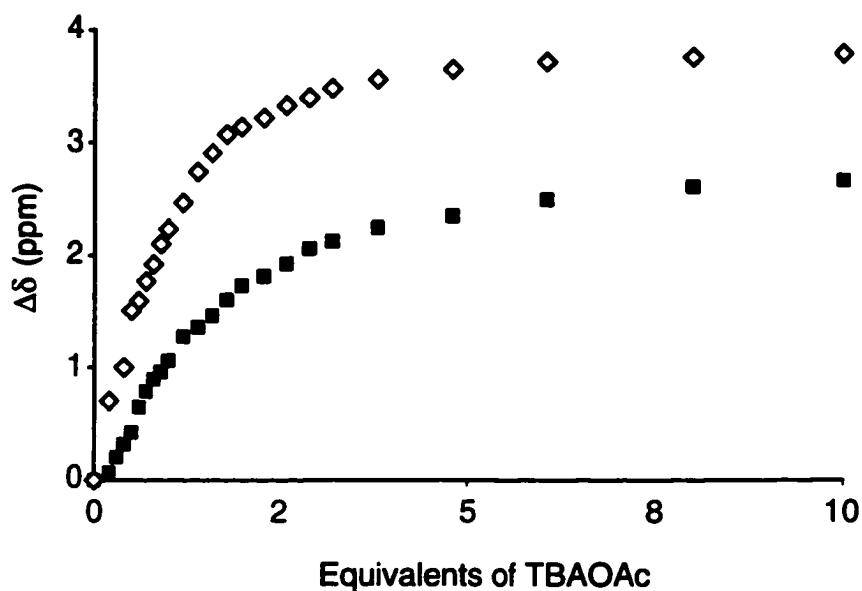


**Figure 2.13** Titration curves of receptor **8** (5 mM) with TBAOAc (100 mM) in DMSO- $d_6$  (◇) and in 1:1 CDCl<sub>3</sub>/CD<sub>3</sub>CN (■).

The <sup>1</sup>H NMR titration of the thiourea receptor **8** with TBA acetate (100 mM) was repeated in CD<sub>3</sub>CN/CDCl<sub>3</sub> (1:1) to determine the extent of the solvent effect on the affinity of the receptor for its substrate (Figure 2.13). A 5 mM solution of thiourea receptor **8** CD<sub>3</sub>CN/CDCl<sub>3</sub> (1:1) was treated with aliquot amounts of TBA acetate (100 mM) in the same solvent. Before the addition of the acetate, the signal corresponding to the N—H protons of the receptor appeared at 6.82 ppm as a very broad signal. As the acetate was added, the signal became sharper and its chemical shift moved significantly downfield ( $\Delta\delta$  about 4 ppm) indicating the formation of effective hydrogen bonding between the substrate and the receptor. After the addition of 1-2 equivalents of the acetate, the observable shift of the signal corresponding to the N—H protons of the thiourea receptor was insignificant. This observation implies that the receptor has reached saturation. After 10 equivalents of the acetate were added the signal for the N—H protons reached 10.63 ppm. The obtained titration curve was fit to 1:1 binding model giving an association constant  $K_a$  of 5790 M<sup>-1</sup>. This value indicates that the



hydrogen-bonded complex **8**•acetate is more stable in a 1:1 mixture of chloroform and acetonitrile than it is in DMSO. This reflects the negative effect of the high polarity and the electron donating ability of DMSO on hydrogen bonding complexation.

The study of the effect of Cu(I) ions on the binding of the thiourea receptor **8** was not possible because the preparation of the copper complex failed to produce the complex **8**•Cu. The <sup>1</sup>H NMR spectrum of the product obtained from the reaction of Cu(CH<sub>3</sub>CN)<sub>4</sub>PF<sub>6</sub> with the thiourea receptor **8** showed peaks that were so broad and poorly resolved it was impossible to characterize the complex. Moreover, the electrospray mass spectrum of the brown solid did not show the presence of the target copper complex of receptor **8**. These observations suggest that the oxidation state of the metal is affected by the presence of sulfur as similar behavior was previously reported for systems with thiol groups.<sup>15b, 16</sup> The formation of the complex, where the copper ion is chelated by the bipyridine ligands of the receptor, is vital to satisfy the allosteric inhibition principle for which the receptor was designed. Since it was not possible to fulfill this goal, all studies on this receptor were terminated at this point of research.

### 2.5.6 The Binding Activity of Squarate Receptor **10** Toward Acetate

The squaric amide scaffold of receptor **10** provides another donor-donor hydrogen bonding site suitable for binding of carboxylates. The binding of the squarate receptor **10** was studied, similar to receptor **8**, using isothermal calorimetry. A solution of TBA acetate (100 mM) in 1:1 mixture of CH<sub>3</sub>CN/CHCl<sub>3</sub> was injected into a solution of receptor **10** (5 mM) in the same solvent. The heat evolved with each injection is displayed versus the time in the top panel in Figure 2.13. The first few injections deviated from ideal binding behavior due to the presence of the squaric amide receptor **10** in large excess compared to the substrate. The heat evolved in the initial injections produced larger

signals due to the complete complexation of the added acetate substrate, but as titration proceeded the signal became smaller due to the saturation of receptor **10** by the acetate substrate. The heat produced at saturation is due to the dilution of the acetate substrate. The binding isothermal was generated by integrating each peak and plotting the resulting data versus molar ratio of the acetate substrate (Figure 2.14, bottom panel (■)). The heat evolved due to the dilution of the injectant substrate was evaluated by taking the average value of the heat produced in the last 25 injections. This value was then subtracted from the isothermal curve before the fitting analysis. The data points corresponding to the heat produced by the first few injections were also removed from the curve. The fitting of this curve to a one-site binding model receptor (the solid line in the bottom panel, Figure 2.13) gave a  $K_a$  value of  $7254 \pm 405.9 \text{ M}^{-1}$ . The values of  $\Delta H$  ( $-2239 \pm 54.64 \text{ cal mol}^{-1}$ ) and  $\Delta S$  ( $10.16 \text{ cal mol}^{-1} \text{ K}^{-1}$ ) indicate that the binding is both enthalpy and entropy driven. A similar value ( $K_a = 7390 \text{ M}^{-1}$ ) was obtained from  $^1\text{H}$  NMR titration experiments of squarate receptor **10** with TBA acetate performed under similar conditions. This correlation of the ITC experiment with the NMR titration indicates that ITC is a useful technique to study the association of a hydrogen bonding receptor with its substrate.

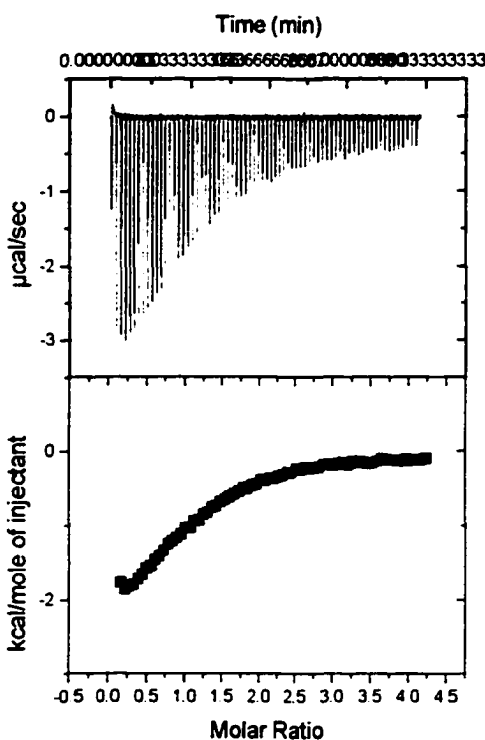


**Figure 2.14** Calorimetric titration of thiourea receptor **10** (5 mM) with TBAOAc (100 mM) in 1:1 mixture of  $\text{CH}_3\text{CN}/\text{CHCl}_3$  at 25°C. Top panel: raw data showing heat evolved with each injection of the acetate. Bottom panel: integrated curve of the raw titration; the solid line represents a nonlinear least squares fit using 1:1 binding model.

The binding of squarate receptor **10** was also studied  $^1\text{H}$  by NMR titration in  $\text{CD}_3\text{CN}/\text{CDCl}_3$  where the change in the chemical shift of the N—H peaks of the squaric amide receptor **10** (5 mM) was monitored as TBA acetate (100 mM) was added in the same solvent. The signal for the N—H protons of the receptor appeared at 6.85 ppm before the addition of the acetate. As the acetate was added the signal of the N—H protons shifted significantly downfield ( $\Delta\delta$  about 4 ppm) indicating a strong association of the squaric amide receptor **10** with the acetate guest. The receptor reached saturation after 1-2 equivalents of guest were added. After the addition of 10 equivalents of the acetate ion, the signal for the N—H protons reached 10.66 ppm. It was also observed that at saturation the signals corresponding to the bipyridine protons were sharper than before

the addition of the acetate ion. This observation was attributed to the limited rotation around the squaric amide C—N bonds imposed by the hydrogen bonding of the receptor to the N—H protons. The association constant was calculated to be  $7390 \text{ M}^{-1}$  when the titration curve was fit to a 1:1 binding model (Figure 2.15). This was similar to the value obtained from the ITC experiments indicating a good correlation between the two methods.

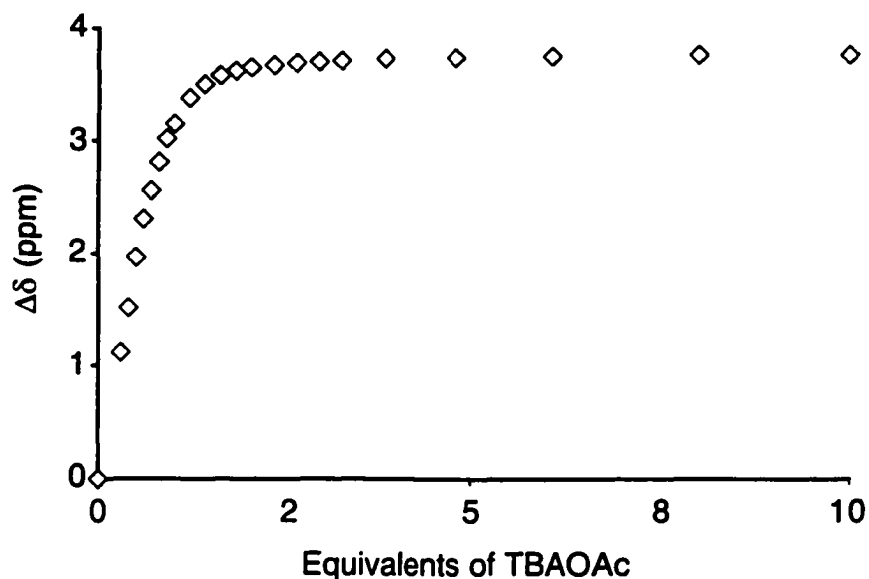


**Figure 2.15** Titration curves of squarate receptor **10** (5 mM) with TBAOAc (100 mM) in 1:1  $\text{CDCl}_3/\text{CD}_3\text{CN}$  ( $\diamond$ ).

The study of the effect of Cu(I) ions on the binding of the squaric amide receptor **10** was not possible since the preparation of the copper complex failed to produce the complex **10**•Cu. The  $^1\text{H}$  NMR spectrum of the product obtained from the reaction of  $\text{Cu}(\text{CH}_3\text{CN})_4\text{PF}_6$  with squarate receptor **7** could not be characterized due to broad peaks. However, the electrospray mass spectrum of the complex showed a peak that corresponding to the  $m/z$  of  $[\mathbf{10}+\text{Cu}]^+$ . Although this peak indicated the presence of a species where the copper may be coordinated to the ligand, it did not verify that the metal

was chelated by the bipyridines in a tetrahedral fashion and it did not rule out the presence of metal-ligand aggregate. The formation of the complex, where the copper ion is chelated by the bipyridine ligands of the receptor, is vital to satisfy the allosteric inhibition principle for which the receptor was designed. Since it was not possible to fulfill this goal, all studies on this receptor were terminated at this point of research.

**Table 2.2** The results of the isothermal titration calorimetry (T= 25 °C).

Receptor	Solvent	n	$K_a$ ( $M^{-1}$ )	$\Delta H$ (cal mol <sup>-1</sup> )	$\Delta S$ (cal mol <sup>-1</sup> K <sup>-1</sup> )
<b>8</b>	DMSO	1.00 <sup>a</sup>	172.1±9.5	-563.2±14.21	8.340
<b>10</b>	CH <sub>3</sub> CN/CHCl <sub>3</sub>	1.12	7254±405.9	-2239±54.64	10.16

a) The stoichiometry of the binding was fixed at one equivalent in the binding analysis.

## 2.6 Conclusions

Nature has been successfully using allostery as a means to regulate the functions of its systems. These systems use allosteric cofactors to process the "orders" for the tasks to be performed by each component. The presence of an allosteric activator induces an enzyme, for example, to start its task. The removal of the activator or the appearance of an allosteric inhibitor causes the enzyme to shut down its operation. Such a mode of function requires a reversible binding of the cofactor to an allosteric site which receives the "order" and transmits it to the active site through conformational changes in the structure of the enzyme. Chemists have long tried to mimic the systems of Nature and have built tailored molecular systems in which they can control their functions. In order to fully achieve this goal, the systems must be designed to respond to a stimulus and

adjust their functions accordingly. Only by controlling the stimulus, will the chemist be able to control the function of the molecules.

This chapter has shown that the presence or absence of Cu(I) ions can be used as a stimulus to control the binding of hydrogen-bonding receptors to their substrates. The studies of the triazine receptor **6** have successfully shown that the presence of Cu(I) ions inhibits the binding of *N*-butyluracil to the receptor. The chelation of the metal ion by the bipyridine ligands anchored to the receptor causes the destruction of the active site of the receptor. This is clearly an example of negative allosteric effect of an inhibitor (the Cu(I) ions) on the binding of a receptor. The effect of the copper ion on the triazine receptor is reversed by the removal of the metal providing a level of reversible control. This concept will be expanded upon in subsequent chapters of this thesis.

The use of Cu(I) ions as negative allosteric cofactors for the urea receptor **7** was not as successful as for the triazine receptor. Cu(I) ions were able to inhibit the binding of the urea receptor **7** to the acetate substrate at low concentrations of the substrate. As the concentration of the acetate increased, the conformation of the receptor changed to accommodate the substrate. This behavior of the urea receptor **7**, although it was not planned, it is an interesting form of substrate feedback effect on the binding of an inhibitor. It is most likely the nature of DMSO as a good solvent for cations that helped the rearrangement of the copper complex from the inactive monomer  $7 \cdot \text{Cu}$  to the active dimer  $(7 \cdot \text{Cu})_2$ . Therefore, a possible solution for this situation could be the use of a more soluble derivative of the urea receptor allowing the binding to exist in less competitive solvents than DMSO.

The thiourea receptor **8** and the squaric amide receptor **10** both displayed high affinity for acetate substrates. The binding studies using these receptors showed that isothermal titration calorimetry is a useful technique to obtain the thermodynamic data

about the formation of a hydrogen-bonded complex (Table 2.2). Also, the solvent effect on the stability of the hydrogen-bonded complex was evident through the increase in the association constant for thiourea receptor **8** to the acetate guest species as the solvent was changed from DMSO to a 1:1 mixture of  $\text{CDCl}_3/\text{CD}_3\text{CN}$ . These receptors (**8** and **10**) failed, however, to form well characterizable Cu(I) complexes. Therefore, the binding of thiourea receptor **8** and squaric amide receptor **10** can not yet be controlled through allosteric inhibition by copper ions. This instability of the copper complexes of the thiourea receptor is probably due to the redox effect of sulfur on the metal. Meanwhile, the presence of the carbonyl groups in the squaric amide receptor provides another possible site for copper coordination in molecule than the bipyridine ligands. This will lead to mixed forms of complexes.

## 2.7 Experimental

**General Information.** All solvents (Caledonia) for synthesis and purification were used as received. Solvents used for UV-Vis absorption and fluorescence spectroscopy analysis were deoxygenated by bubbling argon through the solvent. Solvents used for NMR analysis (Cambridge Isotope Laboratories) were used as received. All reagents and starting materials were purchased from Aldrich or Acros Organics.

$^1\text{H}$  NMR characterizations were performed on a Varian Inova-300 instrument, working at 299.96 MHz, or on a Varian Inova-500 instrument, working at 499.92 MHz. Chemical shifts ( $\delta$ ) are reported in parts per million relative to tetramethylsilane using the residual solvent peak as a reference standard. Coupling constants ( $J$ ) are reported in hertz.  $^{13}\text{C}$  NMR characterizations were performed on a Bruker-300 instrument, working at 74.99 MHz or a Varian Inova-500 instrument, working at 125.29 MHz. FT-IR measurements were performed using a Nicolet Magna-IR 750. UV-Vis spectra were recorded on a Varian Cary 400 Scan spectrophotometer.

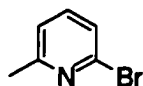
Mass spectrometry measurements were performed a Kratos MS-50 with an electron impact source or by positive mode electrospray ionization on a Micromass ZabSpec Hybrid Sector-TOF. The liquid carrier was infused into the electrospray source by means of a Harvard syringe pump at a flow rate of 10  $\mu\text{L}/\text{minute}$ . The sample solution, in the same solvent, was introduced *via* a 1  $\mu\text{L}$ -loop-injector. Pre-purified nitrogen was used as a spray pneumatic aid and filtered air as the bath gas, heated at *ca.* 80  $^\circ\text{C}$ . For low resolution, the mass spectra were acquired by magnet scan at a rate of 5 seconds/decade at *ca.* 1000 resolution. For exact mass measurements, the spectra were obtained by voltage scan over a narrow mass range at *ca.* 10000 resolution. Data acquisition and processing was achieved by using the OPUS software package on a Digital Alpha station with VMS operating system.



**General Procedure to Measure Association Constants Using  $^1\text{H}$  NMR Titration Experiments.** A solution of the host at a concentration between 2 mM and 5 mM was prepared in an appropriate deuterated solvent. A measured amount (500-600  $\mu\text{L}$ ) of this solution was immediately transferred into an NMR tube fitted with a rubber septum to minimize the evaporation of the solvent. A solution of the guest at a concentration of 20-100 mM was prepared in the same solvent. The guest solution was prepared in a vial fitted with a controlled seal or a septum to minimize the evaporation of the solvent. Aliquot amounts of the guest solution were added to the NMR tube through the rubber septum via a syringe. The number of additions varied between 25 and 30 with an increase in the amount of guest solution added until a total of 10 equivalents of the guest was attained. A  $^1\text{H}$  NMR spectrum was recorded after each addition. The chemical shift of the protons associated with the recognition process was recorded after each  $^1\text{H}$  NMR spectrum was run. The collected data was analyzed using a non-linear least square regression program to fit the data to a theoretical model for the binding process. The programs used were either HOSTEST or SIMPLEX which were kindly provided by Dr. Craig Wilcox (University of Pittsburgh, Pittsburgh, PA, USA) and Dr. Christopher A. Hunter (Department of Chemistry, University of Sheffield, UK), respectively.

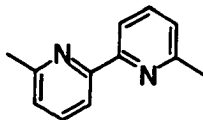
**General Procedure to Measure Association Constants Using Isothermal Titration Calorimeter (ITC) Experiments.** All of the calorimetric binding experiments were performed using an Isothermal Titration Calorimeter (ITC) from Microcal Inc. In a typical experiment a 5 mM receptor solution was added to the calorimetry cell (1.47 mL). A 100 mM solution of the substrate was introduced in fifty 5  $\mu\text{L}$  injections, for a total of 250  $\mu\text{L}$  added substrate. The solution was continuously stirred to ensure rapid mixing

and kept at an operating temperature of 25 °C through the combination of an external cooling bath (at 18 °C) and an internal heater. Dilution effects were determined by a second experiment adding the same guest solution into pure solvent and subtracting this data from the raw titration data to produce the final binding isotherm. Association parameters were calculated by applying a one-site model using the Origin® software. These methods rely on standard non-linear least square regression to fit the titration curves, taking into account the change in observable volume that occurs during the calorimetric titration. In some cases, where the complex formed has weak association, the stoichiometry of the binding was fixed at one equivalent in the binding analysis.



**6-Bromo-2-methylpyridine (1).**<sup>17</sup> A mixture of 2-aminopyridine (25.0 g, 0.23 mole) and an aqueous HBr solution (115 mL of a 48% solution) was stirred at -10 °C in a two-liter 3-neck round-bottom flask fitted with a mechanical stirrer. The temperature was maintained by immersing the round-bottom flask in an ice bath. Bromine (35 mL) was added dropwise from a dropping funnel while maintaining the temperature of the reaction solution below -5 °C. A solution of sodium nitrite (40.0 g, 0.58 mole) in water (60 mL) was added at sufficient a rate to keep the solution temperature below 0 °C. After stirring for 1 h at 0 °C, a solution of NaOH (87.0 g, 2.17 mole) dissolved in water (95 mL) was slowly added. The ice bath was removed and the reaction allowed to warm to room temperature when it was extracted with ether (4 × 100 mL). The combined organic layers were washed with water (2 × 100 mL), followed by saturated NaCl (1 × 100 mL), dried over MgSO<sub>4</sub> and filtered. The solvent was evaporated under vacuum affording a red-brown oil. The product was isolated as a yellow oil by distillation under reduced pressure

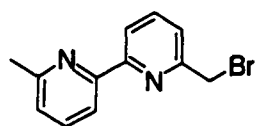
(< 5 mm) at 72-74 °C (25.0 g, 45%). <sup>1</sup>H NMR (CDCl<sub>3</sub>, 300 MHz) δ 7.40 (t, *J*=8 Hz, 1H), 7.24 (d, *J*=8 Hz, 1H), 7.06 (d, *J*=8 Hz, 1H), 2.50 (s, 3H).



**6,6'-Dimethyl-2,2'-bipyridine (2). Procedure A**<sup>18</sup> A solution of NiCl<sub>2</sub>·6H<sub>2</sub>O (8.2 g, 35.0 mmol) and triphenylphosphine (36.0 g, 140.1 mmol) in DMF (135 mL) at 50 °C under argon was treated with zinc powder (2.2 g, 33.6 mmol). After 1 h of stirring at 50 °C, the color of the mixture changed from deep blue to red-brown. At this time, 6-bromo-2-methylpyridine (6.0 g, 35.1 mmol) was added and the reaction was stirred at 50 °C for 4 h. The mixture was then poured into ammonium hydroxide (600 mL) and extracted with chloroform (4 × 100 mL). The combined organic layers were washed with water (2 × 100 mL) followed by brine (100 mL), dried over MgSO<sub>4</sub> and filtered. The solvent was evaporated under vacuum affording a yellow solid. The solid was dissolved in toluene (200 mL) and dry HCl gas was bubbled through the solution continuously for 15 min. The precipitate that formed was collected by filtration, dissolved in water (30 mL) and the solution was made basic by the careful addition of NaHCO<sub>3</sub>. The solution was extracted with chloroform (3 × 10 mL). The combined organic layers were washed with water (2 × 10 mL) followed by brine (10 mL), dried over MgSO<sub>4</sub> and filtered. The solvent was evaporated under vacuum to afford a beige solid. The product was recrystallized as a beige solid from ethanol/water (2.0 g, 62%).

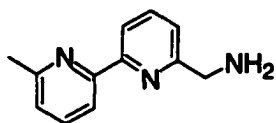
**Procedure B**<sup>19</sup> A slurry of Raney Nickel (10.0 g) in water was poured into a 3-neck round-bottom flask fitted with a rubber septum, a condenser and a gas-outlet equipped with a stopcock. The flask was connected through the gas outlet to vacuum (< 5 mm) and placed in hot water bath at 60 °C for 6 h. The bath was removed and the flask was cooled

to room temperature. At that time, the vacuum was disconnected and the dry Raney Nickel was placed under argon. (CAUTION: dry Raney Nickel should be handled very carefully to prevent its contact with air). A solution of 6-bromo-2-methylpyridine (40.0 g, 0.23 mole) in dry toluene (150 mL) was then added through a canula into the flask and the mixture was heated under reflux for 24 h. After cooling the mixture to room temperature, a violet precipitate was formed. The precipitate was filtered off, washed with toluene (100 mL) and dried under vacuum. This solid was then added in small portions to water (300 mL) at 40 °C. After stirring for 2 h at 40 °C, the color of the solution changed from violet to green and a precipitate was formed. The solid was filtered, washed with water (30 mL), and recrystallized as a beige solid from ethanol/water (10.0 g, 73%). M.p. 85-87 °C (lit.<sup>19</sup> 88 °C); <sup>1</sup>H NMR (300 MHz, CDCl<sub>3</sub>) δ 8.23 (d, *J*=8 Hz, 2H), 7.74 (t, *J*=7 Hz, 2H), 7.19 (d, *J*=7 Hz, 2H), 2.61 (s, 3H).

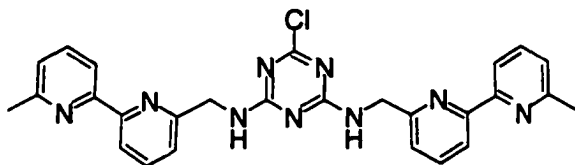


**6-Bromomethyl-6'-methyl-2,2'-bipyridine (3).**<sup>20</sup> A mixture of 6,6'-dimethyl-2,2'-bipyridine (2.0 g, 10.9 mmol), NBS (1.9 g, 10.7 mmol) and a catalytic amount of AIBN dissolved in CCl<sub>4</sub> (20 mL) was heated under reflux for 5 h under argon. The mixture was filtered while hot and the filtrate was evaporated to afford a yellow solid. The solid was dissolved in chloroform (30 mL) and the solution was washed consecutively with 5% Na<sub>2</sub>CO<sub>3</sub> solution (10 mL), water (10 mL) and brine (10 mL). After drying over Na<sub>2</sub>SO<sub>4</sub>, the mixture was filtered and the solvent was evaporated under vacuum to afford a white residue. The product was isolated by flash chromatography (silica, 1% MeOH in CH<sub>2</sub>Cl<sub>2</sub>) as a white solid (1.9 g, 72%). M.p. 90-92 °C (lit.<sup>20</sup> 88 °C); <sup>1</sup>H NMR (300 MHz, CDCl<sub>3</sub>) δ

8.33 (d,  $J=7$  Hz, 1H), 8.22 (d,  $J=7$  Hz, 1H), 7.79 (t,  $J=7$  Hz, 1H), 7.68 (t,  $J=7$  Hz, 1H), 7.44 (dd,  $J_1=7$  Hz,  $J_2=1$  Hz, 1H), 7.61 (d,  $J=7$  Hz, 1H), 4.62 (s, 2H), 2.62 (s, 3H).



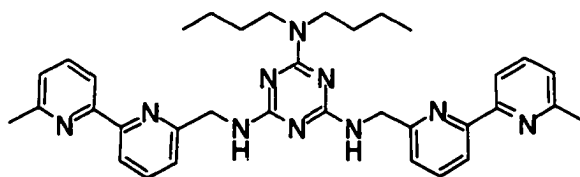
**6-Aminomethyl-6'-methyl-2,2'-bipyridine (4).**<sup>21</sup> A solution of hexamethylenetetramine (0.8 g, 5.7 mmol) in  $\text{CH}_2\text{Cl}_2$  (20 mL) heated at reflux was treated with a solution of 6-bromomethyl-6'-methyl-2,2'-bipyridine (1.0 g, 5.4 mmol) in  $\text{CH}_2\text{Cl}_2$  (10 mL). The mixture was heated under reflux for 3 h. The deposited white solid was filtered off, dried and suspended in a solution of EtOH (20 mL) and concentrated HCl (3 mL). After it was stirred at 80 °C for 24 h in an oil bath, the heat was removed and the mixture was allowed to cool to room temperature at which point the solvent was evaporated under vacuum. Water (20 mL) was added to the residue and the mixture was made basic with a concentrated NaOH solution until the pH reached 13. The yellow precipitate that formed was filtered off, washed with water (10 mL) and air dried. The product was recrystallized as a white solid from EtOH/ $\text{H}_2\text{O}$  (0.6 g, 56%). M.p. >180 °C (dec.);  $^1\text{H}$  NMR (300 MHz,  $\text{CDCl}_3$ )  $\delta$  8.26 (d,  $J=6$  Hz, 1H), 8.19 (d,  $J=8$  Hz, 1H), 7.72 (t,  $J=8$  Hz, 1H), 7.66 (t,  $J=8$  Hz, 1H), 7.20 (d,  $J=8$  Hz, 1H), 7.12 (d,  $J=8$  Hz, 1H), 4.01 (s, 2H), 2.58 (s, 3H).



**6-Chloro-*N,N'*-bis(6'-methyl-2,2'-bipyridin-6-yl)-1,3,5-triazine-2,4-diamine (5).**

A solution of 6-aminomethyl-6'-methyl-2,2'-bipyridine (4) (0.25 g, 1.25 mmol) and triethylamine (0.13 g, 1.25 mmol) in freshly distilled THF (10 mL) was added dropwise

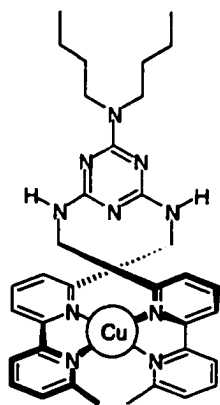
(15–30 min) to a solution of cyanuric chloride (0.23 g, 1.25 mmol) in freshly distilled THF (20 mL) at 0 °C under argon. After the addition was complete, the ice bath was removed and the mixture was allowed to warm to room temperature, where it was stirred for 1 h. The reaction mixture was then heated in an oil bath at 40–50 °C, and an additional batch of 6-aminomethyl-6'-methyl-2,2'-bipyridine (1.25 mmol) and triethylamine (1.25 mmol) in THF (10 mL) was added dropwise. After stirring at this temperature for 5–6 h, the reaction was cooled and concentrated to dryness under vacuum. The residue was dissolved in EtOAc (20 mL), washed with water (3 × 10 mL), brine (10 mL), and dried over Na<sub>2</sub>SO<sub>4</sub>. After filtration, the solvent was evaporated under vacuum affording a white solid that was further purified by recrystallization from CH<sub>2</sub>Cl<sub>2</sub>/benzene (0.46 g, 72%). M.p. 113–115 °C; <sup>1</sup>H NMR (300 MHz, CDCl<sub>3</sub>) δ 8.33 (t, *J*=5 Hz, 2H), 8.22 (t, *J*=5 Hz, 2H), 7.78–7.68 (m, 4H), 7.20–7.16 (m, 4H), 6.62 (br t, 2H), 4.78 (d, *J*=3 Hz, 4H), 2.61 (s, 6H); <sup>13</sup>C NMR (125.3 MHz, CDCl<sub>3</sub>) δ 165.8, 158.0, 155.8, 155.5, 155.2, 155.1, 137.6, 137.2, 123.5, 121.8, 121.3, 119.8, 118.3, 118.2, 446.1, 24.7; FT-IR (cast) ν 3257, 2957, 1621, 1571, 1549, 1439, 1407, 1386, 1329, 1312, 1291, 1240, 1150, 1116, 1081, 991, 805, 781, 753, 634 cm<sup>-1</sup>; HRMS (ES) *m/z*: 510.1923 [M+H]<sup>+</sup>, C<sub>27</sub>H<sub>25</sub>ClN<sub>9</sub>; calculated 510.1921 [M+H]<sup>+</sup>, C<sub>27</sub>H<sub>25</sub>ClN<sub>9</sub>



***N*<sup>2</sup>,*N*<sup>2</sup>-Dibutyl-*N*<sup>4</sup>,*N*<sup>6</sup>-bis(6'-methyl-2,2'-bipyridin-6-yl)-1,3,5-triazine-2,4,6-triamine**

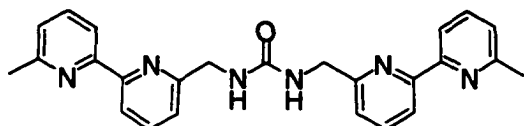
(6). A mixture of 6-Chloro-*N,N*-bis(6'-methyl-2,2'-bipyridin-6-yl)-1,3,5-triazine-2,4-diamine (5) (0.2 g, 0.4 mmol) and dibutylamine (0.1 g, 0.8 mmol) in THF (20 mL) was heated at reflux for 12 h under argon. After cooling to room temperature, the mixture was

added to water (100 mL) and the aqueous layer was extracted with chloroform ( $3 \times 10$  mL). The combined organic layer was dried over  $\text{Na}_2\text{SO}_4$ , filtered and evaporated under vacuum to afford a yellow sticky residue. The product was isolated by flash chromatography (alumina, 1% MeOH in  $\text{CHCl}_3$ ) and was recrystallized as a white solid from  $\text{CH}_2\text{Cl}_2$ /hexane (125 mg, 52%). M.p. 88-90 °C (dec.);  $^1\text{H}$  NMR (300 MHz,  $\text{CDCl}_3$ )  $\delta$  8.23 (t,  $J=8$  Hz, 4H), 7.62-7.73 (m, 4H), 7.26 (d,  $J=8$  Hz, 2H), 7.11 (d,  $J=7$  Hz, 2H), 5.99 (br s, 2H), 4.74 (d,  $J=6$  Hz, 4H), 3.42 (t,  $J=7$  Hz, 4H), 2.60 (s, 6H), 1.47 (br s, 4H), 1.23 (br s, 4H), 0.83 (br s, 6H);  $^{13}\text{C}$  NMR (75.5 MHz,  $\text{CDCl}_3$ )  $\delta$  157.9, 155.8, 155.5, 137.4, 137.1, 124.3, 123.3, 121.2, 119.4, 118.4, 46.9, 46.2, 30.1, 24.7, 20.2, 14.0; FT-IR (cast)  $\nu$  3323, 2956, 2929, 2870, 1572, 1540, 1511, 1438, 1375, 1328, 1253, 1151, 1111, 1081, 992, 811, 782, 7542, 664, 634, 418  $\text{cm}^{-1}$ ; HRMS (EI)  $m/z$ : 602.3603  $[\text{M}]^+$ ,  $\text{C}_{35}\text{H}_{42}\text{N}_{10}$ ; calculated 602.3594  $[\text{M}]^+$ ,  $\text{C}_{35}\text{H}_{42}\text{N}_{10}$ .



**Copper Complex 6•Cu.** A mixture of  $N^2,N^2$ -dibutyl- $N^4,N^6$ -bis(6'-methyl-2,2'-bipyridin-6-yl)-1,3,5-triazine-2,4,6-triamine (**6**) (15 mg,  $2.5 \times 10^{-2}$  mmol) and  $\text{Cu}(\text{CH}_3\text{CN})_4\text{PF}_6$  (8 mg,  $2.5 \times 10^{-2}$  mmol) in  $\text{CH}_3\text{CN}$  (3 mL) was stirred for 1 h at room temperature under argon. Diethyl ether (5 mL) was then added to the mixture at which point a red-orange precipitate formed. The solid was filtered off, washed with diethyl ether (1 mL), and dried under vacuum (19 mg, 93 %).  $^1\text{H}$  NMR (300 MHz,  $\text{CD}_3\text{CN}$ )  $\delta$  8.27 (d,  $J=8$  Hz, 2H),

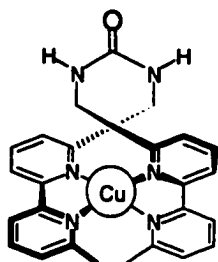
8.23 (d,  $J=8$  Hz, 2H), 8.06 (t,  $J=8$  Hz, 2H), 8.03 (t,  $J=8$  Hz, 2H), 7.62 (d,  $J=8$  Hz, 2H), 7.45 (d,  $J=8$  Hz, 2H), 6.13 (br s, 2H), 4.66 (d,  $J=6$  Hz, 1H), 4.61 (d,  $J=6$  Hz, 1H), 4.09 (d,  $J=6$  Hz, 1H), 4.04 (d,  $J=6$  Hz, 1H), 3.51-3.42 (m, 2H), 3.27-3.17 (m, 2H), 2.10 (s, 6H), 1.48-1.38 (m, 4H), 1.25-1.15 (m, 4H), 0.88 (t,  $J=7$  Hz, 6H);  $^{13}\text{C}$  NMR (100.5 MHz,  $\text{CD}_3\text{CN}$ )  $\delta$  (17 of 18 carbons) 167.0, 162.0, 158.5, 152.6, 151.9, 139.5, 139.3, 126.8, 125.4, 121.5, 120.4, 49.6, 46.6, 30.7, 24.9, 20.8, 14.2; FT-IR (cast)  $\nu$  3304, 2956, 2870, 2870, 1720, 1596, 1571, 1540, 1509, 1462, 1438, 1374, 843, 784  $\text{cm}^{-1}$ ; UV-VIS ( $\text{CH}_3\text{CN}$ )  $\lambda_{\text{max}}/\text{nm}$  ( $\log \epsilon/\text{M}^{-1} \text{cm}^{-1}$ ) 455 (3900); HRMS (EI)  $m/z$ : 665.2885  $[\text{M}]^+$ ,  $\text{C}_{35}\text{H}_{42}\text{CuN}_{10}$ ; calculated 665.2890  $[\text{M}]^+$ ,  $\text{C}_{35}\text{H}_{42}\text{CuN}_{10}$ .



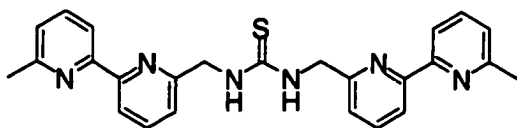
***N,N'*-Bis(6'-methyl-2,2'-bipyridin-6-yl)urea (7).** A solution of 6-bromomethyl-6'-methyl-2,2'-bipyridine (0.12 g, 0.6 mmol) in dry THF (40 mL) was added dropwise into a stirred solution of carbonyl diimidazole (49 mg, 0.3 mmol) at room temperature under argon. The mixture was stirred for 12 h at room temperature at which time the solvent was evaporated under vacuum. The yellow residue was dissolved in EtOAc (20 mL) where a white solid separated upon standing at room temperature for 1 h. The solid was filtered off and washed with EtOAc (10 mL) followed by water (20 mL). After drying under vacuum, a beige solid was collected (95 mg, 75%). M.p. 240-242 °C (dec.);  $^1\text{H}$  NMR (300 MHz,  $\text{DMSO}-d_6$ )  $\delta$  8.23 (t,  $J=7$  Hz, 4H), 7.85 (t,  $J=8$  Hz, 2H), 7.80 (t,  $J=8$  Hz, 2H), 7.33 (d,  $J=7$  Hz, 2H), 7.28 (d,  $J=7$ , 2H), 6.89 (t,  $J=3$  Hz, 2H), 4.43 (d,  $J=6$  Hz, 4H), 2.60 (s, 6H);  $^{13}\text{C}$  NMR (75.5 MHz,  $\text{DMSO}-d_6$ )  $\delta$  189.2, 159.3, 158.2, 157.4, 154.5, 137.6, 137.3, 123.4, 121.0, 118.4, 117.6, 45.1, 24.2; FT-IR (microscope)  $\nu$  3325, 3147, 3057, 2949, 2913, 1618, 1571, 1440, 1415, 1391, 1372, 1340, 1290, 1261, 1149, 1109,



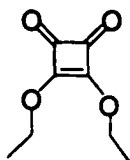
1081, 1057, 993, 777, 736, 656, 630  $\text{cm}^{-1}$ ; HRMS (EI)  $m/z$ : 424.1992  $[\text{M}]^+$ ,  $\text{C}_{25}\text{H}_{24}\text{N}_6\text{O}$ ; calculated 424.2012  $[\text{M}]^+$ ,  $\text{C}_{25}\text{H}_{24}\text{N}_6\text{O}$ .



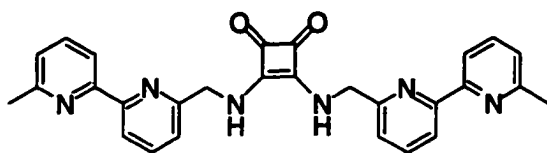
**Copper Complex 7•Cu.** A mixture of *N,N'*-bis(6'-methyl-2,2'-bipyridin-6-yl)urea (**7**) (11 mg,  $2.5 \times 10^{-2}$  mmol) and  $\text{Cu}(\text{CH}_3\text{CN})_4\text{PF}_6$  (8 mg,  $2.5 \times 10^{-2}$  mmol) in  $\text{CH}_3\text{CN}$  (3 mL) was stirred for 1 h at room temperature under argon. The solution was filtered to remove any non-reacting ligand. Diethyl ether (5 mL) was added to the filtrate where a red-orange precipitate was formed. The solid was filtered off, washed with diethyl ether (1 mL), and dried under vacuum (14 mg, 91 %).  $^1\text{H}$  NMR (300 MHz,  $\text{CD}_3\text{CN}$ )  $\delta$  8.28 (d,  $J=8$  Hz, 2H), 8.22 (d,  $J=8$  Hz, 2H), 8.11 (br s, 2H), 7.80 (t,  $J=8$  Hz, 2H), 7.68 (br s, 2H), 7.45 (d,  $J=8$  Hz, 2H), 6.31 (br s, 2H), 4.32 (br s, 2H), 3.89 (br s, 2H), 2.08 (s, 6H);  $^{13}\text{C}$  NMR (100.5 MHz,  $\text{CD}_3\text{CN}$ )  $\delta$  159.9, 158.9, 158.6, 152.7, 152.3, 140.2, 139.5, 127.0, 124.8, 121.9, 120.7, 47.4, 25.2; FT-IR (cast)  $\nu$  3328, 1644, 1597, 1568, 1462, 1377, 1253, 1036, 838, 785, 739, 654, 559, 482, 418  $\text{cm}^{-1}$ ; UV-VIS ( $\text{CH}_3\text{CN}$ )  $\lambda_{\text{max}}/\text{nm}$  ( $\log \epsilon/\text{M}^{-1} \text{cm}^{-1}$ ) 448 (3900); HRMS (ES)  $m/z$ : 487.1300  $[\text{M}]^+$ ,  $\text{C}_{25}\text{H}_{24}\text{CuN}_6\text{O}$ ; calculated 487.1307  $[\text{M}]^+$ ,  $\text{C}_{25}\text{H}_{24}\text{CuN}_6\text{O}$ .



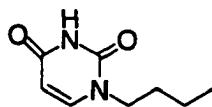
***N,N'*-Bis(6'-methyl-2,2'-bipyridin-6-yl)thiourea (8).** Thiophosgene (59 mg, 0.5 mmol) was added to a solution of 6-methyl-6'-bromomethyl-2,2'-bipyridine (300 mg, 1.5 mmol) and triethylamine (155 mg, 1.5 mmol) in dry  $\text{CH}_2\text{Cl}_2$  (30 mL) at room temperature. The solution was stirred for 2 h at room temperature under argon. The mixture was then washed with water ( $3 \times 10$  mL), dried over  $\text{Na}_2\text{SO}_4$  and filtered. The solvent was evaporated under vacuum to afford a yellow residue. The product was isolated from the residue by flash chromatography (alumina, 1% MeOH in  $\text{CHCl}_3$ ) (0.26 g, 78%). M.p.  $>128$  °C;  $^1\text{H}$  NMR (300 MHz,  $\text{DMSO}-d_6$ )  $\delta$  8.41 (t,  $J=6$  Hz, 2H), 8.26 (d,  $J=8$  Hz, 2H), 7.87 (t,  $J=7$  Hz, 2H), 7.78 (t,  $J=7$  Hz, 2H), 7.38 (d,  $J=7$  Hz, 2H), 7.31 (d,  $J=8$  Hz, 2H), 4.89 (br, s, 4H), 2.55 (s, 6H);  $^{13}\text{C}$  NMR (75.5 MHz,  $\text{CDCl}_3$ )  $\delta$  182.3, 158.0, 155.8, 155.1, 154.9, 137.9, 137.0, 123.4, 121.9, 120.1, 118.0, 49.7, 24.6; FT-IR (cast)  $\nu$  3247, 3060, 1706, 1572, 1439, 1364, 1263, 1152, 1108, 1082, 991, 956, 783, 753, 663., 634  $\text{cm}^{-1}$ ; HRMS (ES)  $m/z$ : 441.1857  $[\text{M}+\text{H}]^+$ ,  $\text{C}_{25}\text{H}_{25}\text{N}_6\text{S}$ ; calculated 441.1861  $[\text{M}+\text{H}]^+$ ,  $\text{C}_{25}\text{H}_{25}\text{N}_6\text{S}$ .



**3,4-Diethoxycyclobut-3-ene-1,2-dione (9).** A solution of squaric acid (1.2 g, 10.7 mmol) and ethanol (30 mL) in dry benzene (10 mL) was heated under reflux for 10 h in a Dean-Stark apparatus. After removing the heating source and allowing the reaction to cool to room temperature, the solvent was evaporated under vacuum and the residue was dissolved in 1% MeOH in  $\text{CHCl}_3$  mixture (20 mL). The solution was filtered through a plug of neutral alumina. Evaporation of the solvent under vacuum afforded a colorless oil (1.45 g, 85%).  $^1\text{H}$  NMR (300 MHz,  $\text{CDCl}_3$ )  $\delta$  4.78 (q,  $J=7$  Hz, 4H), 1.51 (t,  $J=7$  Hz, 6H).



**3,4-Bis[(6'-methyl-2,2'-bipyridin-6-yl)amino]cyclobut-3-ene-1,2-dione (10).** A mixture of diethyl squarate (0.20 mg, 1.2 mmol) and 6-methyl-6'-bromomethyl-2,2'-bipyridine (0.50 mg, 2.5 mmol) in ethanol (20 mL) was stirred at room temperature for 24 h. The solvent was then evaporated under vacuum to afford a yellow residue. The product was isolated for the residue by column chromatography (alumina, 1% MeOH in  $\text{CHCl}_3$ ) (0.48 g, 82%). M.p. >160 °C (dec.);  $^1\text{H}$  NMR (300 MHz,  $\text{CDCl}_3$ )  $\delta$  8.23 (dd,  $J_1=8$  Hz,  $J_2=1$  Hz, 2H), 7.59 (d,  $J=8$  Hz, 2H), 7.71 (t,  $J=8$  Hz, 2H), 7.42 (t,  $J=8$  Hz, 2H), 7.25 (d,  $J=7$  Hz, 2H), 7.03 (d,  $J=7$  Hz, 2H), 4.87 (d,  $J=7$  Hz, 2H), 2.54 (s, 6H);  $^{13}\text{C}$  NMR (75.5 MHz,  $\text{CDCl}_3$ )  $\delta$  183.7, 168.9, 158.2, 156.3, 155.0, 138.2, 137.1, 123.6, 122.2, 120.5, 118.2, 49.4, 24.8; FT-IR (microscope)  $\nu$  3252, 3002, 1797, 1666, 1580, 1537, 1439, 1388, 1350, 1243, 1151, 1082, 992, 783, 752, 665, 634, 584  $\text{cm}^{-1}$ ; HRMS (ES)  $m/z$ : 477.2033  $[\text{M}+\text{H}]^+$ ,  $\text{C}_{28}\text{H}_{25}\text{N}_6\text{O}_2$ ; calculated 477.2039  $[\text{M}+\text{H}]^+$ ,  $\text{C}_{28}\text{H}_{25}\text{N}_6\text{O}_2$ .



**1-Butylpyrimidine-2,4(1H,3H)-dione (11).** A solution of uracil (1.0 g, 8.9 mmol) in DMF (10 mL) was treated with NaH (0.2 g, 8.9 mmol) at room temperature. The mixture was stirred for 10 min under argon before it was treated with a solution of *N*-*n*-butylbromide (1.2 g, 8.9 mmol) in DMF (1 mL). After stirring for 2 h at room temperature, the mixture was poured into water (100 mL) and the mixture was extracted with chloroform (3  $\times$  20 mL). The combined organic layers were dried over  $\text{Na}_2\text{SO}_4$ ,

filtered and evaporated under vacuum to afford a beige residue. The product was isolated from the residue by column chromatography (silica, hexane/EtOAc (9:1)) and recrystallized as a white solid from ethanol/water (0.92 g, 61%). M.p. 102-104 °C; <sup>1</sup>H NMR (300 MHz, CDCl<sub>3</sub>) δ 8.65 (br s, 1H), 7.11 (t, *J*=8 Hz, 1H), 5.65 (dd, *J*<sub>1</sub>=8 Hz, *J*<sub>2</sub>=2 Hz, 1H), 3.70 (t, *J*=7 Hz, 2H), 1.60-1.70 (m, 2H), 1.28-1.40 (m, 2H), 0.94 (t, *J*=7 Hz, 3H); <sup>13</sup>C NMR (75.6 MHz, CDCl<sub>3</sub>,) δ 163.8, 150.9, 144.4, 102.1, 48.6, 31.1, 19.7, 13.9; FT-IR (cast) ν 3174, 3050, 2959, 2873, 1678, 1459, 1421, 1356, 1283, 1234, 1206, 1180, 1153, 988, 941, 809, 765, 722, 619, 548, 532, 416 cm<sup>-1</sup>; HRMS (EI) *m/z*: 168.0898 [M]<sup>+</sup>, C<sub>8</sub>H<sub>12</sub>N<sub>2</sub>O<sub>2</sub>; calculated 168.0899 [M]<sup>+</sup>, C<sub>8</sub>H<sub>12</sub>N<sub>2</sub>O<sub>2</sub>

## 2.8 References

1. M. D. Hollenberg in *Receptor Pharmacology and Function, Vol. 13* (Eds. M. Williams, R. A. Glennon, P. B. M. W. M. Timmermans) Marcel Dekker, Inc., New York **1989**, pp. 1-16.
2. A. Levitzki, *Quantitative Aspects of Allosteric Mechanisms*, Springer-Verlag, Heidelberg **1978**, pp. 3-5; K. G. Scrimgeour, *Chemistry and Control of Enzyme Reactions*, Academic Press Inc., New York **1977**.
3. (a) M. Takeuchi, M. Ikeda, A. Sugasaki, S. Shinkai, *Acc. Chem. Res.* **2001**, *34*, 865; (b) S. Shinkai, M. Ikeda, A. Sugasaki, M. Takeuchi, *Acc. Chem. Res.* **2001**, *34*, 494; (c) T. Nabeshima, S. Akine, T. Shaiki, *Rev. Heteroatom Chem.* **2000**, *22*, 219; (d) J. Rebek, Jr., *Acc. Chem. Res.* **1984**, *17*, 258.
4. (a) J. Rebek, Jr., J. Trend, R. V. Wattley, S. Chakravorti, *J. Am. Chem. Soc.* **1979**, *101*, 4333; (b) J. Rebek, Jr., R. V. Wattley, *Heterocycl. Chem.* **1980**, *17*, 749; J. Rebek, Jr., R. V. Wattley, *J. Am. Chem. Soc.* **1980**, *102*, 4853.
5. For other reported positive allosteric systems see: (a) T. Nabeshima, A. Hashiguchi, S. Yazawa, T. Haruyama, Y. Yano, *J. Org. Chem.* **1998**, *63*, 2788; (b) T. Haino, Y. Katsutani, H. Akii, Y. Fukazawa, *Tetrahedron Lett.* **1998**, *39*, 8133; (c) T. Nabeshima, *Coord. Chem. Rev.* **1996**, *148*, 151; (d) T. Nabeshima, T. Inaba, N. Furukawa, T. Hosoya, Y. Yano, *Inorg. Chem.* **1993**, *32*, 1407; (e) M. Inouye, T. Konishi, K. Isagawa, *J. Am. Chem. Soc.* **1993**, *115*, 8091; (f) H. -J. Schneider, D. Ruf, *Angew. Chem. Int. Ed. Engl.* **1990**, *29*, 1159; (g) J. Rebek, Jr., T. Costello, L. Marshall, R. Wattley, R. C. Gadwood, K. Onan, *J. Am. Chem. Soc.* **1985**, *107*, 7481.
6. J. C. Rodriguez-Ubis, O. Juanes, E. Brunet, *Tetrahedron Lett.* **1994**, *35*, 1295.
7. For other reported negative allosteric systems see: (a) H. -J. Schneider, F. Werner, *J. Chem. Soc., Chem. Commun.* **1992**, 490; (b) A. M. Castero, S. Rodriguez,

- Tetrahedron Lett.* **1992**, *33*, 623; (c) A. M. Castero, S. Rodriguez, *Tetrahedron* **1992**, *48*, 6265; d) P. D. Beer, A. S. Rothin, *J. Chem. Soc., Chem. Commun.* **1988**, 52.
8. (a) F. H. Beijer, R. P. Sijbesma, J. A. J. M. Vekemans, E. W. Meijer, H. Kooijman, A. L. Spek, *J. Org. Chem.* **1996**, *61*, 6371; (b) I. Willner, J. Rosengaus, S. Biali, *Tetrahedron Lett.* **1992**, *33*, 3805; (c) T. K. Park, J. Schroeder, J. Rebek, Jr., *J. Am. Chem. Soc.* **1991**, *113*, 5125, (d) A. Niemz, E. Breinlinger, V. Rotello, *J. Am. Chem. Soc.* **1997**, *119*, 10863 (e) F. Ilhan, M. Gray, K. Blanchette, V. Rotello, *Macromolecules* **1999**, *32*, 6159; (f) T. Galow, F. Ilhan, G. Cooke, V. Rotello, *J. Am. Chem. Soc.* **2000**, *122*, 3595; (g) F. Ilhan, T. Galow, M. Gray, G. Clavier, V. Rotello, *J. Am. Chem. Soc.* **2000**, *122*, 5895.
9. (a) K. A. Haushalter, J. Lau, J. D. Roberts, *J. Am. Chem. Soc.* **1996**, *118*, 8891; (b) Y. Mido, *Bull. Chem. Soc. Jpn.* **1974**, *47*, 1833; (c) T. R. Kelly, M. H. Kim, *J. Am. Chem. Soc.* **1994**, *116*, 7072.
10. For recent reports of thioureas as carboxylate receptors for see (a) J. M. Benito, M. Gomez-Garcia, J. L. J. Blanco, C. O. Mellet, J. M. G. Fernandez, *J. Org. Chem.* **2001**, *66*, 1366; (b) V. Jullian, E. Shephard, M. B. Hursthouse, J. D. Kilburn, *Tetrahedron Lett.* **2000**, *41*, 3963; (c) S. Sasaki, M. Mizuno, K. Naemura, Y. Tobe, *J. Am. Chem. Soc.* **2000**, *65*, 275; (d) B. R. Linton, M. S. Goodman, A. D. Hamilton, *Chem. Eur. J.* **2000**, *6*, 2449; (e) Y. Tobe, S. Sasaki, M. Mizuno, K. Naemura, *Chem. Lett.* **1998**, 835 (f) E. Fan, A. V. Arman, S. Kincaid, A. D. Hamilton, *J. Am. Chem. Soc.* **1993**, *115*, 369.
11. (a) R. Prohens, M. C. Rotger, M. N. Pina, P. M. Deya, J. Morey, P. Ballester, A. Costa, *Tetrahedron Lett.* **2001**, *42*, 4933; (b) R. Prohens, S. Tomas, J. Morey, P. M. Deya, P. Ballester, A. Costa, *Tetrahedron Lett.* **2001**, *42*, 4933.
12. L. G. Borchardt, J. P. Butler, *Anal. Chem.* **1957**, *29*, 414.

13. (a) J. S. Klassen, Y. Ho, A. T. Blades, P. Kebarle, *Adv. Gas Ph. Ion Chem.* **1998**, *3*, 255; (b) J. S. Klassen, A. T. Blades, P. Kebarle, *J. Am. Chem. Soc.* **1996**, *118*, 12437; (c) L. Tang, P. Kebarle, *Anal. Chem.* **1993**, *65*, 3654; (d) L. Tang, P. Kebarle, *Anal. Chem.* **1993**, *65*, 972 A.
14. G. A. Breault, C. A. Hunter, P. C. Mayers, *J. Am. Chem. Soc.* **1998**, *120*, 3402.
15. (a) K. A. Haushalter, J. Lau, J. Roberts, *J. Am. Chem. Soc.* **1996**, *118*, 8891; (b) F. G. Bordwell, D. J. Algrim, J. A. Harrelson, Jr., *J. Am. Chem. Soc.* **1988**, *110*, 5903.
16. L. Rehm, C. Hamann, J.-M. Kern, J.-P. Sauvage, *Org. Lett.* **2000**, *2*, 1991.
17. S. R. Admas, M. J. Seiji, *J. Am. Chem. Soc.* **1954**, *76*, 3168.
18. M. Tiecco, L. Testakerri, M. Tingoli, D. Chianelli, M. Montanucci, *Synthesis* **1984**, 737.
19. T. Rode, E. Breitmaier, *Synthesis* **1987**, 574.
20. J.-C. Rodriguez-Ubis, B. Alpha, D. Plancherel, J.-M. Lehn, *Helv. Chem. Acta* **1984**, *67*, 2264.
21. R. Stiller, J.-M. Lehn, *Eur. J. Inorg. Chem.* **1998**, *7*, 977.
22. (a) J. -M. Kern, L. Raehm, J.-P. Sauvage, B. Divisia-Blohorn, P.-L. Vidal, *Inorg. Chem.* **2000**, *39*, 1555; (b) L. Raehm, J.-M. Kern, J.-P. Sauvage, *Chem. Eur. J.* **1999**, *5*, 3310; (c) A. Livoreil, J.-P. Sauvage, N. Armaroli, V. Balzani, L. Flamigni, b. Ventura, *J. Am. Chem. Soc.* **1997**, *119*, 12114; (d) J.-P. Collin, P. Gavina, J.-P. Sauvage, *Chem. Comm.* **1996**, 2005; (e) A. Livoreil, O. Dietrich-Buchecker, J.-P. Sauvage, *J. Am. Chem. Soc.* **1994**, *116*, 9399.

## **Chapter 3- Controlling Copper's Allosteric Effects Through Redox Chemistry**

### **3.1 "Molecular Machines"**

Supramolecular chemists have recently paid a lot of attention to the investigation of so called "molecular machines".<sup>1</sup> These are molecules or molecular assemblies whose shape, physical, chemical and dynamic properties can be controlled by using an external stimulus. Similar to its macroscopic equivalent, a molecular machine needs 1) a form of applied energy to make it function, 2) a manner to control and monitor its function, 3) a task compatible with the movement of its components, and 4) the ability to repeat the task at will.<sup>11</sup>

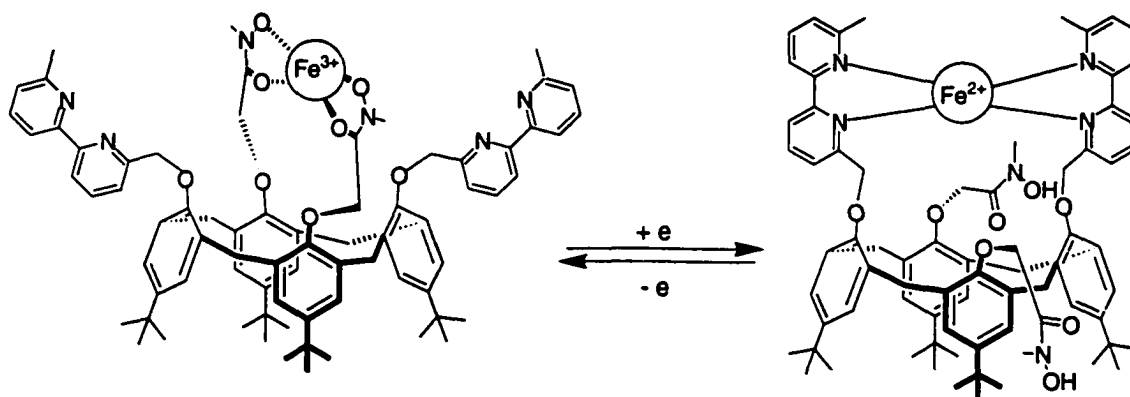
In principle, photons and electrons are the preferred forms of energy to make a molecular machine work.<sup>1d,1</sup> The consumption of these forms of energy does not usually produce any waste products which, if not removed, will compromise the function of the machine. Also, the ability to switch this photo- and electrochemical supply of energy on and off provides a means to control the operation of the machine. However, to regulate and monitor the machine's operation, the motions of the component parts should bring about chemical or physical changes that can be detected. In this regard, photons and electrons can play a dual role of causing change in the system and reporting the resulting state. Any change in the system, nonetheless, should be reversible in order for the machine to work in repeating cycles.

Recently there has been substantial growth in the number of research groups interested in constructing artificial molecular machines. Many molecular systems where mechanical movement can be induced and controlled by chemical, electrical, or light energy have been reported.<sup>1-5</sup> In most cases mechanical movement occurs between two different, well defined stable states, and is accompanied by "on/off" switching of an observable spectroscopic property. This reversible switching is usually monitored by



NMR, electronic absorption and luminescence spectroscopies, and/or by electrochemical techniques. Such molecules are usually termed "molecular switches".

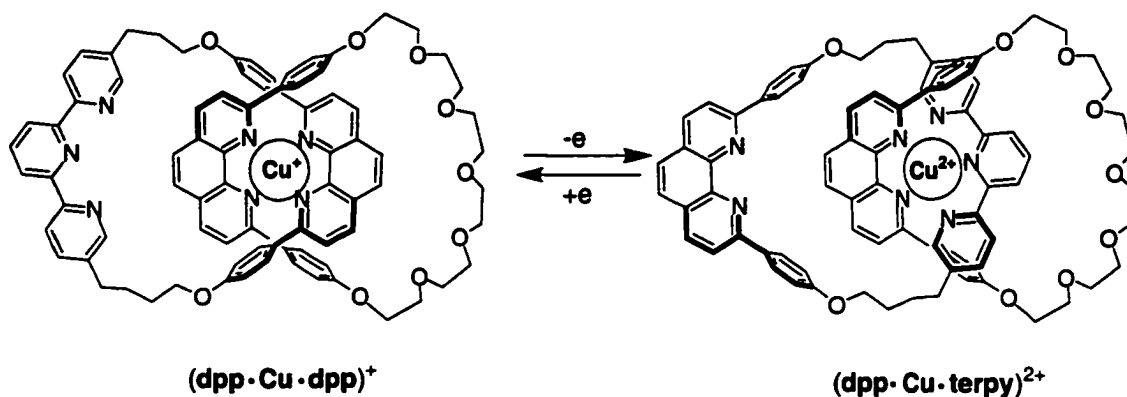
Shanzer and coworkers have utilized the different coordination requirements of Fe(II) and Fe(III) cations to build redox-controlled molecular switches.<sup>4</sup> Their design involved two pairs of binding ligands (2,2'-bipyridines and hydroxyamides) anchored onto a calix[4]arene scaffold in an alternating fashion as shown in Scheme 3.1.<sup>4a</sup> When loaded with Fe(III) the "harder" hydroxyamide ligands converge to embrace the "harder" metal ion and the bipyridine ligands are forced into a divergent pattern. Upon reduction of the metal ion, the molecule rearranges in order to enclose the "softer" Fe(II) ion with its "softer" bipyridyl ligands. In this case, it is the hydroxyamide ligands that are forced to diverge. Subsequent oxidation of the metal ion reverses the process. This structural regulation can be readily monitored because of color change from pink (for the Fe(II) complex) to orange (for the Fe(III) complex).



Scheme 3.1

Sauvage and coworkers<sup>5</sup> described another example of electron-induced switching of a metal complex (Scheme 3.2). The system is based on an asymmetric catenate, a compound made up of two ring-shaped molecules mechanically interlocked. <sup>5a,c</sup> A 2,9-

diphenyl-1,10-phenanthroline (**dpp**) bidentate ligand is included in one of the cycles. The other ring contains two different subunits: a **dpp** moiety and a terdentate ligand, 2,2',6',2''-terpyridine (**terpy**). The addition of Cu(I) ion leads to a tetrahedral complex (**dpp**•Cu•**dpp**)<sup>+</sup> involving the two **dpp** ligands, while Cu(II) ion favors the 5-coordinate complex (**dpp**•Cu•**terpy**)<sup>2+</sup>. Consequently, oxidation of the Cu(I) complex (**dpp**•Cu•**dpp**)<sup>+</sup> generates the unstable compound (**dpp**•Cu•**dpp**)<sup>2+</sup>, which rearranges through a gliding motion of one ring through the other, leading to Cu(II) complex (**dpp**•Cu•**terpy**)<sup>2+</sup> which best suits the new coordination geometry of the metal center (Scheme 3.2). The reduction of the Cu(II) complex leads to the reverse rearrangement. This rearrangement is accompanied by a reversible change in color from green (for (**dpp**•Cu•**terpy**)<sup>2+</sup>) to red (for (**dpp**•Cu•**dpp**)<sup>+</sup>).



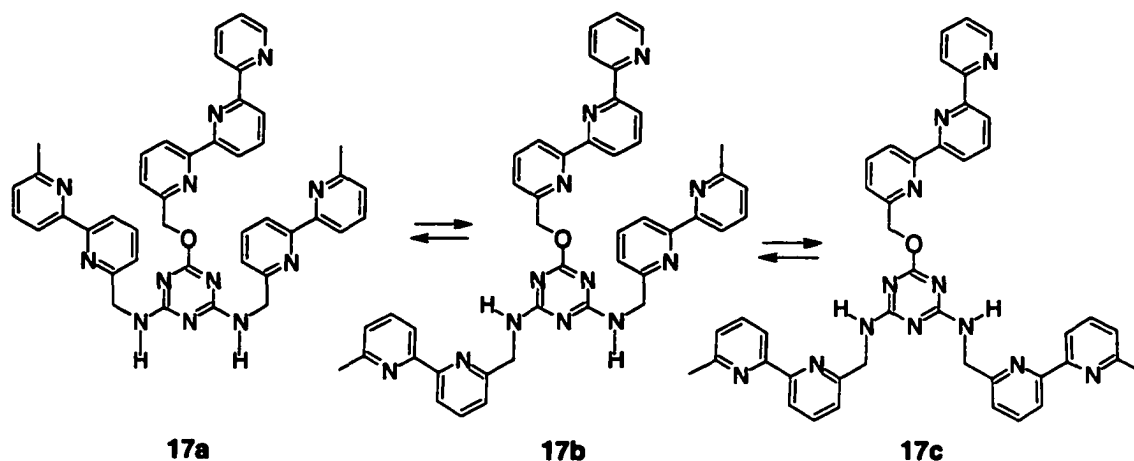
Scheme 3.2

Molecular switches such as those described above consume electrical energy to induce conformational and topological changes within their component parts. Electricity is used as the energy source and as the external stimulus to control the "machines". The state of each device is monitored by color changes in the UV-Vis range of the electronic absorption spectrum. However, in the examples described above, the motion of the

machine's components was not used to perform a specific task such as binding or transport. This chapter introduces a molecular receptor whose activity toward binding uracil derivatives can be controlled by electrochemistry. In a manner similar to the literature examples above, the state of this receptor can be monitored by UV-Vis absorption and NMR spectroscopy.

### **3.2 Receptor Design**

The previous chapter introduced the triaminotriazine receptor **6**, which provided a hydrogen bonding donor-acceptor-donor site for imide guests. The binding of the receptor to its substrate was controlled through the allosteric effect of Cu(I) ions. Each on/off binding cycle required the addition of a Cu(I) ion and a neocuproine ligand to the solution. This requirement for chemical energy limits the use of receptor **6** as a molecular machine due to the accumulation of added chemicals. In this chapter, the control of diaminotriazine receptor **17** binding to imide substrates is based on harnessing changes in the allosteric cofactor (the copper ion). Electrochemical energy is used to regulate the allosteric effect of the metal, hence, the stimulus is mild, noninvasive and easy to control. The result is a molecular machine that binds and releases imide derivatives, a task controlled by the addition or removal of an electron.

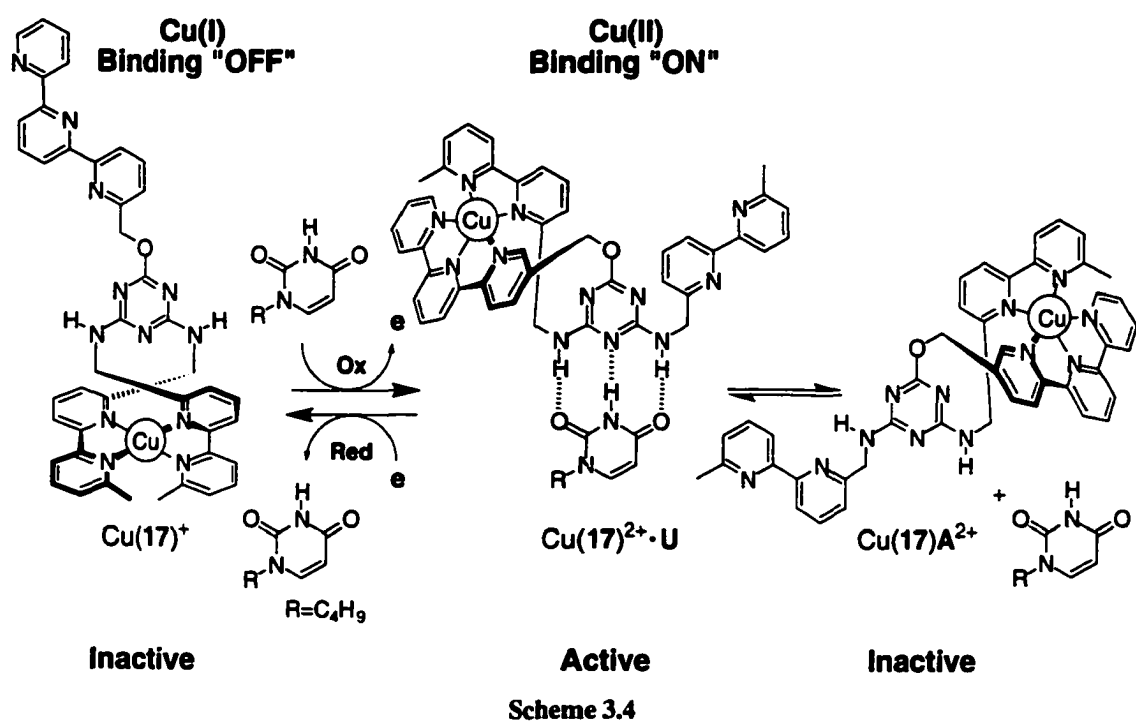


Scheme 3.3

Diaminotriazine receptor **17** provides the requisite donor-acceptor-donor hydrogen bond site needed to target imide guests as shown in Chapter 2. The receptor is based on the same triazine scaffold as found in the original triaminotriazine receptor, **6**. However, the diaminotriazine receptor **17** brandishes two bidentate bipyridine ligands and one tridentate terpyridine ligand (Scheme 3.3). This particular receptor exists in three unique conformations (**17a**, **17b** and **17c**) as a result of the limited rotation of the triazine's exocyclic C–N bonds. Such a limited rotation was also observed for triaminotriazines but to a lesser extent.<sup>6</sup> Only rotomer **17a** possesses a hydrogen-bonding site where both N–H donors project in a fashion suitable to bind imide guests. Rotation around one and both C–N bonds generates the non-binding rotomers **17b** and **17c**, respectively. Increasing the ratio of "active" rotomer **17a** relative to **17b** and **17c** will enhance the binding efficiency of the receptor toward imide substrates. The reverse is also true. Favoring the presence of rotomers **17b** and/or **17c** will lead to low activity of the receptor for imide substrates.

The ability to control molecular topology can be accomplished through metal coordination to the receptor as shown in Chapter 2.<sup>1g-i,4,5</sup> This strategy can be similarly

applied to control the relative ratios of the rotomers of diaminotriazine **17** (Scheme 3.4). Coordination of the bipyridine ligands to Cu(I) ion forces the exocyclic C—N bonds to rotate so that the N—H bonds project in a divergent manner similar to that found in rotomer **17c**. The result is a 4-coordinate Cu(I) complex locked into a single non-effective conformation that lacks a hydrogen bond array suitable for binding the imide substrate (Cu(**17**)<sup>+</sup> in Scheme 3.4). Therefore, Cu(I) ion is a negative allosteric cofactor for receptor **17** since its presence results in a decrease in the concentration of the "active" receptor in solution and an increase in the inactive forms.



The Cu(II) ion, on the other hand, prefers to reside in a 5- or 6-coordinate fashion which is provided by the terpyridine ligand and one of the bipyridine ligands (Scheme 3.4).<sup>5</sup> To achieve this coordination, one of the C—N bonds is locked while the other remains free to rotate. The result is a species that can exist in two possible

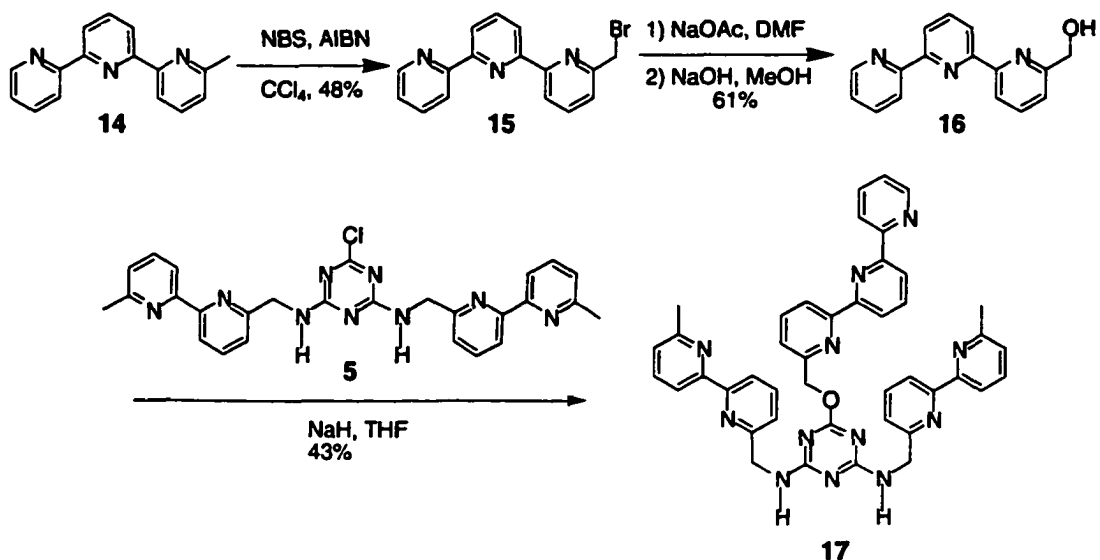
conformations. (1) An "active" conformation where the two N—H bonds converge in a similar fashion to receptor **17a**. Thus the donor–acceptor–donor hydrogen bonding surface is present ( $\text{Cu}(\mathbf{17})^{2+}$  in Scheme 3.4). (2) An "inactive" conformation where the two N—H bonds project in a divergent manner similar to that of receptor **17b** ( $\text{Cu}(\mathbf{17})\text{A}^{2+}$  in Scheme 3.4). Either way, the effective concentration of the active receptor is higher than in the presence of the Cu(I) negative allosteric cofactor as well as higher than the receptor alone. Therefore, the Cu(II) ion acts as a positive allosteric cofactor for receptor **17** because it increases the effective concentration of the active receptor by eliminating one of the non-binding conformations (**17c**) and increasing the ratio of the binding conformation (**17a**) to half.

The different conformational preferences of Cu(I) and Cu(II) ions provide a means to regulate the binding of the receptor to its substrate using electrons as an external stimulus as shown in Scheme 3.4. The metal can be electrochemically and reversibly switched between its Cu(I) and Cu(II) states causing the molecule to alter its conformation to afford the coordinating environment favorable to the corresponding oxidation state. These conformational changes are contemporary with either destroying ( $\text{Cu}(\mathbf{17})^+$ ) or re-creating ( $\text{Cu}(\mathbf{17})^{2+}$ ) the binding site of the receptor to its substrate. Therefore, the binding of the receptor to its imide substrates can be turned on or off by the addition or removal of an electron.

### 3.3 Synthesis and Characterization of Diaminotriazine Receptor **17**

The diaminotriazine receptor **17** was prepared in two steps from 6-aminomethyl-6'-methyl-2,2''-bipyridine and 2-hydroxymethyl-2,2'-6',2''-terpyridine<sup>9</sup> as shown in Scheme 3.5. The latter was prepared by brominating 2-methyl-2,2'-6',2''-terpyridine<sup>7</sup> with NBS in carbon tetrachloride to afford bromide **39**. Conversion of this bromide to

the acetate followed by base hydrolysis produced the alcohol **40** in 61% yield. Reaction of terpyridine **40** and chlorotriazine **4** (prepared as described in Chapter 2) in the presence of NaH afforded the final receptor **17** in 43% yield.



Scheme 3.5

The <sup>1</sup>H NMR spectrum of the diaminotriazine receptor **17** showed the presence of broad peaks in the aromatic region due to the rotomers that were expected to be present in solution. The signal corresponding to the triazine N—H protons appeared as a broad singlet at 6.28 ppm, while the CH<sub>2</sub> protons of the bipyridine and terpyridine groups appeared as singlets at 5.62 and 4.79 ppm, respectively. As the temperature was increased to 60 °C, the aromatic signals sharpened as did those corresponding to the N—H protons and the CH<sub>2</sub> protons of the bipyridines. These observations were expected as rotation around the triazine exocyclic C—N bonds is easier at elevated temperatures and lead to rapid interconversion of the rotomers.

### 3.4 Synthesis and Characterization of the Metal Complexes

The copper complexes  $\text{Cu}(\mathbf{17})^+$  and  $\text{Cu}(\mathbf{17})^{2+}$  of the receptor were prepared by adding the corresponding copper salt to a solution of the receptor dissolved in a chloroform/acetonitrile (1:1) mixture. The addition of  $\text{Cu}(\text{CH}_3\text{CN})_4\text{PF}_6$  to a solution of receptor **17** caused immediate formation of a red-brown color. The addition of diethyl ether induced precipitation of  $\text{Cu}(\mathbf{17})\text{PF}_6$  in 95% yield. The  $\text{Cu}(\text{II})$  complex  $\text{Cu}(\mathbf{17})^{2+}$  was prepared by the addition  $\text{Cu}(\text{OTf})_2$  to a solution of receptor **17**. The addition of diethyl ether caused the precipitation of a green solid  $\text{Cu}(\mathbf{17})(\text{OTf})_2$  in 93% yield.

#### 3.4.1 UV-Vis Spectra

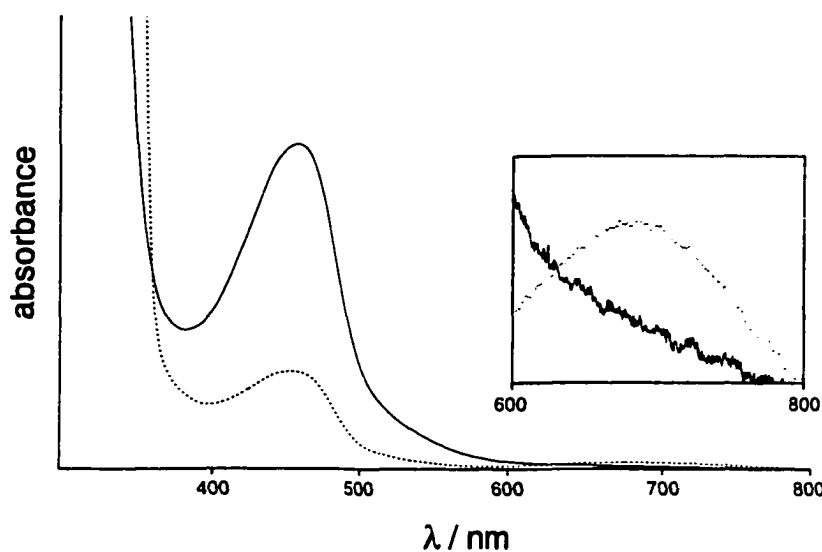


**Figure 3.1.** The UV-Vis absorption spectra of  $\text{Cu}(\mathbf{17})^+$  (—) and  $\text{Cu}(\mathbf{17})^{2+}$  (⋯) in  $\text{CH}_3\text{CN}$  ( $1 \times 10^{-4}$  M). The inset shows the expansion of the absorbances (20×) in the region between 600 and 800 nm.

The copper complexes were first characterized by UV-Vis absorption spectroscopy where the colors of the complexes are characteristic of a particular coordination mode. The spectrum of complex  $\text{Cu}(\mathbf{17})^+$  possessed a strong absorption band in the visible region at  $\lambda_{\text{max}} = 440$  nm ( $\epsilon = 5700$ ), characteristic of a tetrahedral  $\text{Cu}(\text{I})$



4-coordinated complex with diimine ligands (solid line in Figure 3.1).<sup>5</sup> This observation supports the claim that the bipyridine ligands chelate the Cu(I) ion as such phenomena has previously been reported for similar copper complexes.<sup>5</sup> The spectrum of the Cu(II) complex Cu(17)<sup>2+</sup>, on the other hand, showed a weak absorption band at  $\lambda_{\text{max}} = 700 \text{ nm}$  ( $\epsilon = 102$ ), indicating formation of a 5-coordinate Cu(II) complex (broken line in Figure 3.1).<sup>5</sup> This observation suggests that Cu(II) is coordinated by one bipyridine ligand and the terpyridine.

### 3.4.2 <sup>1</sup>H NMR and X-Ray Crystallography

Structural changes associated with the coordination of the metal were immediately apparent from the <sup>1</sup>H NMR spectrum of the complexes. All signals in the spectrum of complex Cu(17)<sup>+</sup> were sharper than those of the original receptor **17** due to locked rotation around the triazine's exocyclic C—N bonds as the metal is coordinated by the 2,2'-bipyridine ligands. Signals corresponding to these bipyridine ligands and the exocyclic N—H protons appeared as a single set of peaks, indicating that the molecule is symmetrical. The methylene CH<sub>2</sub> protons of the bipyridine groups emerged as a doublet-of-doublets at 5.37 and 4.67 ppm. These signals are characteristic (see Chapter 2) of a tetrahedral geometry of the complex which places each proton of the CH<sub>2</sub> group in two different environments leading to the splitting of the doublet signal observed in receptor **17**. The signal corresponding to the methylene CH<sub>2</sub> protons of the terpyridine group was split into a quartet-like signal in the spectrum of the complex. This was attributed to the diastereotopic environment of these protons created by the tetrahedral geometry around the metal center and the limited rotation around the triazine exocyclic C—O bond. The resulting quartet-shaped signal is due to coincidental overlapping of the four doublets corresponding to the AB splitting of CH<sub>2</sub> protons of the two diastereoisomers L-Cu(17)<sup>+</sup> (H<sub>a</sub> and H<sub>b</sub>) and R-Cu(17)<sup>+</sup> (H<sub>c</sub> and H<sub>d</sub>) (Figure 3.2).

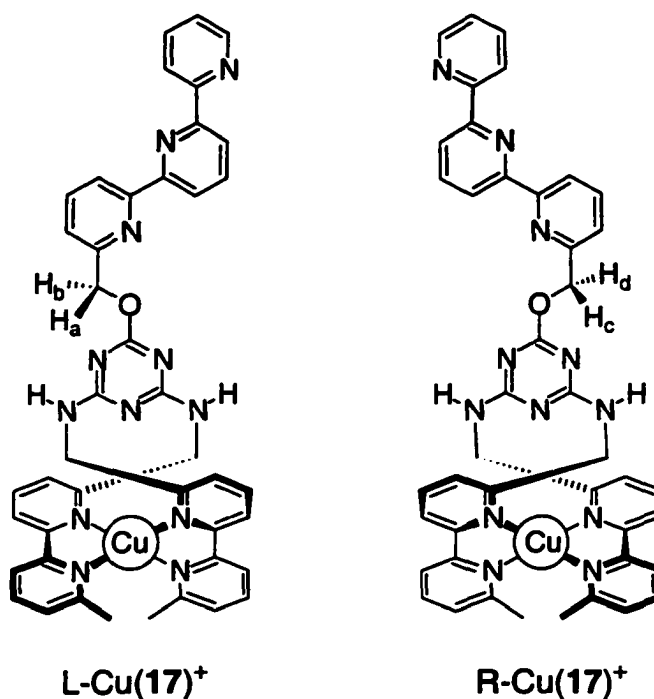


**Figure 3.2** The diastereoisomers of Cu(17)<sup>+</sup> created by the limited rotation around exocyclic C—O bond and the tetrahedral geometry around the metal center.

The symmetrical nature of the Cu(I) complex and the tetrahedral geometry around the metal was supported by X-ray analysis of single crystals of Cu(17)<sup>+</sup> (Figure 3.3). The structure shows coordination of the Cu(I) ion by the bipyridine ligands in a tetrahedral arrangement around the metal center. The terpyridine ligand is directed away from the coordination site. This structure also shows that both C—N bonds have rotated almost 180° from their original position in order to form the coordination compound (the torsional angles for C4—N4—C3—N1 and C5—N5—C2—N2 are 175° and 179°, respectively). The structural changes that accompany the coordination event perturb the hydrogen bond sites (HN(4), N2, HN(5)), and only two low-affinity donor-acceptor (HN(4), N1, HN(5), N3) recognition sites remain in Cu(17)<sup>+</sup>.

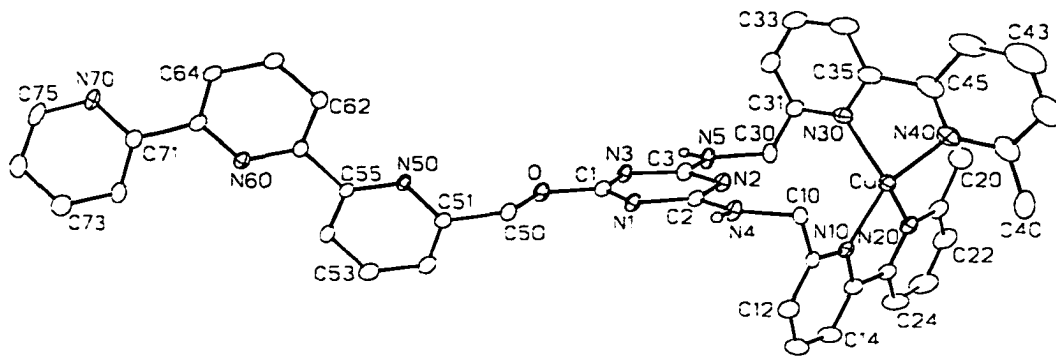


**Figure 3.3** Molecular structure of Cu(17)<sup>+</sup> in the crystal. The PF<sub>6</sub><sup>-</sup> counterion and all non-heteroatomic hydrogens have been removed for clarity. The thermal ellipsoids are drawn at the 20% probability level.

The structural changes that accompanied the complexation of diaminotriazine receptor **17** to the Cu(II) ion were readily obtained from the <sup>1</sup>H NMR spectrum of Cu(17)<sup>2+</sup>, despite the fact that the signals were uniformly broad due to the diamagnetic effect of Cu(II) ions. Signals corresponding to the N–H protons appeared at 8.19 ppm and 8.12 ppm and vanished from the spectrum when a drop of D<sub>2</sub>O was added to the NMR tube. The protons of the methyl groups on the two bipyridine ligands appeared as two independent sets of peaks at 2.58 ppm and 2.55 ppm in the <sup>1</sup>H NMR spectrum, implying that the two bipyridine groups were not in identical environments. This doubling of signals is an outcome of the dissymmetric nature of the Cu(II) complex, where the two bipyridine ligands cannot simultaneously coordinate the metal cation. Only one bipyridine ligand partners with the terpyridine ligand to provide the 5-coordinate binding site suited to Cu(II) ions.

The peak at  $m/z = 400$  in the positive electrospray mass spectrum of Cu(17)<sup>2+</sup> clearly reveals the presence of a doubly charged Cu(II) complex of the diaminotriazine receptor **17**. Also, the appearance of peak at  $m/z = 948$ , corresponding to a singly charged ion consisting of the complex Cu(17)<sup>2+</sup> and one triflate counterion, affirms the

formation of  $\text{Cu}(\mathbf{17})^{2+}$ . The spectrum showed a peak at  $m/z = 799$  corresponding to a singly charged copper complex of receptor **17**. This peak was attributed to the reduction of Cu(II) ion of the complex in the gas-phase during analysis of the sample by the mass spectrometer. Such behavior of transition metals during electrospray mass spectrometry analysis has been previously reported.<sup>10</sup>

### 3.4.3 Cyclic Voltammetry

The metal complexes were also characterized by cyclic voltammetry where the oxidation state of the metal and its coordination number are reflected by the trends observed in the voltammograms. Cyclic voltammetry experiments were performed on  $\text{CH}_3\text{CN}$  solutions of the complexes ( $10^{-4}$  M) using tetrabutylammonium hexafluorophosphate ( $\text{BuN}_4\text{PF}_6$ ) (0.1 M) as an electrolyte. A platinum working electrode, a platinum counter electrode, and a Ag/AgCl reference electrode were used at a potential sweep rate of 200 mV/sec.

The cyclic voltammogram (CV) of  $\text{Cu}(\mathbf{17})^+$  exhibits the characteristic redox couple for a 4-coordinate (labeled with the notation ' $\text{N}_4$ ') complex ( $\text{Cu}^{\text{III}}\text{N}_4$ ) at +0.62 V as shown in the top CV of Figure 3.4.<sup>5</sup> The oxidation wave consists of a peak that corresponds to oxidation of the 4-coordinate complex of Cu(I) ( $\text{Cu}^{\text{I}}\text{N}_4$ ) to form a 4-coordinate complex of Cu(II) ( $\text{Cu}^{\text{II}}\text{N}_4$  in Scheme 3.6). The subsequent reduction wave has a slight decrease in peak intensity corresponding to reduction of  $\text{Cu}^{\text{II}}\text{N}_4$  to  $\text{Cu}^{\text{I}}\text{N}_4$  with the concomitant appearance of an additional peak at -0.15 V corresponding to reduction of 5-coordinate (labeled with the notation ' $\text{N}_5$ ')  $\text{Cu}^{\text{II}}\text{N}_5$  to  $\text{Cu}^{\text{I}}\text{N}_5$ . This indicates that within this time-scale a small amount of the 4-coordinate Cu(II) complex ( $\text{Cu}^{\text{II}}\text{N}_4$ ) rearrange to the 5-coordinate Cu(II) complex ( $\text{Cu}^{\text{II}}\text{N}_5$ ) after the initial oxidation of  $\text{Cu}(\mathbf{17})^+$  (Scheme 3.6).<sup>5</sup>

The voltammogram of  $\text{Cu(17)}^{2+}$  displays a reduction wave with a peak at  $-0.15$  V corresponding to the reduction of  $\text{Cu}^{\text{II}}\text{N}_5$  to  $\text{Cu}^{\text{I}}\text{N}_5$ . However, a significant decrease in the oxidation peak of  $\text{Cu}^{\text{I}}\text{N}_5$  and the concomitant appearance of the oxidation peak of  $\text{Cu}^{\text{I}}\text{N}_4$  was observed. This can be explained by the rapid and virtually quantitative rearrangement of  $\text{Cu}^{\text{I}}\text{N}_5$  to  $\text{Cu}^{\text{I}}\text{N}_4$  immediately after it is generated (Scheme 3.6). The rates of change-over from  $\text{Cu}^{\text{II}}\text{N}_4$  to  $\text{Cu}^{\text{II}}\text{N}_5$  and from  $\text{Cu}^{\text{I}}\text{N}_5$  to  $\text{Cu}^{\text{I}}\text{N}_4$  was not measured but similar electrochemical trends have been reported by Sauvage and coworkers.<sup>5</sup>

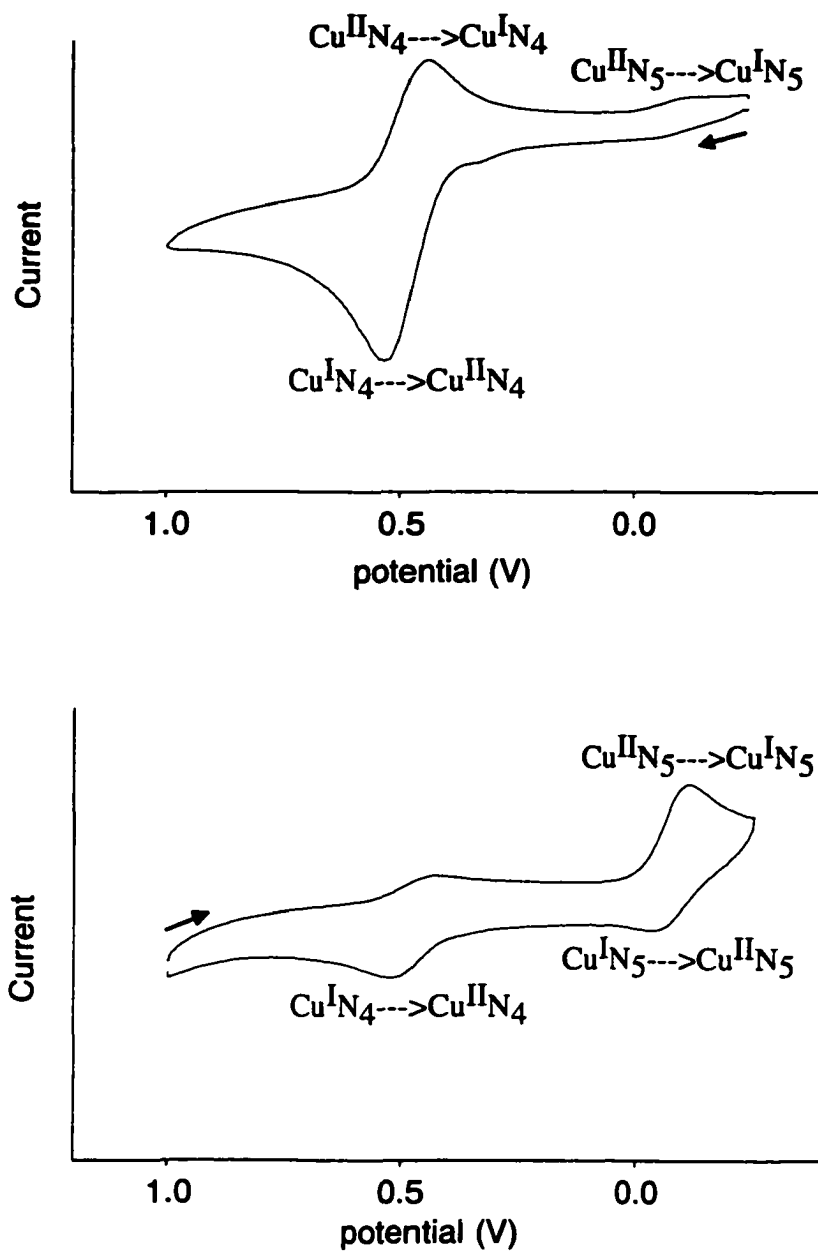
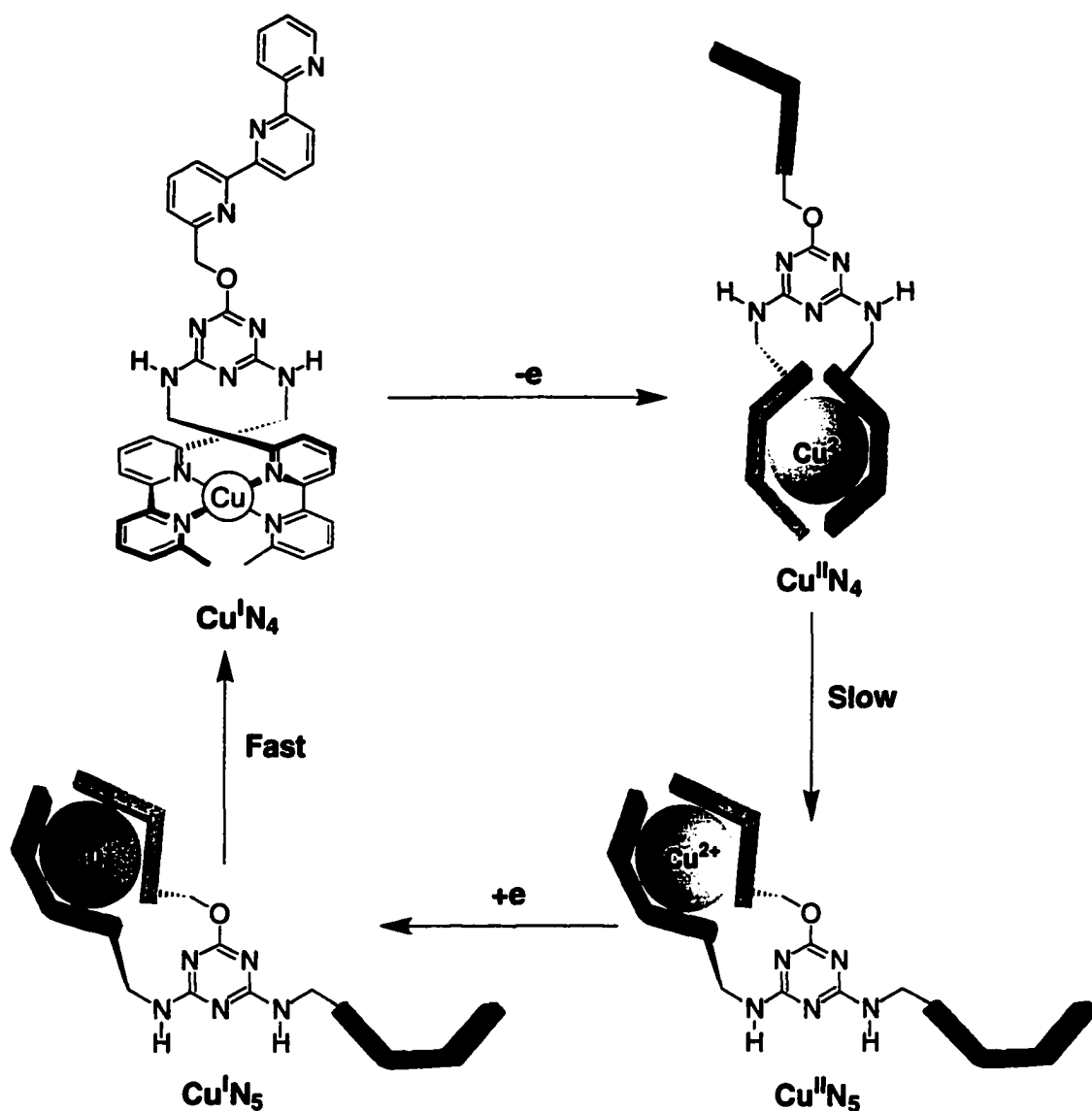


**Figure 3.4** Cyclic voltammograms of  $\text{CH}_3\text{CN}$  solutions ( $1 \times 10^{-4}$  M) of  $\text{Cu(17)}^+$  (top) and  $\text{Cu(17)}^{2+}$  (bottom) using Pt electrode and Ag/AgCl reference electrode ( $[\text{Bu}_4\text{N}_4\text{PF}_6] = 0.1\text{M}$ ,  $200\text{ mV/sec}$ ).



Scheme 3.6

### 3.5 Redox Switching Studies of the Copper Complexes

#### 3.5.1 Redox Switching Between $\text{Cu}(\mathbf{17})^+$ and $\text{Cu}(\mathbf{17})^{2+}$ Using Chemical Means

UV-Vis absorption spectroscopy provided a convenient means to monitor the changes in coordination behavior of diaminotriazine **17** and copper as the metal ion was switched between its two oxidation states. When a  $\text{CH}_3\text{CN}$  solution of  $\text{Cu}(\mathbf{17})^+$  ( $10^{-4}$  M) was treated with a bromine solution which is a strong oxidizing agent ( $E^\circ = +1.09\text{V}$ ) (0.1

M in CH<sub>3</sub>CN), there was an immediate change in color from red-brown ( $\lambda_{\text{max}} = 440 \text{ nm}$ ,  $\epsilon = 5700$ ), characteristic of the 4-coordinated complex, to yellow-green ( $\lambda_{\text{max}} = 700 \text{ nm}$ ,  $\epsilon = 102$ ). This observation indicates that the chemical oxidation of Cu(I) to Cu(II) was accompanied by transformation to the 5-coordinate complex Cu(17)<sup>2+</sup> (Scheme 3.6). After addition of 4 equivalents of bromine, a UV-Vis absorption spectrum identical to that of Cu(17)<sup>2+</sup> was observed, implying a complete transformation from Cu(17)<sup>+</sup> to the 5-coordinate complex.

The reverse reaction (Cu(II) → Cu(I)) was also tracked by a color change, in this case from yellow-green to red-brown. As a hydrazine which is a strong reducing agent, ( $E^\circ = -1.16\text{V}$ ) solution (0.1 M in CH<sub>3</sub>CN) was added to a solution of Cu(17)<sup>2+</sup> there was an immediate change in the color of the solution from yellow-green ( $\lambda_{\text{max}} = 700 \text{ nm}$ ,  $\epsilon = 102$ ), characteristic of the 5-coordinated complex, to red-brown ( $\lambda_{\text{max}} = 440 \text{ nm}$ ,  $\epsilon = 5700$ ). This observation indicates that the chemical reduction of the metal (Cu(II) → Cu(I)) was accompanied by transformation to the 4-coordinate complex Cu(17)<sup>+</sup> (Scheme 3.6). After addition of 4 equivalents of hydrazine, a UV-Vis absorption spectrum identical to that of Cu(17)<sup>+</sup> was observed, implying a complete transformation from Cu(17)<sup>2+</sup> to the 4-coordinate complex.

### 3.5.2 Redox Switching Between Cu(17)<sup>+</sup> and Cu(17)<sup>2+</sup> Using Electrochemical Means

Reversible interconversion between Cu(17)<sup>+</sup> and Cu(17)<sup>2+</sup> was also induced using electrochemical means. Electrolysis experiments were performed in the cyclic voltammetry apparatus after replacing the working electrode with a platinum-wire coil. A CH<sub>3</sub>CN solution ( $1 \times 10^{-4} \text{ M}$ ) of Cu(17)<sup>+</sup> was placed in the cyclic voltammetry cell and the potential of the working electrode was set at +800 mV to cause oxidation of the Cu(I) complex ( $E^\circ = +0.62\text{V}$ ). The UV-Vis absorption spectrum of the solution was recorded



every 3 minutes. A reduction in intensity of the absorption at 440 nm and the appearance of a new absorption at 700 nm was observed (Figure 3.5 (A)). This change in the UV-Vis absorption spectrum was accompanied by a visual change in color from red–brown to yellow–green. After 9 minutes of oxidation, the UV-Vis absorption spectrum was identical to that of the preformed complex  $\text{Cu}(\mathbf{17})^{2+}$ . This observation indicates a full transformation of the 4-coordinate Cu(I) complex  $\text{Cu}(\mathbf{17})^+$  to the 5-coordinate Cu(II) complex  $\text{Cu}(\mathbf{17})^{2+}$ .

The potential of the working electrode was then switched to -200 mV to induce reduction of the resulting Cu(II) complex ( $E^\circ = -0.15\text{V}$ ). The UV-Vis absorption spectrum of the solution was recorded every 3 minutes. It showed a decrease in intensity of the absorption at 700 nm and a reappearance of absorption at 440 nm (Figure 3.5 (A)). This change in UV-Vis absorption spectrum was accompanied by a visual change in color from yellow–green to red–brown. After 24 minutes of reduction, the UV-Vis absorption spectrum was identical to that of the preformed complex  $\text{Cu}(\mathbf{17})^+$ . This observation indicates a full transformation of the 5-coordinate Cu(II) complex  $\text{Cu}(\mathbf{17})^{2+}$  to the 4-coordinate Cu(I) complex  $\text{Cu}(\mathbf{17})^+$ . At this stage, one cycle of the redox process was completed. Several cycles of the redox process (at +800 mV and -200 mV) commencing with either  $\text{Cu}(\mathbf{17})^+$  (Figure 3.6 (A)) or  $\text{Cu}(\mathbf{17})^{2+}$  (Figure 3.6(B)) were achieved with quantitative conversion.

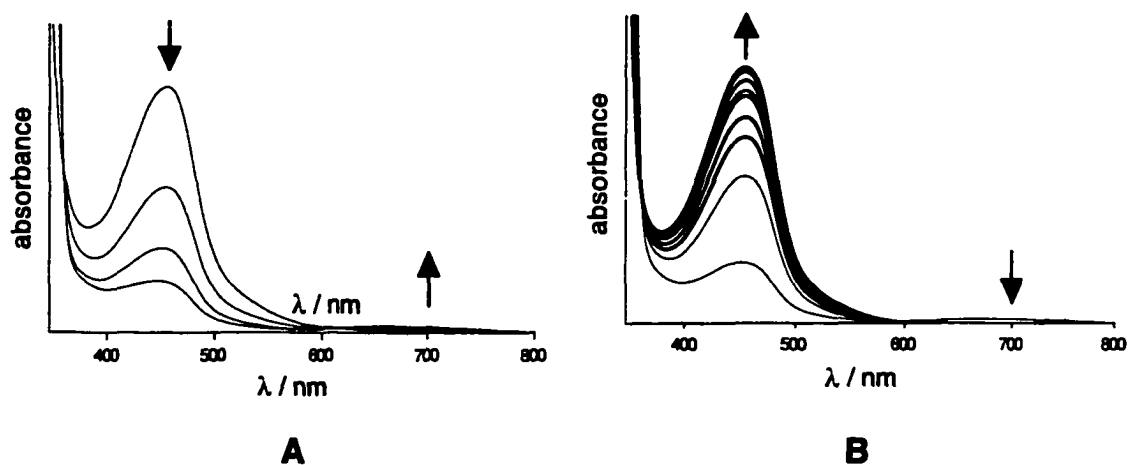


**Figure 3.5** Changes in the UV-Vis absorption spectra of  $\text{CH}_3\text{CN}$  solutions of (A)  $\text{Cu}(\mathbf{17})^+$  ( $1 \times 10^{-4}$  M) upon electrochemical oxidation at +800 mV (electrolysis periods are 0, 3, 6, and 9 minutes), and of (B)  $\text{Cu}(\mathbf{17})^{2+}$  ( $1 \times 10^{-4}$  M) upon electrochemical reduction at -200 mV (electrolysis period is for 24 minutes over 3-minute intervals).

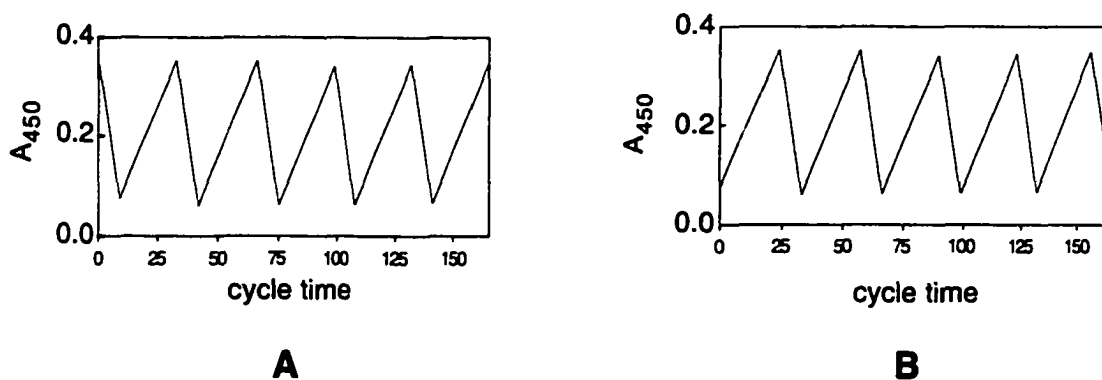


**Figure 3.6** The modulated absorption spectra ( $\lambda = 450$  nm) during alternating electrolysis of  $\text{CH}_3\text{CN}$  solutions of (A)  $\text{Cu}(\mathbf{17})^+$  ( $1 \times 10^{-4}$  M) at +800 mV for 9 minute periods and at -200 mV for 24 minute periods, and of (B)  $\text{Cu}(\mathbf{17})^{2+}$  ( $1 \times 10^{-4}$  M) at -200 mV for 24-minute periods and at +800 mV for 9-minute periods.

### 3.6 Binding Studies of the Complexes

The binding abilities of receptor **17** and its corresponding metal complexes for imide substrates were studied using  $^1\text{H}$  NMR spectroscopy (Figure 3.7). For these NMR studies, the change in the chemical shift of the N—H proton of *N*-butyluracil was followed as it was treated with 2 equivalents of the receptor or its complexes. The signal

that corresponds to the imide N—H proton of *N*-butyluracil appears at 8.71 ppm, an uncluttered region of the spectrum (Figure 3.7(a)) which made it easy to follow during the studies. The triazine N—H protons of the receptor and its complexes, however, appears at  $\delta$  6.0-7.0 ppm. Thus, hydrogen bonding of these N—H protons shifted their signal to the aromatic region of the spectrum making it impossible to follow.

The addition of the diaminotriazine receptor **17** (2 equivalents) to a solution of *N*-butyluracil (2.0 mM) in CDCl<sub>3</sub>/CD<sub>3</sub>CN (1:1) resulted in a downfield shift of the signal corresponding to the uracil N—H protons from 8.71 to 8.93 ppm. This observation is indicative of effective hydrogen bonding between the receptor and the uracil substrate (Figure 3.7(b)). When Cu(CH<sub>3</sub>CN)<sub>4</sub>PF<sub>6</sub> (2 equivalents) was added directly to the NMR tube, all signals corresponding to receptor **17** were replaced by those corresponding to Cu(**17**)<sup>+</sup> (Figure 3.7(c)). Peaks in the aromatic region became sharper as chelation of the metal by bipyridine locked the molecule into a single conformation. The signal for the N—H proton of *N*-butyluracil returned to 8.75 ppm, indicating that a virtually ineffective hydrogen bonding receptor had been formed. A similar spectrum was obtained when pre-formed complex Cu(**17**)<sup>+</sup> was added to the substrate (Figure 3.7(d)). These observations show that Cu(I) inhibits the binding of diaminotriazine receptor **17** of uracil derivatives.

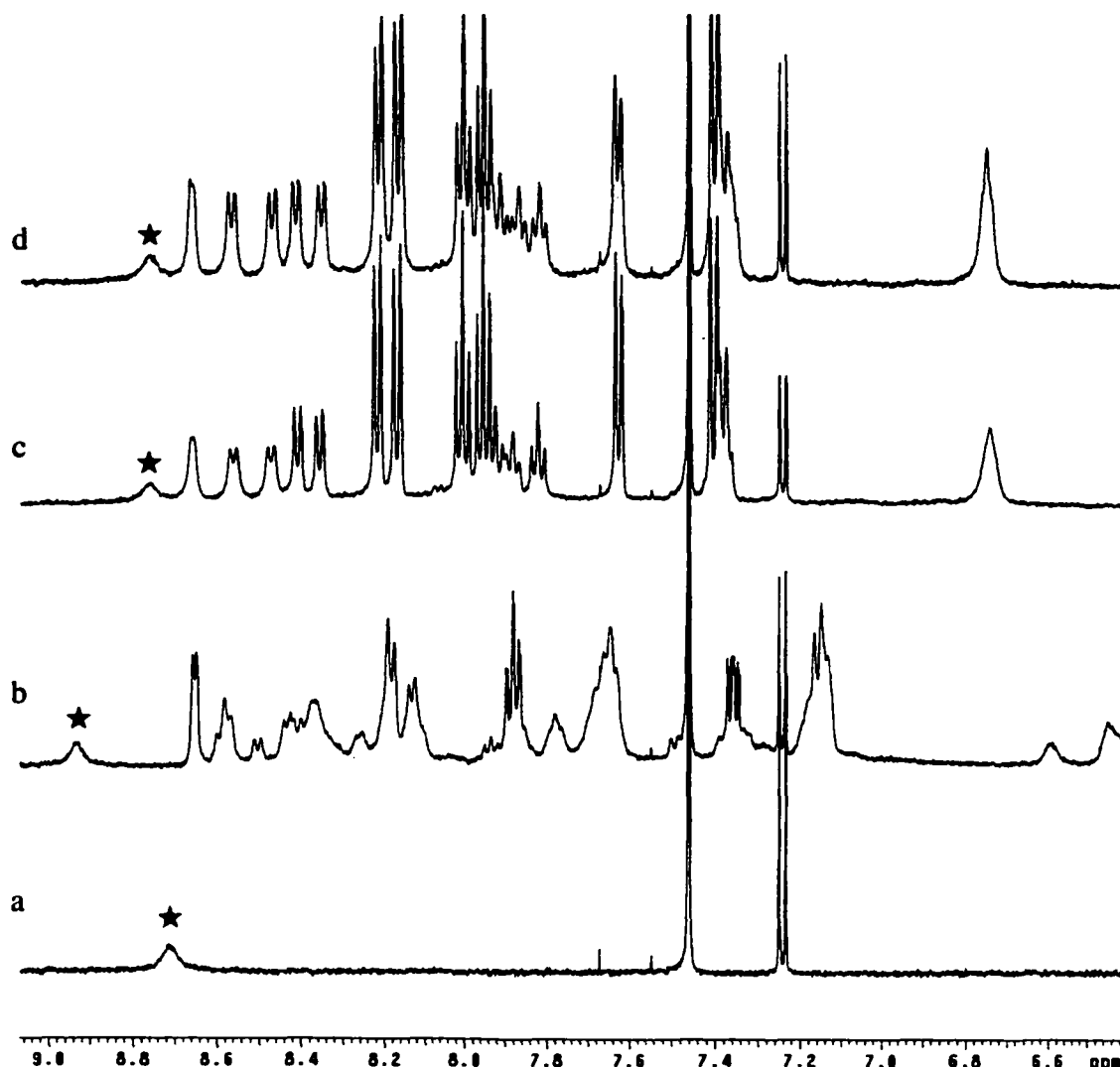


**Figure 3.7** Partial <sup>1</sup>H NMR (500 MHz, 1:1 CD<sub>3</sub>CN/CDCl<sub>3</sub>) spectra showing the change in the chemical shift of the N—H proton signal (★) of (a) *N*-butyluracil (2 mM) upon the subsequent addition of (b) 2 equivalents of **17** and (c) 2 equivalents of Cu(CH<sub>3</sub>CN)<sub>4</sub>PF<sub>6</sub>. (d) Partial <sup>1</sup>H NMR (500 MHz, 1:1 CD<sub>3</sub>CN/CDCl<sub>3</sub>) spectrum of *N*-butyluracil (2 mM) and 2 equivalents of the pre-formed complex Cu(**17**)<sup>+</sup>. (The chemical shifts were referenced to the residual peak of CD<sub>3</sub>CN at δ 1.93 ppm).

In order to study the effect of the Cu(II) ions on the binding of the diaminotriazine receptor **17**, the above experiment was repeated replacing the Cu(I) source (Cu(CH<sub>3</sub>CN)<sub>4</sub>PF<sub>6</sub>) with a Cu(II) source (Cu(OTf)<sub>2</sub>). Addition of receptor **17** (2 equivalents) to a solution of *N*-butyluracil (2.0 mM) resulted in a downfield shift of the signal corresponding to the uracil N—H protons from 8.71 to 8.95 ppm (Figure 3.8(b)) as

a result of strong association between receptor **17** and uracil. When  $\text{Cu}(\text{OTf})_2$  (2 equivalents) was added to the NMR tube, all signals corresponding to receptor **17** were replaced by those corresponding to  $\text{Cu}(\mathbf{17})^{2+}$  (Figure 3.7(c)). The signal corresponding to the N–H proton of *N*-butyluracil shifted further downfield from 8.95 to 9.15 ppm (Figure 3.8(c)). A similar spectrum was obtained when preformed  $\text{Cu}(\mathbf{17})^{2+}$  was added to a solution of *N*-butyluracil at similar concentrations (Figure 3.8(d)). This enhanced downfield shift indicates that  $\text{Cu}(\mathbf{17})^{2+}$  acts as an improved hydrogen-bonded receptor compared to receptor **17** alone. This suggests a positive allosteric effect of Cu (II).

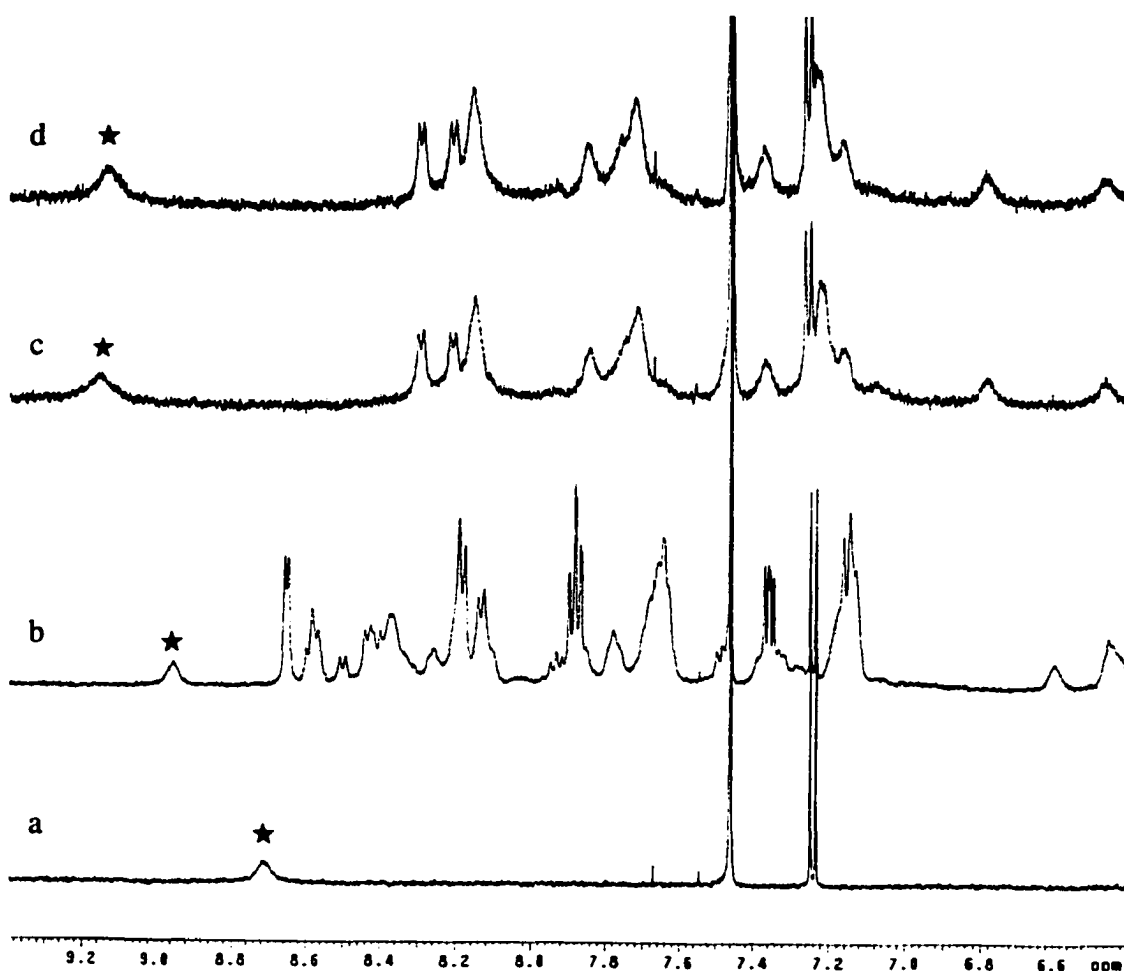


**Figure 3.8** Partial  $^1\text{H}$  NMR (500 MHz, 1:1  $\text{CD}_3\text{CN}/\text{CDCl}_3$ ) spectra showing the change in the chemical shift of the N–H proton signal ( $\star$ ) of (a) *N*-butyluracil (2 mM) upon the subsequent addition of (b) 2 equivalents of **17** and (c) 2 equivalents  $\text{Cu}(\text{OTf})_2$ . (d) Partial  $^1\text{H}$  NMR (500 MHz, 1:1  $\text{CD}_3\text{CN}/\text{CDCl}_3$ )

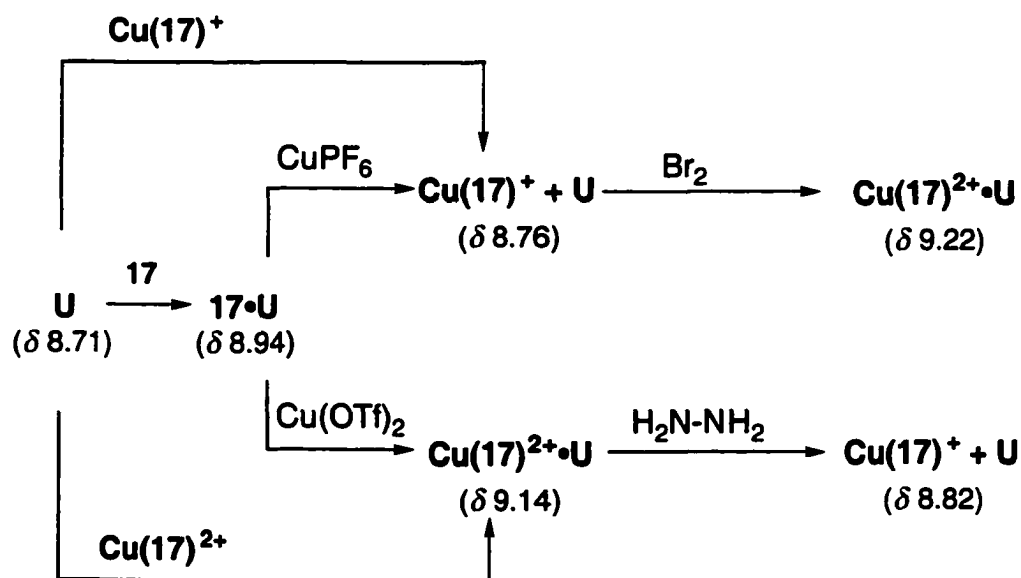
spectrum of *N*-butyluracil (2 mM) and 2 equivalents of the preformed complex  $\text{Cu}(\mathbf{17})^{2+}$ . (The chemical shifts were referenced to the residual peak of  $\text{CD}_3\text{CN}$  at  $\delta$  1.93 ppm).

### 3.7 Redox Effect on Binding of the Complexes

Regulation of the allosteric effect of copper ion was achieved through reversible switching of the metal between its oxidation states. As shown above, the metal ion can be chemically oxidized or reduced by reaction with four equivalents of bromine ( $\text{Cu}(\text{I}) \rightarrow \text{Cu}(\text{II})$ ) or four equivalents of hydrazine ( $\text{Cu}(\text{II}) \rightarrow \text{Cu}(\text{I})$ ), respectively. The redox process and its effect on the binding of receptor to its substrate were followed by  $^1\text{H}$  NMR and the results are shown in Scheme 3.7. Addition of  $\text{Cu}(\text{I})$  complex  $\text{Cu}(\mathbf{17})^+$  (2 equivalents) to a solution of *N*-butyluracil resulted in an insignificant downfield shift of the N—H proton of *N*-butyluracil from 8.71 to 8.76 ppm. This indicates that there is little association between the substrate and the preformed complex  $\text{Cu}(\mathbf{17})^+$ . Addition of eight molar equivalents of bromine to the NMR tube resulted in an immediate change in color from red-orange to green. This color change implies the conversion of the  $\text{Cu}(\text{I})$  complex to the  $\text{Cu}(\text{II})$  complex. The NMR spectrum showed the disappearance of peaks corresponding to  $\text{Cu}(\mathbf{17})^+$  and the appearance of broad spectrum that corresponds to the that of  $\text{Cu}(\mathbf{17})^{2+}$ . The N—H proton signal of *N*-butyluracil shifted from 8.76 to 9.22 ppm similar to the shift observed for the hydrogen bonding complex  $\text{Cu}(\mathbf{17})^{2+}\cdot\text{U}$  (Scheme 3.9).

Similar results were obtained when the experiment was repeated with metal complex  $\text{Cu}(\mathbf{17})^+$  formed *in situ* (Scheme 3.7). The addition of the diaminotriazine receptor **17** (2 equivalents) to a solution of *N*-butyluracil resulted in a downfield shift of the signal corresponding to uracil's N—H proton from 8.71 to 8.94 ppm which is indicative of effective hydrogen bonding between the receptor and uracil. When  $\text{Cu}(\text{CH}_3\text{CN})_4\text{PF}_6$  (2 equivalents) was added directly to the NMR tube, all signals corresponding to receptor **17** were replaced by those corresponding to  $\text{Cu}(\mathbf{17})^+$ . The

signal for the N–H proton of *N*-butyluracil returned to 8.76 ppm indicating a negative allosteric effect of the metal on the binding of the receptor. The addition of eight molar equivalents of bromine to the NMR tube resulted in an immediate change in color from red-orange to green and the NMR spectrum showed the disappearance of peaks corresponding to  $\text{Cu(17)}^+$  and the appearance of broad spectrum that corresponds to the that of  $\text{Cu(17)}^{2+}$ . The N–H proton signal of the uracil shifted from 8.76 to 9.22 ppm similar to the shift observed for the hydrogen bonding complex  $\text{Cu(17)}^{2+}\cdot\text{U}$  (Scheme 3.9). These observations imply that the oxidation of the metal resulted in formation of a stronger hydrogen bonding receptor  $\text{Cu(17)}^{2+}$ . Therefore, the negative allosteric effect of the metal on receptor **17** was turned off by oxidation of the metal ion and, thus, the binding is turned on.



**Scheme 3.7** Chemical shifts in the  $^1\text{H}$  NMR spectrum of  $\text{CDCl}_3/\text{CD}_3\text{CN}$  (1:1) solutions of *N*-butyluracil ( $2 \times 10^{-3}$  M) upon addition of receptor **17**,  $\text{Cu}(\text{CH}_3\text{CN})_4\text{PF}_6$ ,  $\text{Cu}(\text{OTf})_2$ ,  $\text{Cu(17)}^+$ ,  $\text{Cu(17)}^{2+}$ , and after the chemical interconversion of the metal between its two oxidation states. Chemical shift values are averages obtained from 3–6 independent experiments. Errors are  $\pm 0.01$  ppm except in the case of  $\text{Cu(17)}^{2+}\cdot\text{U}$  which has an error of  $\pm 0.03$  ppm. (The chemical shifts were referenced to the residual peak of  $\text{CD}_3\text{CN}$  at  $\delta 1.93$  ppm).

A control experiment was run to ensure that the presence of bromine had no effect on the chemical shift of the N–H proton of *N*-butyluracil. The addition of eight molar equivalents of bromine to a solution of *N*-butyluracil had no effect on the position or shape of the uracil N–H signal at 8.71 ppm. This further supports the claim that the observed changes in the chemical shifts in the above experiments are due to effective hydrogen bonding between the substrate and the Cu(II) complex  $\text{Cu}(\mathbf{17})^{2+}$  that was formed upon addition of bromine.

Alternatively, addition of two molar equivalents of  $\text{Cu}(\mathbf{17})^{2+}$  to *N*-butyluracil resulted in an immediate shift of the N–H proton signal of the substrate from 8.71 to 9.14 ppm due to effective hydrogen bonding between the complex and the imide substrate (Scheme 3.7). The addition of eight molar equivalents of hydrazine to the NMR tube resulted in an immediate change in color from yellow-green to red-orange. This color change implies that the reduction of the Cu(II) complex to the Cu(I) complex was achieved. The spectrum also showed the appearance of sharp peaks corresponding to  $\text{Cu}(\mathbf{17})^+$  and an upfield shift of the N–H proton signal of the uracil substrate from 9.14 to 8.82 ppm (Scheme 3.7) indicating lower affinity of the receptor for the uracil substrate.

Similar results were observed when the metal complex  $\text{Cu}(\mathbf{17})^{2+}$  was prepared *in situ* (Scheme 3.7). The addition of diaminotriazine receptor **17** (2 equivalents) to a solution of *N*-butyluracil (2.0 mM) resulted in a downfield shift of the uracil N–H proton signal from 8.71 to 8.94 ppm as a result of strong association between receptor and substrate. When  $\text{Cu}(\text{OTf})_2$  (2 equivalents) was added to the NMR tube, the signal corresponding to the N–H proton of *N*-butyluracil shifted further downfield from 8.95 to 9.14 ppm indicating a positive allosteric effect of the metal on the binding of the uracil substrate to the receptor. The addition of eight molar equivalents of hydrazine to the



NMR tube resulted in an immediate change in color from yellow-green to red-orange. This color change implies reduction of the Cu(II) complex to the Cu(I) complex. The spectrum also showed the appearance of sharp peaks corresponding to Cu(17)<sup>+</sup> and an upfield shift of the N—H proton signal of the uracil from 9.14 to 8.82 ppm . This upfield shift suggests that a less effective hydrogen-bonding receptor is generated. Thus, the positive allosteric effect of the metal is switched from on to off and, thus, the binding is turned off.

A control experiment was run to ensure that the presence of hydrazine had no effect on the chemical shift of uracil's N—H proton. Addition of eight molar equivalents of hydrazine to a solution of *N*-butyluracil had no effect on the position of the signal corresponding to the uracil's N—H proton at 8.71 but the signal became broader. This change in the shape of the signal was attributed to fast exchange of the uracil's N—H proton with protons of the excess hydrazine. However, since there was no observed change in the chemical shift of the uracil N—H proton, it was concluded that the chemical shifts observed in the above experiments were due to effective hydrogen bonding between the substrate and the Cu(II) complex Cu(17)<sup>2+</sup> that was formed upon addition of bromine.

### 3.8 Conclusion

This chapter has shown that the allosteric effect of copper ion can be modulated by using electricity as an external stimulus to control the binding of diaminotriazine receptor 17 to its imide substrates. Limited rotation around the triazine exocyclic C—N bonds lowered the concentration of the "active" conformation of the receptor in solution to one-third the total concentration of receptor. In the presence of Cu(I) ion, concentration of the "active" conformer became negligible as the coordination of the

metal by the receptor favored an "inactive" conformation of the receptor. Alternatively, chelation of Cu(II) ion favored the "active" conformer enhancing its concentration to half the total concentration of the diaminotriazine receptor. Therefore, Cu(I) ion has a negative (inhibitory) allosteric effect on the triaminotriazine receptor while Cu(II) ion has a positive (activating) allosteric effect .

The ability to toggle between the oxidation states of copper ions provided a means to switch the binding of the triaminotriazine receptor **17** from active (on) to inactive (off) and vice versa. Redox processes were performed using both chemical (bromine/hydrazine) and electrochemical sources of energy. Using electrochemistry, switching between Cu(I) and Cu(II) was possible for several cycles with quantitative conversion. Switching was monitored by UV-Vis absorption spectroscopy as the two copper complexes have different colors (Cu(I) is red-orange, Cu(II) is yellow-green). The effect of the oxidation state of the metal ion on the binding of the diaminotriazine receptor to its imide substrate was also observed by <sup>1</sup>H NMR spectroscopy. The presence of Cu(I) lowered the affinity of receptor **17** for *N*-butyluracil, reflected by an upfield shift of the uracil N—H proton, and turned the binding off. Oxidation of Cu(I), however, caused a downfield shift of this signal indicating that the binding was turned on. These results indicate that the copper complexes of receptor **17** have all the characteristics of a molecular machine. Energy for mechanical movement of the components of these machines can be supplied by electricity and monitored by light absorbance. Movement of the component parts can lead to reversible binding or release of a substrate and this task can be repeated many times at will. The next level of development of this project will be incorporation of an "active site" that can change the substrate. The receptor will be more like an enzyme, a molecule on which a bound substrate is processed into

products and released. Such a controlled catalyst that can be mounted on an electrode is valuable for processing of organic compounds.

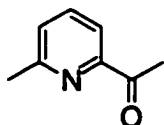
### 3.9 Experimental

**General Information.** All solvents (Caledonia) for synthesis and purification were used as received. Solvents used for UV-Vis absorption and fluorescence spectroscopy analysis were deoxygenated by bubbling argon through the solvent. Solvents used for NMR analysis (Cambridge Isotope Laboratories) were used as received. All reagents and starting materials were purchased from Aldrich or Acros Organics.

<sup>1</sup>H NMR characterizations were performed on a Varian Inova-300 instrument, working at 299.96 MHz, or on a Varian Inova-500 instrument, working at 499.92 MHz. Chemical shifts ( $\delta$ ) are reported in parts per million relative to tetramethylsilane using the residual solvent peak as a reference standard. Coupling constants ( $J$ ) are reported in hertz. <sup>13</sup>C NMR characterizations were performed on a Bruker-300 instrument, working at 74.99 MHz or a Varian Inova-500 instrument, working at 125.29 MHz. FT-IR measurements were performed using a Nicolet Magna-IR 750. UV-Vis spectra were recorded on a Varian Cary 400 Scan spectrophotometer.

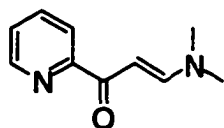
Mass spectrometry measurements were performed a Kratos MS-50 with an electron impact source or by positive mode electrospray ionization on a Micromass ZabSpec Hybrid Sector-TOF. The liquid carrier was infused into the electrospray source by means of a Harvard syringe pump at a flow rate of 10  $\mu$ L/minute. The sample solution, in the same solvent, was introduced *via* a 1  $\mu$ L-loop-injector. Pre-purified nitrogen was used as a spray pneumatic aid and filtered air as the bath gas, heated at *ca.* 80 °C. For low resolution, the mass spectra were acquired by magnet scan at a rate of 5 seconds/decade at *ca.* 1000 resolution. For exact mass measurements, the spectra were obtained by voltage scan over a narrow mass range at *ca.* 10000 resolution. Data acquisition and processing was achieved by using the OPUS software package on a Digital Alpha station with VMS operating system.

**Electrochemistry experiments.** Cyclic voltammetry experiments was performed using a platinum electrode, a platinum counter electrode, and an Ag/AgCl reference electrode in a glass cell. All experiments were run at room temperature under argon using a PINE bipotentiostat and tetrabutylammonium hexafluorophosphate ( $10^{-3}$  M) as the electrolyte in deoxygenated  $\text{CH}_3\text{CN}$ . The CV was measured at 200mV/sec potential sweep rate. Electrolysis was conducted under the same conditions after replacing the platinum electrode with platinum-wire (0.5 mm diameter, 50 cm long) coil. The electrode was set a controlled potential with a maximum current of 500  $\mu\text{A}$ .

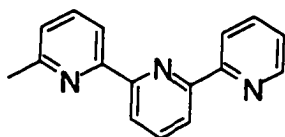


**1-(6-Methylpyridin-2-yl)ethanone (12).**<sup>7</sup> A solution of *n*-BuLi in hexane (7.2 mL, 2.5 M) was injected into dry THF (80 mL) and the mixture was stirred at  $-80^\circ\text{C}$  (dry-ice/acetone bath) under argon. A solution of 2-bromo-6-methylpyridine (3 g, 17 mmol) in dry THF (140 mL) was added dropwise while maintaining the temperature of the reaction solution below  $-75^\circ\text{C}$ . After stirring for 1 h at  $-78^\circ\text{C}$ , a solution of dimethyl acetamide (2 mL) in THF (40 mL) was added dropwise and the mixture was further stirred for 2 h at  $-78^\circ\text{C}$ . The cooling bath was removed and the mixture was left to warm to  $-10^\circ\text{C}$ . At this time, an HCl solution (6N, 16 mL) was added slowly and the mixture warmed to room temperature. The mixture was then concentrated under vacuum to half its volume and treated with concentrated NaOH solution until a pH value of 9 was achieved. The solution was extracted with  $\text{CHCl}_3$  ( $3 \times 20$  mL) and the combined organic layers were dried over  $\text{Na}_2\text{SO}_4$ , filtered and evaporated under reduced pressure to afford a

yellow oil (2.0 g, 60%).  $^1\text{H NMR}$  (300 MHz,  $\text{CDCl}_3$ )  $\delta$  7.79 (d,  $J=8$  Hz, 1H), 7.66 (t,  $J=8$  Hz, 1H), 7.27 (d,  $J=8$  Hz, 1H), 2.68 (s, 3H), 2.58 (s, 3H).

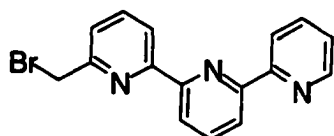


**(2E)-3-(Dimethylamino)-1-pyridin-2-ylprop-2-en-1-one (13).**<sup>8</sup> A mixture of 2-acetylpyridine (5.0 g, 41.3 mmol) and *N,N*-dimethylformamide dimethyl acetal (6.0 g, 50.2 mmol) in toluene (25 mL) was heated at reflux in an apparatus fitted with a Dean-Starck condenser for 15 h. After cooling to room temperature, the solvent was evaporated under vacuum to afford an oily residue. Cyclohexane (100 mL) was added causing the crystallization of a yellow solid that was filtered off and air dried (7.9 g, 75%). M.p. 126–128 °C (lit.<sup>8</sup> 125–127 °C);  $^1\text{H NMR}$  (300 MHz,  $\text{CDCl}_3$ )  $\delta$  8.59 (d,  $J=5$  Hz, 1H), 8.13 (d,  $J=8$  Hz, 1H), 7.86 (d,  $J=13$  Hz, 1H), 7.77 (dt,  $J_1=6$  Hz,  $J_2=2$  Hz, 1H), 7.33 (dt,  $J_1=5$  Hz,  $J_2=2$  Hz, 1H), 6.44 (d,  $J=13$  Hz, 1H), 3.16 (s, 3H), 2.980 (s, 3H).

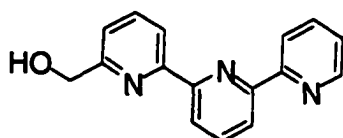


**6-Methyl-2,2':6',2''-terpyridine (14).**<sup>8</sup> A mixture of *t*-BuOK (2.24 g, 20.0 mmol), and 2-acetyl 6-methylpyridine (1.35 g, 10.0 mmol) in dry THF (50 mL) was stirred for 2 h at room temperature under argon. (2E)-3-(Dimethylamino)-1-pyridin-2-ylprop-2-en-1-one (13) (1.76 g, 10.0 mmol) was added in a single portion and the mixture was further stirred for 15 h. Then, a solution of ammonium acetate (7.7 g, 100 mmol) in acetic acid (25 mL) was added and the mixture was heated at reflux for 2 h. After cooling to room temperature, the solvent was evaporated under reduced pressure to afford a black sticky

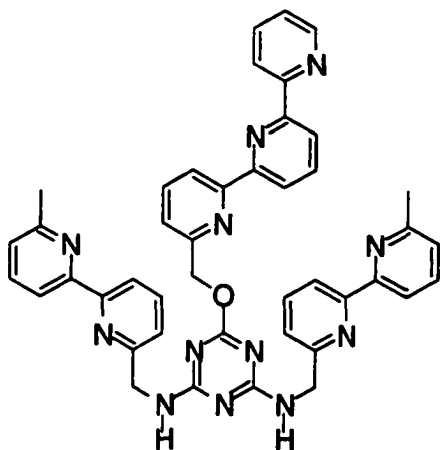
residue which was treated with water (200 mL). The solution was then neutralized with  $\text{Na}_2\text{CO}_3$  and the mixture was extracted with  $\text{CHCl}_3$  ( $3 \times 50$  mL). The combined organic layers were evaporated under reduced pressure to afford a black sticky residue. The product was isolated by flash chromatography (alumina, 1:1  $\text{CH}_2\text{Cl}_2$ /hexane) as a yellow-brown solid (3.0 g, 61%). M.p. 108-110 °C (lit.<sup>8</sup> 111-113 °C);  $^1\text{H}$  NMR (300 MHz,  $\text{CDCl}_3$ )  $\delta$  8.68 (dd,  $J_1=4$  Hz,  $J_2=1$  Hz, 1H), 8.61 (dd,  $J_1=8$  Hz,  $J_2=1$  Hz, 1H), 7.83 (dt,  $J_1=8$  Hz,  $J_2=1$  Hz, 1H), 8.40 (dd,  $J_1=8$  Hz,  $J_2=1$  Hz, 2H), 7.92 (t,  $J=8$  Hz, 1H), 7.83 (dt,  $J_1=8$  Hz,  $J_2=1$  Hz, 1H), 7.72 (t,  $J=7.8$  Hz, 1H), 7.30 (dd,  $J_1=5$  Hz,  $J_2=1$  Hz, 1H), 7.16 (dd,  $J_1=7$  Hz,  $J_2=1$  Hz, 1H), 2.62 (s, 3H).



**6-(Bromomethyl)-2,2':6',2''-terpyridine (15).**<sup>9</sup> A mixture of 6-methyl-2,2':6',2''-terpyridine (0.4 g, 1.60 mmol), NBS (0.30 g, 1.70 mmol), AIBN (50 mg) and  $\text{CCl}_4$  (20 mL) was heated at reflux for 6 h under argon. The mixture was filtered while hot and the filtrate was evaporated under vacuum to afford a yellow solid. The product was isolated by flash chromatography (alumina, 3:2  $\text{CHCl}_3$ /toluene) as a white solid (0.25 g, 48%). M.p. 118-120 °C (lit.<sup>9</sup> 124-125 °C);  $^1\text{H}$  NMR (300 MHz,  $\text{CDCl}_3$ )  $\delta$  8.69 (dd,  $J_1=5$  Hz,  $J_2=1$  Hz, 1H), 8.60 (dd,  $J_1=8$  Hz,  $J_2=2$  Hz, 1H), 8.52 (dd,  $J_1=8$  Hz,  $J_2=1$  Hz, 1H), 8.46 (dt,  $J_1=8$  Hz,  $J_2=1$  Hz, 1H), 7.94 (t,  $J=8$  Hz, 1H), 7.84 (dt,  $J_1=8$  Hz,  $J_2=1$  Hz, 2H), 7.47 (dd,  $J_1=7$  Hz,  $J_2=1$  Hz, 1H), 7.26-7.34 (m, 1H), 4.46 (s, 2H).



**2,2':6',2''-Terpyridin-6-ylmethanol (16).**<sup>9</sup> A mixture of 6-bromomethyl-2,2':6',2''-terpyridine (0.5 g, 1.9 mmol) and sodium acetate (1.6 g, 19 mmol) in DMF (3 mL) was heated at 140 °C for 20 h. After cooling to room temperature, the mixture was added to water (20 mL) and the aqueous layer was extracted with CH<sub>2</sub>Cl<sub>2</sub> (3 × 10 mL). The combined organic layers were dried (Na<sub>2</sub>SO<sub>4</sub>), filtered, and evaporated under vacuum to leave a brown residue. This residue was dissolved in MeOH (30 mL), treated with NaOH (0.2 g, 5 mmol) and heated at reflux for 3 h. After cooling to room temperature, the solvent was evaporated under vacuum and the residue was dissolved in water (30 mL). The solution was neutralized with dilute HCl and extracted with CH<sub>2</sub>Cl<sub>2</sub> (3 × 10 mL). The combined organic layers were dried over Na<sub>2</sub>SO<sub>4</sub>, filtered and evaporated to afford a yellow residue. The product was isolated by column chromatography (alumina, a gradient of 1-5% MeOH in CH<sub>2</sub>Cl) as a beige solid (0.3 g, 61%). M.p. 109-111 °C (lit.<sup>9</sup> 111-112 °C); <sup>1</sup>H NMR (500 MHz, CDCl<sub>3</sub>) δ 8.70 (m, 1H), 8.61 (dt, *J*<sub>1</sub>=8.0 Hz, *J*<sub>2</sub>=1.0 Hz, 1H), 8.54 (d, *J*=8 Hz, 1H), 8.47 (m, 2H), 7.97 (t, *J*=8 Hz, 1H), 7.85 (td, *J*<sub>1</sub>=8.0 Hz, *J*<sub>2</sub>=1.0 Hz, 2H), 7.34 (m, 1H), 7.26 (d, *J*=8 Hz, 1H), 4.84, (s, 2H), 4.00 (br s, 1H).



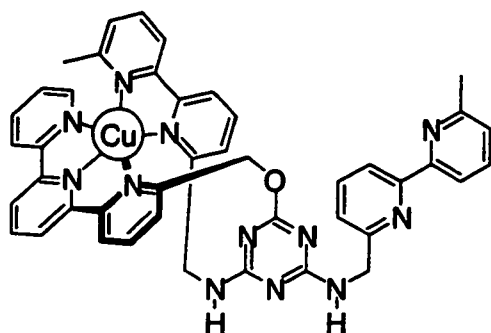
***N,N'*-Bis[(6'-methyl-2,2'-bipyridin-6-yl)methyl]-6-(2,2':6',2''-terpyridin-6-ylmethoxy)-1,3,5-triazine-2,4-diamine (17).** A solution of 6-aminomethyl-6'-methyl-



2,2'-bipyridine (**4**) (0.25 g, 1.25 mmol) and triethylamine (0.13 g, 1.25 mmol) in freshly distilled THF (10 mL) was added dropwise (15–30 min) to a solution of cyanuric chloride (0.23 g, 1.25 mmol) in freshly distilled THF (20 mL) at 0°C under argon. After the addition was complete, the mixture was allowed to warm to room temperature, then it was stirred for 1 h. The reaction mixture was then heated in an oil bath at 40–50°C, and an additional batch of 6-aminomethyl-6'-methyl-2,2'-bipyridine (1.25 mmol) and triethylamine (1.25 mmol) in THF (10 mL) was added dropwise. After stirring at this temperature for 5–6 h, the reaction was cooled and concentrated to dryness under vacuum. The residue was dissolved in EtOAc (20 mL), washed with water (3 × 10 mL), dried over Na<sub>2</sub>SO<sub>4</sub>, filtered, and concentrated affording a crude solid that was used without further purification. The crude solid was added to a mixture of 6-hydroxymethyl-2,2';6',2"-terpyridine (0.33 g, 1.25 mmol), NaH (30 mg, 1.25 mmol) and dry THF (20 mL). After heating at reflux under argon overnight, the reaction was cooled and concentrated to dryness. The residue was taken up in EtOAc (25 mL), washed with water (3 × 10 mL), dried over Na<sub>2</sub>SO<sub>4</sub> and concentrated under vacuum. The residue was purified by flash chromatography (alumina 1:1 hexane/EtOAc) and recrystallized from hexane/EtOAc to afford the product as a white solid (0.4g, 43%). M.p. 174–176 °C; <sup>1</sup>H NMR (500 MHz, CDCl<sub>3</sub>) δ 8.68 (m, 1H), 8.61 (d, *J*=8.5 Hz, 1H), 8.47 (br d, *J*=8.0 Hz, 2H), 8.41 (d, *J*=8.0 Hz, 1H), 8.27 (br t, *J*=6.5 Hz, 2H), 8.21 (br t, *J*=6.5 Hz, 2H), 7.89 (br t, *J*=8.0 Hz, 1H), 7.84 (dt, *J*<sub>1</sub>=8.0, *J*<sub>2</sub>=1.5 Hz, 2H), 7.79 (br s, 1H), 7.68 (br d, *J*=6.5 Hz, 4H), 7.50 (br s, 1H), 7.31 (m, 2H), 7.14 (d, *J*=8.0 Hz, 2H), 6.28 (br s, 2H) 5.62 (s, 2H), 4.79 (br s, 4H), 2.60 (s, 6H); <sup>13</sup>C NMR (125.7 MHz, CDCl<sub>3</sub>) δ 167.4, 157.9, 156.7, 156.3, 155.8, 155.5, 155.3, 149.2, 137.8, 137.5, 137.1, 136.9, 123.7, 123.4, 121.7, 121.2, 120.9, 119.8, 119.6, 118.2, 69.1, 68.8, 46.2, 45.9, 24.7; FT-IR ν 3405, 3264, 3058, 2925, 1569, 1551, 1438, 1427, 1384, 1336, 1265, 115, 1081, 991, 813, 779, 738, 632 cm<sup>-1</sup>; HRMS



1336, 1149, 1062, 844, 781  $\text{cm}^{-1}$ ; UV-Vis ( $\text{CH}_3\text{CN}$ )  $\lambda_{\text{max}}/\text{nm}$  ( $\log \epsilon/\text{M}^{-1} \text{cm}^{-1}$ ) 450 (5700); HRMS (ES)  $m/z$  799.24454  $[\text{M}]^+$ ,  $\text{C}_{43}\text{H}_{36}\text{CuN}_{12}\text{O}$ ; calculated 799.2431  $[\text{M}]^+$ ,  $\text{C}_{43}\text{H}_{36}\text{CuN}_{12}\text{O}$ .



**[Cu(17)](OTf)<sub>2</sub>.** A solution of 17 (50 mg, 0.07 mmol) in  $\text{CHCl}_3/\text{CH}_3\text{CN}$  (1:1, 3.0 mL) was treated with  $\text{Cu}(\text{OTf})_2$  (25 mg, 0.07 mmol). After stirring at room temperature for 1 h,  $\text{Et}_2\text{O}$  (10 mL) was added and the green precipitate that formed was collected by filtration, washed with  $\text{Et}_2\text{O}$  (5 mL) and dried under vacuum (69 mg, 93%).  $^1\text{H}$  NMR (500 MHz,  $\text{CD}_3\text{CN}$ )  $\delta$  8.33 (d,  $J=7.5$  Hz, 2H), 8.22 (d,  $J=6.5$  Hz, 2H), 8.19 (br s, 2H), 8.12 (br s, 2H), 7.78 (br s, 4H), 7.44 (d,  $J=7.0$  Hz, 1H), 7.37 (br s, 1H), 7.25 (br s, 4H), 7.18 (br s, 2H), 6.62 (br s, 1H), 6.50 (br s, 2H), 4.78 (br d,  $J=2.1$  Hz, 2H), 4.49 (br s, 4H), 4.36 (br s, 2H), 2.58 (s, 3H), 2.55 (s, 3H); FT-IR  $\nu$  3426, 3104, 2923, 1583, 1440, 1332, 1253, 1149, 1012, 842, 782  $\text{cm}^{-1}$ ; UV-Vis ( $\text{CH}_3\text{CN}$ )  $\lambda_{\text{max}}/\text{nm}$  ( $\log \epsilon/\text{M}^{-1} \text{cm}^{-1}$ ) 690 (102); HRMS (ES)  $m/z$ : 948.194858  $[\text{M}+\text{OTf}]^+$ ,  $\text{C}_{44}\text{H}_{36}\text{CuF}_3\text{N}_{12}\text{O}_4\text{S}$ ; calculated 948.195129  $[\text{M}+\text{OTf}]^+$ ,  $\text{C}_{44}\text{H}_{36}\text{CuF}_3\text{N}_{12}\text{O}_4\text{S}$ .

### 3.10 References

1. For recent reviews about "Molecular Machines" see: (a) C. Bustamante, D. Keller, G. Oster, *Acc. Chem. Res.* **2001**, *34*, 412; (b) A. N. Shipway, I. Willner, *Acc. Chem. Res.* **2001**, *34*, 421; (c) A. R. Pease, J. O. Jeppesen, J. F. Stoddart, Y. Luo, C. P. Collier, J. R. Heath, *Acc. Chem. Res.* **2001**, *34*, 433; (d) R. Ballardini, V. Balzani, A. Credi, M. T. Gandolfi, M. Venturi, *Acc. Chem. Res.* **2001**, *34*, 445; (e) A. Harada, *Acc. Chem. Res.* **2001**, *34*, 456; (f) C. A. Schalley, K. Beizai, F. Vögtle, *Acc. Chem. Res.* **2001**, *34*, 465; (g) J.-P. Collin, C. Dietrich-Buchecker, P. Gaviña, M. C. Jimenez-Molero, J.-P. Sauvage, *Acc. Chem. Res.* **2001**, *34*, 477; (h) V. Amendola, L. Fabbrizzi, C. Mangano, P. *Acc. Chem. Res.* **2001**, *34*, 488; (i) S. Shinkai, M. Ikeda, A. Sugasaki, M. Takeuchi, *Acc. Chem. Res.* **2001**, *34*, 494; (j) B. L. Feringa, *Acc. Chem. Res.* **2001**, *34*, 504; (k) T. R. Kelly, *Acc. Chem. Res.* **2001**, *34*, 514; (l) V. Balzani, A. Credi, F. Raymo, J. F. Stoddart, *Angew. Chem. Int. Ed.* **2000**, *39*, 3348.
2. (a) A. P. de Sliva, C. P. McCoy, *Chem. Ind.* **1994**, 992; (b) L. Fabbrizzi, A. Poggi, *Chem. Soc. Rev.* **1995**, *24*, 197; (c) A. C. Benniston, *Chem. Soc. Rev.* **1996**, *25*, 427; (d) M. Gómez-López, J. A. Preece, J. F. Stoddart, *Nanotechnology* **1996**, *7*, 183; (e) M. D. Ward, *Chem. Ind.* **1997**, 640; (f) P. D. Beer, *Acc. Chem. Res.* **1998**, *31*, 71; (g) P. L. Boulas, M. Gómez-López, L. Echegoyen, *Angew. Chem. Int. Ed.* **1998**, *37*, 216; (h) V. Balzani, M. Gómez-López, J. F. Stoddart, *Acc. Chem. Res.* **1998**, *31*, 405; (i) J.-P. Sauvage, *Acc. Chem. Res.* **1998**, *31*, 611; (j) J.-C. Chambron, J.-P. Sauvage, *Chem. Eur. J.* **1998**, *4*, 1362;
3. (a) R. Deans, A. Niemz, E. Breinlinger, V. Rotello, *J. Am. Chem. Soc.* **1997**, *119*, 10863; (b) A. Niemz, V. Rotello, *Acc. Chem. Res.* **1999**, *3*, 747; (c) A. Boal, V. Rotello, *J. Am. Chem. Soc.* **1999**, *121*, 9419.

4. (a) C. Canevet, J. Libman, A. Shanzer, *Angew. Chem. Int. Ed.* **1996**, *35*, 2657; (b) L. Zelikovich, J. Libman, A. Shanzer, *Nature* **1995**, *374*, 790.
5. (a) J.-M. Kern, L. Raehm, J.-P. Sauvage, B. Divisia-Blohorn, P.-L. Vidal, *Inorg. Chem.* **2000**, *39*, 1555; (b) L. Raehm, J.-M. Kern, J.-P. Sauvage, *Chem. Eur. J.* **1999**, *5*, 3310; (c) A. Livoreil, J.-P. Sauvage, N. Armaroli, V. Balzani, L. Flamigni, b. Ventura, *J. Am. Chem. Soc.* **1997**, *119*, 12114; (d) J.-P. Collin, P. Gavina, J.-P. Sauvage, *Chem. Comm.* **1996**, 2005; (e) A. Livoreil, O. Dietrich-Buchecker, J.-P. Sauvage, *J. Am. Chem. Soc.* **1994**, *116*, 9399.
6. I. Willner, J. Rosengaus and S. Biali, *Tetrahedron Lett.*, **1992**, *33*, 3805.
7. K. T. Potts, K. A. G. Raiford, M. Kesharvarzk, *J. Am. Chem. Soc.*, **1993**, *115*, 2803.
8. D. L. Janeson, L. E. Gusie, *Tetrahedron. Lett.* **1991**, *32*, 1999.
9. J. Uenishi, T. Tanaka, K. Nishiwaki, S. Wakabayashi, S. Oae, H. Tsukube, *J. Org. Chem.* **1993**, *58*, 4382.
10. (a) K. P. Madhusudanan, B. A. Bhat, S. N. Suryawanshi, *Rapid Comm. Mass Spec.* **2001**, *15*, 788; (b) O. Schramel, B. Michalke, A. Kettrup, *J. Chromat A.* **1998**, *819*, 231; (c) B. J. Hall, J. S. Brodbelt, *J. Am. Chem. Soc. Mass Spec.* **1999**, *10*, 402.

## Chapter 4 – Metal Ions as Allosteric Inhibitors of Hydrogen Bonding Receptors

### Approach 2: Cavity Size Alteration

#### 4.1 Introduction to the Cavity Size Alteration Approach

The previous two chapters introduced the use of metal ions as allosteric cofactors where they effectively destroy the hydrogen bonding molecular recognition surface responsible for interacting with the substrate. This chapter introduces an alternative to distorting a molecular recognition site. The receptors described here were designed such that the binding of the cofactor alters the accessibility to and the size of the binding pocket rendering it unsuitable to accommodate the guest species (Figure 4.1). In this approach, the shape and the multiple-point hydrogen bonding surface of the binding pocket is not altered or deformed upon the binding of the cofactor. Instead, the allosteric binding of the cofactor induces conformational changes that block the entrance of the binding pocket and cause minor shrinkage in its size. These two factors furnish the basis for the negative allosteric effect of the metal.

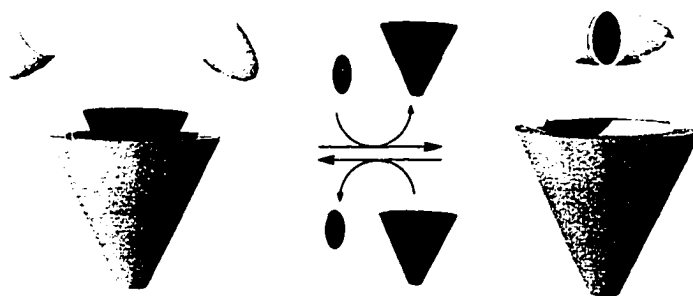


**Figure 4.1** A schematic representation of the cavity-size alteration approach. The binding of the allosteric cofactor (●) within the allosteric binding site blocks entrance of the substrate (▼) to the active site.

Barbituric acid derivatives were chosen as the target substrates since their binding is well understood and receptors specific for them are easy to prepare.<sup>1-3</sup> Barbiturates

have a framework containing eight potential hydrogen bonding sites: two N–H hydrogen bond donors and six carbonyl oxygen lone pairs that act as hydrogen bond acceptors (Figure 4.2). Two of the lone pairs on the carbonyl groups at C-4 and C-6 are usually not accessible for hydrogen bonding due to the steric effect of the substituents at the 5-position. Therefore, a barbiturate guest typically provides two divergent hydrogen bonding donor-acceptor-donor (DAD) arrays. A suitable receptor for barbiturates must, therefore, provide a triangular-shaped cleft with two convergent hydrogen bonding acceptor-donor-acceptor arrays to furnish a complementary binding site for the substrate.

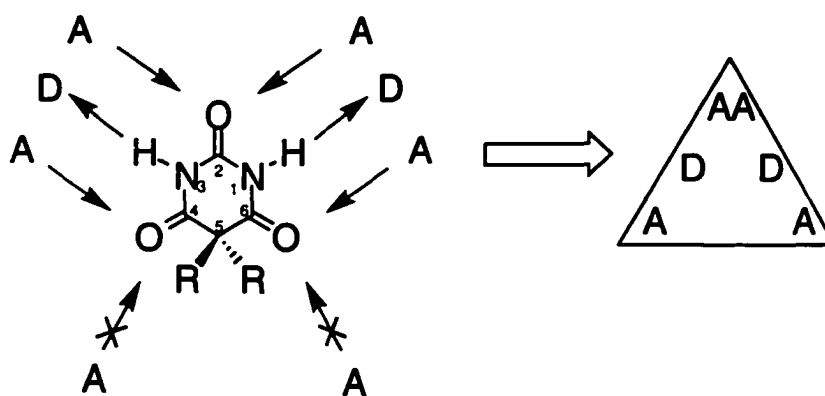


**Figure 4.2** The hydrogen-bonding motif of 5,5-disubstituted barbiturate

#### 4.2 Designing A Specific Allosteric Receptor for Barbiturate Guests

The receptor was designed based on the framework previously reported by Hamilton and coworkers.<sup>1</sup> They have reported the binding of barbiturates using macrocyclic and acyclic receptors containing two 2,6-diaminopyridine units linked via an isophthoyl group (X) (Figure 4.3). The diaminopyridine unit provides the complementary donor-acceptor-donor hydrogen bonding surface suitable for binding the barbiturate guest. The isophthoyl spacer furnishes the correct shape and size of the binding pocket and prevents intramolecular hydrogen bonding between the two

diaminopyridine units. In the case of the cyclic receptors, another spacer (Y) was varied to achieve some selectivity in binding barbiturates based on the different substituents ( $R_1$  and  $R_2$ ) at position 5. However, no significant selectivity was observed. These cyclic receptors associated much more strongly ( $K_a = 10^6 \text{ M}^{-1}$ ) with barbiturate derivatives than did their flexible acyclic counterparts ( $K_a = 10^3 \text{ M}^{-1}$ )<sup>3b,4</sup> due to high entropy loss associated with the binding of the latter to the guest leading to the formation of a less stable host-guest complex.

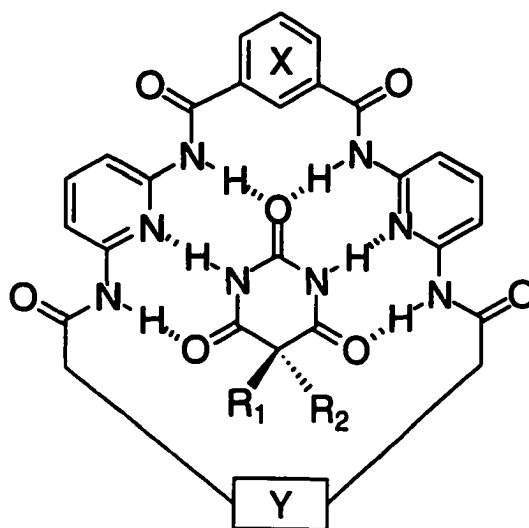
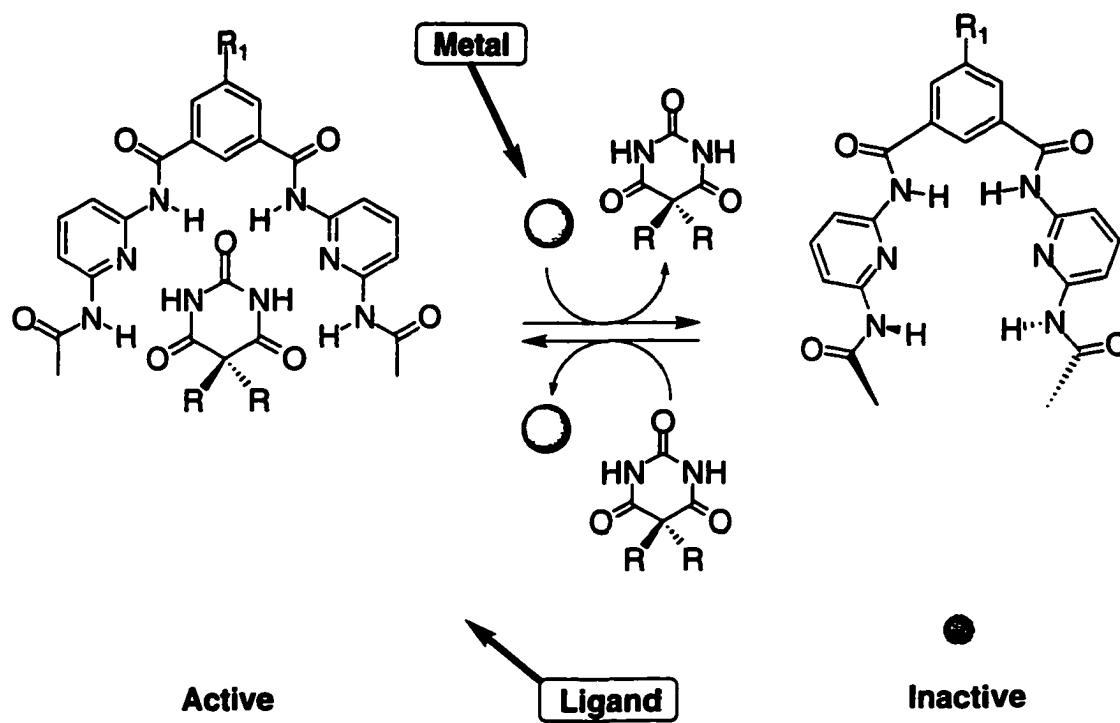


**Figure 4.3** A schematic representation of Hamilton's receptor for barbiturates.<sup>1</sup> The spacer Y is a variable group that is absent in acyclic receptors.

The targeted receptor is composed of two diaminopyridines units linked together by an isophthyl group, while the other amino groups are appended by two metal-coordinating ligands through amide linkages (Scheme 4.1). In the presence of a metal ion, the ligands swing towards each other to chelate the metal. This metal complexation blocks the entrance of the guest into the hydrogen bonding pocket and forces the two aminopyridine groups to be closer to each other causing a shrinkage in the binding cavity.



These effects render the binding site unsuitable to accommodate the guest and, as a result, the binding of the barbiturate by the receptor is inhibited (Scheme 4.1).



Scheme 4.1

### 4.3 Synthesis of the Bipyridyl Receptor 26

Analogous to the triaminotriazine and urea receptors (6 and 7) described in Chapter 2, receptor 26 was designed such that the allosteric binding site is a 6,6'-disubstituted-2,2'-bipyridine ligand and the copper ion is used as a negative allosteric cofactor. The chelation of the metal ion by the bipyridine ligands should block the entrance of the substrate to the binding pocket. Molecular modeling suggests that metal binding should also alter the size of the pocket and the hydrogen bonding surface rendering the binding site unsuitable for binding the barbiturate (Figure 4.4).

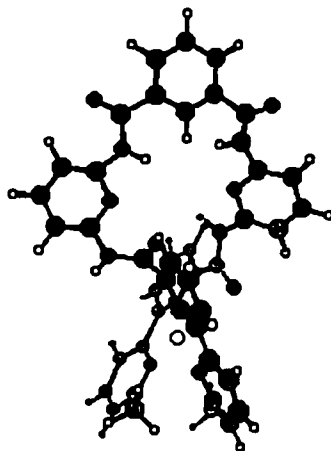
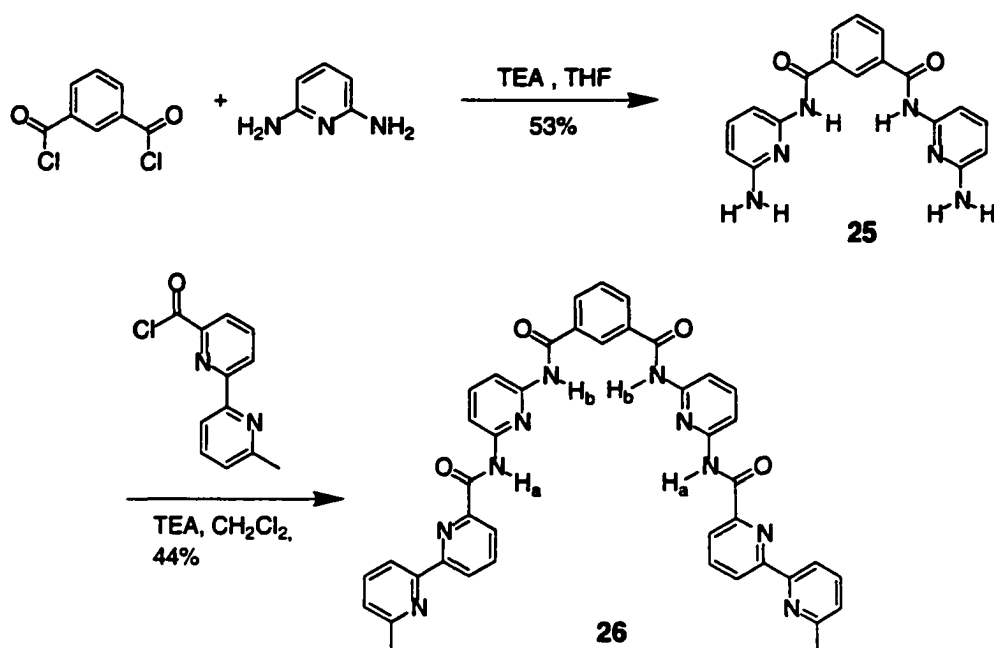


**Figure 4.4** The structure of the metal complex of bipyrindyl receptor **26** generated by MacroModel® software. The structure shows the tetrahedral coordination of the metal ion by the bipyridine ligands blocking the entrance to the binding pocket. The size and the shape of the cavity is altered and a rotation in one of the N—H bonds of the hydrogen bonding surface is also noticed.

A series of receptors were prepared using a procedure adapted from the literature.<sup>1a</sup> The synthesis began with the preparation of the *N,N'*-bis(6-aminopyridin-2-yl)-isophthalamide **25** scaffold which was prepared in 53% yield by adding a THF solution of isophthoyl chloride into an excess of 2,6-diaminopyridine in dry THF (Scheme 4.2). The appearance in the <sup>1</sup>H NMR spectrum of a broad singlet at 10.25 ppm corresponding to the N—H protons clearly reveals the formation of the amide group. The signals corresponding to the N—H protons of the amino group appeared at 5.78 ppm.

Receptor **26** was prepared in 44% yield by the reaction of **25** with the acid chloride of 6'-methyl-2,2'-bipyridine-6-carboxylic acid **22** in dry CH<sub>2</sub>Cl<sub>2</sub> (Scheme 4.2). The <sup>1</sup>H NMR (CDCl<sub>3</sub>) spectrum showed the signal corresponding to the N—H proton (H<sub>a</sub>) of the newly formed amide group at 10.34 ppm. The appearance of the molecular ion peak at *m/z*=741.2845 in the electrospray mass spectrum further supports that the targeted receptor **26** was obtained.



It was observed that the signal corresponding to the amide  $H_a$  protons (Scheme 4.2) at 10.34 ppm is further downfield than would be expected for these types of protons which have been previously reported to appear between 8.2 and 8.8 ppm.<sup>1,3</sup> The signal that corresponds to the  $H_b$  protons appeared at 8.58 ppm similar to previously reported data. These observations imply that  $H_a$  must be involved in hydrogen bonding. Also, because the chemical shift of the signal corresponding to  $H_a$  protons of the bipyridyl **26** did not change their position or shape upon diluting the solution, it was concluded that any hydrogen bonding present was not intermolecular. It can be concluded that the downfield shift is due to the presence of an intramolecular hydrogen bond between  $H_a$  and a hydrogen bond acceptor, most likely one of the nitrogen atoms in the bipyridine rings or one of the oxygen atoms of the carbonyl groups.

## 4.4 Binding Studies

### 4.4.1 Studies on the Binding of the Bipyridyl Receptor **26** to Barbiturate Guests

The binding efficacy of the bipyridyl receptor **26** to its barbiturate substrate was evaluated by monitoring the changes in the chemical shifts of the signals corresponding to protons  $H_a$  and  $H_b$ , which are involved in the recognition process, upon the addition of the substrate. A solution of the bipyridyl receptor **26** (5 mM) in  $CD_2Cl_2$  was treated with aliquot amounts of 5,5-dibutylbarbiturate solution (100 mM) in the same solvent. Before the addition of the substrate, the signals for protons  $H_a$  and  $H_b$  appeared at 10.35 and 8.83 ppm, respectively. As 5,5-dibutylbarbiturate was added, there was insignificant changes in the positions ( $\Delta\delta$  less than 0.1 ppm) of the signals corresponding to the N—H protons  $H_a$  (Figure 4.5 (A)) and  $H_b$  (Figure 4.5 (B)). This observation indicates that there were no effective hydrogen bonds formed between the bipyridyl receptor and the barbiturate. As a consequence, the titration curves of the collected data sets were too shallow to be fit to any binding model implying that receptor **26** exhibits a very low and uncharacterizable affinity for its barbiturate guest.

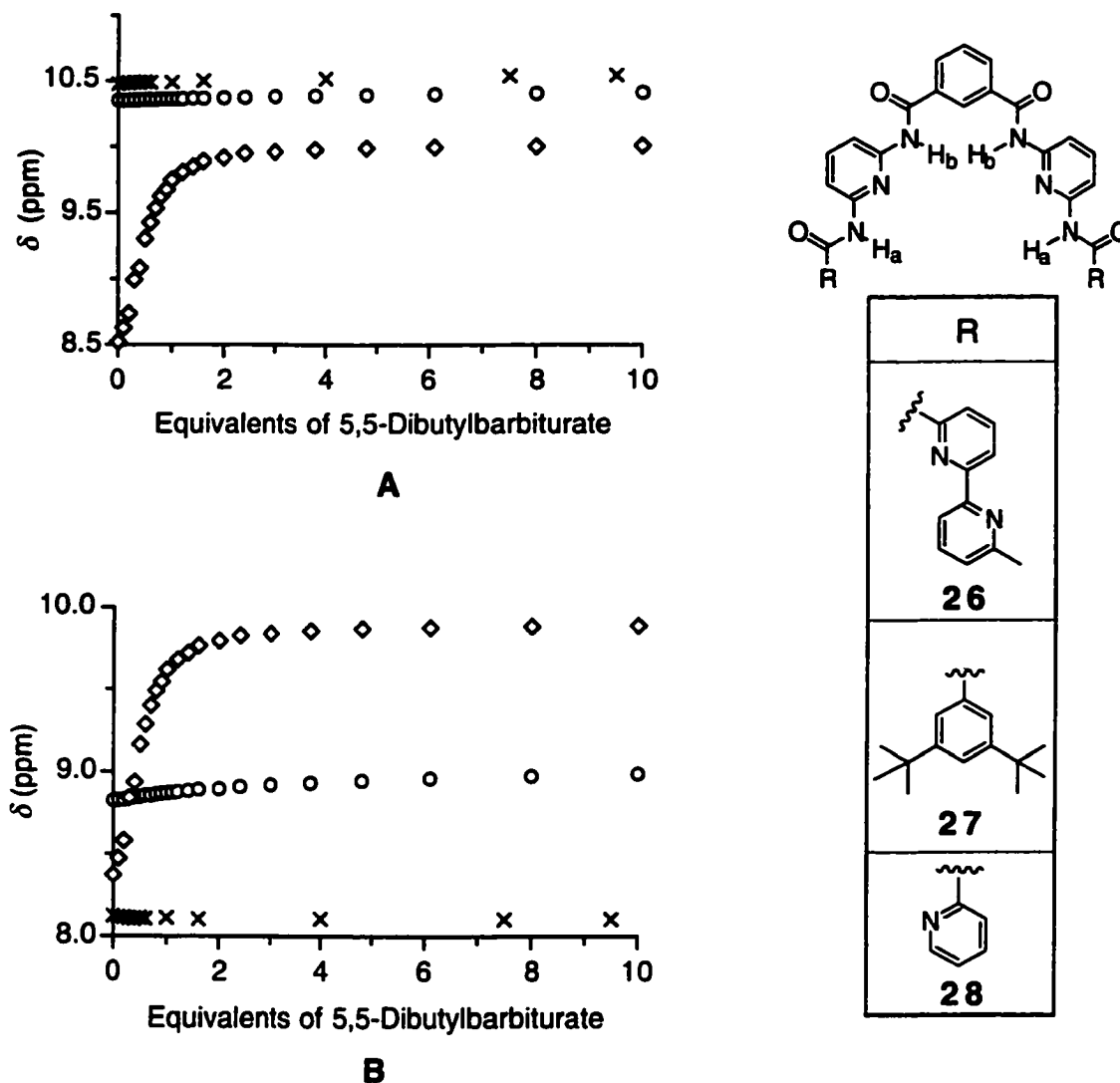


**Figure 4.5** Titration curves for receptors **26**, **27**, and **28**. Changes in the chemical shifts of  $H_a$  (A) and  $H_b$  (B) for receptors (5 mM) **26** (o), **27** ( $\diamond$ ) and **28** (x) upon the addition of 5,5-dibutylbarbiturate (100 mM) in  $CD_2Cl_2$ .

Such a low affinity is surprising as previously reported examples of similar acyclic receptors displayed high affinity for barbiturate derivatives ( $K_a = 10^4 M^{-1}$ ).<sup>1b,2,3</sup> However, these previously reported systems differ from the bipyridyl receptor **26** as they do not have aromatic rings directly attached to the 2,6-diaminopyridyl group but, instead, alkyl chains. These observations raised many issues about the rationale of the design of receptor **26** that needed to be investigated individually. First, the bipyridine ligands are

composed of electron withdrawing heterocyclic rings that, because they are conjugated with the amide group bearing  $H_a$ , will exert a different electronic effect on the  $H_a$  protons than will the alkyl chains in the previously reported systems (Figure 4.6). Second, the steric effect of a long flexible alkyl chain is different from that of an aromatic ring which could block the entrance of the binding pocket and inhibit the binding of the substrate even in the absence of the metallic allosteric cofactor. Finally, the alkyl chains of the previously reported systems lacks any heteroatoms that could play the role of hydrogen bond acceptors in the intramolecular hydrogen bonds to  $H_a$ . Such acceptors, however, may be provided by the nitrogen atoms on either of the bipyridine rings (C or D) in receptor **26**. The effect of these intramolecular hydrogen bonds on the receptor's affinity for its barbiturate substrate is not clear. Therefore, in order to address these three points of concern, it was important to investigate model receptors in which each point is studied separately from the others.

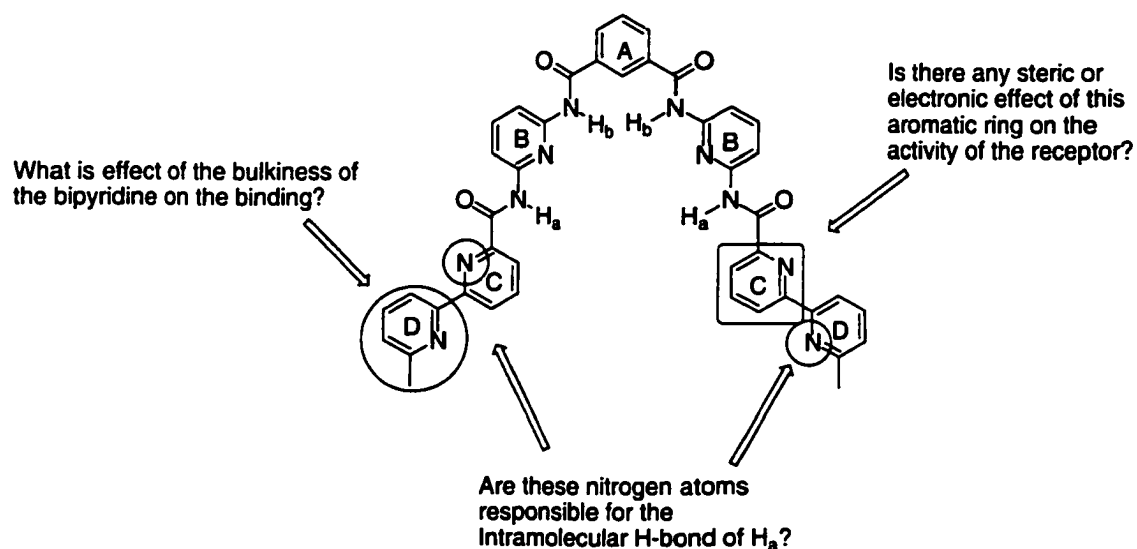


**Figure 4.6** The possible effects of bipyridine substituents on the binding of receptor **26**

## 4.4.2 Binding Studies on the Model Receptors for the Bipyridyl Receptor 26

### 4.4.2.1 Design, Synthesis and Binding Studies of the Di-*tert*-butyl Receptor 27

In order to study the electronic and the steric effect that the aromatic rings labeled as 'C' in Scheme 4.4 has on the affinity of the bipyridyl receptor **26** for its barbiturate substrate, model receptor **27** was designed such that two bulky aromatic groups replace the bipyridine ligands (Figure 4.7). If the steric bulk of the C-rings is blocking the substrate's entrance to binding pocket, then the di-*tert*-butylphenyl receptor **27** should exhibit an even lower affinity. This is because 3,5-di-*tert*-butylphenyl groups are bulkier than the pyridine rings in **26** and, thus, it should be even harder for the substrate to reach the binding pocket in receptor **27**. However, if the di-*tert*-butylphenyl receptor **27** exhibited a high affinity for barbiturates, this will rule out the steric effect of the C-rings as a reason for the low association of the bipyridyl receptor **26** with its substrate.

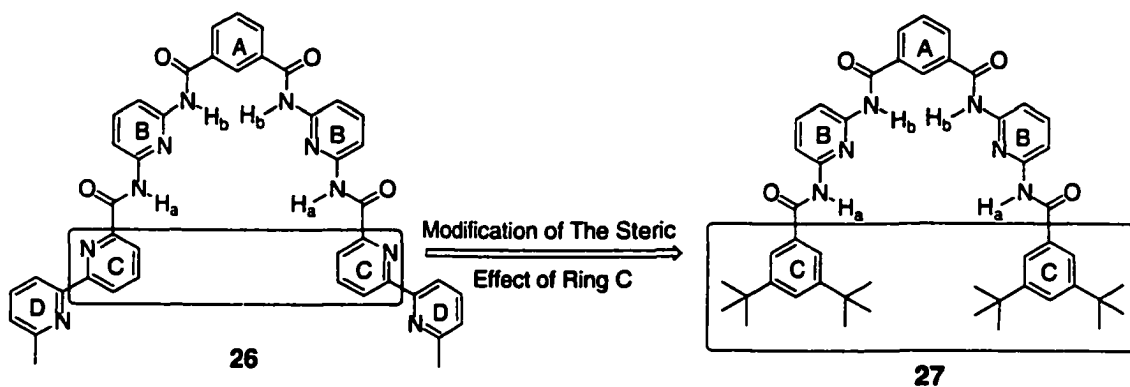
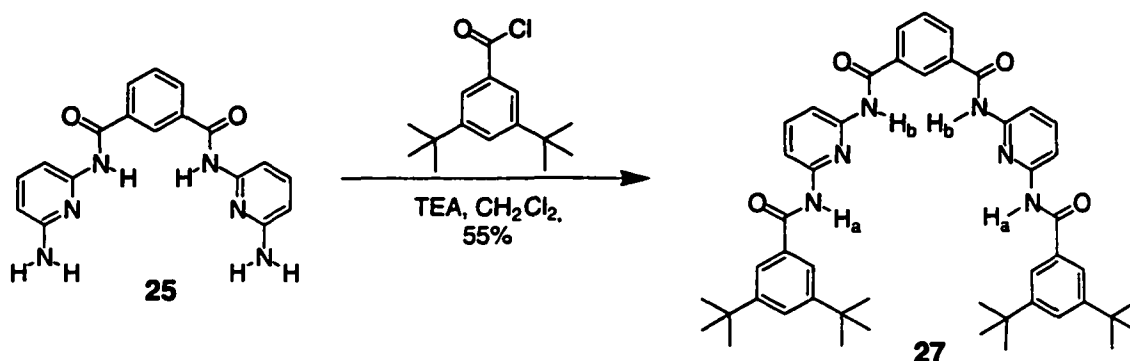


Figure 4.7 Modification of ring C of the bipyridyl receptor **26**

The di-*tert*-butylphenyl receptor **27** was prepared by reacting 3,5-di-*tert*-butylbenzoic acyl chloride with diamine **25** in the presence of triethylamine to afford the receptor **27** in 55% yield (Equation 4.1). The disappearance of the characteristic signal corresponding to the amino protons of diamine **25** at 4.30 ppm in the  $^1\text{H}$  NMR spectrum

(in  $\text{CDCl}_3$ ) and the appearance of a new signal at 8.48 ppm clearly revealed the formation of the amide group. The electrospray mass spectrum of receptor **27** supported the formation of the molecule as the molecular ion peak appeared at  $m/z=803.4261$  corresponding to  $[\text{M}+\text{Na}]^+$ .



Equation 4.1

The binding efficacy of the di-*tert*-butylphenyl receptor **27** to 5,5-dibutylbarbiturate was studied by performing similar  $^1\text{H}$  NMR titration experiments as already described for the bipyridyl receptor **26**. The changes in the chemical shifts of  $\text{H}_a$  and  $\text{H}_b$  protons were monitored as a  $\text{CD}_2\text{Cl}_2$  solution of the receptor (5 mM) was treated with a solution 5,5-dibutylbarbiturate (100 mM) in the same solvent (Figure 4.5 (p: 107)). Before the addition of the barbiturate guest, the signals corresponding to  $\text{H}_a$  and  $\text{H}_b$  protons appeared at 8.52 ppm and 8.37 ppm in the  $^1\text{H}$  NMR spectrum, respectively. The low chemical shift of  $\text{H}_a$  protons' signal, as compared to that of the bipyridyl receptor **26**, implies that the protons of the di-*tert*-butylphenyl receptor **27** are not involved in intramolecular hydrogen bonding. As the barbiturate guest was added, these peaks shifted significantly downfield ( $\Delta\delta$  more than 1.5 ppm) indicating a strong association between the receptor and its substrate through hydrogen bonding (Figure 4.5, (page:



107)). At saturation, when 10 equivalents of the barbiturate was added, the two signals of  $H_a$  and  $H_b$  shifted to 10.01 ppm and 9.89 ppm, respectively.

The collected data sets correlate well with the calculated curves for a 1:1 binding model giving an association constant of  $8.0 \times 10^3 \text{ M}^{-1}$ . This high affinity of the di-*tert*-butylphenyl receptor **27** for 5,5-dibutylbarbiturate indicates that the presence of the bulky aromatic substituents next to the entrance of the binding pocket does not prevent the access of the substrate in receptor **27**. Consequently, the presence of the C-rings of the bipyridines next to the entrance of the active site in receptor **26** is not the reason for the low affinity of the receptor for the barbiturate substrate. Moreover, the absence of the intramolecular hydrogen bonding to the  $H_a$  protons of the di-*tert*-butylphenyl receptor **27**, suggests that the nitrogen atoms of the bipyridines are acting as acceptors for this hydrogen bonding in receptor **26**.

#### 4.4.2.2 Design, Synthesis and Binding Studies of 2-Pyridyl Receptor **28**

The removal of rings labeled 'D' in Figure 4.8 from the bipyridyl receptor **26** would increase the affinity of the receptor if the steric effects of the corresponding rings were responsible for the low association of the bipyridyl receptor **26** with its substrate. Also, removing the nitrogen atoms of the D-rings would prevent the intramolecular hydrogen bonding of  $H_a$  if these nitrogen atoms were acting as the hydrogen bond acceptors. However, if the 2-pyridyl receptor **28** exhibits a similar behavior as receptor **26**, then the presence of the D-rings has no effect on the association of the bipyridyl receptor **26** to its substrate or on the chemical shift of  $H_a$ .

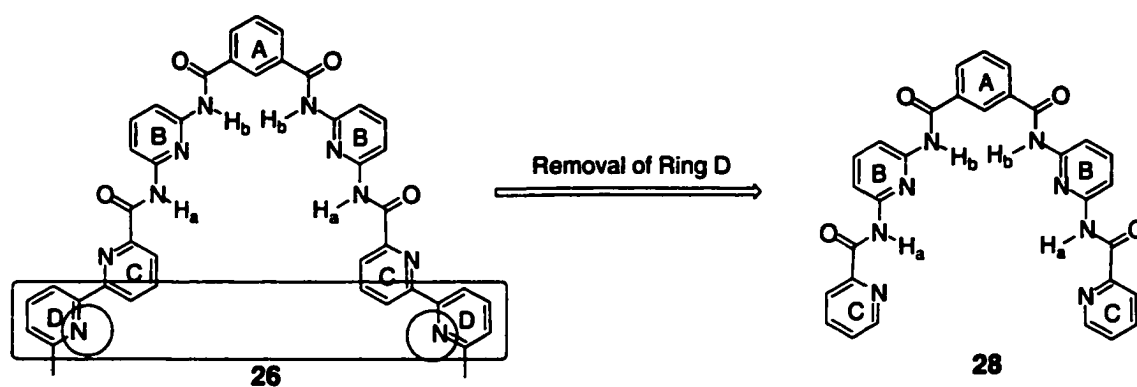
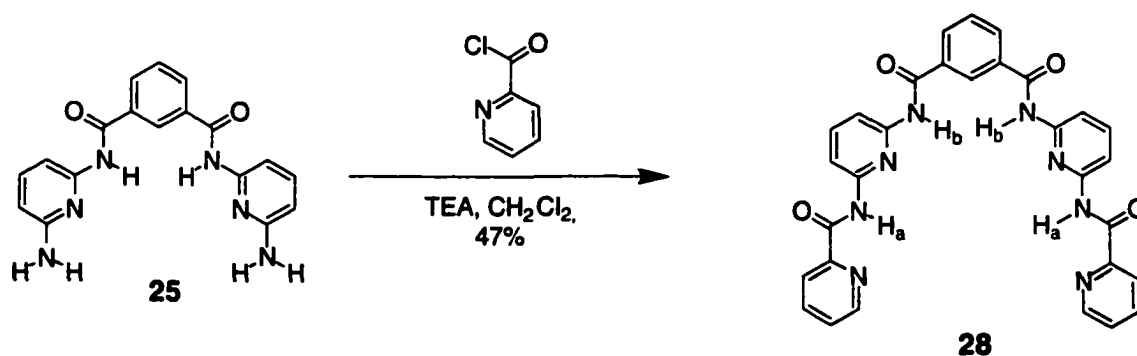


**Figure 4.8** Removal of ring D of the bipyridyl receptor **26**

The preparation of 2-pyridyl receptor **28** started with the reaction of picolinic acid with thionyl chloride to afford the picolinic acyl chloride which was reacted with the diamine **25** in  $\text{CH}_2\text{Cl}_2$  in the presence of triethylamine to give receptor **28** in 47% yield (Equation 4.2). The disappearance of the characteristic signal of the amino protons of the diamine **25** at 4.30 ppm in the  $^1\text{H}$  NMR spectrum (in  $\text{CDCl}_3$ ) and the appearance of a new signal at 10.41 ppm revealed the formation of the amide group. The electrospray mass spectrum of 2-pyridyl receptor **28** supported the formation of the molecule as its molecular ion peak appeared at  $m/z = 581.1664$  corresponding to  $[\text{M}+\text{Na}]^+$ .



**Equation 4.2**

The binding of 2-pyridyl receptor **28** to 5,5-dibutylbarbiturate was studied in a similar fashion as receptors **26** and **27** by performing  $^1\text{H}$  NMR titration experiments. The receptor (5 mM in  $\text{CD}_2\text{Cl}_2$ ) was treated with 5,5-dibutylbarbiturate (100 mM in  $\text{CD}_2\text{Cl}_2$ ) and the chemical shifts of the protons corresponding to  $\text{H}_a$  and  $\text{H}_b$  were followed. The binding trend of receptor **28** to the barbiturate was similar to that of the bipyridyl receptor **26**. The signals for the  $\text{H}_a$  and  $\text{H}_b$  protons of 2-pyridyl receptor **28** appeared initially at 10.48 and 8.12 ppm, respectively, and exhibited little change ( $\Delta\delta$  less than 0.1) in their chemical shift upon the addition of 5,5-dibutylbarbiturate (Figure 4.5, (page: 107)). The downfield chemical shift of the  $\text{H}_a$  protons was similar to that of the bipyridyl receptor **26** indicating that the removal of the D-rings has no effect on the position of this signal. It can, therefore, be concluded that the intramolecular hydrogen bond must be between the nitrogen atoms of the pyridine C-rings and the  $\text{H}_a$  protons. Also, since the chemical shift of  $\text{H}_a$  exhibited very little change upon the addition of 5,5-dibutylbarbiturate (Figure 4.5 (A), (page: 107)), it was concluded that there was no association between the 2-pyridyl receptor **28** and its barbiturate substrate, similar to the bipyridyl receptor **26**.

X-ray quality crystals of the 2-pyridyl receptor **28** were collected via a slow evaporation of a chloroform solution of the receptor. The crystal structure of receptor **28** provided more insight into the possible reasons for its low affinity for the barbiturate substrate. The structure (Figure 4.9) revealed that the molecule adopts a non-binding conformation where the two donor-acceptor-donor hydrogen bonding surfaces ( $\text{H}(\text{N}1)$ ,  $\text{N}10$ ,  $\text{H}(\text{N}2)$ , and  $\text{H}(\text{N}3)$ ,  $\text{N}30$ ,  $\text{H}(\text{N}4)$ ) of the active site are divergent. The torsional angle of  $\text{C}6\text{-C}1\text{-C}9\text{-N}3$  is  $7.4^\circ$ , implying that the regeneration of the hydrogen-bonding pocket of the 2-pyridyl receptor **28** requires a rotation around the  $\text{C}1\text{-C}9$  bond by  $173^\circ$ . The structure also shows the presence of an intramolecular hydrogen bond between the  $\text{H}_a$  protons ( $\text{H}(\text{N}2)$  and  $\text{H}(\text{N}4)$ ) and the nitrogen atoms ( $\text{N}30$  and  $\text{N}40$ ) on the pyridine C-

rings. The torsional angles of N2-C8-C21-N20 and N4-C10-C41-N40 are  $3.7^\circ$  and  $8.0^\circ$ , respectively while the interatomic non-bonded distances between N20 and H(N2) and between N40 and H(N40) are 2.16 Å and 21.9 Å, respectively (Figure 4.9). However, such geometry could be strongly influenced by crystal packing in the solid state and it does not necessary represent the most stable conformation in solution.

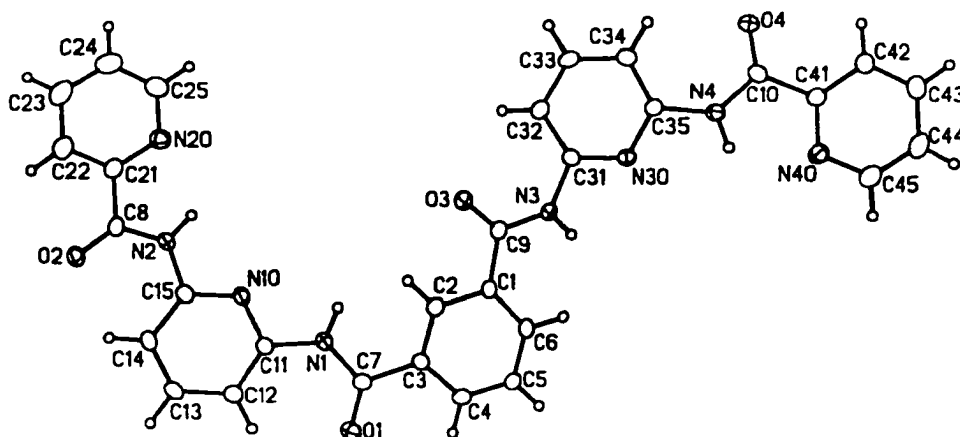


**Figure 4.9** The crystal structure of receptor **28** showing the presence of hydrogen bonding between N30 and N40 and the protons on the adjacent amide linkages, HN(2) ( $H_a$ ) and HN(4) ( $H_b$ ), respectively.

The binding studies and the structure analysis of the 2-pyridyl receptor **28** uncovered two important aspects about the inactivity of the bipyridyl receptor **26**. (1) The intramolecular hydrogen bonds in receptors **26** and **28** are between the  $H_a$  protons and the nitrogen atoms on the pyridine C-rings. (2) The low affinity of the bipyridyl receptor **26** and the 2-pyridyl receptor **28** for the barbiturate substrate is associated with the presence of these intramolecular hydrogen bonds. This is supported by the fact that the di-*tert*-butylphenyl receptor **27**, which lacks these intramolecular hydrogen-bonds, exhibited a strong binding of 5,5-dibutylbarbiturate.

An important technical point was also induced from the results of the binding studies of receptors **26**, **27** and **28**. It was observed that during the titration of the active

*di-tert*-butylphenyl receptor **27** with the barbiturate substrate, the signals corresponding to H<sub>a</sub> and H<sub>b</sub> protons shifted significantly downfield ( $\Delta\delta$  about 1.5 ppm) and reached its saturation value just after 1-2 equivalents of the substrate were added (see Figure 4.5 (page: 107)). Meanwhile, there was no significant change in the chemical shift of the signals corresponding to H<sub>a</sub> and H<sub>b</sub> protons of the inactive receptors (**26** and **28**). In these cases, the chemical shift of H<sub>a</sub> and H<sub>b</sub> signals were the same in absence and in the presence of one equivalent and in the presence of ten equivalents of the barbiturate substrate. It was thus concluded that there was no need for time-consuming full <sup>1</sup>H NMR titration experiments to evaluate future receptors' abilities to bind to the substrate. Instead, the change in chemical shift of the signals corresponding to H<sub>a</sub> and H<sub>b</sub> protons can be monitored as one equivalent of the barbiturate substrate is added (Table 4.1). If these signals are shifted significantly downfield upon the addition of the substrate, then the receptor is active. However, if there was no significant change in the chemical shift of the signals corresponding to H<sub>a</sub> and H<sub>b</sub> protons, then the receptor has low affinity for the barbiturate substrate and is inactive. Therefore, this experimental procedure was followed in studying the model receptors **29**, **30**, **31** and **32**. A full NMR titration was performed only when an estimation of the association constant ( $K_d$ ) of the receptor to its substrate was absolutely indispensable.

**Table 4.1.** The chemical shifts ( $\delta$ /ppm) of  $H_a$  and  $H_b$  in the  $^1H$  NMR spectrum before and after the addition of 1 equivalent of 5,5-dibutylbarbiturate (100 mM, in  $CD_2Cl_2$ ) to a 5 mM  $CD_2Cl_2$  solution of the receptor.

Receptor	Additive			
	none	none	5,5-dibutylbarbiturate	5,5-dibutylbarbiturate
	$\delta H_a$	$\delta H_b$	$\delta H_a$	$\delta H_b$
<b>26</b>	10.35	8.83	10.36	8.87
<b>27</b>	8.52	8.37	9.75	9.62
<b>28</b>	10.48	8.12	10.49	8.11
<b>30</b>	8.56	8.33	9.74	9.52
<b>31</b>	9.30	9.20	9.84	9.77
<b>34</b>	8.83	8.68	9.55	9.49

#### 4.4.2.3 Design, Synthesis and Binding Studies of the 3-Pyridyl Receptors (29, 30 and 31)

In order to estimate the effect of the intramolecular hydrogen bonds to the  $H_a$  protons on the affinity of the receptor **26** and **28** for their barbiturate substrate, the 2-pyridyl group of receptor **28** was replaced with the 3-pyridyl group (Figure 4.10). The result was the formation of the 3-pyridyl receptor **29** where the nitrogen atom of the pyridine C-ring was moved further away from  $H_a$  to prevent the formation of the intramolecular hydrogen bonds. Therefore, if the 3-pyridyl receptor **29** shows a high association with the barbiturate substrate, then it can be concluded that the intramolecular hydrogen bonding to  $H_a$  protons was responsible for the low affinity of the 2-pyridyl receptor **28** and the bipyridyl receptor **26** (Figure 5.6 (page: 108)).

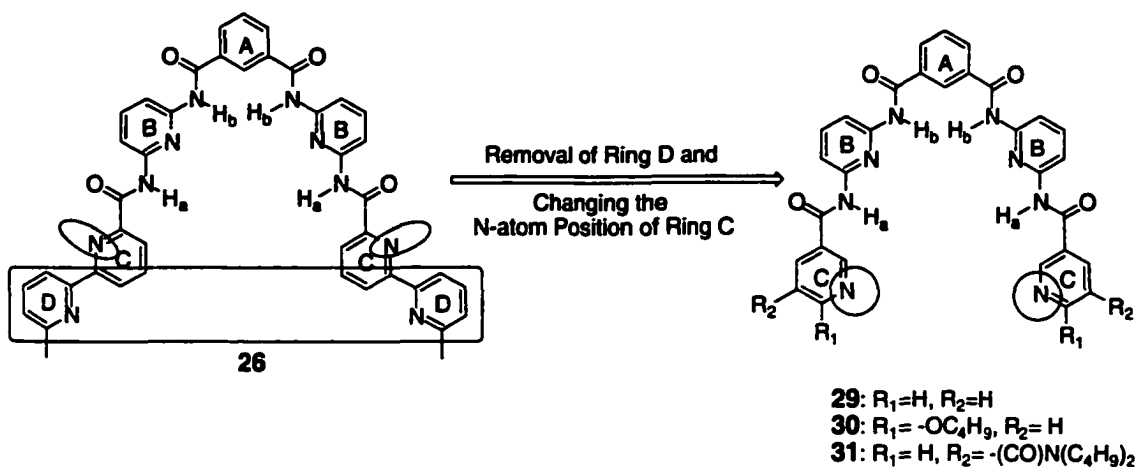
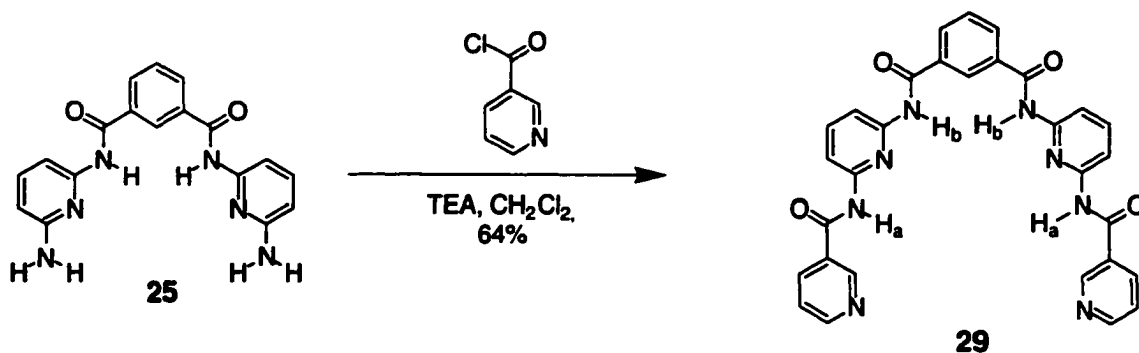


**Figure 4.10** Removal of ring D and changing the N-atom position of ring C of the bipyridyl receptor **26**

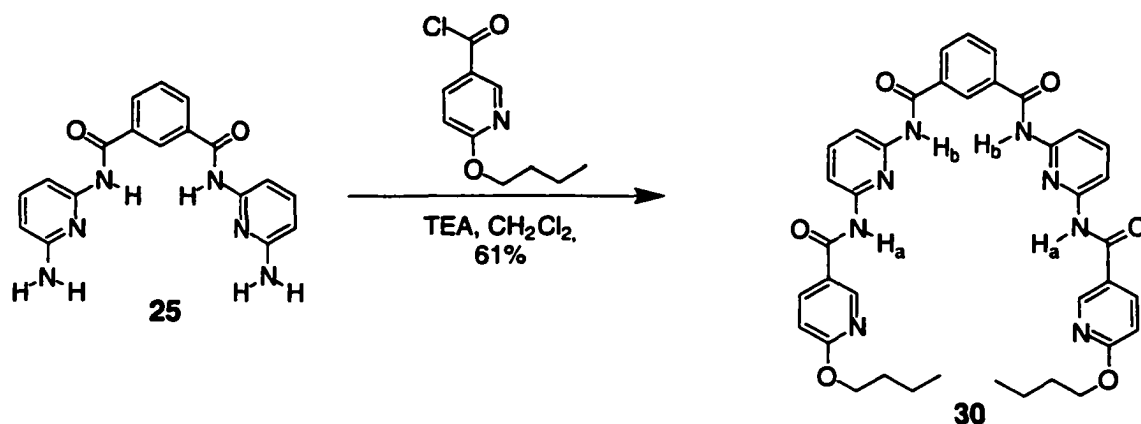
The synthesis of receptor **29** started with the reaction of thionyl chloride with nicotinic acid to form the acid chloride of the latter. This acid chloride was reacted with the diamine **25** in  $CH_2Cl_2$  in the presence of triethylamine to give receptor **29** in 64% yield (Equation 4.3). The receptor was insoluble in most organic solvents such as  $CH_2CH_2$  and  $CHCl_3$  but soluble in DMSO. The disappearance of the characteristic signal of the amino protons of the diamine **25** at 5.78 ppm on the  $^1H$  NMR spectrum (in  $DMSO-d_6$ ) and the appearance of a new signal at 10.77 ppm clearly revealed the formation of the amide group. The electrospray mass spectrum of receptor **28** supported the formation of the molecule as its molecular ion peak appeared at  $m/z=581.1656$  corresponding to  $[M+Na]^+$ .



The 3-pyridyl receptor **29** was insoluble in  $\text{CH}_2\text{Cl}_2$  which was the solvent used to study the binding activity of the 2-pyridyl and the bipyridyl receptors **28** and **26**. Therefore, the binding studies of the 3-pyridyl receptor **28** to the 5,5-dibutylbarbiturate were attempted in DMSO, a highly competitive solvent for hydrogen bonding (see Chapter 2). The chemical shifts of the signals corresponding to  $\text{H}_a$  and  $\text{H}_b$  protons of the 3-pyridyl receptor **29** (5 mM in  $\text{DMSO}-d_6$ ) were monitored as one equivalent of 5,5-dibutylbarbiturate (30 mM in  $\text{DMSO}-d_6$ ) was added to the NMR tube. Initially, the signals for  $\text{H}_a$  and  $\text{H}_b$  protons appeared at 10.76 and 10.61 ppm, respectively. These downfield shifting of the signals was attributed to the strong association of the solvent with the receptor although the presence of an intramolecular hydrogen bonding to  $\text{H}_a$  cannot be ruled out in this case. The 5,5-dibutylbarbiturate (one molar equivalent) was added but there was no change in the position or shape of the signal corresponding to  $\text{H}_a$  indicating that there was no formation of effective hydrogen bonding between the 3-pyridyl receptor **29** and the barbiturate. It was not possible to establish the reasons behind this low association because of the solvent effect on the formation of hydrogen bonding (see Chapter 2). Therefore, an alkyl chain was incorporated into the 3-pyridyl receptor (**30**) to make it more soluble in organic solvents such as  $\text{CHCl}_3$  and  $\text{CH}_2\text{Cl}_2$  which are less competitive solvents for hydrogen bonding.



The 3-pyridyl receptor, **30**, was prepared by the reaction of the diamine **25** with the acyl chloride derivative of 6-butoxy nicotinic acid (Equation 4.4). The receptor was collected in 61% yield and was characterized by  $^1\text{H}$  NMR spectroscopy and electrospray mass spectrometry. The disappearance of the characteristic signal of the amino protons of the diamine **25** at 4.30 ppm in the  $^1\text{H}$  NMR spectrum (in  $\text{CDCl}_3$ ) and the appearance of a new signal at 8.56 ppm clearly revealed the formation of the amide group. The electrospray mass spectrum of receptor **28** supported the formation of the molecule as its molecular ion peak appeared at  $m/z=703.2993$  corresponding to  $[\text{M}+\text{H}]^+$ .

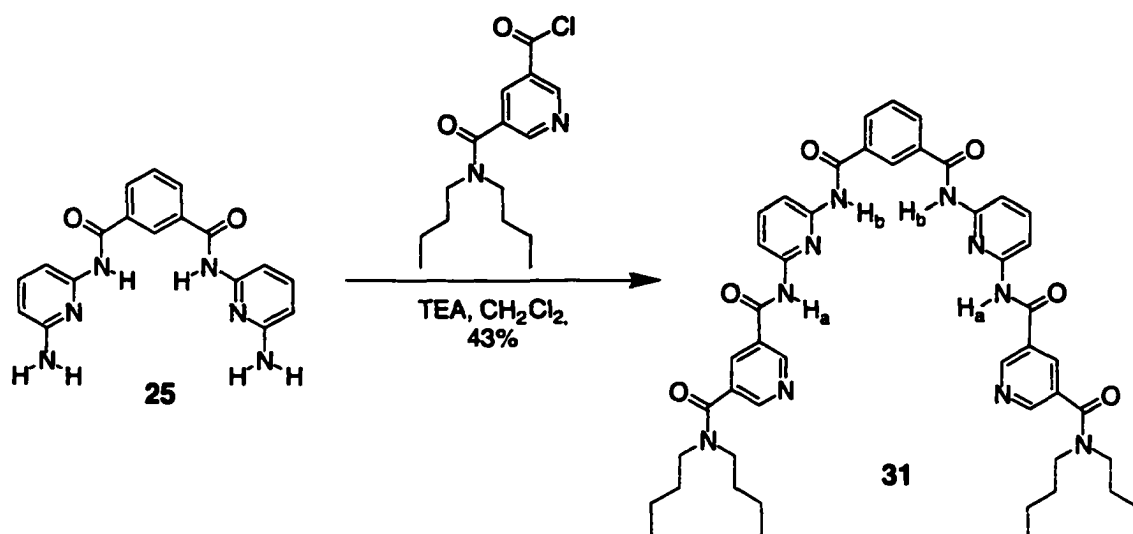


Equation 4.4

Receptor **30** was soluble in  $\text{CH}_2\text{Cl}_2$  where its  $^1\text{H}$  NMR spectrum showed the presence of the signals corresponding to  $\text{H}_a$  and  $\text{H}_b$  protons at 8.56 ppm and 8.33 ppm, respectively. The former chemical shift implies that  $\text{H}_a$  is not hydrogen bonded and, thus, the substituting of 2-pyridine (as in **28**) with 3-pyridine (as in **30**) prevented the formation of this hydrogen bond. The addition of one equivalent of 5,5-dibutylbarbiturate to a 5 mM solution of the 3-pyridyl receptor **30** in  $\text{CD}_2\text{Cl}_2$  shifted these signals to 9.74 ppm and 9.52 ppm, respectively (Table 4.1). This was an indication of an effective association between the receptor and the substrate through hydrogen bonding. Therefore, by moving

the nitrogen atom, the intramolecular hydrogen bonds of the H<sub>a</sub> protons were eliminated, as indicated by the upfield chemical shift of these protons, and the affinity of the receptor to the substrate which was significantly enhanced.

It was important, however, to rule out the possibility that the steric effect of the butoxy group attached close to the nitrogen atoms of the C-rings has prevented the formation of the intramolecular hydrogen bond. Thus, another 3-pyridyl receptor **31** was prepared (Equation 4.5) such that the incorporated alkyl groups are further away from the nitrogen atoms. This will remove any possible interference of the alkyl chains with the formation of an intramolecular hydrogen bond between the nitrogen atoms of the C-rings and H<sub>a</sub> protons. The reaction of 5-[(dibutylamino)carbonyl]nicotinic acid chloride with the diamine **25** in CH<sub>2</sub>Cl<sub>2</sub> afforded receptor **31** in 43% yield (Equation 4.5). The disappearance of the characteristic signal of the amino protons of the diamine **25** at 4.30 ppm in the <sup>1</sup>H NMR spectrum (in CDCl<sub>3</sub>) and the appearance of a new signal at 9.13 ppm clearly revealed the formation of the amide group. The <sup>1</sup>H NMR spectrum also showed the presence of two sets of signals corresponding to the butyl chains. The electrospray mass spectrum of receptor **31** supported the formation of the molecule as its molecular ion peak appeared at m/z=891.4282 corresponding to [M+Na]<sup>+</sup>.



The  $^1\text{H}$  NMR spectrum of 3-pyridyl receptor **31** in  $\text{CD}_2\text{Cl}_2$  showed the signals corresponding to  $\text{H}_a$  and  $\text{H}_b$  protons at 9.30 and 9.20 ppm, respectively. Since these peaks shifted to 9.04 ppm and 8.93 ppm, respectively, as the NMR sample was diluted from 5 mM to 0.3 mM concentration, it was concluded that  $\text{H}_a$  and  $\text{H}_b$  protons of receptor **31** undergo intermolecular hydrogen bonding causing a downfield shift of these signals when solutions of the 3-pyridyl receptor **31** are concentrated. Also, since the chemical shift of the signal corresponding to  $\text{H}_a$  protons changed by varying the concentration, it implied that there was no intramolecular hydrogen bonding between  $\text{H}_a$  protons and any other atom. On the other hand, the addition of one molar equivalent of 5,5-dibutylbarbiturate to the 3-pyridyl receptor **31** solution (5 mM in  $\text{CD}_2\text{Cl}_2$ ) induced a downfield shift of the signals corresponding to  $\text{H}_a$  and  $\text{H}_b$  protons to 9.84 ppm and 9.77 ppm, respectively (Table 4.1). This indicates that there is a strong association between the receptor and its substrate.

#### 4.4.2.4 Conclusions of the Binding Studies on the Control Receptors

The studies on the model receptors, **27**, **28**, **30** and **31**, highlighted three main points (Figure 4.11). (1) The high affinity of the di-*tert*-butylphenyl receptor **27** for its barbiturate substrate indicates the steric bulkiness of the C-rings has no effect on the binding ability of the bipyridyl receptor **26**. (2) Since the 2-pyridyl receptor **28** exhibited similar binding behavior to the bipyridyl receptor **26**, it can be concluded that the affinity of the latter for the barbiturate substrate is not affected by the D-rings. (3) There is a direct relation between the presence of the intramolecular hydrogen bond between H<sub>a</sub> and the nitrogen atoms on the pyridine C-rings of receptors **26** and **28**, and the low affinity of these receptors for the barbiturate substrate. This is supported by the fact that receptors **27**, **30** and **31**, which lack this intramolecular hydrogen bond, exhibited strong association with 5,5-dibutylbarbiturate.

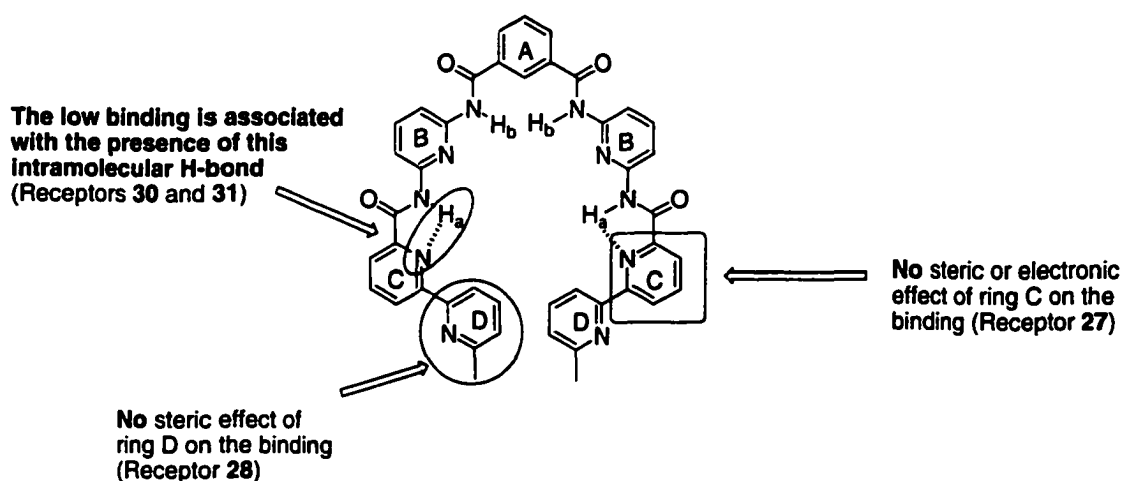


**Figure 4.11** The effects of bipyridine substituents on the binding of receptor **26**

It can be argued that the intramolecular hydrogen bonds between the H<sub>a</sub> protons and the nitrogen atoms of the pyridine C-rings in receptor **26** force the bipyridine ligands to converge toward the entrance of the binding pocket as illustrated by conformer **26A**

illustrated in Figure 4.12. This orientation forces the  $H_a$  protons to be in close proximity with the protons at the 3'-position of D-ring. Thus, a simple 1-dimensional NOE experiment was run on the bipyridyl receptor **26** (in  $CD_2Cl_2$ ) to verify the presence of this conformation. The  $H_a$  protons were irradiated and the signals corresponding to the C—H protons at the 3'-position (D-ring) and the 5-position (B-ring) were monitored. An enhancement of the signal corresponding to the C—H protons at the 3'-position was only observed indicating a close proximity of these protons with the  $H_a$  protons. No enhancement of the signal corresponding to the C—H protons at the 5-position on the B-ring was noticed. These observations support the convergent orientation of the bipyridine arms toward the entrance of the binding pocket (conformer **26A** in Figure 4.12). Otherwise, if the bipyridines were diverging away from the entrance to the binding pocket,  $H_a$  protons should have been in close proximity with the protons at the 5-position of B-ring as shown in conformer **26B** (Figure 4.12). This conformer is not particularly stable due to the electronic repulsion of the lone pairs of the nitrogen atoms of the B-rings and those on the oxygen atoms of the amide group.

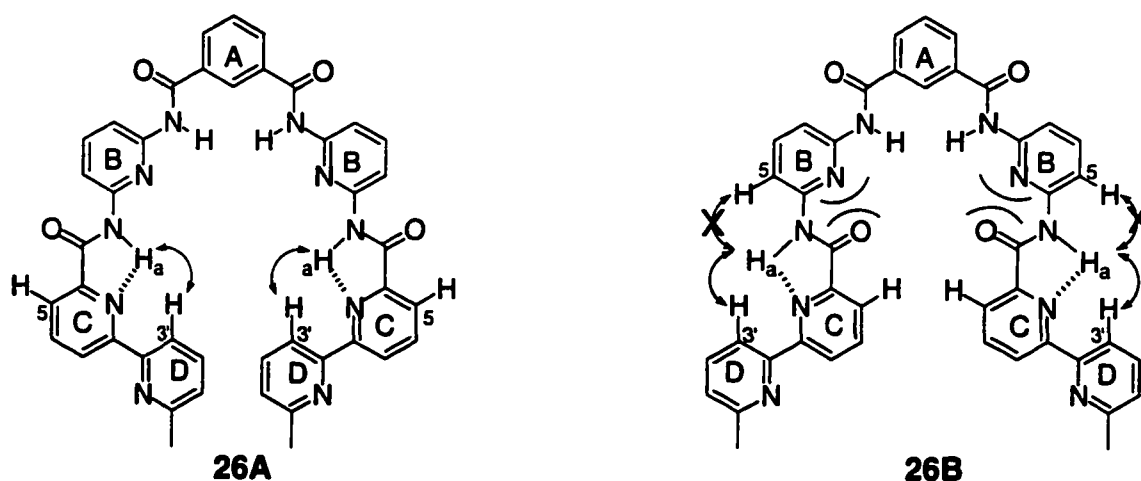
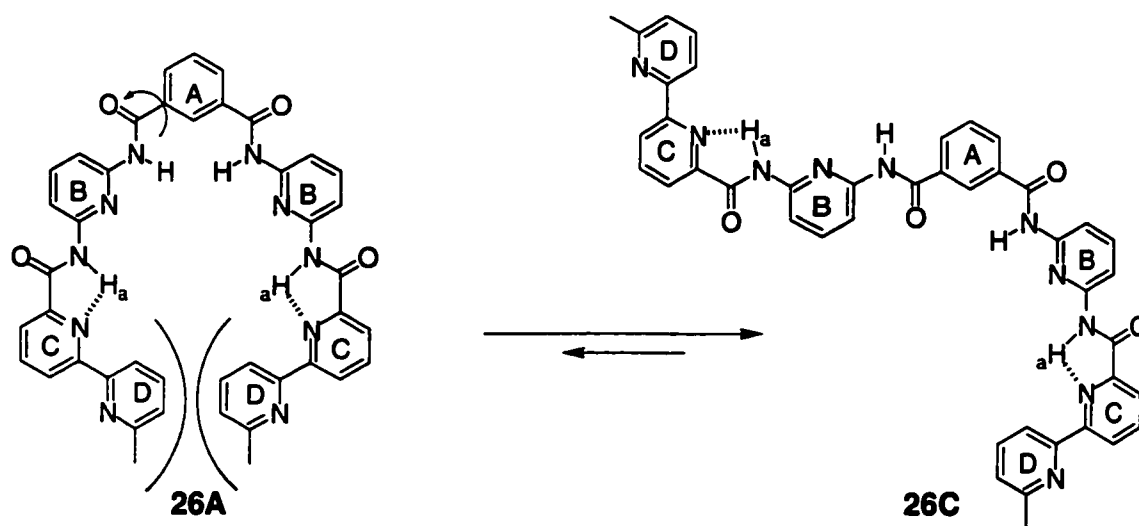


**Figure 4.12** The possible conformers of receptor **26**

The low affinity of the bipyridyl receptor **26** for the barbiturate substrate was attributed to the converging orientation of the bipyridines toward the entrance of the binding pocket. This orientation has led to two possible factors that inhibited the binding of receptor **26** to its substrate. (1) The converging conformation of the bipyridine arms blocked the entrance of the binding pocket preventing the access of the barbiturate substrate to the binding site, thus, inhibiting the formation of the receptor-substrate complex. (2) Alternatively, the steric effect of the two bipyridines bumping into each other destabilized conformer **26A** of the receptor favoring the formation of the divergent conformer **26C** (illustrated in Scheme 4.3). In conformer **26C**, the hydrogen bonding donor-acceptor-donor surfaces of the active site are diverging away from each other leading to the destruction of the binding pocket of the bipyridyl receptor **26** and rendering it unsuitable to accommodate the barbiturate substrate. In conclusion, both conformers **26A** and **26C** of the receptor are unable to bind the substrate leading to the low affinity of the bipyridyl receptor **26** towards the barbiturate substrate.



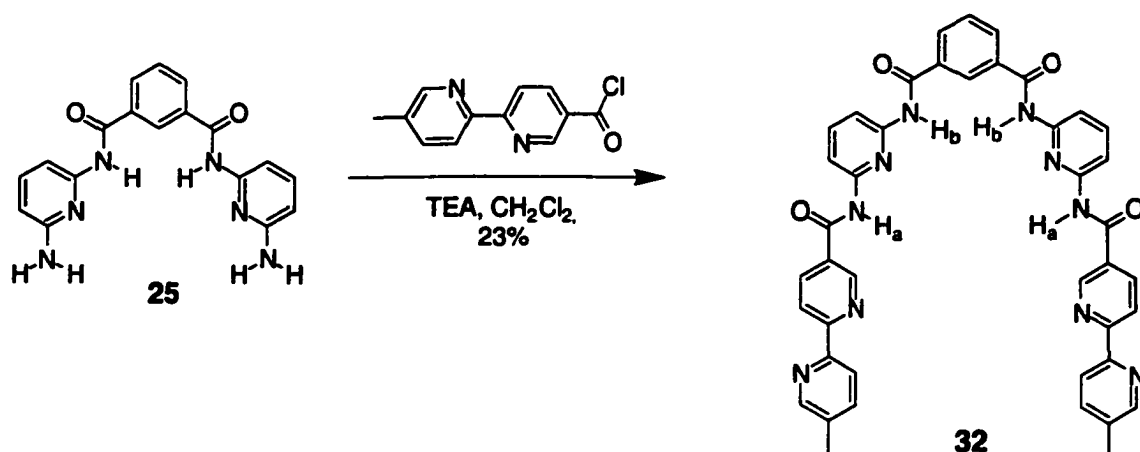
Scheme 4.3

## 4.5 New Bipyridyl Receptors for Barbiturate Guests

### 4.5.1 Design, Synthesis and Binding Studies of Bipyridyl Receptor 32

In order to overcome the problems associated with the intramolecular hydrogen bonding of the bipyridyl receptor **26**, a new bipyridyl receptor **32** was prepared such that the bipyridine ligands are connected to the active site at the 5-position of the C-rings. This change in the connectivity moved the nitrogen atoms of the C-rings away from the H<sub>3</sub> protons and, thus, no intramolecular hydrogen bond can be formed. Similar to the 3-pyridyl receptors **30** and **31**, the bipyridyl receptor **32** should show a high affinity for the barbiturate substrate. On the other hand, the 5,5'-disubstituted bipyridine can still bind to the metal cofactor and act as the allosteric binding site of receptor **32**. However, the disadvantage of using 5,5'-disubstituted bipyridine ligands is the lower stability of their Cu(I) complexes as compared to those of the 6,6'-disubstituted bipyridines.<sup>4</sup>

The bipyridyl receptor **32** was prepared by the reaction of the diamine **25** with 5'-methyl-2,2'-bipyridine-5-carboxylic acyl chloride in CH<sub>2</sub>Cl<sub>2</sub> in the presence of triethylamine. The receptor was collected in 23% yield and was very insoluble in organic solvents such as CH<sub>2</sub>Cl<sub>2</sub>, CHCl<sub>3</sub>, acetone and THF, however, it exhibited a limited solubility in DMSO. Since DMSO is a highly competitive solvent for hydrogen bonding as was observed for the 3-pyridyl receptor **29**, and due to the insolubility of the receptor in less competitive solvent such as CH<sub>2</sub>Cl<sub>2</sub>, it was impossible to study the binding of the bipyridyl receptor **32** to the barbiturate substrate. Therefore, the receptor was made more soluble by the incorporation of a *tert*-butyl group at the 5-position of the isophthylamide moiety rendering the bipyridyl receptor **34** soluble in CH<sub>2</sub>Cl<sub>2</sub> and CHCl<sub>3</sub>.

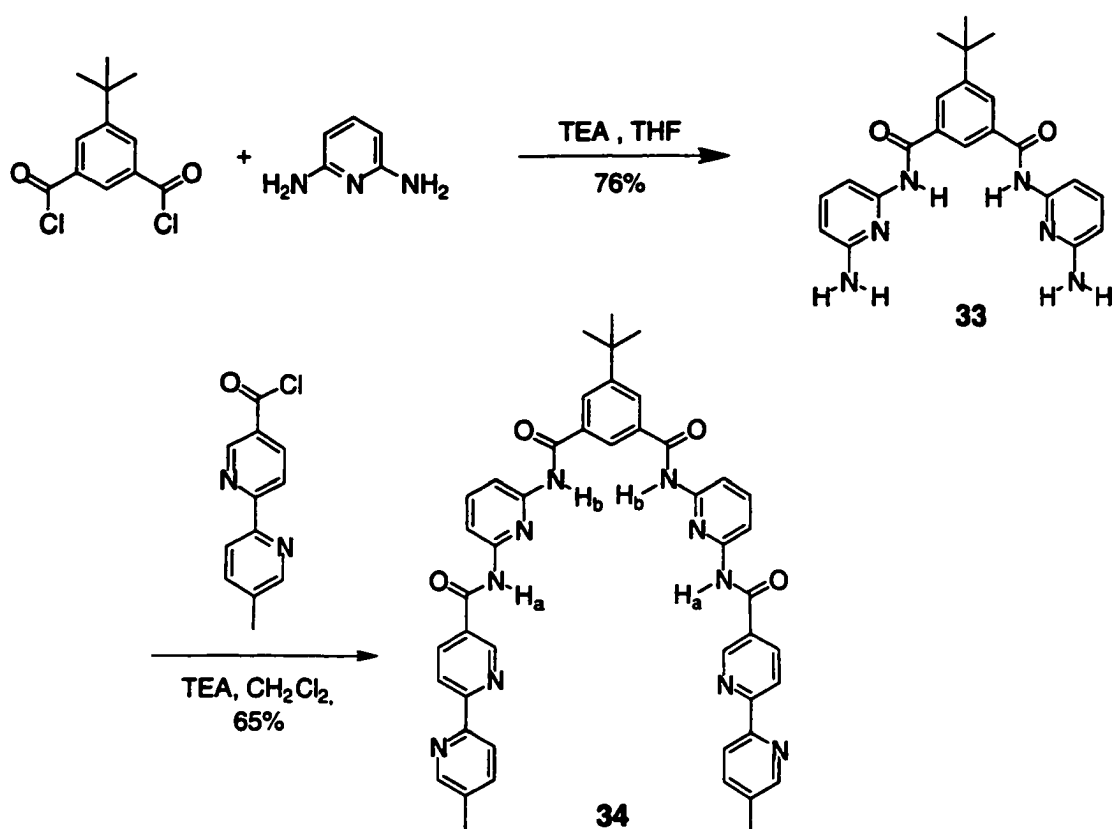


Equation 4.6

#### 4.5.2 Synthesis and Binding Studies of the Bipyridyl Receptor 34

The synthesis of the bipyridyl receptor **34** started with preparation of the diamine **33** from the 5-*tert*-butylisophthaloyl chloride with excess 2,6-diaminopyridine (Scheme 4.4). The reaction of the diamine **33** with 5'-methyl-2,2'-bipyridine-5-carboxylic acyl chloride in  $\text{CH}_2\text{Cl}_2$  afforded receptor **34** in 65% yield. The disappearance of the characteristic signal of the amino protons of the diamine **33** at 4.35 ppm in the  $^1\text{H}$  NMR spectrum and the appearance of a new signal at 8.83 ppm clearly revealed the formation of the amide group. The electrospray mass spectrum of receptor **34** supported the formation of the molecule as its molecular ion peak appeared at  $m/z=797.3312$  corresponding to  $[\text{M}+\text{H}]^+$ .





Scheme 4.4

The binding ability of the bipyridyl receptor **34** to its barbiturate receptor was studied by monitoring the change in the chemical shifts of the signals corresponding to H<sub>a</sub> and H<sub>b</sub> protons upon the addition of one molar equivalent of 5,5-dibutylbarbiturate to 5 mM solution of the receptor in CD<sub>2</sub>Cl<sub>2</sub>. Before the addition of the substrate, the signals corresponding to the H<sub>a</sub> and H<sub>b</sub> protons appeared at 8.83 ppm and 8.68 ppm, respectively. After the addition of one molar equivalent of 5,5-dibutylbarbiturate, these signals shifted downfield to 9.55 and 9.49 ppm, respectively, indicating the formation of effective hydrogen bonding between the receptor and the substrate. Consequently, the bipyridyl receptor **34** is active and has a high affinity for barbiturate substrates as shown in the following experiment.

<sup>1</sup>H NMR titration experiments were run on the bipyridyl receptor **34** to calculate the association constant for its binding to 5,5-dibutylbarbiturate. Receptor **34** was dissolved in a 10% CD<sub>3</sub>CN/CD<sub>2</sub>Cl<sub>2</sub> mixture (2 mM) and treated with aliquot amounts of a 20 mM solution of 5,5-dibutylbarbiturate in the same solvent system. This mixture of solvents was used because it dissolves the metal complexes of receptor **34**, *vide infra*. Before any guest was added, the signals corresponding to H<sub>a</sub> and H<sub>b</sub> protons appeared at 8.84 and 8.70 ppm, respectively in the <sup>1</sup>H NMR spectrum. As the substrate was added, these signals shifted significantly downfield ( $\Delta\delta$  about 1 ppm) indicating the presence of strong hydrogen bonding between the receptor and its substrate (Figure 4.13). After two equivalents of the substrate were added, the signal corresponding to H<sub>b</sub> protons merged with the signal corresponding to H<sub>a</sub> protons and the merged signal continued to shift downfield upon the addition of the substrate. After 10 equivalents of the barbiturate substrate were added, the receptor reached saturation where the merged signal corresponding to both H<sub>a</sub> and H<sub>b</sub> protons reached a chemical shift of 9.88 ppm. The data sets collected from three different runs correlated well with the calculated curves using 1:1 binding models. The value of K<sub>a</sub> was calculated to be  $2.8 \pm 0.7 \times 10^3 \text{ M}^{-1}$  when the chemical shift of the signal corresponding to H<sub>a</sub> was monitored and  $3.2 \pm 0.8 \times 10^3 \text{ M}^{-1}$  when the chemical shift of the signal corresponding to H<sub>b</sub> was monitored. These values indicated a strong association of the substrate by the bipyridyl receptor **34**.

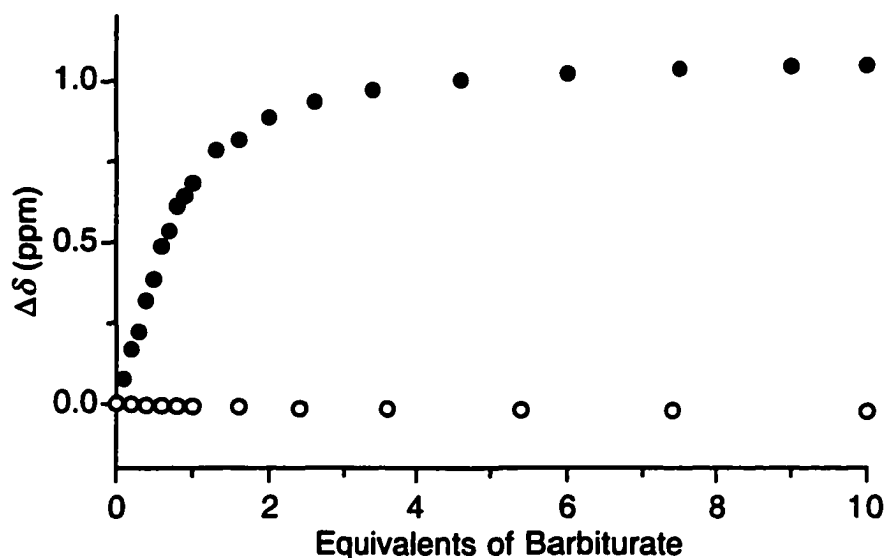


**Figure 4.13** Titration curves of **34** and **34•Zn**. The change in the chemical shift of  $H_a$  protons' signal as **34** (●) and **34•Zn** (○) are treated with 5,5-dibutyl barbiturate (20 mM) in  $CD_2Cl_2/CD_3CN$  (9:1).

#### 4.5.3 The Effect of Metal Ions on the Activity of the Bipyridyl Receptor **34**

The chelation of a metal cofactor by the bipyridine ligands in **34** should induce conformational changes in the receptor leading to the blocking of the entrance of the binding pocket. These changes inhibit the binding of the barbiturate guest to the bipyridyl receptor **34**. In order to study the effect of the metal on the affinity of receptor **34** for barbiturate guests, the preparation of the Cu(I) complex of the receptor was attempted. The addition of one molar equivalent of  $Cu(CH_3CN)_4PF_6$  to a solution of the bipyridyl receptor **34** in a 10%  $CH_3CN/CH_2Cl_2$  mixture produced an instantaneous change in the color of the solution from colorless to dark brown. This color was much darker than the characteristic red-orange color of the tetrahedral Cu(I) complexes with 2,2'-bipyridine ligands that was observed of the receptors in Chapters 2 and 3. Ether was added to the solution to induce the precipitation of the brown solid that was collected by filtration, washed with ether and dried under vacuum. The  $^1H$  NMR spectrum (in  $CD_3CN$ ) of this solid showed broad peaks which were uncharacterizable.<sup>4</sup> This broadness

of the peaks in the NMR spectrum implies that either (1) a partial oxidation of Cu(I) to Cu(II) has occurred and the broad peaks are due to the diamagnetic effect of Cu(II) or (2) polymolecular aggregates have formed through the coordination of the metal by the bipyridine ligands of neighboring molecules or (3) a combination of the two possibilities. The electrospray mass spectrum of this solid did not show any peaks that corresponds to either  $[M+Cu]^+$  or  $[M+Cu]^{2+}$ . This indicates that the target complex of receptor **34** where the copper ion is coordinated by the bipyridine ligands is not a product of the reaction. Therefore, copper ions can not be used as allosteric cofactors since their coordination to the allosteric bipyridine ligands of receptor **34** was not foreseeable.

The Zn(II) complex of receptor **34** was prepared by reacting the bipyridyl receptor **34** with one equivalent of zinc triflate in a 10%  $CH_3CN/CH_2Cl_2$  mixture. The solvent was removed under vacuum and the solid residue was washed with small amount of  $CH_2Cl_2$  and filtered. After drying under vacuum, the product was collected as a colorless solid that was characterized by multi-dimensional NMR spectroscopy and electrospray mass spectrometry. The  $^1H$  NMR spectrum of the complex, **34•Zn**, exhibited significant changes in the chemical shifts of the aromatic peaks which correspond to chelation of the Zn(II) ion by the bipyridine ligands of receptor **34**. Figure 4.14 shows the  $^1H$  NMR spectra of the aromatic regions of receptor **34** (bottom) and its Zn(II) complex **34•Zn** (top). The spectrum of **34•Zn** reveals that the signals corresponding to the aromatic protons of the bipyridine rings ( $H_d$ ,  $H_e$ ,  $H_f$ ,  $H_g$ ,  $H_h$ ) have shifted downfield indicating that the metal coordination by the ligand withdrew the electronic density on the rings causing the downfield shift of its protons. The upfield shift of  $H_c$  was attributed to the distorted octahedral geometry of the Zn(II) complex which places  $H_c$  within the shielding cone of the D-ring of the opposite bipyridine ligand. Such an upfield shift of the protons on the 6-position of the bipyridine has been previously observed for similar zinc complexes.<sup>5</sup>

The downfield shift of  $H_a$  protons signal of  $34 \bullet Zn$  is attributed to the coordination of the strong Lewis acidic Zn(II) by the bipyridines which increases the acidity of  $H_a$  protons shifting their signal to higher  $\delta$ . The upfield shift of the signal corresponding to  $H_i$  protons upon the complexation of the metal, suggests that this proton is less deshielded by the carbonyl of the adjacent amide which is rotated away from  $H_i$  due to the geometric requirements of the metal coordination (Figure 4.13). Finally, the downfield shift of  $H_i$  is attributed to limiting the rotation of the adjacent C—CO bond which forces the carbonyl to be in close proximity to  $H_i$ , deshielding the latter by the carbonyl (C=O) magnetic field.

The electrospray mass spectrum of  $34 \bullet Zn$  showed the presence of peak at  $m/z$  1159.1648 corresponding to the mass of  $[34+Zn+2 Otf+H]^+$  and another peak at  $m/z$  859.2445 which corresponds to  $[34+Zn-H]^+$ . These two peaks clearly supports the formation of the complex  $34 \bullet Zn$  where the metal is coordinated by one molecule of the receptor.

The effect that the metal has on the binding ability of bipyridyl receptor **34** to the guest was studied by treating the preformed complex  $34 \bullet Zn$  (5 mM) with 5,5-dibutylbarbiturate substrate in  $CD_2Cl_2/CD_3CN$  (9:1). The addition of the barbiturate to the Zn(II) complex led to an insignificant ( $\Delta\delta$  less than 0.1 ppm) but observable upfield shift in the signals corresponding to  $H_a$  and  $H_b$  (Figure 4.12). This was attributed to the dilution of the receptor solution upon the addition of the substrate solution. This also indicates that there is no association between the receptor and its substrate. Therefore, the metal has prevented the binding of the substrate and has turned the activity of the receptor “off”.

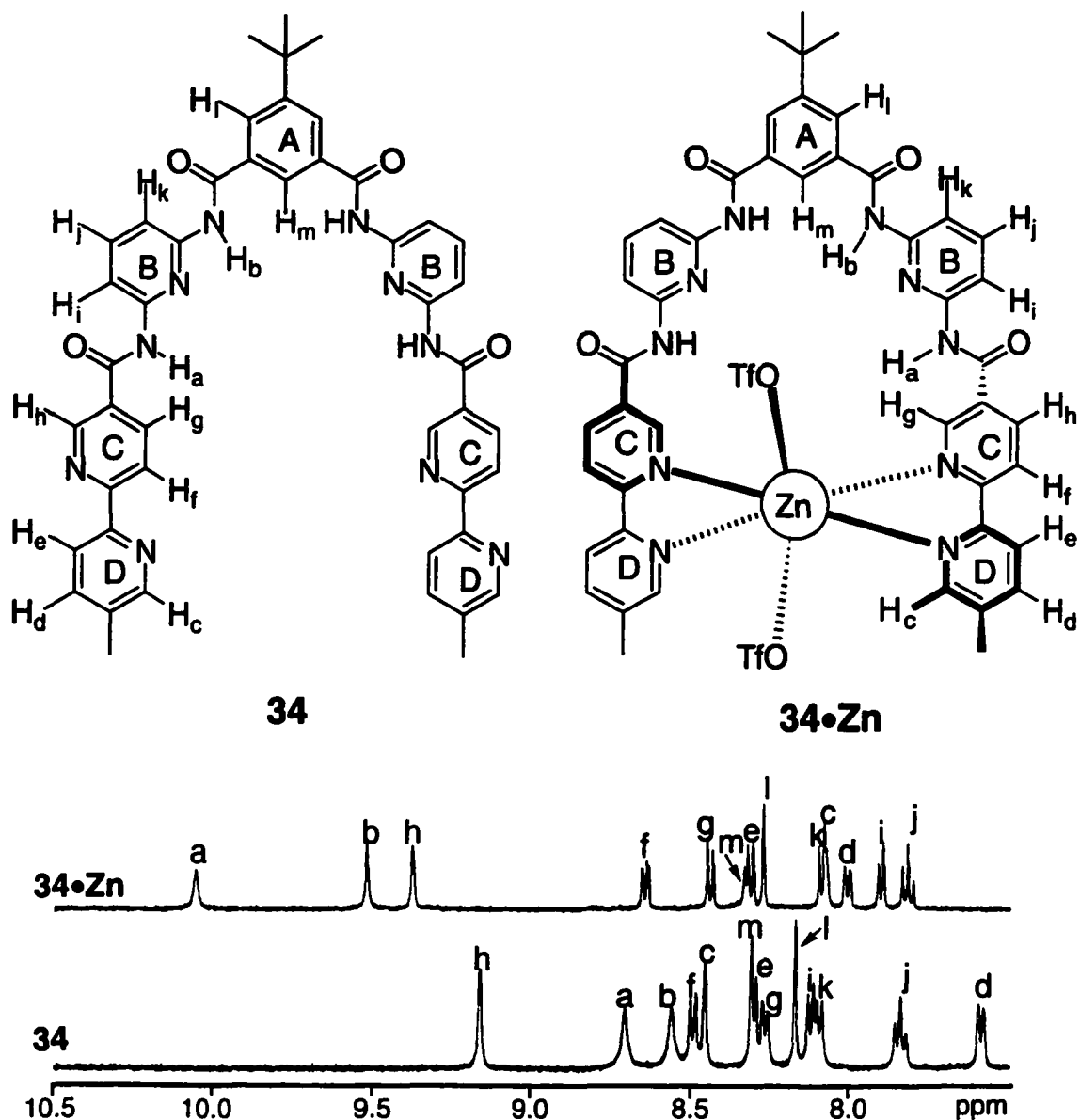


**Figure 4.14** Partial <sup>1</sup>H NMR (500 MHz, 9:1 CD<sub>2</sub>Cl<sub>2</sub>/CD<sub>3</sub>CN) spectrum of the bipyridyl receptor **34** and its zinc complex **34•Zn**. The aromatic peaks are assigned to the structures based on 2-dimensional NMR studies (GCOSEY and TROESY) of the two compounds.

#### 4.6 Conclusions

The bipyridyl receptor **26** was designed such that it provides a hydrogen-bonding site for barbiturates. The activity of the receptor was to be controlled by the allosteric effect of copper ions as their chelation by the bipyridine ligands blocks the entrance of

the binding site of the receptor rendering it “inactive”. The bipyridyl receptor **26**, however, turned out to be “inactive” without the presence of the metal.

After careful investigation of the bipyridyl receptor’s computer-generated model and the similar systems that have been reported in literature, three factors in the design of the receptor were proposed as reasons of low affinity of the bipyridyl receptor **26** for the barbiturate substrate. (1) The electronic effect of the bipyridines on the protons involved in the molecular recognition process. (2) The presence of a bulk aromatic group (such as bipyridine) next to the binding pocket interferes with the access of the substrate to the pocket. (3) The nitrogen atoms of the bipyridine rings form intramolecular hydrogen bonds with the N—H protons responsible for the recognition of the substrate. These bonds result in the existence of inactive conformations of the bipyridyl receptor **26**. Therefore, control receptors were prepared in order to study the effect these factors have on the binding efficacy.

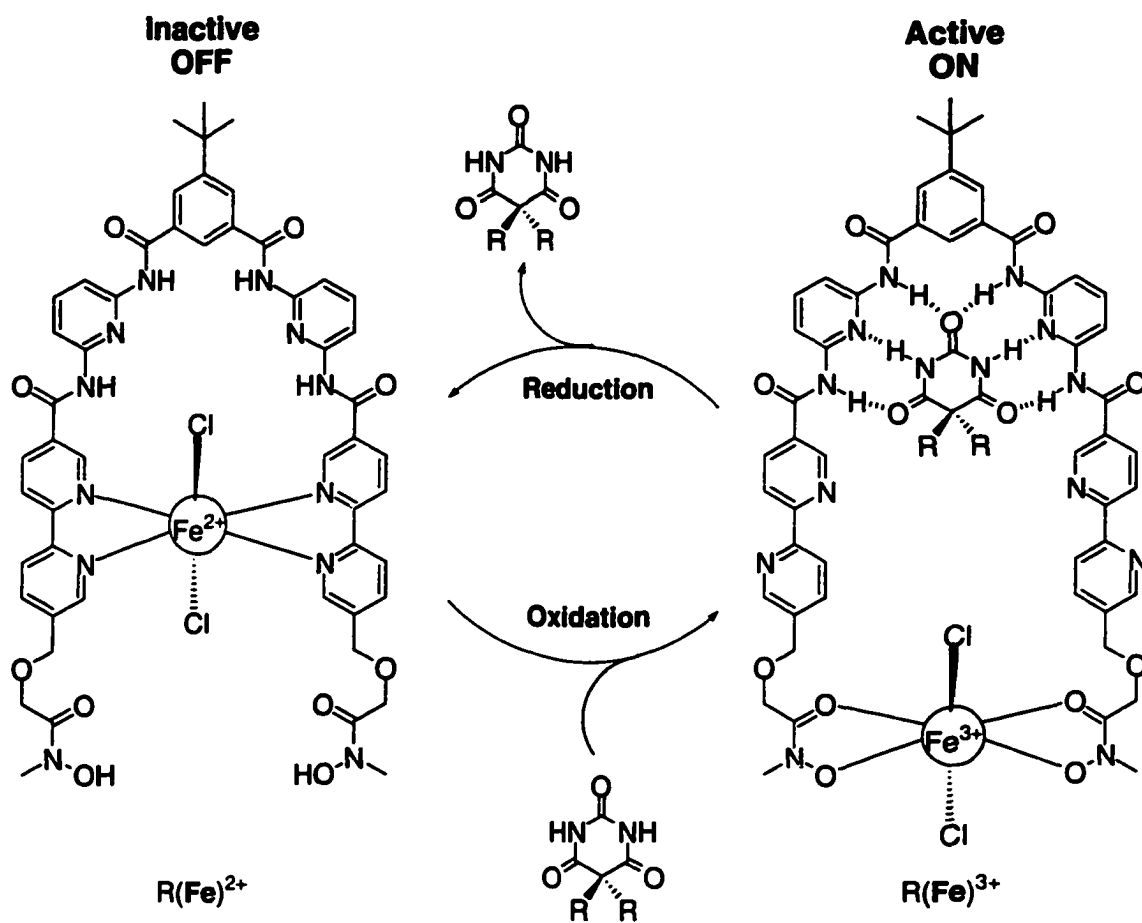
The study of the di-*tert*-butyl receptor **27** concluded that the steric bulkiness of the bipyridine arms had no effect on the activity of bipyridyl receptor **26**. The 2-pyridyl receptor **28** also showed a low affinity toward binding the barbiturate substrate most likely due to the presence of an intramolecular hydrogen bond involving the N—H protons. These observations, supported by the crystal structure, showed that the N—H protons in the 2-pyridyl receptor **28** are hydrogen bonded to the nitrogen atoms of the pyridine C-rings. The study of the 3-pyridyl receptors **30** and **31** determined that these intramolecular hydrogen bonds are responsible for the inactivity of bipyridyl receptor **26**.

Based on the results of the control receptors, the design of the original bipyridyl receptor **26** was modified to prevent the formation of the intramolecular hydrogen bonds. The connectivity of the allosteric bipyridine ligands to the binding site was changed such that the bipyridines are 5,5'-disubstituted. The result was a new bipyridyl receptor **34**

which exhibited a high affinity for the barbiturate substrate in the absence of Zn(II) ions. Upon the addition of the zinc triflate, the bipyridine ligands coordinated to the metal blocking the entrance of the binding pocket. This inhibited the binding of the substrate by the receptor. Therefore, the binding activity of bipyridyl receptor **34** and its Zn(II) complex represents an example of the allosteric inhibition of binding by metal cofactors through the cavity-size alternation approach.

Future extension of this project would include developing the bipyridyl receptor **34** such that its binding can be controlled by an external stimulus leading to the construction of a “molecular machine”. The incorporation of hydroxamide ligands onto the bipyridyl receptor **34** would provide a suitable allosteric binding site for Fe(III) ions (Scheme 4.11). The chelation of Fe(III) by the hydroxamide ligands should lead to the formation of a cyclic receptor for barbiturate substrates (positive allostery). Fe(II) ions, on the other hand, prefer the complexation with bipyridine ligands.<sup>9</sup> Thus, the complexation of Fe(II) ions with bipyridine ligands of receptor **34** should inhibit (negative allosteric) the binding of the barbiturate substrate to the binding site in similar manner to Zn(II) complex of receptor **34**. Therefore, by electrochemical switching between Fe(II) and Fe(III) one should be able to switch the binding of the receptor between “ON” and “OFF” states (Scheme 4.5). Using a similar approach to that of the triaminotriazine receptor **17** (Chapter 3), the redox processes can be performed chemically or electrochemically and can be monitored by light (UV-Vis).<sup>9</sup>





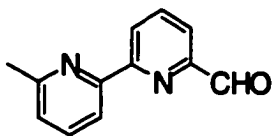
Scheme 4.5

## 4.7 Experimental

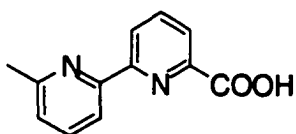
**General Information.** All solvents (Caledonia) for synthesis and purification were used as received. Solvents used for UV-Vis absorption and fluorescence spectroscopy analysis were deoxygenated by bubbling argon through the solvent. Solvents used for NMR analysis (Cambridge Isotope Laboratories) were used as received. All reagents and starting materials were purchased from Aldrich or Acros Organics.

$^1\text{H}$  NMR characterizations were performed on a Varian Inova-300 instrument, working at 299.96 MHz, or on a Varian Inova-500 instrument, working at 499.92 MHz. Chemical shifts ( $\delta$ ) are reported in parts per million relative to tetramethylsilane using the residual solvent peak as a reference standard. Coupling constants ( $J$ ) are reported in hertz.  $^{13}\text{C}$  NMR characterizations were performed on a Bruker-300 instrument, working at 74.99 MHz or a Varian Inova-500 instrument, working at 125.29 MHz. FT-IR measurements were performed using a Nicolet Magna-IR 750. UV-Vis spectra were recorded on a Varian Cary 400 Scan spectrophotometer.

Mass spectrometry measurements were performed a Kratos MS-50 with an electron impact source or by positive mode electrospray ionization on a Micromass ZabSpec Hybrid Sector-TOF. The liquid carrier was infused into the electrospray source by means of a Harvard syringe pump at a flow rate of 10  $\mu\text{L}/\text{minute}$ . The sample solution, in the same solvent, was introduced *via* a 1  $\mu\text{L}$ -loop-injector. Pre-purified nitrogen was used as a spray pneumatic aid and filtered air as the bath gas, heated at *ca.* 80  $^\circ\text{C}$ . For low resolution, the mass spectra were acquired by magnet scan at a rate of 5 seconds/decade at *ca.* 1000 resolution. For exact mass measurements, the spectra were obtained by voltage scan over a narrow mass range at *ca.* 10000 resolution. Data acquisition and processing was achieved by using the OPUS software package on a Digital Alpha station with VMS operating system.

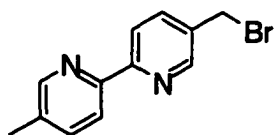


**6'-Methyl-2,2'-bipyridine-6-carbaldehyde (18).**<sup>6</sup> A solution of 6,6'-Dimethyl-2,2'-bipyridine (1.00 g, 5.4 mmol) in dioxane (25 mL) was treated with SeO<sub>2</sub> (0.70 g, 6.3 mmol) and heated at reflux for 24 h. The mixture was filtered while hot through Celite and the filtrate was concentrated under reduced pressure to afford a yellow solid. This solid was dissolved in ethyl acetate (100 mL) and the solution was extracted with 0.3 M Na<sub>2</sub>S<sub>2</sub>O<sub>5</sub> solution (3 × 30 mL). The combined aqueous layers were treated with Na<sub>2</sub>CO<sub>3</sub> until a pH value of 10 was attained and then it was extracted with CH<sub>2</sub>Cl<sub>2</sub> (4 × 50 mL). The combined organic layers were dried over Na<sub>2</sub>SO<sub>4</sub>, filtered and concentrated under reduced pressure to afford a beige solid (4.71 g, 45%). M.p. 140-142 °C (lit.<sup>6</sup> 135-136 °C); <sup>1</sup>H NMR (300 MHz, CDCl<sub>3</sub>) δ 10.14 (s, 1H), 8.66 (dd, *J*<sub>1</sub>=6 Hz, *J*<sub>2</sub>=2 Hz, 1 H), 8.33 (d, *J*=6 Hz, 1H), 7.95-7.97 (m, 2H), 7.74 (t, *J*=8 Hz, 1H), 7.20 (d, *J*=8 Hz, 1H), 2.62 (s, 3H).

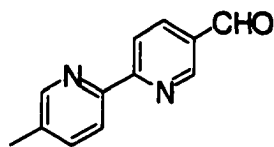


**6'-Methyl-2,2'-bipyridine-6-carboxylic acid (19).** A rapidly stirred suspension of 6'-methyl-2,2'-bipyridine-6-carbaldehyde **18** (0.50 g, 2.5 mmol) in EtOH (20 mL) was treated with a solution of silver nitrate (0.45 g, 2.6 mmol) in water (4.5 mL). Then, 1 M NaOH solution (11.1 mL) was added dropwise over a period of 20 min. The black mixture was stirred for 24 h at room temperature. The mixture was filtered through Celite and the filtrate was washed with CH<sub>2</sub>Cl<sub>2</sub> (2 × 10 mL) to remove unreacted starting material. The pH of the water layer was adjusted to 3.5 by the addition of a 1:1 mixture

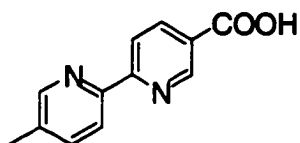
of 4 N HCl and acetic acid. The solution was extracted with  $\text{CHCl}_3$  ( $5 \times 20$  mL) and the combined organic layers were dried over  $\text{Na}_2\text{SO}_4$  and filtered. Concentration of the filtrate under reduced pressure afforded a yellowish solid (0.29 g, 53%). M.p. 189-190 °C;  $^1\text{H}$  NMR (300 MHz,  $\text{CDCl}_3$ )  $\delta$  8.68 (d,  $J=8$  Hz, 1H), 8.22 (d,  $J=8$  Hz, 1H), 8.11 (t,  $J=8$  Hz, 1H), 8.06 (t,  $J=8$  Hz, 1H), 7.76 (t,  $J=8$ , 1H), 7.26 (d,  $J=5$  Hz, 1H), 2.62 (s, 3H);  $^{13}\text{C}$  NMR (125.3 MHz,  $\text{DMSO}-d_6$ )  $\delta$  166.7, 158.4, 156.1, 154.5, 149.2, 139.3, 138.3, 125.4, 124.7, 124.1, 118.8, 25.1; FT-IR (microscope)  $\nu$  2998, 2919, 2616, 2566, 1769, 1704, 1584, 1474, 1447, 1416, 1323, 1261, 1155, 805, 770, 724, 634  $\text{cm}^{-1}$ ; HRMS (EI)  $m/z$ : 214.0746  $[\text{M}]^+$ ,  $\text{C}_{12}\text{H}_{10}\text{N}_2\text{O}_2$ ; calculated 214.0742  $[\text{M}]^+$ ,  $\text{C}_{12}\text{H}_{10}\text{N}_2\text{O}_2$ .



**5-(Bromomethyl)-5'-methyl-2,2'-bipyridine (20).**<sup>7</sup> A mixture of 5,5'-dimethyl-2,2'-bipyridine (2.00 g, 10.9 mmol) and NBS (1.90 g, 10.6 mmol) in  $\text{CCl}_4$  (20 mL) was treated with a catalytic amount of AIBN and heated at reflux for 8 h under argon. The mixture was filtered while hot and the filtrate was cooled to room temperature and concentrated under reduced pressure to afford a yellow solid. The product was isolated by flash chromatography (alumina, 1% methanol in  $\text{CH}_2\text{Cl}_2$ ) as a white solid (1.2 g, 43%). M.p. 151-153 °C (lit:<sup>7</sup> 153-154 °C);  $^1\text{H}$  NMR (300 MHz,  $\text{CDCl}_3$ )  $\delta$  8.66 (s, 1H), 8.51 (s, 1H), 8.40 (d,  $J=8$  Hz, 1H), 8.30 (d,  $J=8$  Hz, 1H), 7.83 (dd,  $J_1=8$  Hz,  $J_2=2$  Hz, 1H), 7.66 (d,  $J=8$  Hz, 1H), 4.51 (s, 2H), 2.40 (s, 3H).

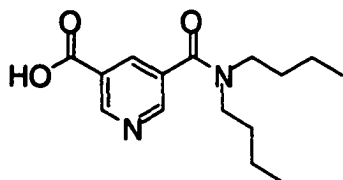


**5'-Methyl-2,2'-bipyridine-5-carbaldehyde (21).**<sup>7b</sup> A solution of hexamethylenetetramine (1.10 g, 7.6 mmol) in CH<sub>2</sub>Cl<sub>2</sub> (20 mL) heated at reflux was treated with a solution of 5-methyl-5'-bromomethyl-2,2'-bipyridine (20) (1.00 g, 3.8 mmol) in CH<sub>2</sub>Cl<sub>2</sub> (20 mL) dropwise and the mixture was further heated for 3 h. After cooling to room temperature, the deposited white solid (1.98 g, 77 %) was filtered off, washed with CH<sub>2</sub>Cl<sub>2</sub> (10 mL) and air-dried. This solid was then treated with a 1:1 solution of acetic acid/water (20 mL) and the mixture was heated at reflux for 1 h. Concentrated HCl (2 mL) was added and the solution was further heated at reflux for 10 min. The acidic mixture was cooled in an ice bath and treated with 10% NaOH solution until a pH of 10 was attained. The precipitate that formed was filtered off, washed with water (20 mL) and dried under vacuum (0.48 g, 64%). M.p. 135-137 °C; <sup>1</sup>H NMR (500 MHz, CDCl<sub>3</sub>) δ 10.14 (s, 1H), 9.09 (d, *J*=1.5 Hz, 1H), 8.56 (d, *J*=8.0 Hz, 1H), 8.53 (s, 1H), 8.39 (d, *J*=8.0 Hz, 1H), 8.26 (dd, *J*<sub>1</sub>=8.5 Hz, *J*<sub>2</sub>=2.0 Hz, 1H), 7.66 (d, *J*=8.5 Hz, 1H), 2.41 (s, 3H); <sup>13</sup>C NMR (75.5 MHz, CDCl<sub>3</sub>) δ 190.7, 161.0, 152.3, 151.8, 150.1, 137.6, 136.9, 134.9, 130.9, 121.8, 121.0, 18.5; FT-IR (cast) ν 2918, 2829, 1689, 1593, 1551, 1471, 1402, 1384, 1361, 1254, 1207, 1180, 1141, 1075, 1053, 1031, 847, 826, 734, 710, 651, 459, 418 cm<sup>-1</sup>; HRMS (EI) *m/z*: 198.0792 [M]<sup>+</sup>, C<sub>12</sub>H<sub>10</sub>N<sub>2</sub>O; calculated 198.0793 [M]<sup>+</sup>, C<sub>12</sub>H<sub>10</sub>N<sub>2</sub>O.



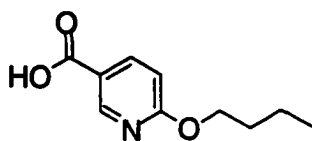
**5'-Methyl-2,2'-bipyridine-5-carboxylic acid (22).** A solution of 5'-methyl-2,2'-bipyridine-5-carbaldehyde (21) (0.40 g, 2.0 mmol) and 35% aqueous solution of H<sub>2</sub>O<sub>2</sub> (0.5 mL) in acetonitrile (10 mL) was treated with NaH<sub>2</sub>PO<sub>4</sub> (100 mg, 0.8 mmol) dissolved in water (2 mL). The mixture was stirred in a cold water bath at 5-10°C and treated with

an aqueous solution (10 mL) of NaClO<sub>2</sub> (0.50 g, 5.52 mmol) dropwise over a period of 1 h maintaining the temperature at less than 10°C. After stirring for another 2 h at 5-10°C, a small amount of Na<sub>2</sub>SO<sub>3</sub> (100 mg) was added to destroy the unreacted HOCl and H<sub>2</sub>O<sub>2</sub>. The mixture was cooled in an ice bath and treated with 10% HCl solution until a pH of 3.5 was obtained. The deposited solid was filtered off, washed with water (10 mL) and vacuum dried as a beige solid (0.21 g, 49%). M.p. > 300 °C; <sup>1</sup>H NMR (500 MHz, DMSO-*d*<sub>6</sub>) δ 10.31 (br s, 1H), 9.13 (d, *J*=2.5 Hz, 1H), 8.56 (s, 1H), 8.47 (d, *J*=8.0 Hz, 1H), 8.38 (dd, *J*<sub>1</sub>=8.5 Hz, *J*<sub>2</sub>=2.5 Hz, 1H), 8.35 (d, *J*=8.5 Hz, 1H), 7.80 (dd, *J*<sub>1</sub>=7.5 Hz, *J*<sub>2</sub>=2.0 Hz, 1H), 2.37 (s, 3H); <sup>13</sup>C NMR (75.5 MHz, DMSO-*d*<sub>6</sub>) δ 166.2, 158.5, 151.8, 150.1, 149.9, 138.1, 137.6, 134.6, 126.3, 120.8, 119.9, 17.9; FT-IR (microscope) ν 3060, 2921, 2473, 1703, 1594, 1557, 1469, 1369, 1265, 1143, 1053, 1033, 839, 788, 766, 744, 714, 659 cm<sup>-1</sup>; HRMS (EI) *m/z*: 214.0741 [M]<sup>+</sup>, C<sub>12</sub>H<sub>10</sub>N<sub>2</sub>O<sub>2</sub>; calculated 214.0742 [M]<sup>+</sup>, C<sub>12</sub>H<sub>10</sub>N<sub>2</sub>O<sub>2</sub>.



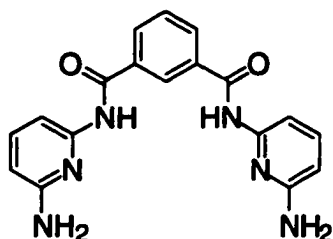
**5-[(Dibutylamino)carbonyl]nicotinic acid (23).** A solution of 3,5-pyridinedicarboxylic acid (1.00 g, 6.0 mmol) in dry CH<sub>2</sub>Cl<sub>2</sub> (25 mL) was treated with SOCl<sub>2</sub> (10 mL) and heated at reflux overnight under argon. After cooling to room temperature, the mixture was concentrated under reduced pressure and the residue was dried under vacuum for 5 h to remove traces of SOCl<sub>2</sub>. The residue was dissolved in dry THF (25 mL) and treated with a THF solution (20 mL) of dibutylamine (0.77 g, 6.0 mmol) and TEA (0.60 g, 6.0 mmol) dropwise. The mixture was stirred overnight at room temperature under argon. An aqueous solution (3 mL) of 10% NaOH was added and the mixture was further stirred

for another 30 min. The solvent was removed under reduced pressure and the residue was treated with water (20 mL). The solution was washed with  $\text{CH}_2\text{Cl}_2$  ( $3 \times 10$  mL) and treated with 10% HCl solution until a pH of 3 was attained. The mixture was extracted with  $\text{CH}_2\text{Cl}_2$  ( $3 \times 20$  mL) and the combined organic layers were dried over  $\text{Na}_2\text{SO}_4$ , filtered and concentrated under reduced pressure to afford a beige solid (0.78 g, 47%). M.p. 158-160 °C;  $^1\text{H}$  NMR (300 MHz,  $\text{CDCl}_3$ )  $\delta$  9.30 (d,  $J=2$  Hz, 1H), 8.84 (d,  $J=2$  Hz, 1H), 8.38 (t,  $J=2$  Hz, 1H), 3.52 (t,  $J=7$  Hz, 4H), 3.18 (t,  $J=7$  Hz, 4H), 1.66 (br m, 4H), 1.52 (br. m, 4H), 1.41 (br. m, 4H), 1.16 (br. m, 4H), 0.97 (t,  $J=7$  Hz, 6H), 0.79 (t,  $J=7$  Hz, 6H);  $^{13}\text{C}$  NMR (100.6 MHz,  $\text{CDCl}_3$ )  $\delta$  167.8, 167.1, 151.0, 150.6, 136.3, 133.0, 126.0, 49.2, 45.3, 31.0, 29.7, 20.4, 19.9, 14.0, 13.7; FT-IR (cast)  $\nu$  2957, 2930, 2872, 1632, 1594, 1458, 1310, 1281, 1230, 1197, 1153, 1113, 1102, 747  $\text{cm}^{-1}$ ; HRMS (EI)  $m/z$ : 278.1635  $[\text{M}]^+$ ,  $\text{C}_{15}\text{H}_{22}\text{N}_2\text{O}_3$ ; calculated 278.1630  $[\text{M}]^+$ ,  $\text{C}_{15}\text{H}_{22}\text{N}_2\text{O}_3$ .



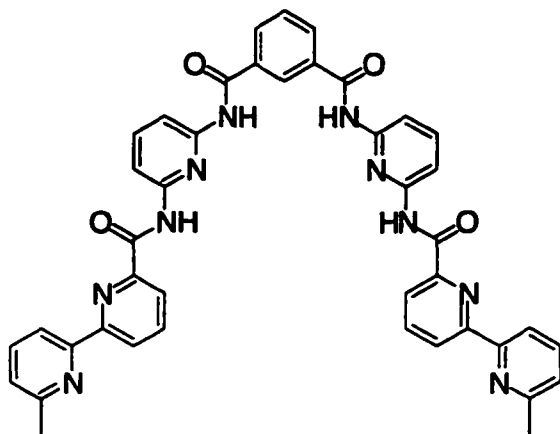
**6-Butoxynicotinic acid (24).**<sup>8</sup> Small pieces of sodium (0.10 g, 4.3 mmol) were added to *n*-butanol (20 mL) and the mixture was stirred under argon until all the sodium dissolved. 2-Bromonicotinic acid (200 mg, 1.0 mmol) was added to the mixture and the solution was heated at reflux overnight under argon. After cooling to room temperature, the solution was treated with water (2 mL) dropwise. The solvent was removed under reduced pressure and the residue treated with water (10 mL). This solution was acidified with 10% HCl solution and the precipitate that formed was filtered off, washed with water (10 mL) and vacuum dried (0.16 g, 83%). M.p. 106-108 °C;  $^1\text{H}$  NMR (300 MHz,  $\text{DMSO}-d_6$ )  $\delta$  12.98 (br s, 1H), 8.70 (dd,  $J_1=1$  Hz,  $J_2=2$  Hz, 1H), 8.13 (dd,  $J_1=9$  Hz,  $J_2=2$

Hz, 1H), 9.88 (dd,  $J_1 = 9$  Hz,  $J_2 = 1$  Hz, 1H), 4.32 (t,  $J = 7$  Hz, 2H), 1.70 (m, 2H), 1.42 (m, 2H), 0.91 (t,  $J = 7$  Hz, 3H).

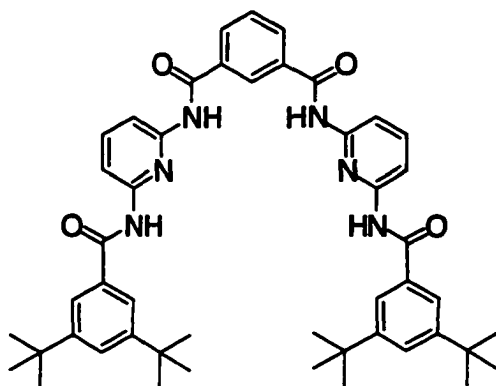


***N,N'*-Bis(6-aminopyridin-2-yl)-isophthalamide (25).**<sup>1a</sup> A solution of isophthaloyl dichloride (**19**) (2.45 g, 12.1 mmol) in THF (60 mL) was added dropwise into a stirred solution of diaminopyridine (20.00 g, 183.5 mmol) and TEA (2.42 g, 24.0 mmol) in THF (200 mL) at room temperature under argon. After the reaction was stirred for 3 h, the solvent was evaporated and the residue was treated with water (100 mL). The precipitate that formed was filtered off, washed with water (500 mL) and dried under vacuum. The product was purified by column chromatography (alumina, 10% MeOH in CHCl<sub>3</sub>) and recrystallized from THF/hexane as a white solid (1.36 g, 53%). M.p. 198-200 °C (lit:<sup>1a</sup> 201-202 °C); <sup>1</sup>H NMR (300 MHz, DMSO-*d*<sub>6</sub>) δ 10.25 (s, 2H), 8.49 (s, 1H), 8.06 (dd,  $J_1 = 8$  Hz,  $J_2 = 2$  Hz, 2H), 7.62 (t,  $J = 8$  Hz, 1H), 7.32-7.67 (m, 4H), 6.25 (dd,  $J_1 = 8$  Hz,  $J_2 = 1$  Hz, 2H), 5.78 (s, 4H).



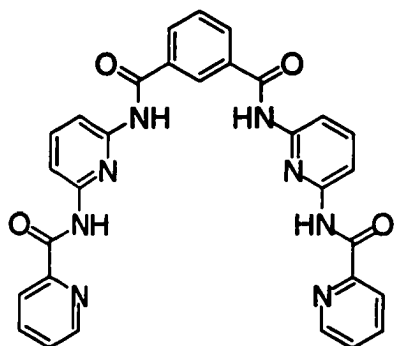


***N,N'*-Bis{6-[(6'-methyl-2,2'-bipyridin-6-yl)carbonyl]amino}pyridin-2-yl}isophthalamide (26).** A solution of 6'-methyl-2,2'-bipyridine-6-carboxylic acid (**20**) (46 mg, 0.2 mmol) in  $\text{SOCl}_2$  (15 mL) was heated at reflux for 4 h under argon.  $\text{SOCl}_2$  was then removed under reduced pressure and the residue was vacuum dried for 5 h. The obtained solid was dissolved in THF (20 mL) and treated with a solution of *N,N'*-bis(6-aminopyridin-2-yl)-isophthalamide (**25**) (38 mg, 0.1 mmol) and TEA (0.22 g, 0.2 mmol) in THF (20 mL) dropwise at room temperature under argon. The mixture was stirred overnight at room temperature. The solution was washed with water ( $3 \times 10$  mL), dried over  $\text{Na}_2\text{SO}_4$  and filtered. Concentration under reduced pressure of the filtrate afforded a yellow residue. The product was purified by flash chromatography (alumina, 1% to 10% gradient of MeOH in  $\text{CHCl}_3$ ) and recrystallized from ethanol/water as a white solid (36 mg, 44%). M.p.  $>300$  °C;  $^1\text{H}$  NMR (300 MHz,  $\text{CDCl}_3$ )  $\delta$  10.34 (s, 2H), 8.74 (s, 2H), 8.58 (d,  $J=7$  Hz, 2H), 8.53 (s, 1H), 8.13-8.27 (m, 10H), 7.98 (t,  $J=5$  Hz, 2H), 7.85 (t,  $J=8$  Hz, 2H), 7.64-7.72 (m, 3H), 7.12 (d,  $J=8$  Hz, 2H), 2.58 (s, 6H);  $^{13}\text{C}$  NMR (75.5 MHz,  $\text{CDCl}_3$ )  $\delta$  164.5, 162.5, 5.1, 149.9, 149.4, 148.3, 141.1, 138.5, 137.4, 134.7, 131.4, 129.7, 125.4, 124.4, 123.9, 122.4, 118.0, 110.1, 24.5; FT-IR (cast)  $\nu$  3346, 1692, 1583, 1507, 1447, 1391, 1301, 1243, 1156, 1074, 994, 797, 758, 712, 634  $\text{cm}^{-1}$ ; HRMS (EI)  $m/z$ : 741.2685  $[\text{M}+\text{H}]^+$ ,  $\text{C}_{42}\text{H}_{33}\text{N}_{10}\text{O}_4$ ; calculated 741.2686  $[\text{M}+\text{H}]^+$ ,  $\text{C}_{42}\text{H}_{33}\text{N}_{10}\text{O}_4$ .



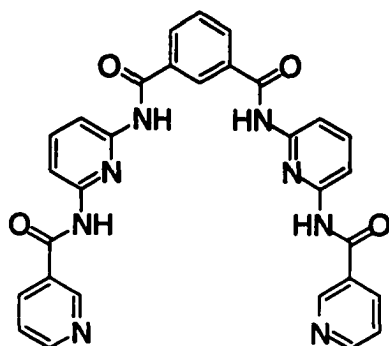
***N,N'*-Bis[6-[(3,5-di-*tert*-butylbenzoyl)amino]pyridin-2-yl]isophthalamide (27).** A solution of 3,5-di-*tert*-butylbenzoic acid (0.05 g, 0.2 mmol) in oxalyl chloride (15 mL) was heated at reflux for 4 h under argon. The oxalyl chloride was removed under reduced pressure and the residue was vacuum dried for 5 h. The obtained solid was dissolved in THF (30 mL) and treated with a solution of *N,N'*-bis(6-aminopyridin-2-yl)-isophthalamide (25) (38 g, 0.1 mmol) and TEA (0.22 g, 0.2 mmol) in THF (20 mL) dropwise at room temperature under argon. After stirring the mixture overnight at room temperature, the solvent was evaporated to afford a yellow residue which was purified by flash chromatography (alumina, 1% MeOH in CHCl<sub>3</sub>) to give a white solid (48 mg, 55%). M.p. >180 °C (dec.); <sup>1</sup>H NMR (300 MHz, CDCl<sub>3</sub>) δ 8.48 (s, 2H), 8.35 (s, 2H), 8.15 (d, *J*=8 Hz, 2H), 8.09 (dd, *J*<sub>1</sub>=8 Hz, *J*<sub>2</sub>=2 Hz, 2H), 8.08 (d, *J*=8 Hz, 2H), 7.82 (t, *J*=8 Hz, 2H), 7.72 (d, *J*=1 Hz, 2H), 7.60-7.65 (m, 3H), 1.36 (s, 36H); <sup>13</sup>C NMR (75.5 MHz, CDCl<sub>3</sub>) δ 166.6, 164.3, 151.8, 150.1, 149.4, 141.1, 134.9, 133.7, 130.8, 129.6, 126.7, 125.9, 121.4, 110.3, 109.8, 35.12, 31.5; FT-IR (cast) ν 3421, 3285, 3015, 2963, 2905, 2868, 1680, 1584, 1506, 1478, 1449, 1393, 1363, 1307, 1242, 1158, 1136, 898, 885, 800, 756, 704, 666, 596, 543 cm<sup>-1</sup>; HRMS (EI) *m/z*: 803.4261 [M+Na]<sup>+</sup>, C<sub>48</sub>H<sub>56</sub>N<sub>6</sub>NaO<sub>4</sub>; calculated 803.4261 [M+Na]<sup>+</sup>, C<sub>48</sub>H<sub>56</sub>N<sub>6</sub>NaO<sub>4</sub>.

**General procedure for the preparation of 28, 29, 30, 31, and 32.** A solution of the corresponding carboxylic acid (1.2 mmol) in  $\text{SOCl}_2$  (15 mL) was heated at reflux for 4 h under argon. Excess  $\text{SOCl}_2$  was removed under reduced pressure and the residue was dried under vacuum for 5 h. The obtained solid was dissolved in  $\text{CH}_2\text{Cl}_2$  (20 mL) and treated with a solution of *N,N'*-bis(6-aminopyridin-2-yl)-isophthalamide (**25**) (175 mg, 0.5 mmol) and TEA (0.10 g, 1.0 mmol) in THF (20 mL) dropwise at room temperature under argon. After the mixture was stirred overnight, the solvent was evaporated under reduced pressure. The residue was treated with water (20 mL) and the precipitate that formed was filtered off, washed with water (10 mL) and vacuum dried. The product was purified by chromatography over alumina using a gradient of 1% to 10% MeOH in  $\text{CHCl}_3$  as the eluant.

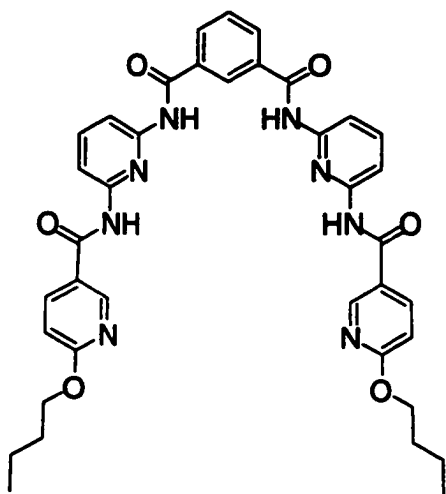


***N,N'*-Bis[6-[(pyridin-2-ylcarbonyl)amino]pyridin-2-yl]isophthalamide (28).** The carboxylic acid was picolinic acid (0.14 g, 1.2 mmol) and the product was collected as a beige solid (0.13 g, 47%). M.p. >270 °C (dec.);  $^1\text{H}$  NMR (300 MHz,  $\text{CDCl}_3$ )  $\delta$  10.41 (s, 2H), 8.72 (br s, 2H), 8.63 (d,  $J=5$  Hz, 2H), 8.57 (s, 1H), 8.30 (d,  $J=8$  Hz, 2H), 8.17-8.13 (m, 6H), 7.94 (m, 6H), 7.67 (t,  $J=8$  Hz, 1H), 7.50-7.46 (m, 2H);  $^{13}\text{C}$  NMR (75.5 MHz,  $\text{DMSO-}d_6$ )  $\delta$  182.3, 176.2, 175.7, 165.2, 161.7, 150.8, 149.0, 148.6, 141.0, 138.6, 131.6, 128.4, 127.6, 127.1, 124.5, 122.2, 110.2, 108.6; FT-IR (microscope)  $\nu$  3330, 1089, 1053, 1680, 1667, 1589, 1514, 1482, 1449, 1393, 1307, 1245, 1229, 1155, 1090, 1076, 999,

800, 748, 714, 691, 613, 590  $\text{cm}^{-1}$ ; HRMS (EI)  $m/z$ : 581.1664  $[\text{M}+\text{Na}]^+$ ,  $\text{C}_{30}\text{H}_{22}\text{N}_8\text{NaO}_4$ ; calculated 581.1662  $[\text{M}+\text{Na}]^+$ ,  $\text{C}_{30}\text{H}_{22}\text{N}_8\text{NaO}_4$ .

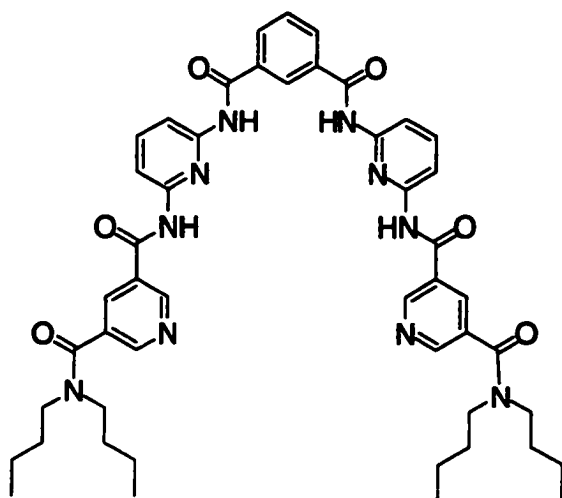


***N,N'*-Bis(6-[(pyridin-3-ylcarbonyl)amino]pyridin-2-yl)isophthalamide (29).** The carboxylic acid was nicotinic acid (0.14 g, 1.2 mmol) and the product was collected as a white solid (0.18 g, 64%). M.p. 192-194 °C;  $^1\text{H}$  NMR (300 MHz,  $\text{DMSO}-d_6$ )  $\delta$  10.77 (s, 2H), 10.60 (s, 2H), 9.12 (d,  $J=2$  Hz, 2H), 8.77 (m, 2H), 8.58 (br s, 1H), 8.33 (dt,  $J_1=8$  Hz,  $J_2=2$  Hz, 2H), 8.20 (dd,  $J_1=8$  Hz,  $J_2=2$  Hz, 2H), 7.95 (d,  $J=4$  Hz, 2H), 7.93 (s, 2H), 7.89 (m, 2H), 7.69 (t,  $J=8$ , 1H), 7.55 (m, 2H);  $^{13}\text{C}$  NMR (75.5 MHz,  $\text{DMSO}-d_6$ )  $\delta$  165.2, 164.6, 152.4, 150.4, 150.2, 148.8, 140.2, 135.6, 134.1, 131.4, 129.8, 128.9, 127.3, 123.4, 111.6, 111.4; FT-IR (microscope)  $\nu$  3428, 3319, 3233, 3042, 1667, 1590, 1524, 1477, 1444, 1391, 1304, 1239, 1160, 1028, 805, 733, 715  $\text{cm}^{-1}$ ; HRMS (EI)  $m/z$ : 581.1656  $[\text{M}+\text{Na}]^+$ ,  $\text{C}_{30}\text{H}_{22}\text{N}_8\text{NaO}_4$ ; calculated 581.1662  $[\text{M}+\text{Na}]^+$ ,  $\text{C}_{30}\text{H}_{22}\text{N}_8\text{NaO}_4$ .

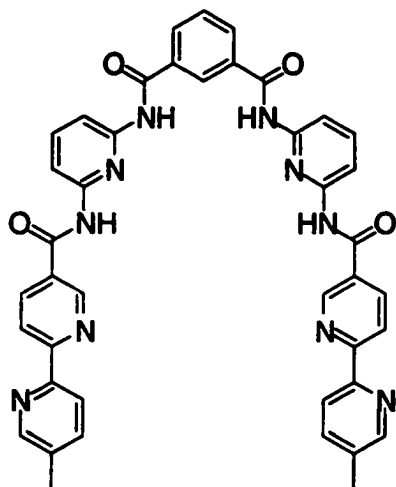


***N,N'*-Bis(6-((6-butoxypyridin-3-yl)carbonyl)amino)pyridin-2-yl)isophthalamide**

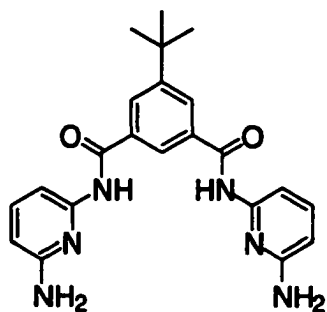
**(30).** The carboxylic acid was 6-butoxynicotinic acid (0.23 g, 1.2 mmol) and the product was collected as a white solid (0.21 g, 61%). M.p. 244-246 °C; <sup>1</sup>H NMR (500 MHz, CD<sub>2</sub>Cl<sub>2</sub>) δ 8.72 (s, 2H), 8.56 (s, 2H), 8.48 (s, 1H), 8.33 (s, 2H), 8.13-8.06 (m, 8H), 7.82 (t, *J*=8.5 Hz, 2H), 7.67 (t, *J*=8.5 Hz, 1H), 6.81 (d, *J*=8.5 Hz, 2H), 4.36 (t, *J*=7 Hz, 4H), 1.79-1.73 (m, 4H), 1.50-1.45 (m, 4H), 0.97 (t, *J*=7 Hz, 6H); <sup>13</sup>C NMR (75.5 MHz, CDCl<sub>3</sub>) δ 166.6, 164.4, 163.9, 149.8, 149.5, 147.2, 141.1, 137.7, 134.8, 131.0, 129.7, 125.8, 122.9, 111.3, 110.5, 110.1, 66.7, 31.0, 19.3, 13.9; FT-IR (cast) ν 3315, 2957, 1677, 1600, 1514, 1487, 1446, 1398, 1369, 1293, 1241, 797 cm<sup>-1</sup>; HRMS (EI) *m/z*: 703.2984 [M+H]<sup>+</sup>, C<sub>38</sub>H<sub>39</sub>N<sub>8</sub>O<sub>6</sub>; calculated 703.2993 [M+H]<sup>+</sup>, C<sub>38</sub>H<sub>39</sub>N<sub>8</sub>O<sub>6</sub>.



***N***-[6-((3-((2-((5-(Dibutylaminocarbonyl)pyridin-3-yl)carbonyl)amino)pyridin-6-yl))carbonyl]benzoyl)amino)pyridin-2-yl]-*N'*-dibutylpyridine-3,5-dicarboxamide (31). The carboxylic acid was 5-[(dibutylamino)carbonyl]nicotinic acid (23) (0.33 g, 1.2 mmol) and the product was collected as a yellow solid (0.19 g, 43%). M.p. 140-142 °C; <sup>1</sup>H NMR (300 MHz, CDCl<sub>3</sub>) δ 9.13 (d, *J*=2 Hz, 2H), 9.06 (br s, 2H), 8.95 (br s, 2H), 8.84 (d, *J*=2 Hz, 2H), 8.61 (s, 1H), 8.27 (t, *J*=2 Hz, 2H), 8.19 (dd, *J*<sub>1</sub>=8 Hz, *J*<sub>2</sub>=2 Hz, 2H), 8.13 (d, *J*=8 Hz, 2H), 8.01 (d, *J*=8 Hz, 2H), 7.79 (t, *J*=8 Hz, 2H), 7.64 (t, *J*=8 Hz, 1H), 3.41 (br. t, 4H), 3.16 (br. t, 4H), 1.56 (br. m, 4H), 1.47 (br. m, 4H), 1.32 (br. m, 4H), 1.12 (br. m, 4H), 0.91 (t, *J*=8 Hz, 6H), 0.75 (t, *J*=7 Hz, 6H); <sup>13</sup>C NMR (75.5 MHz, CDCl<sub>3</sub>) δ 167.9, 165.2, 163.6, 150.6, 149.9, 149.6, 149.0, 140.7, 134.4, 134.1, 132.7, 131.8, 129.7, 129.3, 125.1, 111.1, 110.9, 49.0, 44.9, 30.8, 29.5, 20.2, 19.7, 12.8, 13.5; FT-IR (cast) ν 3266, 2958, 2931, 2872, 1680, 1620, 1587, 1515, 1446, 1299, 1241, 1158, 1109, 1026, 799, 751, 584 cm<sup>-1</sup>; HRMS (EI) *m/z*: 891.4292 [M+Na]<sup>+</sup>, C<sub>48</sub>H<sub>56</sub>N<sub>10</sub>NaO<sub>6</sub>; calculated 891.4282 [M+Na]<sup>+</sup>, C<sub>48</sub>H<sub>56</sub>N<sub>10</sub>NaO<sub>6</sub>.

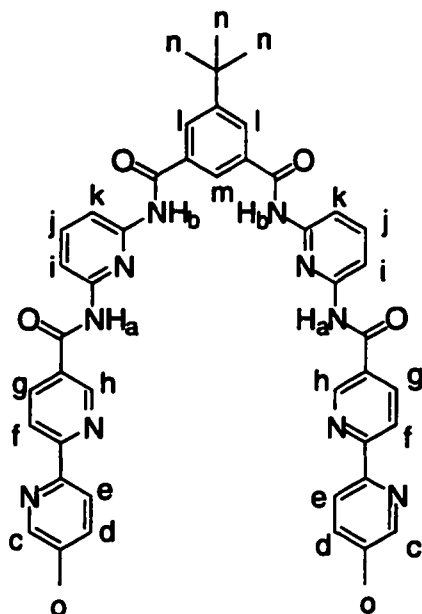


***N,N'*-Bis{6-[(5'-methyl-2,2'-bipyridin-5-yl)carbonyl]amino}pyridin-2-yl}isophthalamide (32).** The carboxylic acid was 5'-methyl-2,2'-bipyridine-5-carboxylic acid (19) (0.26 g, 1.2 mmol) and the product was collected as a beige solid (0.08 g 23%). M.p. >250°C (dec.); <sup>1</sup>H NMR (500 MHz, DMSO-*d*<sub>6</sub>) δ 10.88 (s, 2H), 10.69 (s, 2H), 9.21 (s, 2H), 8.58 (s, 1H), 8.54 (s, 2H), 8.46 (s, 4 H), 8.34 (d, *J* = 8 Hz, 2H), 8.20 (dd, *J*<sub>1</sub> = 8 Hz, *J*<sub>2</sub> = 2 Hz, 2H), 7.95 (dd, *J*<sub>1</sub> = 6 Hz, *J*<sub>2</sub> = 2 Hz, 4H), 7.91 (dd, *J*<sub>1</sub> = 5 Hz, *J*<sub>2</sub> = 5 Hz, 2H), 7.79 (d, *J* = 9 Hz, 2H), 7.71 (t, *J* = 9 Hz, 1H) 2.37 (s, 6H); <sup>13</sup>C NMR (125.7 MHz, DMSO-*d*<sub>6</sub>) δ 165.3, 164.4, 157.7, 151.7, 150.5, 150.3, 149.7, 148.7, 140.3, 137.8, 136.9, 134.6, 134.1, 132.1, 131.4, 129.5, 129.0, 127.4, 120.7, 119.7, 111.5, 111.3, 17.9; FT-IR (microscope) ν 3341, 3300, 3066, 3027, 2918, 1649, 1592, 1518, 1453, 1370, 1310, 1241, 1096, 1030, 834, 796, 782, 743, 728, 685, 658, 635 cm<sup>-1</sup>; HRMS (EI) *m/z*: 741.2688 [M+H]<sup>+</sup>, C<sub>42</sub>H<sub>33</sub>N<sub>10</sub>O<sub>4</sub>; calculated 741.2686 [M+H]<sup>+</sup>, C<sub>42</sub>H<sub>33</sub>N<sub>10</sub>O<sub>4</sub>.



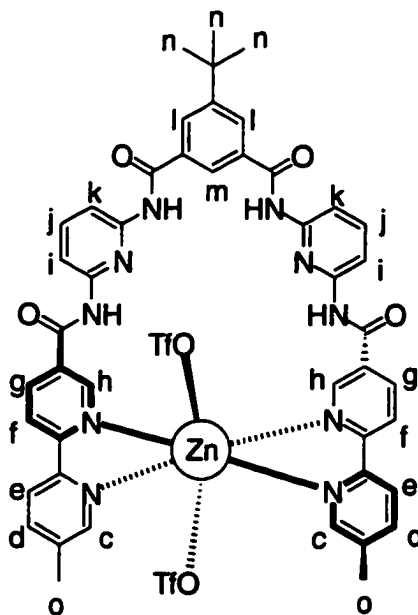
***N,N'*-Bis(6-aminopyridin-2-yl)-5-tert-butyl-isophthalamide (33).** A solution of 5-*tert*-butylisophthalic acid (1.00 g, 4.5 mmol) in SOCl<sub>2</sub> (15 mL) was heated at reflux overnight under argon. The mixture was cooled to room temperature and the excess thionyl chloride was removed under reduced pressure. The oily residue was vacuum dried for 5 h. The residue was dissolved in CH<sub>2</sub>Cl<sub>2</sub> (40 mL) and added to a solution of diaminopyridine (2.50 g, 22.9 mmol) and TEA (0.76 g, 7.6 mmol) in CH<sub>2</sub>Cl<sub>2</sub> (20 mL) dropwise at room temperature. After the mixture was stirred for 3 h, the solvent was evaporated and the residue was treated with water (50 mL). The precipitate that formed was filtered off, washed with 20% aqueous EtOH (200 mL) and vacuum dried. The product was recrystallized from EtOH/water as a white solid (1.31 g, 76%). M.p. 152-154 °C; <sup>1</sup>H NMR (300 MHz, CDCl<sub>3</sub>) δ 8.44 (s, 2H), 8.172 (t, *J*=2 Hz, 1H), 8.10 (d, *J*=2 Hz, 2H), 7.70 (d, *J*=8 Hz, 2H), 7.49 (t, *J*=8 Hz, 2H), 6.30 (d, *J*=8 Hz, 2H), 4.35 (s, 4H), 1.37 (s, 9H); <sup>13</sup>C NMR (75.6 MHz, CDCl<sub>3</sub>) δ 164.9, 157.2, 153.3, 149.9, 140.3, 135.0, 128.1, 122.5, 104.1, 103.7, 35.1, 31.3; FT-IR (cast) ν 3450, 3369, 3295, 3030, 2965, 1689, 1659, 1614, 1577, 1526, 1450, 1347, 1327, 1293, 1250, 1230, 1164, 1151, 791, 752, 614, 576 cm<sup>-1</sup>; HRMS (ES) *m/z*: 404.1955 [M]<sup>+</sup>, C<sub>16</sub>H<sub>15</sub>N<sub>2</sub>O<sub>4</sub>; calculated 404.1960 [M]<sup>+</sup>, C<sub>16</sub>H<sub>15</sub>N<sub>2</sub>O<sub>4</sub>.





**5-*tert*-Butyl-*N,N'*-bis(6-((5'-methyl-2,2'-bipyridin-5-yl)carbonyl)amino)pyridin-2-yl)isophthalamide (34).** A solution of 5'-methyl-2,2'-bipyridine-5-carboxylic acid (**19**) (0.26 g, 1.2 mmol) in  $\text{SOCl}_2$  (15 mL) was heated at reflux for 4 hours under argon. The excess  $\text{SOCl}_2$  was removed under reduced pressure and the residue was vacuum dried for 5 h. The obtained solid was dissolved in  $\text{CH}_2\text{Cl}_2$  (20 mL) and treated with a solution of *N,N'*-bis(6-aminopyridin-2-yl)-5-*tert*-butylisophthalamide (**33**) (200 mg, 0.5 mmol) and TEA (0.10 g, 1.0 mmol) in  $\text{CH}_2\text{Cl}_2$  (20 mL) dropwise at room temperature under argon. After the mixture was stirred overnight, it was washed with water (3 × 10 ml), dried over anhydrous  $\text{Na}_2\text{SO}_4$  and filtered. Concentration of the filtrate under reduced pressure afforded a beige residue. The product was purified by flash chromatography (alumina, 1% to 10% MeOH in  $\text{CHCl}_3$ ) as a white solid (0.26 g, 65%). M.p. >190 °C (dec.);  $^1\text{H}$  NMR (500 MHz,  $\text{CD}_2\text{Cl}_2$ )  $\delta$  9.17 (s, H(h)), 8.71 (br s, H(a)), 8.62 (br s, H(b)), 8.53 (d,  $J=5.5$  Hz, H(f)), 8.51 (s, H(c)), 8.48 (s, H(m)), 8.34 (d,  $J=8.5$  Hz, H(e)), 8.29 (s, H(g)), 8.28 (s, H(l)), 8.17 (d,  $J=8.0$  Hz, H(i)), 8.12 (d,  $J=8.0$  Hz, H(k)), 7.86 (t,  $J=8.5$  Hz, H(j)), 7.63 (d,  $J=8.5$  Hz, H(d)), 2.38 (s, H(o)), 1.43 (s, H(n));  $^{13}\text{C}$  NMR (125.3 MHz,  $\text{CDCl}_3$ )  $\delta$

164.8, 163.4, 162.3, 158.5, 151.7, 149.6, 149.5, 149.3, 147.9, 140.9, 137.6, 136.4, 136.3, 134.6, 134.2, 128.9, 128.7, 122.3, 121.3, 120.6, 110.3, 35.3, 31.3, 29.8; FT-IR (cast)  $\nu$  3288, 2964, 1682, 1588, 1513, 1447, 1396, 1298, 1241, 1158, 1128, 1028, 896, 838, 798, 744, 651  $\text{cm}^{-1}$ ; HRMS (ES)  $m/z$ : 797.3312  $[\text{M}+\text{H}]^+$ ,  $\text{C}_{46}\text{H}_{41}\text{N}_{10}\text{O}_4$ , calculated 797.3312  $[\text{M}+\text{H}]^+$ ,  $\text{C}_{46}\text{H}_{41}\text{N}_{10}\text{O}_4$ .



**Complex 34•Zn.** A solution of **34** (5 mg,  $6.3 \times 10^{-3}$  mmol) in  $\text{CH}_2\text{Cl}_2$  (5 mL) was treated with a solution of  $\text{Zn}(\text{OTf})_2$  (2.3 mg,  $6.3 \times 10^{-3}$  mmol) in  $\text{CH}_3\text{CN}$  (1 mL) and the mixture was stirred for 15 min at room temperature under argon. The solvent was evaporated under reduced pressure and the residue treated with  $\text{CH}_2\text{Cl}_2$  (1 mL). The deposited colorless solid was filtered off and vacuum dried (7.3 mg, 100%).  $^1\text{H}$  NMR (500 MHz, 10%  $\text{CD}_3\text{CN}$  in  $\text{CD}_2\text{Cl}_2$ )  $\delta$  10.50 (s, H(a)), 9.52 (s, H(b)), 9.38 (s, H(h)), 8.65 (d,  $J=8$  Hz, H(f)), 8.45 (d,  $J=8.5$  Hz, H(g)), 8.33 (s, H(m)), 8.31 (d,  $J=8.5$  Hz, H(e)), 8.27 (s, H(l)), 8.09 (d,  $J=8$  Hz, H(k)), 8.07 (s, H(c)), 8.01 (d,  $J=8.0$  Hz, H(d)), 7.90 (d,  $J=7.5$  Hz, H(i)), 7.816 (t,  $J=8.5$  Hz, H(j)), 2.36 (s, H(o)), 1.40 (s, H(n));  $^{13}\text{C}$  NMR (125.7 MHz, 10%

$\text{CD}_3\text{CN}$  in  $\text{CD}_2\text{Cl}_2$ )  $\delta$  165.0, 163.6, 153.6, 151.6, 150.8, 149.9, 148.5, 147.5, 146.1, 142.1, 141.8, 140.8, 139.1, 134.7, 134.3, 129.5, 122.9, 122.6, 122.2, 110.4, 109.7, 35.2, 31.0, 18.4; FT-IR (cast)  $\nu$  3270, 2963, 1681, 1586, 1522, 1477, 1449, 1390, 1245, 1161, 1031, 901, 840, 799, 737, 639  $\text{cm}^{-1}$ ; HRMS (ES)  $m/z$ : 859.2445  $[\text{M}-\text{H}]^+$ ,  $\text{C}_{46}\text{H}_{39}\text{N}_{10}\text{O}_4\text{Zn}$ ; calculated 859.2447  $[\text{M}-\text{H}]^+$ ,  $\text{C}_{46}\text{H}_{39}\text{N}_{10}\text{O}_4\text{Zn}$ ; 1159.1648  $[\text{M}+2\text{Tf}+\text{H}]^+$ ,  $\text{C}_{48}\text{H}_{41}\text{F}_6\text{N}_{10}\text{O}_{10}\text{S}_2\text{Zn}$ ; calculated 1159.1644  $[\text{M}+2\text{Tf}+\text{H}]^+$ ,  $\text{C}_{48}\text{H}_{41}\text{F}_6\text{N}_{10}\text{O}_{10}\text{S}_2\text{Zn}$ .

## 4.8 References

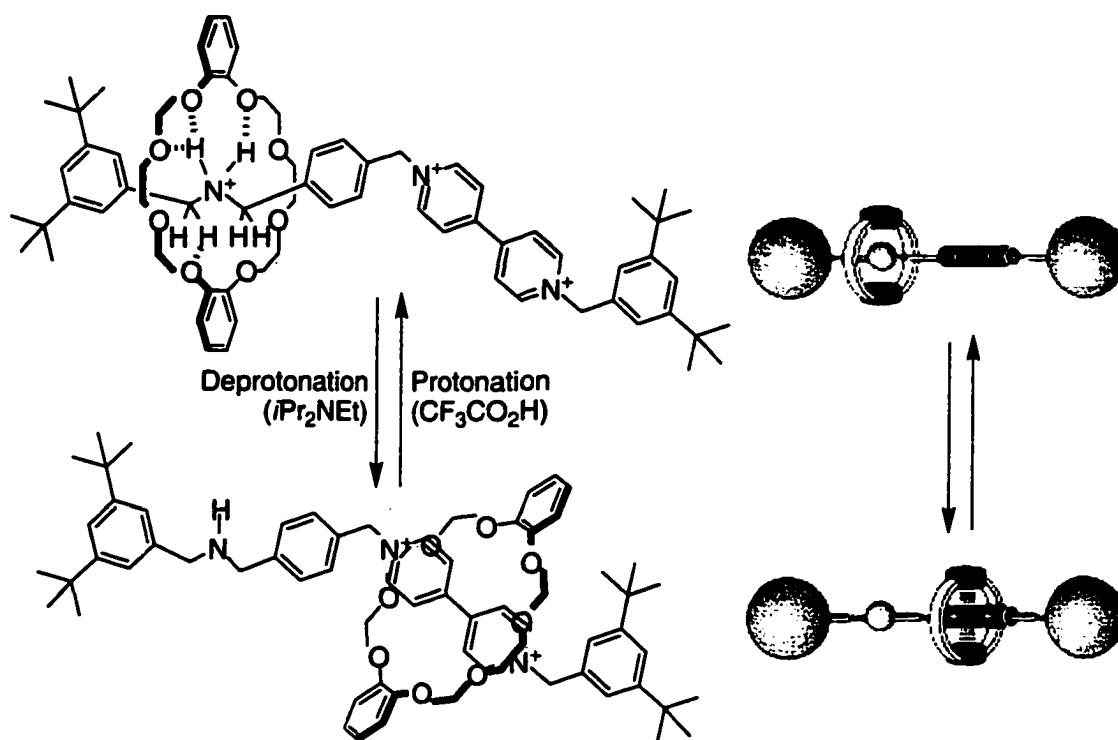
1. (a) S.-K. Chang, D. Van Engen, E. Fan, A. D. Hamilton, *J. Am. Chem. Soc.* **1991**, *113*, 7640; (b) S.-K. Chang, A. D. Hamilton, *J. Am. Chem. Soc.* **1988**, *110*, 1318.
2. S. R. Collinson, T. Gelbrich, M. B. Hursthouse, J. H. R. Tucker, *Chem. Comm.* **2001**, 555.
3. V. Berl, I. Huc, J. –M. Lehn, A. DeCian, J. Fischer, *Eur. J. Org. Chem.*, **1999**, 3089.
4. K. Chichak, Ph.D. Dissertation, University of Alberta, **2001**.
5. (a) A. Bilyk, M. M. Harding, P. Turner, T. W. Hambley, *J. Chem. Soc., Dalton Trans.* **1994**, 2783; (b) T. Nabeshima, T. Inaba, N. Furukawa, T. Hosoya, Y. Yano, *Inorg. Chem.* **1993**, *32*, 1407.
6. R. Stiller, J. –M. Lehn, *Eur. J. Org. Chem.* **1998**, *7*, 977.
7. (a) R. Ziessel, M. Hissler, G. Ulrich, *Synthesis* **1998**, *9*, 1339; (b) M. H. Al-Sayah, A. S. Salameh, *Arab. J. Sci. Eng.* **2000**, *25* (2A), 67.
8. J. Barbera, E. Melendez, P. Romero, J. L. Serrano, *Mol. Crystal Liq. Crystal* **1985**, *126*, 259.
9. a) C. Canevet, J. Libman, A. Shanzer, *Angew. Chem. Int. Ed.* **1996**, *35*, 2657; (b) L. Zelikovich, J. Libman, A. Shanzer, *Nature* **1995**, *374*, 790.

## Chapter 5- Protons As Allosteric Modulators for Hydrogen Bonding Receptors

### 5.1 Introduction

The structural changes that regulate the activity of natural receptors are often induced by subtle variations in the pH of the environment.<sup>1</sup> In many cases, changes in pH lead to direct alterations in the electronic environments of the active sites of the receptors rendering them unsuitable for binding their substrates. More often, however, it is the reversible protonation at a location distant from the active binding site that induces a conformational change in the receptor and subsequently affects its affinity for its substrate. This form of allosteric regulation is used, for example, to control the binding site of the D<sub>4</sub> dopamine receptor.<sup>2</sup>

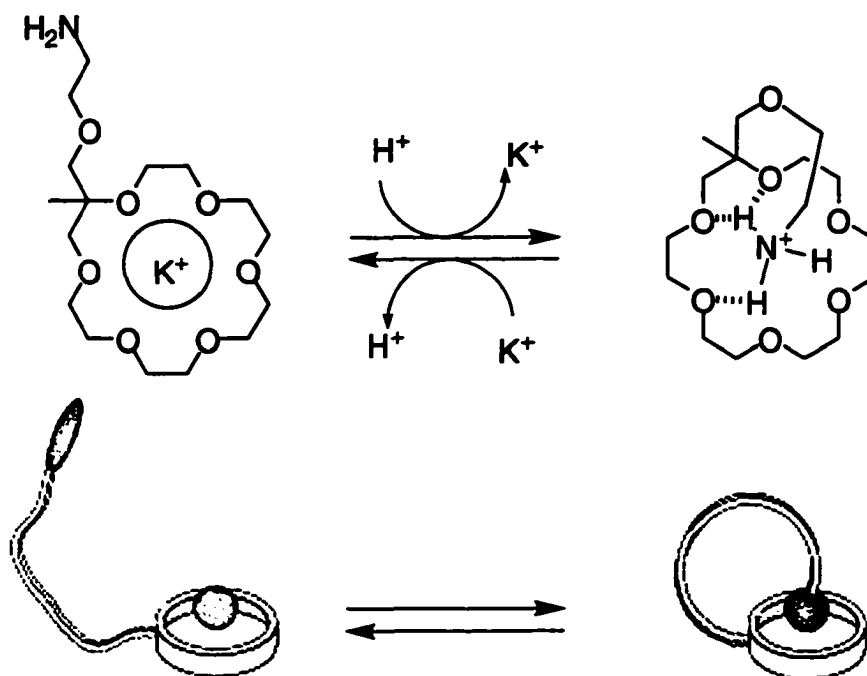
Several synthetic systems have borrowed from Nature's use of variations in pH as a regulatory tool. For example, Stoddart employed a change in pH to induce movement of a rotaxane "wheel" between two stations along a molecular "axle".<sup>3a</sup> A rotaxane is composed of two interlocked molecules, a macrocycle (the "wheel") and a longitudinal-shaped molecule (the "axle"). This pH-controlled "molecular shuttle" is based on dialkylammonium and bipyridinium recognition sites (Scheme 5.1). The macrocyclic crown ether resides exclusively at the cationic ammonium site due to a combination of  $^+N-H\cdots O$  and  $C-H\cdots O$  interactions between the  $CH_2NH_2^+$  hydrogen atoms of the axle component and the oxygen atoms of the macrocyclic wheel component. Upon addition of excess *i*Pr<sub>2</sub>NEt, deprotonation of the ammonium group occurs. As a result, intercomponent hydrogen bonds are destroyed and the macrocycle shuttles along the axle to the bipyridinium recognition site. The initial rotaxane is restored after addition of CF<sub>3</sub>CO<sub>2</sub>H to reprotonate the amine. The ammonium recognition site is regenerated and the macrocycle shuttles back to encircle the NH<sub>2</sub><sup>+</sup> center.



Scheme 5.1

Okahara and coworkers<sup>3d</sup> introduced a pH-regulated ionophore that transports potassium and sodium ions from an aqueous basic phase to an acidic phase across an organic liquid membrane. The molecule is composed of an alkylamine group tethered to an 18-crown-6 ether (Scheme 5.2). At the interface between the organic and aqueous basic phases, the ionophoric macrocycle binds potassium ions and transports them through the organic layer to the acidic phase. When the ionophore comes in contact with the acidic phase, the amino group becomes protonated. This induces an intramolecular complexation of the crown ether with the primary ammonium salt formed under these acidic conditions. It is this intramolecular complexation that competes with binding of the crown to the potassium ion. The result is the release of potassium ions into the acidic phase while the protonated ionophore travels back to the basic phase where the amine is

deprotonated and the crown ether is free to bind another potassium ion and begin the transport cycle once more.

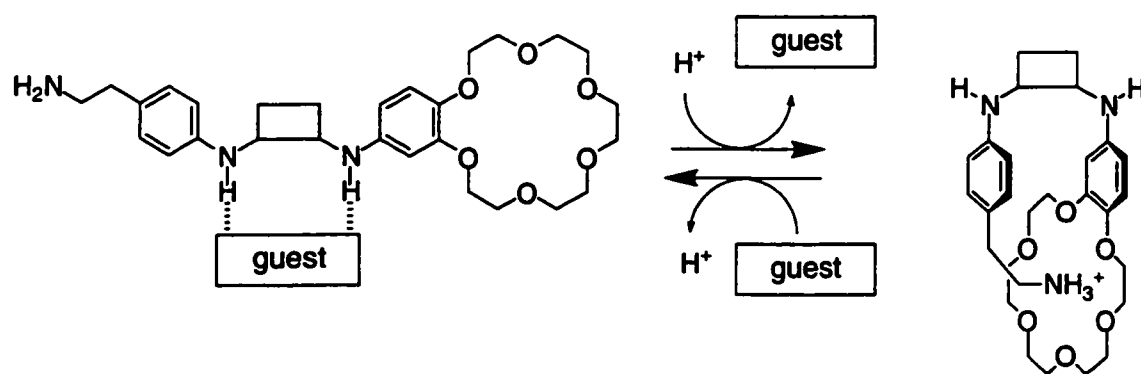


Scheme 5.2

## 5.2 Design of the Receptors

The systems described above use changes in pH to directly alter the recognition site in a system where the proton is an integral part of the site.<sup>3</sup> In the first example, protonation of the amino group of the rotaxane axle (Scheme 5.1) creates a new binding site for the wheel, inducing movement of the wheel. Meanwhile, formation of the ammonium ion creates a better guest for the crown ether (binding site) forcing the release of potassium ion (Scheme 5.2). In both cases, protonation directly alters the binding site of the molecule. This chapter introduces two artificial hydrogen bonding receptors that use a single proton as a negative allosteric cofactor to inhibit substrate recognition. The function of the receptors is designed around the same principle. Both receptors possess a multiple-point hydrogen bonding recognition site specific for their substrates (Scheme

5.3). Tethered to these molecular recognition sites, in a divergent conformation, are the two groups responsible for the allosteric mechanism. The protonation of the amino functional group creates a complementary species for the crown ether which results in the converging of the two groups toward each other and the formation of an intramolecular hydrogen-bonding complex. This change in the conformation of the molecules leads to a distortion of the hydrogen bond sites and inhibition of substrate binding (Scheme 5.3).

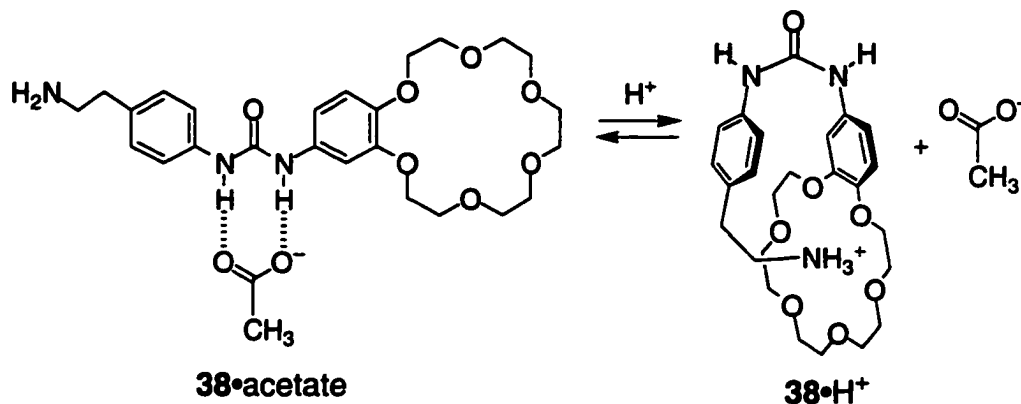


Scheme 5.3

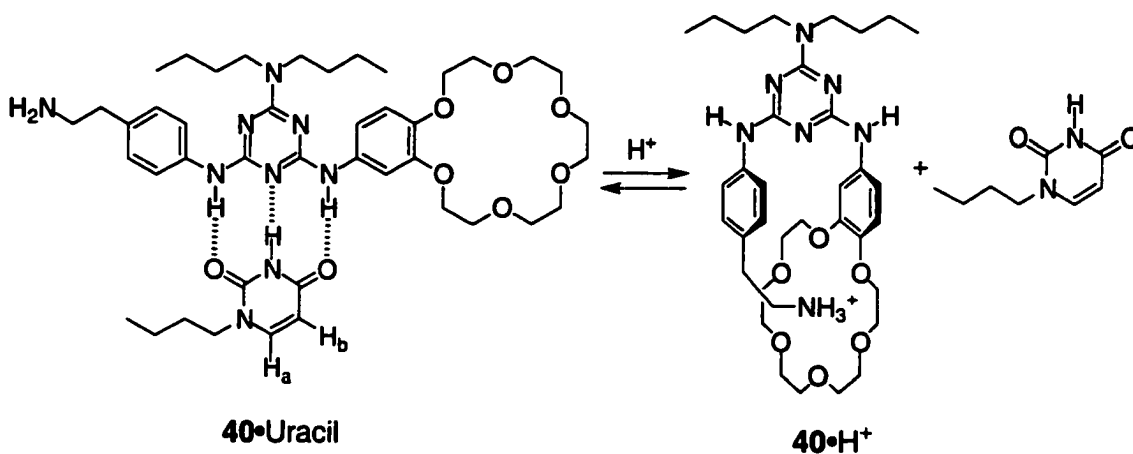
In a manner similar to receptors **6** and **7** presented in Chapter 2, receptor **38** presents a two-point donor-donor hydrogen-bonding urea appropriate for binding anionic carboxylate guests (Scheme 5.4), while receptor **40** possesses a three-point triaminotriazine donor-acceptor-donor site suited to bind imides (Scheme 5.5). Both receptors function with two components responsible for the allosteric event, a primary amine and a crown-ether. In the presence of one equivalent of acid, the amine changes into an ammonium cation, a suitable guest for the crown ether macrocycle. Formation of this ammonium-crown host-guest pair induces a conformational change which forces the receptor C–N bonds to rotate into a non-productive geometry that inhibits the binding of the receptors. Deprotonation destroys the ammonium–crown ether complex and allows



rotation around the C—N bonds to regenerate the hydrogen bonding sites. This reactivates the receptors.



Scheme 5.4

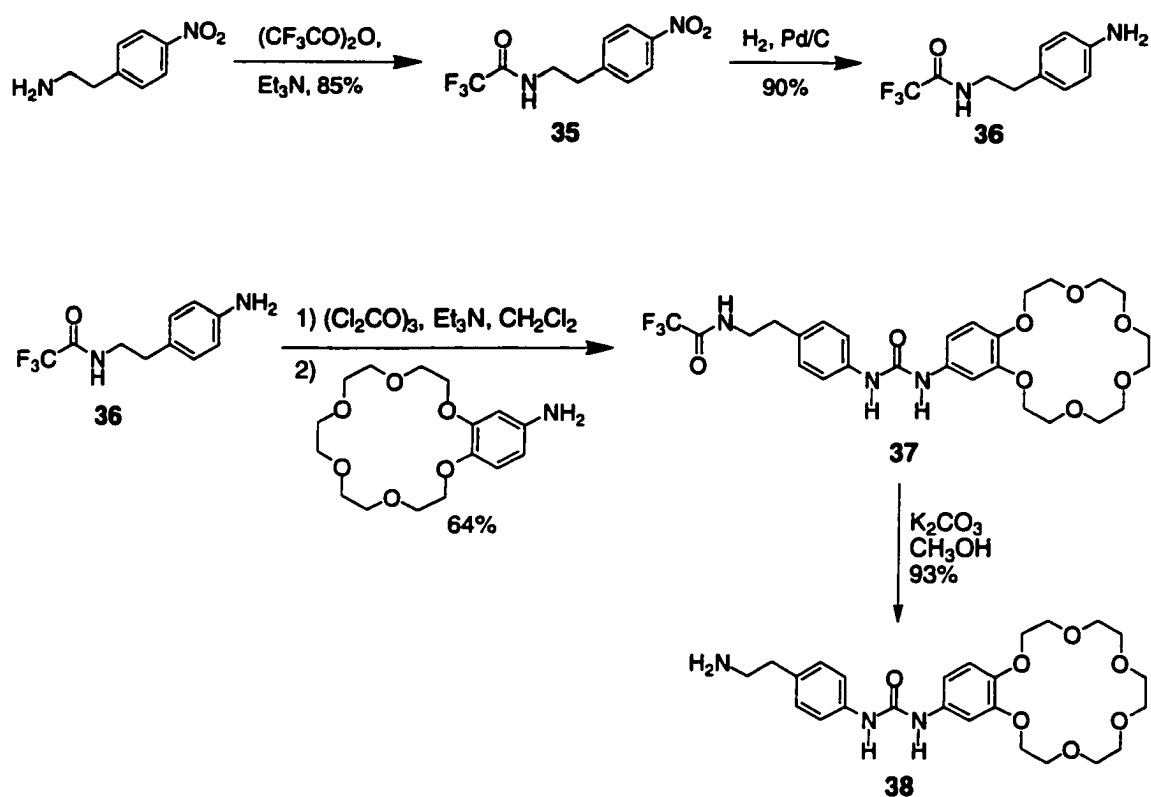


Scheme 5.5

### 5.3 Synthesis of Receptors and Their Protonated Complexes

Synthesis of the two receptors described above started with the preparation of *N*-[2-(4-amino-phenyl)-ethyl]-2,2,2-trifluoro-acetamide (**36**) (Scheme 5.6) as described in a previously reported procedure.<sup>4</sup> The first step was protection of the amino group of *p*-ethylamino-nitrobenzene with trifluoroacetic anhydride to produce **35** in 85% yield. The

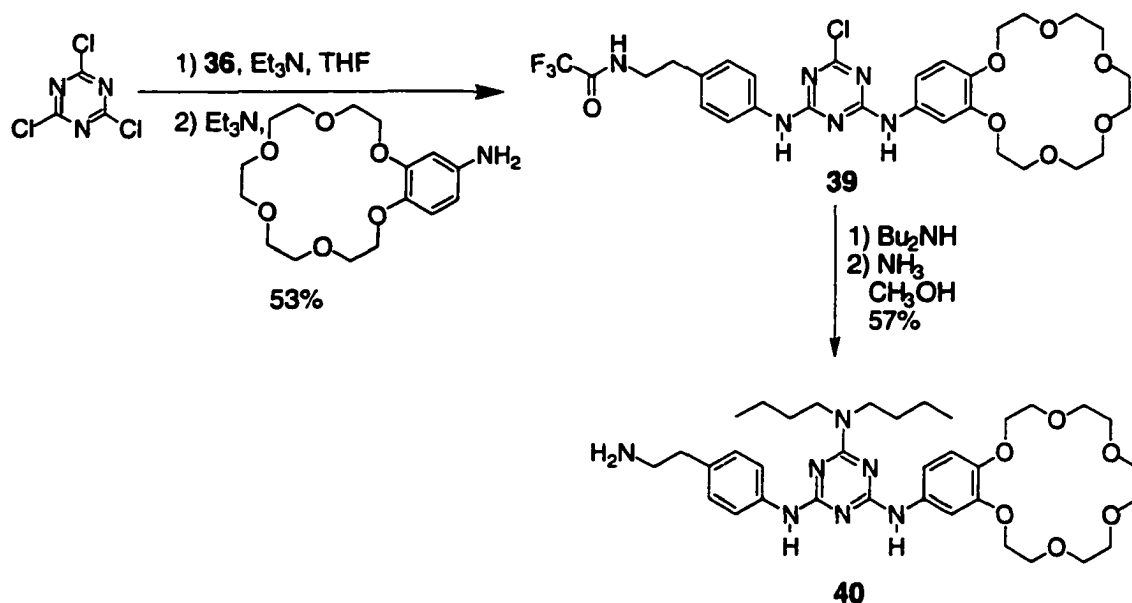
nitro group of **35** was reduced with  $H_2$  in the presence of Pd/C in 15 minutes to produce the amine (**36**) in 93% yield. Urea receptor **38** was prepared in two steps by treating the protected amine **36** with triphosgene, followed by 4-aminobenzo-18-crown-6 in dichloromethane at room temperature (Scheme 5.6). Primary amine **30** was then deprotected with 10%  $K_2CO_3/MeOH$  affording the final receptor **38** as a white solid in nearly quantitative yield. The ammonium form,  $38 \cdot H^+$ , was generated as its tetrafluoroborate salt by careful addition of a methanolic solution of  $HBF_4$  (1.2 equivalents) to the receptors, followed by drying under vacuum.



Scheme 5.6

Triaminotriazine receptor **40** was prepared as illustrated in Scheme 5.7. Addition of protected amine **36** to cyanuric chloride in dry THF at  $0^\circ C$ , followed by addition of 4-

aminobenzo-18-crown-6 at 50°C afforded the triazine **39**. Heating **39** with two equivalents of dibutylamine in THF under reflux, followed by deprotection of the amino group with methanolic ammonia at room temperature, afforded **40** in 57% yield. Similar to the urea receptor **38**, the ammonium tetrafluoroborate salt of the triaminotriazine receptor,  $40\bullet\text{H}^+$ , was generated by careful addition of a methanolic solution of  $\text{HBF}_4$  (1.2 equivalents) to the receptor, followed by drying under vacuum.



Scheme 5.7

#### 5.4 Characterization of Receptors and Their Protonated Complexes

The receptors were characterized by multi-dimensional NMR and mass spectroscopy. The  $^1\text{H}$  NMR spectrum of receptor **38** in  $\text{CD}_3\text{OD}$  showed four signals in the aromatic region and five signals which corresponded to protons of the crown ether. The methylene protons of the ethylamino group appeared as triplets at 2.7 and 2.9 ppm. The former signal corresponds to the  $\text{CH}_2$  protons at the  $\alpha$ -position to the amino group (denoted by "a" in Figure 5.2), while the latter signal is due to the  $\text{CH}_2$  at the  $\beta$ -position

position (denoted by "b" in Figure 5.2). These two peaks shifted to 3.2 and 2.9 ppm, respectively, in the spectrum of the protonated form  $38\bullet\text{H}^+$ . This indicates that these protons are more deshielded after addition of acid to the receptor. This suggests that protonation of the amino group with  $\text{HBF}_4$  created an electron withdrawing ammonium group next to the methylene protons. Moreover, the  $^1\text{H}$  NMR spectrum of  $38\bullet\text{H}^+$  exhibited broadness in all peaks. This can be explained by the dynamics associated with on/off binding of the ammonium salt to the crown ether.

The intramolecular association between the ammonium group and the crown ether macrocycle in  $38\bullet\text{H}^+$  was diagnosed by 2-dimensional  $^1\text{H}$  NMR spectroscopy (TROESY) which showed correlation peaks between the methylene  $\text{CH}_2$  protons of the ethylamino chain and those of the crown ether (Figure 5.1). These correlation peaks were absent in the TROESY spectrum of the neutral form of receptor **38** (Figure 5.2) suggesting that protonation forces the receptor to turn in on itself. However, these observations alone do not completely rule out the presence of intermolecular associations between the cation of one receptor and the macrocycle of another. In fact, the electrospray mass spectrum of  $38\bullet\text{H}^+$  exhibited a major peak corresponding to the molecular mass of the monomer  $38\bullet\text{H}^+$  as well a minor peak corresponding to the dimer  $(38\bullet\text{H}^+)_2$ .

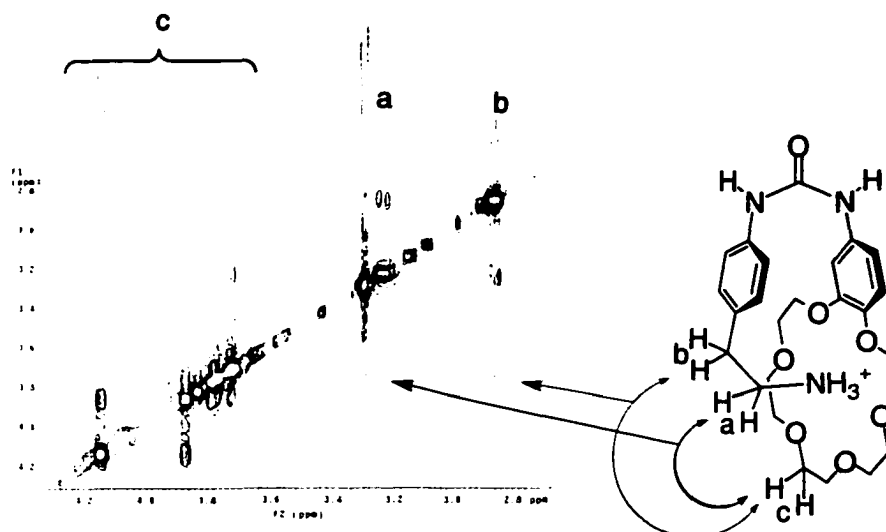


**Figure 5.1** Partial TROESY spectrum (500 MHz) of  $38 \bullet H^+$  in  $CD_3OD$ . The observed cross-peaks between the ethyl protons and those of the crown ether implies that they are in close proximity in space ( $< 4 \text{ \AA}$ ).

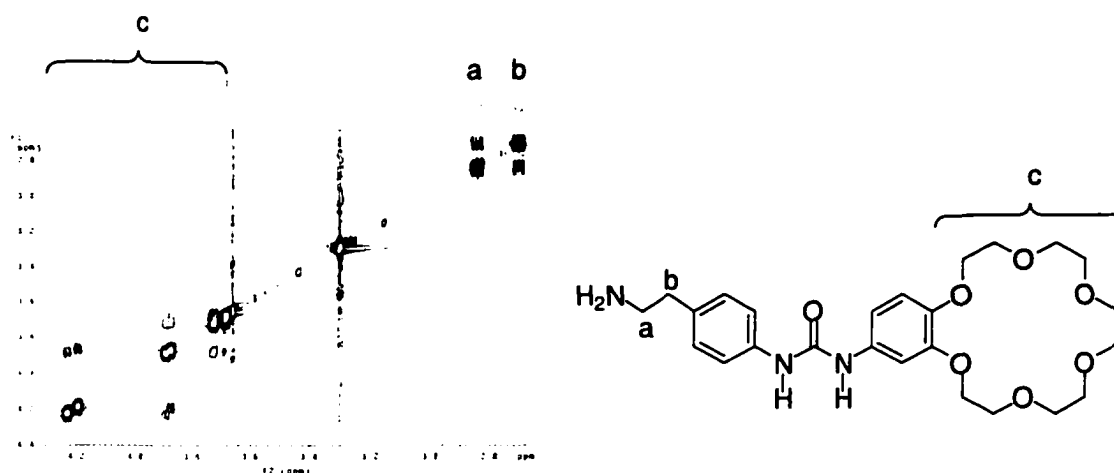


**Figure 5.2** Partial TROESY spectrum (500 MHz) of urea **38** in  $CD_3OD$ . No cross peaks are observed between the protons on the ethyl linkage and those of the crown ether.

The triaminotriazine receptor **40** was also characterized by multi-dimensional NMR spectroscopy and mass spectrometry. The 1-dimensional  $^1H$  NMR spectrum of a  $CD_3OD$  solution of receptor **40** showed the presence of two signals for the protons of the ethylamino group at 2.82 and 3.26 ppm. These signals shifted to 2.90 and 3.39 ppm, respectively, in the NMR spectrum of the protonated complex  $40 \bullet H^+$  in the same solvent. This observation indicates that the amino group is protonated in the complex.

The 2-dimensional  $^1\text{H}$  NMR of  $40\bullet\text{H}^+$  failed to show any correlation peaks between the methylene  $\text{CH}_2$  protons of the ethylamino chain and those of the crown ether. However, the absence of these correlation peaks does not mean that intramolecular association between the ammonium group and the crown ether macrocycle in  $40\bullet\text{H}^+$  were absent. The electrospray mass spectrum of  $[40+\text{H}]^+$  indicated the presence of only the monomer. There were no traces of the dimer in the spectrum. Also, no peaks corresponding to  $m/z$  of  $[\text{M}+\text{Na}]^+$  or  $[\text{M}+\text{K}]^+$  were observed in the spectrum (Figure 5.3). Such peaks are expected to appear since the crown ether has a strong affinity for these ions, which are usually present in trace amounts in solvents used for mass spectrum analysis. The absence of these peaks suggests that the crown ether is not able to bind these ions due to intramolecular association with the ammonium salt.

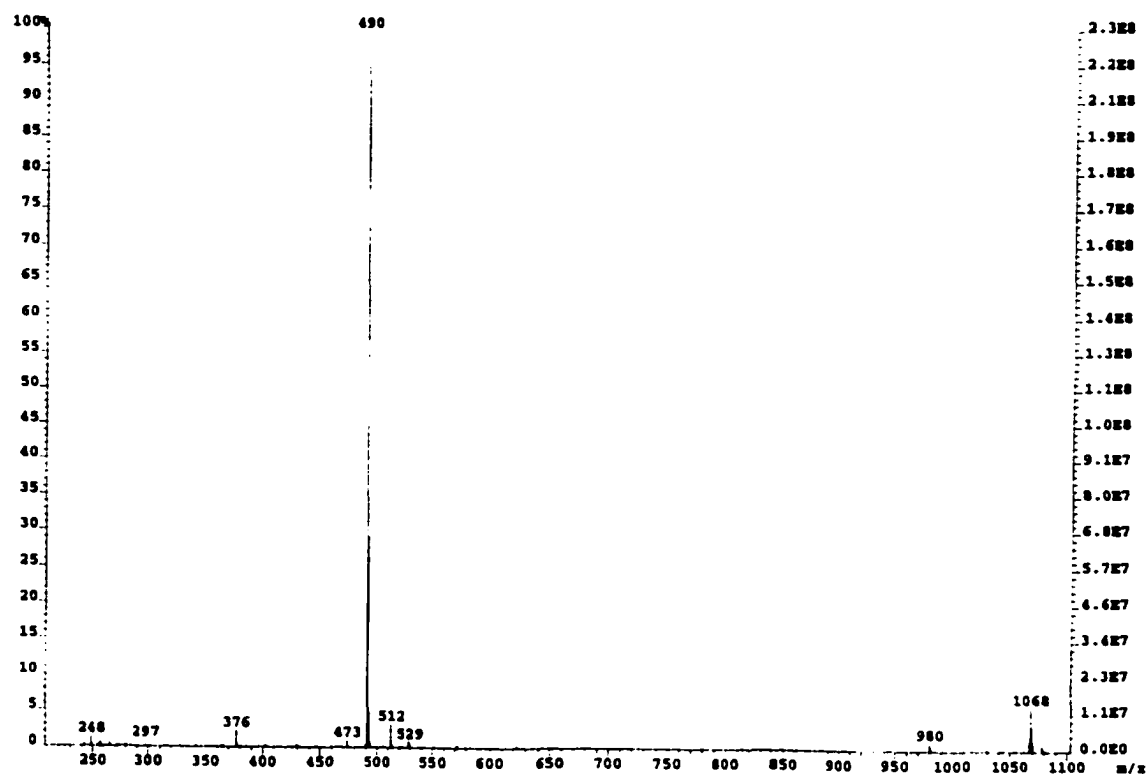
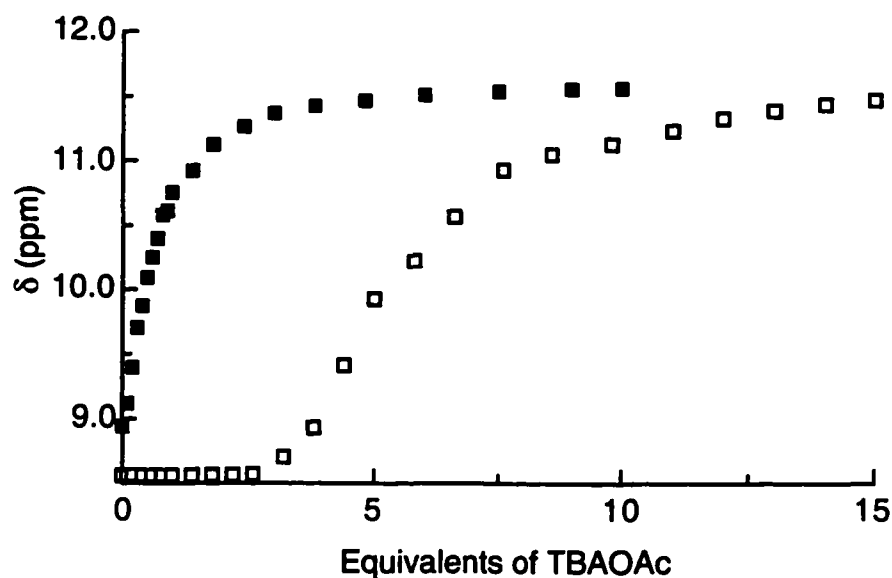


Figure 5.3 Electrospray mass spectrum of  $40\bullet\text{H}^+$

## 5.5 Binding Studies

### 5.5.1 The Binding of Receptor 38 to Tetrabutylammonium (TBA) Acetate

The binding efficiency of urea receptor **38** to its substrate was evaluated by analyzing the  $^1\text{H}$  NMR spectral changes that occurred upon titrating  $\text{DMSO-}d_6$  solutions of receptor **38** ( $2 \times 10^{-3}$  M) with tetrabutylammonium (TBA) acetate ( $2 \times 10^{-2}$  M). As aliquot amounts of the acetate solution were added, a downfield shift in the N—H protons of the urea was observed (Figure 5.4). This indicates the formation of hydrogen bonding between receptor **38** and the acetate. A significant downfield shift ( $\Delta\delta$  greater than 2.5 ppm) was observed until about 2-3 equivalents of acetate had been added. At this point, the neutral form of the receptor reaches saturation where further changes in N—H chemical shift were insignificant. The signal corresponding to this N—H proton appeared at 11.60 ppm.



**Figure 5.4** Observed chemical shifts ( $\delta$ ) of urea N—H resonances in the  $^1\text{H}$  NMR spectra of urea receptor **38** when it is treated with aliquot amounts of TBA acetate (■) and when  $38\cdot\text{H}^+$  is treated with TBA acetate (□) in  $\text{DMSO-}d_6$ .

The titration experiment was repeated three times with three different samples at the same concentrations. Data collected from each experiment were fit against curves

calculated using a 1:1 binding model and gave an average association constant ( $K_a$ ) value of  $4400 \pm 1100 \text{ M}^{-1}$  over three experiments. This value is large when compared to those reported for the complexation between alkylurea hosts and carboxylate guests which are typically in the range of  $50\text{--}100 \text{ M}^{-1}$  in this solvent.<sup>5,6</sup> This discrepancy can be attributed to the fact that reported values of  $K_a$  are for dialkylureas which possess significantly less acidic N–H protons than their diaryl counterparts. In fact, diphenylurea has a  $\text{p}K_a$  value of  $19.5^{7a}$  while diethylurea has a  $\text{p}K_a$  value of  $26.^{7b}$  The low acidity of the protons involved in the formation of the hydrogen bonds results in weaker hydrogen bonding and thus a lower association constant between the receptor and its substrate. Such a correlation between the acidity of the N–H protons and  $K_a$  was previously reported by Hamilton and coworkers.<sup>6</sup> They observed nearly a 10-fold increase in binding of carboxylate guests as less acidic urea receptors ( $\text{p}K_a \sim 27$ ) were replaced by more acidic thiourea analogs ( $\text{p}K_a \sim 21$ ).<sup>6</sup> In our case, receptor **38** should be treated as a diphenylurea derivative instead of a diethylurea derivative. As a consequence, the urea in **38** will act as a better hydrogen bond donor and the larger value of  $K_a$  is not unexpected.

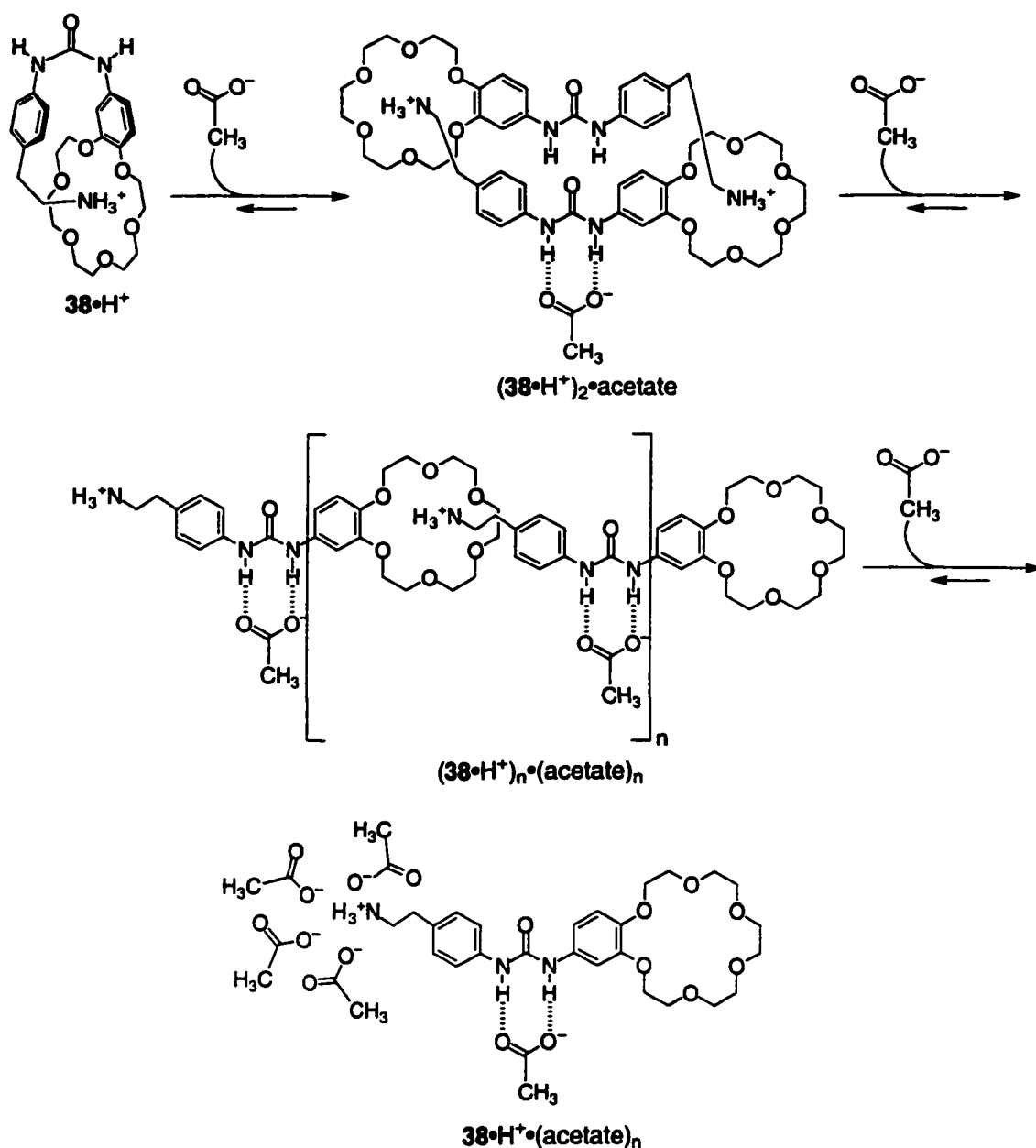
### 5.5.2 Effect of Protons on the Binding of Receptor **38**

The effect of the presence of a proton on the binding of receptor **38** was studied by repeating the titration experiments after replacing the active urea receptor with the preformed complex  $\mathbf{38} \cdot \text{H}^+$ . In the early phase of the titration, signals corresponding to the N–H protons in the  $^1\text{H}$  NMR spectra showed insignificant shifting ( $\Delta\delta$  less than 0.1 ppm) upon the addition of a DMSO- $d_6$  solution of TBA acetate. This signified that the receptor and acetate only associated to a very small extent as was anticipated for the protonated form of the receptor. As the experiment progressed and 2-3 equivalents of TBA acetate were added to the solution, a sudden downfield shift of the N–H signal was



observed. This change in the chemical shift implies that the receptor was reactivated and the hydrogen bonding recognition site for the acetate anion was reconstructed in response to excess guest species.

The receptor  $38\bullet\text{H}^+$  reached saturation after more than 10 equivalents of TBA acetate had been added. The  $^1\text{H}$  NMR spectrum of this solution showed that the chemical shift of the N—H signal and the aromatic region of  $38\bullet\text{H}^+$  was similar to that of the neutral receptor  $38$  in the presence of excess guest. This implies that a host-guest complex,  $38\bullet\text{H}^+\bullet(\text{acetate})_n$  has adopted a similar geometry to that of  $38\bullet\text{acetate}$ . Consequently, the intramolecular association between the crown and the ammonium salt is not possible. However, an intermolecular association between these species to form dimers ( $(38\bullet\text{H}^+)_2\bullet\text{acetate}$ ) and/or oligomers ( $(38\bullet\text{H}^+)_n\bullet(\text{acetate})_n$ ) would provide the necessary geometry for reactivating the receptor (Scheme 5.8). In fact, electrospray mass spectrometry studies of the protonated form,  $38\bullet\text{H}^+$ , showed peaks corresponding to both the monomer ( $38\bullet\text{H}^+$ ) and the dimer ( $(38\bullet\text{H}^+)_2$ ) in a 9:1 ratio. When more TBA acetate was added, this ratio remained unchanged even in the presence of up to 20 equivalents of acetate. At this high concentration of acetate, three factors could favor the formation of the active form of the receptor. (1) The ammonium group is solvated by the excess acetate instead of forming an intermolecular interaction with the macrocycle. (2) Urea derivatives prefer to exist in the *trans-trans* conformation which is satisfied in the "open" acetate-solvated form ( $38\bullet\text{H}^+\bullet(\text{acetate})_n$ ) but not in its "closed" protonated state ( $38\bullet\text{H}^+$ ) (Scheme 5.8). (3) The hydrogen bonding site of the receptor is regenerated and is satisfied by binding to the acetate substrate.



Scheme 5.8

### 5.5.3 Binding of Triaminotriazine Receptor 40 to *N*-Butyluracil

In order to estimate the association constant for the binding of the triaminotriazine receptor **40** to its imide guests, <sup>1</sup>H NMR titration experiments were performed by treating CD<sub>2</sub>Cl<sub>2</sub> solutions of *N*-butyluracil with aliquot amounts of the receptor. Similar to the studies performed on receptor **6** in Chapter 2, it was more convenient to titrate the uracil

substrate with the triaminotriazine receptor **40** because the  $^1\text{H}$  NMR signal that corresponds to the N—H hydrogen-bond-donor protons of the triazine lies in the region between 6.00 and 7.00 ppm. As the *N*-butyluracil substrate was added, this signal shifted downfield into the aromatic region of the spectrum which made it impossible to follow throughout the entire titration experiment. However, the signal corresponding to the imide N—H proton of *N*-butyluracil appears at 8.05 ppm, an uncluttered region of the spectrum. The downfield shift of this imide signal as receptor **40** was added could easily be monitored.

In this case, the signal for the N—H protons of *N*-butyluracil could not be followed because it consistently disappeared after about 0.5 equivalents of the receptor were added, although the significant downfield shift ( $\Delta\delta$  greater than 2 ppm) that occurred before the signal completely vanished clearly indicates effective host-guest association through hydrogen bonding. The disappearance of the N—H signal can be explained by the occurrence of rapid proton exchange between the N—H of the uracil substrate and the alkylamine of receptor **40**. These alkylamine and uracil groups are expected to have acidities similar to ethylammonium cation ( $\text{p}K_{\text{a}} = 10.8$ ) and *N*-pentyluracil ( $\text{p}K_{\text{a}} = 9.98$ ) groups, respectively.<sup>8</sup> This argument was further supported by a simple experiment where one equivalent of *n*-butylamine was added to a  $\text{CD}_2\text{Cl}_2$  solution of *N*-butyluracil. As a result, the signal corresponding to the N—H proton of *N*-butyluracil immediately disappeared. However, there was no observable effect on the chemical shifts of the methine C—H protons of *N*-butyluracil due to the presence of the amine. This observation is significant because it indicates that the observed change in the chemical shifts of the methine C—H protons of uracil upon titration is due to the binding of the substrate by receptor **40** and not a result of the exchange of the uracil's N—H proton with the alkylamine. Therefore, the small ( $\Delta\delta$  about 0.1 ppm) downfield shift of the signal

corresponding to the C–H<sub>3</sub> proton of the uracil provided a means to measure the association constant of the triaminotriazine receptor **40** with *N*-butyluracil. The value of  $K_a$  was estimated to be  $570 \pm 100 \text{ M}^{-1}$  for an average of three titration experiments (Figure 5.5). The data fit well to a 1:1 binding model.

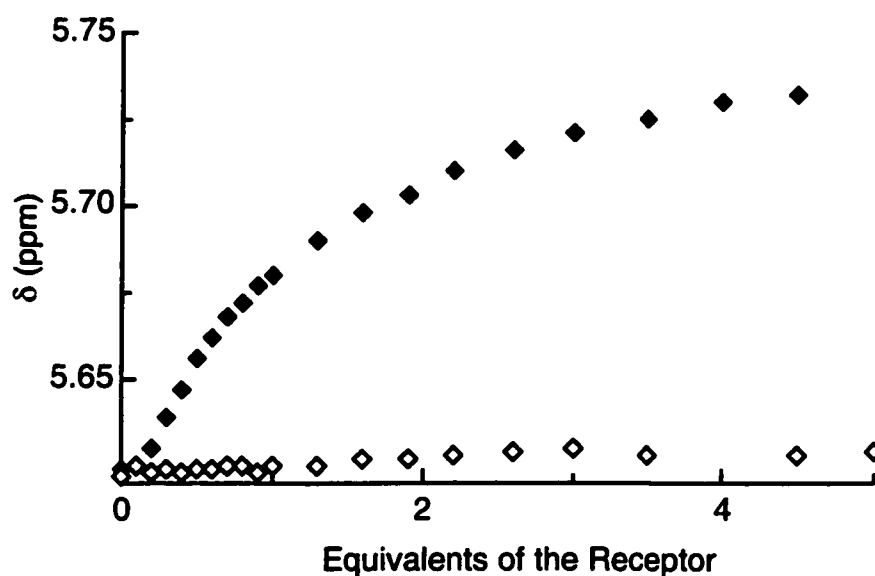


**Figure 5.5** Observed chemical shift ( $\delta$ ) of the C–H signal of *N*-butyluracil in the  $^1\text{H}$  NMR spectra when treated with aliquots of receptor **40** (◆) and when treated with  $40 \cdot \text{H}^+$  (◊) in  $\text{CD}_2\text{Cl}_2$ . [*N*-butyluracil] =  $2 \times 10^{-3} \text{ M}$ , [**40**] and [ $40 \cdot \text{H}^+$ ] =  $2 \times 10^{-2} \text{ M}$ .

In order to further support our claim that the shift in the resonances of these methine protons, which are not involved in the recognition process, reflects an accurate estimation of the association constant, the binding of *N*-butyluracil to diphenyltriazine (**42**) was studied. This receptor (**42**) provides a similar donor-acceptor-donor hydrogen-bonding site to that of **40** while it removes the effect of the alkyamino group (Figure 5.6). The association constant for the binding of *N*-butyluracil to diphenyltriazine (**42**) was measured by titrating a  $\text{CD}_2\text{Cl}_2$  solution of diphenyltriazine (**42**) into an *N*-butyluracil solution in the same solvent. The observed  $K_a$  for receptor **42** was  $487 \text{ M}^{-1}$  and  $508 \text{ M}^{-1}$  when the signals for the N–H and C–H<sub>3</sub> protons of *N*-butyluracil were followed,

respectively. These values indicate that the association constant of receptor **40** can be correctly estimated by following the change in the chemical shift of the C—H<sub>a</sub> proton of uracil. Also, the fact that the signals for the N—H proton could be monitored throughout this last titration experiment supports our claim that the N—H in *N*-butyluracil exchanges with the NH<sub>2</sub> of receptor **40** in an acid-base reaction.

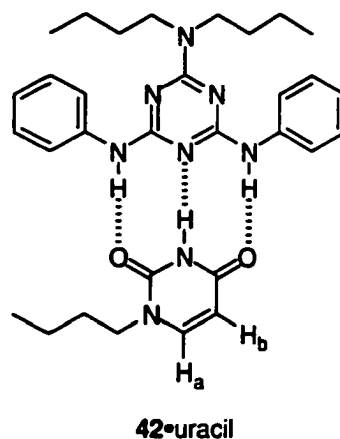


**Figure 5.6** The hydrogen bonding complex of diphenyl triazine receptor **42** and *N*-butyluracil

#### 5.5.4 Effect of Protons on Binding of Triaminotriazine Receptor **40**

The effect of the presence of a proton on the binding of receptor **40** was studied by repeating the titration of *N*-butyluracil with the protonated form of the receptor, **40•H<sup>+</sup>**. The change in the resonance of the uracil C—H<sub>a</sub> was followed as a function of equivalents of receptor **40•H<sup>+</sup>** added. However, the data produced a shallow curve which could not be fit to any binding model (Figure 5.5). Therefore the association constant could only be estimated to be below 10 M<sup>-1</sup>. The small shift in the C—H<sub>a</sub> resonance of *N*-butyluracil ( $\Delta\delta$  less than 0.01 ppm) can be attributed to hydrogen bonding of *N*-butyluracil to the substantially less effective donor-acceptor hydrogen bond sites in **40•H<sup>+</sup>** (Figure 5.7). Despite the existence of two of these sites in the protonated

compound, the reduced inherent binding affinity of recognition surfaces presenting only two hydrogen bonds coupled with the fact that these sites are projecting into the bulky *N*-butyl groups prevent the effective docking of the imide substrate. It is the combination of these factors that are responsible for the substantially reduced efficacy of the protonated receptor.

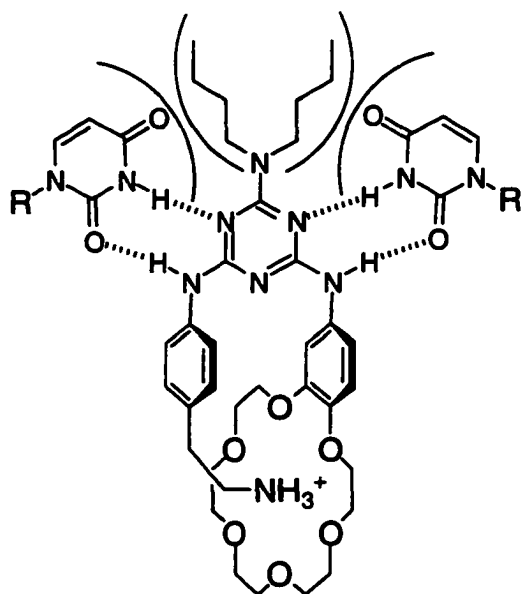


**Figure 5.7** The binding of uracil derivatives to the two less effective sites of  $40\bullet H^+$

The protonated form of the triazine receptor,  $40\bullet H^+$ , did not show the substrate competition observed for the urea receptor  $38\bullet H^+$ . The addition of excess *N*-butyluracil to receptor  $40\bullet H^+$  did not result in any increase in the extent of changes in the  $^1H$  NMR spectra as seen when  $38\bullet H^+$  was treated with excess TBA acetate. Clearly,  $40\bullet H^+$  is not reactivated by the presence of its substrate. This absence of substrate competition can be attributed to three factors. First, because  $CD_2Cl_2$  does not have the same ability to solvate ions as DMSO, the unimolecular complexation equilibrium will lie heavily toward the intramolecularly associated ammonium ion and crown ether. Second, *N*-butyluracil is a neutral substrate and, therefore, cannot effectively solvate the ammonium ion even when

it is in excess. Finally, the rotational barrier imposed on the two exocyclic C–N bonds on the triaminotriazine heterocycle in structures such as receptor **40** is smaller than that of the two C–N bonds in urea derivatives (such as found in receptor **38**).

## 5.6 Conclusions

This chapter has introduced the use of protons as allosteric modulators for hydrogen bonding receptors. The receptors provided hydrogen bonding surfaces through urea and triaminotriazine scaffolds for binding carboxylate and imide substrates, respectively. The allosteric mechanism of the two receptors involved the protonation of an amino group to form an ammonium salt that is a suitable guest for a macrocyclic crown ether. This newly formed guest was then hydrogen bonded by the crown ether host. The formation of this ammonium-crown host-guest complex forced rotation around the C–N bonds of the active sites. This rotation destroyed the hydrogen-bonding surfaces of the receptors rendering them unsuitable to accommodate their substrates.

The urea receptor **38** has exhibited a high affinity for acetates in the absence of a proton. In the presence of one equivalent of an acid, the receptor lost its binding efficacy at low concentrations of the substrate. As the concentration of the acetate increased, the binding of the urea receptor to its substrate became more favorable than the binding of the ammonium salt to the crown ether. This competition between the binding of the substrate to the active site and the allosteric effect led to reactivation of the urea receptor at high concentration of acetate. Weakening of the allosteric ammonium-crown complex in the presence of a high concentration of acetate was attributed to the stabilization of the positively charged ammonium salt by the negatively charged acetate and the binding of acetate to the urea binding site.

The triaminotriazine receptor exhibited a high affinity for *N*-butyluracil in the absence of acid. In the presence of protons, binding of the triaminotriazine receptor to the imide guest was inhibited. This inhibition of the binding sustained even with the addition of excess uracil substrate and no weakening in the allosteric ammonium-crown binding was observed. In this case, the added substrate was neutral and could not stabilize the positively charged ammonium salt if it had to break the ammonium-crown complex.

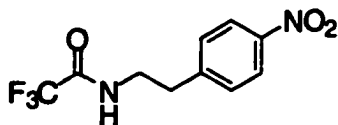


## 5.7 Experimental

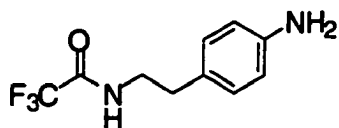
**General Information.** All solvents (Caledonia) for synthesis and purification were used as received. Solvents used for UV-Vis absorption and fluorescence spectroscopy analysis were deoxygenated by bubbling argon through the solvent. Solvents used for NMR analysis (Cambridge Isotope Laboratories) were used as received. All reagents and starting materials were purchased from Aldrich or Acros Organics.

$^1\text{H}$  NMR characterizations were performed on a Varian Inova-300 instrument, working at 299.96 MHz, or on a Varian Inova-500 instrument, working at 499.92 MHz. Chemical shifts ( $\delta$ ) are reported in parts per million relative to tetramethylsilane using the residual solvent peak as a reference standard. Coupling constants ( $J$ ) are reported in hertz.  $^{13}\text{C}$  NMR characterizations were performed on a Bruker-300 instrument, working at 74.99 MHz or a Varian Inova-500 instrument, working at 125.29 MHz. FT-IR measurements were performed using a Nicolet Magna-IR 750. UV-Vis spectra were recorded on a Varian Cary 400 Scan spectrophotometer.

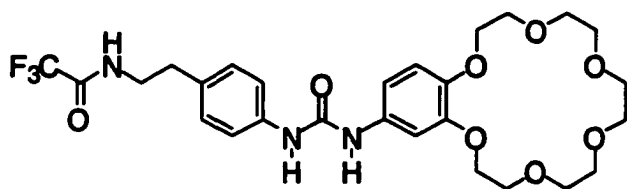
Mass spectrometry measurements were performed a Kratos MS-50 with an electron impact source or by positive mode electrospray ionization on a Micromass ZabSpec Hybrid Sector-TOF. The liquid carrier was infused into the electrospray source by means of a Harvard syringe pump at a flow rate of 10  $\mu\text{L}/\text{minute}$ . The sample solution, in the same solvent, was introduced *via* a 1  $\mu\text{L}$ -loop-injector. Pre-purified nitrogen was used as a spray pneumatic aid and filtered air as the bath gas, heated at *ca.* 80  $^\circ\text{C}$ . For low resolution, the mass spectra were acquired by magnet scan at a rate of 5 seconds/decade at *ca.* 1000 resolution. For exact mass measurements, the spectra were obtained by voltage scan over a narrow mass range at *ca.* 10000 resolution. Data acquisition and processing was achieved by using the OPUS software package on a Digital Alpha station with VMS operating system.



***N*-[2-(4-Nitrophenyl)-ethyl]-2,2,2-trifluoroacetamide (35).**<sup>4</sup> A solution of *p*-nitrophenylethylamine hydrochloride (1.00 g, 4.9 mmol) and TEA (5.00 g, 49.5 mmol) in CH<sub>2</sub>Cl<sub>2</sub> (100 mL) was treated with trifluoroacetic anhydride (4.00 g, 19.0 mmol) and the mixture was stirred for 3 h at room temperature. The solution was washed with 5% HCl (2 × 20 mL), followed by H<sub>2</sub>O (1 × 20 mL) and then saturated NaCl solution (1 × 20 mL). The organic layer was dried over anhydrous Na<sub>2</sub>SO<sub>4</sub>, filtered and concentrated under reduced pressure to afford a yellow oil (1.10 g, 85%). <sup>1</sup>H NMR (300 MHz, CDCl<sub>3</sub>) δ 8.16 (d, *J*=8 Hz, 2H), 7.34 (d, *J*=8 Hz, 2H), 6.58 (br s, 1H), 3.61 (q, *J*=7 Hz, 2H), 3.01 (t, *J*=7 Hz, 2H).



***N*-[2-(4-Aminophenyl)-ethyl]-2,2,2-trifluoroacetamide (36).**<sup>4</sup> A solution of *N*-[2-(4-nitrophenyl)-ethyl]-2,2,2-trifluoroacetamide (35) (1.10 g, 4.2 mmol) in EtOH (100 mL) was treated with 10% Pd/C (0.5 g) and the mixture was hydrogenated under 50 psi of H<sub>2</sub> for 15 min. The mixture was then filtered through Celite to remove the catalyst and the solvent was evaporated to afford a yellow oil. Upon purification by flash chromatography (silica, EtOAc/hexane 1:1), the product was collected as a colorless oil that solidified upon standing (0.88 g, 90%). M.p. 86-88 °C (lit.<sup>4</sup> 83-86 °C); <sup>1</sup>H NMR (300 MHz, CDCl<sub>3</sub>) δ 6.94 (d, *J*=8 Hz, 2H), 6.64 (d, *J*=8 Hz, 2H), 6.22 (br s, 1H), 4.10 (br s, 2H), 4.08 (q, *J*=7 Hz, 2H), 2.75 (t, *J*=7 Hz, 2H).



***N*-[2-[4-(((2,3,5,6,8,9,11,12,14,15-Decalyl)amino)carbonyl)amino)phenyl]ethyl)-2,2,2-**

**trifluoroacetamide (37).** Triphosgene (15 mg,  $0.5 \times 10^{-1}$  mmol) was added to a stirred

mixture of *N*-[2-(4-aminophenyl)-ethyl]-2,2,2-trifluoro-acetamide (36) (35 mg,  $1.5 \times 10^{-1}$

mmol) and triethylamine (46 mg,  $4.5 \times 10^{-1}$  mmol) in dry THF (20 mL) under argon. After

stirring at ambient temperature for 1 h, 4-aminobenzo-18-crown-6 (50 mg,  $1.5 \times 10^{-1}$

mmol) was added and the mixture was stirred for 3 h. After the solvent was removed

under reduced pressure, the product was isolated from the solid residue column

chromatography (alumina, 1% to 5% gradient of MeOH in  $\text{CHCl}_3$ ) and further purified

by recrystallization from EtOH (56 mg, 64%).  $^1\text{H}$  NMR (300 MHz,  $\text{CDCl}_3$ )  $\delta$  7.26 (d,  $J=$

8 Hz, 2H), 7.14 (br s, 1H), 7.01 (d,  $J=8$  Hz, 2H), 6.99 (s, 1H), 6.95 (br s, 1H), 6.70 (s,

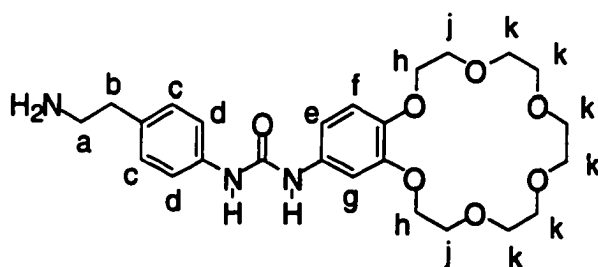
2H), 6.48 (br s, 1H), 4.07 (m, 4H), 3.87 (m, 4H), 3.78-3.67 (m, 12H), 3.53 (q,  $J=6$  Hz,

2H), 2.78 (t,  $J=7$  Hz, 2H);  $^{13}\text{C}$  NMR (75.5 MHz,  $\text{CDCl}_3$ )  $\delta$  157.5, 157.2, 154.1, 148.9,

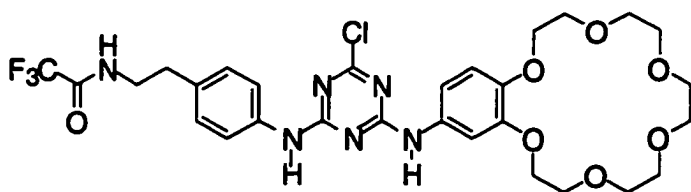
144.9, 137.7, 132.6, 132.2, 129.1, 120.3, 117.0, 114.5, 113.5, 107.6, 77.3, 70.8, 70.7,

70.6, 70.6, 70.5, 69.8, 69.6, 69.3, 68.6, 41.2, 34.2, 29.8; HRMS (ES)  $m/z$  608.2197

[ $\text{M}+\text{Na}$ ] $^+$   $\text{C}_{27}\text{H}_{34}\text{F}_3\text{N}_3\text{NaO}_8$ ; calculated 608.2196 [ $\text{M}+\text{Na}$ ] $^+$   $\text{C}_{27}\text{H}_{34}\text{F}_3\text{N}_3\text{NaO}_8$ .

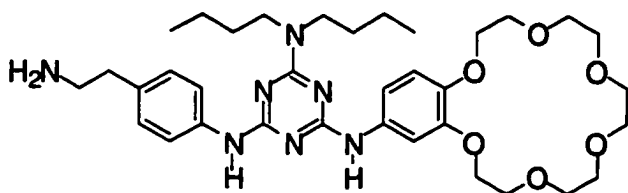


***N*-[4-(2-Aminoethyl)phenyl]-*N'*-(2,3,5,6,8,9,11,12,14,15-decahydro-1,4,7,10,13,16-benzohexaoxacyclooctadec-18-yl)urea (38).** A solution of urea 37 (50 mg,  $8.5 \times 10^{-2}$  mmol) was dissolved in a solution of  $K_2CO_3$  (5 mL, 10% in 5:2  $CH_3OH/H_2O$ ) and stirred at ambient temperature over-night. The solvent was evaporated under reduced pressure and water (5 mL) was added to the solid residue. The solid product was collected by vacuum filtration, washed with water and vacuum dried to afford 38 as a white solid (39 mg, 93%). M.p.  $> 198^\circ C$  (dec);  $^1H$  NMR (300 MHz,  $CD_3OD$ )  $\delta$  7.32 (d,  $J=8$  Hz, H(d) +H(g)), 7.12 (d,  $J=8$  Hz, H(c)), 6.92 (d,  $J=8$  Hz, H(f)), 6.80 (dd,  $J_1 = 8$  Hz,  $J_2 = 2$  Hz, H(e)), 4.20 (m, H(h)), 3.89 (m, H(j)), 3.70 (m, H(k)), 2.88 (t,  $J=7$  Hz, H(a)), 2.72 (t,  $J=7$  Hz, H(b));  $^{13}C$  NMR (75.5 MHz,  $CD_3OD$ )  $\delta$  177.1, 176.3, 155.9, 148.4, 144.4, 138.7, 134.5, 130.2, 120.8, 113.1, 112.6, 106.1, 71.3, 71.0, 70.2, 70.1, 68.5, 44.2, 39.3; FT-IR (microscope)  $\nu$  3242, 2919, 1681, 1609, 1547, 1513, 1484, 1457, 1425, 1383, 1353, 1333, 1313, 1278, 1253, 1181, 1133, 1111, 1081, 1072, 1053, 992, 956, 836, 787  $cm^{-1}$ ; HRMS (ES)  $m/z$  490.2545  $[M+H]^+$   $C_{25}H_{36}N_3O_7$ ; calculated 490.2553  $[M+H]^+$ ,  $C_{25}H_{36}N_3O_7$ .



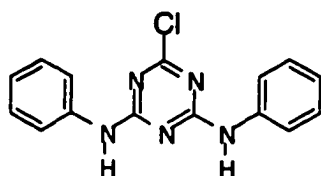
***N*-{2-[4-((4-Chloro-6-[(2,3,5,6,8,9,11,12,14,15-decahydro-1,4,7,10,13,16-benzohexaoxacyclooctadec-18-yl)amino]-1,3,5-triazin-2-yl)amino)phenyl]ethyl}-2,2,2-trifluoroacetamide (39).** Cyanuric chloride (238 mg, 1.3 mmol) was dissolved in dry THF (15 mL) and cooled in an ice bath. This solution was treated with a solution of *N*-[2-(4-aminophenyl)-ethyl]-2,2,2-trifluoro-acetamide (36) (300 mg, 1.3 mmol) and triethylamine (130 mg, 1.3 mmol) in dry THF (15 mL) dropwise. The ice bath was

removed and the reaction mixture allowed to warm to ambient temperature and stirred for 4 h. The mixture was then placed in an oil bath heated to 45 °C and treated with a solution of 4-aminobenzo-18-crown-6 (400 mg, 1.3 mmol) and triethylamine (130 mg, 1.3 mmol) in dry THF (15 mL) dropwise. After stirring at 45 °C for 12 h, the oil bath was removed and the reaction mixture was allowed to cool to ambient temperature. The solvent was removed under vacuum and the residue was dissolved in EtOAc (20 mL). The organic layer was separated and washed with water (2 × 10 mL), dried over Na<sub>2</sub>SO<sub>4</sub> and the solvent was evaporated under reduced pressure. The brown-orange residue was purified by column chromatography (alumina, gradient of 1 to 5% MeOH in CHCl<sub>3</sub>) and recrystallization (EtOAc/hexane) to afford the product as a white solid (450 mg, 53%). M.p. 159-160 °C; <sup>1</sup>H NMR (300 MHz, CDCl<sub>3</sub>) δ 7.45 (br d, *J*=8 Hz, 2H), 7.15 (br d, *J*=8 Hz, 4H), 6.85 (br s, 2H), 4.16 (m, 4H), 3.90 (m, 4H), 3.75-3.68 (m, 12H), 3.61 (dt, *J*<sub>1</sub> = 6 Hz, *J*<sub>2</sub> = 6 Hz, 2H), 2.85 (t, *J*=7 Hz, 2H); <sup>13</sup>C NMR (75.5 MHz, CDCl<sub>3</sub>) δ 149.4, 146.6, 136.2, 133.8, 130.9, 129.3, 121.3, 114.9, 110.0, 70.1, 70.7, 69.8, 69.5, 41.0, 34.4; FT-IR (cast) ν 3200, 2931, 1710, 1613, 1574, 1505, 1454, 1418, 1367, 1220, 1184, 1157, 1121, 1001, 953, 839, 802, 754, 665 cm<sup>-1</sup>; HRMS (ES) *m/z*: 671.2199 [M+H]<sup>+</sup>, C<sub>29</sub>H<sub>35</sub>ClF<sub>3</sub>N<sub>6</sub>O<sub>7</sub>; calculated 671.2209 [M+H]<sup>+</sup>, C<sub>29</sub>H<sub>35</sub>ClF<sub>3</sub>N<sub>6</sub>O<sub>7</sub>.

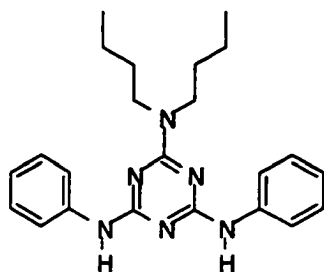


***N*<sup>4</sup>-[4-(2-Aminoethyl)phenyl]-*N*<sup>2</sup>,*N*<sup>2</sup>-dibutyl-*N*<sup>6</sup>-(2,3,5,6,8,9,11,12,14,15-decahydro-1,4,7,10,13,16-benzohexaoxacyclooctadec-18-yl)-1,3,5-triazine-2,4,6-triamine (40).** A mixture of triazine 39 (150 mg, 0.2 mmol), di-*n*-butylamine (60 mg, 0.5 mmol) and THF (20 mL) was heated at reflux for 12 h. The heating source was removed, the reaction

mixture was allowed to cool to ambient temperature and the solvent was removed under vacuum. The residue was dissolved in  $\text{CH}_2\text{Cl}_2$  (50 mL) and washed with water ( $3 \times 10$  mL). The combined organic layers were dried ( $\text{Na}_2\text{SO}_4$ ), filtered and the solvent was removed under reduced pressure affording a brown oil. The oil was dissolved in hot EtOAc (2 mL) and hexane (8 mL) was added. Upon standing at  $-5$  °C overnight, a brown solid separated. The solid was collected by vacuum filtration, washed with a cold mixture of EtOAc/hexane (1:9) and used without further purification. The solid was dissolved in MeOH (15 mL) and gaseous ammonia was bubbled through the resulting solution for 30 min. The source of ammonia was removed and the mixture stirred at ambient temperature overnight. The solvent was removed under reduced pressure and the solid residue was purified by column chromatography (alumina, gradient of 1% to 5% MeOH in  $\text{CHCl}_3$ ) and by recrystallization from EtOAc/hexane affording the product as a beige solid (83 mg, 57%). M.p.  $> 130$  °C (dec);  $^1\text{H}$  NMR (500 MHz,  $\text{DMSO}-d_6$ )  $\delta$  8.92 (s, 1H), 8.74 (s, 1H), 7.73 (d,  $J=7.5$  Hz, 2H), 7.34 (s, 1H), 7.29 (br s, 1H), 7.10 (d,  $J=8.0$  Hz, 2H), 6.83 (d,  $J=9.0$  Hz, 2H), 4.02 (s, 4H), 3.74 (m, 4H), 3.60-3.53 (m, 16H), 2.94 (t,  $J=7.5$  Hz, 2H), 2.74 (t,  $J=7.5$  Hz, 2H), 1.56 (m, 4H), 1.32 (br m, 4H), 0.91 (m, 6H);  $^{13}\text{C}$  NMR (125.7 MHz,  $\text{CD}_2\text{Cl}_2$ )  $\delta$  246.2, 183.2, 163.8, 129.3, 128.2, 120.3, 119.7, 116.8, 112.5, 71.1, 70.5, 69.7, 68.1, 48.2, 41.0, 32.9, 30.5, 20.9, 20.7, 14.2, 13.7; FT-IR (cast)  $\nu$  2927, 1600, 1583, 1551, 1513, 1420, 1315, 1222, 1181, 1118, 750  $\text{cm}^{-1}$ ; HRMS (ES)  $m/z$ : 668.4132  $[\text{M}+\text{H}]^+$ ,  $\text{C}_{35}\text{H}_{54}\text{N}_7\text{O}_6$ ; calculated 668.4136  $[\text{M}+\text{H}]^+$ ,  $\text{C}_{35}\text{H}_{54}\text{N}_7\text{O}_6$ .

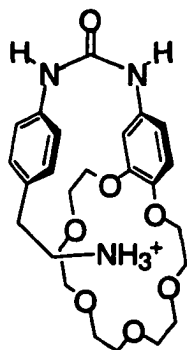


**6-Chloro-*N,N'*-diphenyl-1,3,5-triazine-2,4-diamine (41).**<sup>9</sup> Cyanuric chloride (0.50 g, 2.7 mmol) was dissolved in dry THF (20 mL) and cooled in an ice bath. This solution was treated with a solution of aniline (0.25 g, 2.7 mmol) and of triethylamine (0.27 g, 2.7 mmol) dissolved in THF (10 mL) dropwise. The ice bath was removed and the reaction mixture allowed to warm to ambient temperature and stirred for 4 h. The mixture was placed in an oil bath heated to 45 °C and treated with a solution of (0.25 g, 2.7 mmol) and triethylamine (0.27 g, 2.7 mmol) in dry THF (15 mL) dropwise. After stirring at 50 °C for 6 h, the oil bath was removed and the reaction mixture was allowed to cool to ambient temperature. The white deposited solid was filtered off, washed with water and vacuum dried (0.63 g, 79%). M.p. 197-200 °C; <sup>1</sup>H NMR (500 MHz, DMSO-*d*<sub>6</sub>) δ 9.53 (br. s, 2H), 7.76 (br. d, *J*=7.0 Hz, 4H), 7.30 (t, *J*=7.5 Hz, 4H), 7.03 (t, *J*=7.5 Hz, 2H).

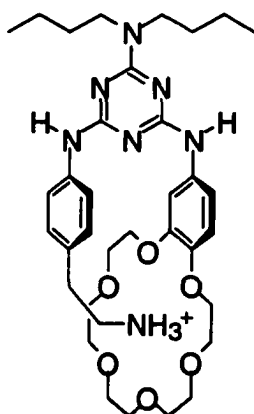


***N*<sup>2</sup>,*N*<sup>2</sup>-Dibutyl-*N*<sup>4</sup>,*N*<sup>6</sup>-diphenyl-1,3,5-triazine-2,4,6-triamine (42).**<sup>10</sup> A solution of 6-chloro-*N,N'*-diphenyl-1,3,5-triazine-2,4-diamine (0.5 g, 1.7 mmol), dibutylamine (0.65 g, 5 mmol) and THF (20 mL) was heated at reflux overnight under argon. After cooling to room temperature, the solvent was evaporated and the residue was treated with CH<sub>2</sub>Cl<sub>2</sub> (20 mL). The solution was washed with 5% HCl (1 × 10 mL), water (1 × 10 mL) and brine (1 × 10 mL). The organic layer was dried over anhydrous Na<sub>2</sub>SO<sub>4</sub>, filtered and concentrated under reduced pressure to afford solid. The product was purified by recrystallization twice from CH<sub>2</sub>Cl<sub>2</sub>/hexane (0.54 g, 82%). M.p. 139-141 °C; <sup>1</sup>H NMR (500 MHz CD<sub>2</sub>Cl<sub>2</sub>) δ 7.66 (d, *J*=7.5 Hz, 4H), 7.30 (t, *J*=7.5 Hz, 4H), 7.09 (br. s, 2H),

7.01 (t,  $J=7.0$  Hz, 2H), 3.55 (t,  $J=8.0$  Hz, 4H), 1.65 (m, 4H), 1.40 (m, 4H), 0.98 (t,  $J=7.5$  Hz, 6H);  $^{13}\text{C}$  NMR (75.5 MHz,  $\text{CDCl}_3$ )  $\delta$  165.0, 164.0, 139.5, 128.7, 122.5, 119.8, 47.5, 30.1, 20.4, 14.0; FT-IR (cast)  $\nu$  3412, 3279, 3055, 2957, 2929, 2871, 1593, 1582, 1543, 1510, 1493, 1433, 1419, 1369, 1313, 1226, 806, 751, 689, 597  $\text{cm}^{-1}$ ; HRMS (ES)  $m/z$ : 390.2528  $[\text{M}]^+$ ,  $\text{C}_{23}\text{H}_{30}\text{N}_6$ ; calculated 390.2532  $[\text{M}]^+$ ,  $\text{C}_{23}\text{H}_{30}\text{N}_6$ .



**Protonated urea receptor 38•HBF<sub>4</sub>.** To a solution of urea receptor **38** (5 mg,  $10.0 \times 10^{-3}$  mmol) in  $\text{CH}_3\text{OH}$  (2 mL), a 0.01 M  $\text{HBF}_4$  solution (1.2 mL,  $12.0 \times 10^{-3}$  mmol) in methanol was added. The mixture was stirred at room temperature for 15 min. The solvent was evaporated under reduced pressure and the residue was dried under vacuum ( $< 5$  mm) overnight. The collected white solid (6 mg) was then used without any further purification.





**Protonated triazine receptor 40•HBF<sub>4</sub>.** To a solution of triazine receptor **40** (5 mg,  $7.5 \times 10^{-3}$  mmol) in CH<sub>3</sub>OH (2 mL), a 0.01 M HBF<sub>4</sub> solution (0.9 mL,  $9.0 \times 10^{-3}$  mmol) in CH<sub>3</sub>OH was added. The mixture was stirred at room temperature for 15 min. The solvent was evaporated under reduced pressure and the residue was dried under vacuum (< 5 mm) overnight. The collected white solid (6 mg) was then used without further purification.

## 5.8. References

1. K. G. Scrimgeour, *Chemistry and Control of Enzyme Reactions*, Academic Press Inc. 1977.
2. J. A. Schetz, D. R. Sibley, *J. Pharmacol. Exp. Thera.* **2000**, 296, 359. (b) S. F. Traynelis, M. F. Burgess, F. Zheng, P. Lyuboslavsky, J. L. Powers, *J. Neurosci.* **1998**, 18, 6163.
3. (a) M.-V. Martinez-Diaz, N. Spencer, J. F. Stoddart, *Angew. Chem. Int. Ed.* **1997**, 36, 1904; (b) R. A. Bissell, E. Cordova, A. E. Kaifer, J. F. Stoddart, *Nature* **1994**, 369, 133; (c) A. E. Cordova, R. A. Bissell, N. Spencer, P. R. Ashton, J. F. Stoddart, A. E. Kaifer, *J. Org. Chem.* **1993**, 58, 6550; (d) Y. Nakatsuji, H. Kobayashi, M. Okahara, *J. Chem. Soc., Chem. Comm.* **1983**, 801; (e) P. R. Ashton, R. Ballardini, V. Balzani, I. Baxter, A. Credi, M. C. T. Gandolfi, M. Gomez-Lopez, M. V. Martinez-Diaz, A. Piersanti, N. Spencer, J. F. Stoddart, M. Venturi, A. J. P. White, D. J. Williams, *J. Am. Chem. Soc.* **1998**, 120, 11932; (f) V. Amendola, L. Fabbrizzi, C. Mangano, P. Pallavicini, A. Perotti, A. Taglietti, *J. Chem. Soc., Dalton Trans* **2000**, 185; (g) A. Harada, J. Li, M. Kamachi, *Nature* **1992**, 356, 325.
4. L. Desaubry, R. Johnson, *Bioorg. Med. Chem. Lett.* **1997**, 7, 123.
5. T. R. Kelly, M. H. Kim, *J. Am. Chem. Soc.* **1994**, 116, 7072.
6. E. Fan, A. V. Arman, S. Kincaid, A. D. Hamilton, *J. Am. Chem. Soc.* **1993**, 115, 369.
7. (a) F. G. Bordwell, D. J. Algrim, J. A. Jr. Harrelson, *J. Am. Chem. Soc.* **1988**, 110, 5903; (b) B. Valter, M. I. Terekhova, E. S. Petrov, J. Stehlicek, J. Sebenda, *Coll. Czech. Chem. Comm.* **1985**, 50, 840.
8. J. Hine, J. S. Hwang, V. Balasubramanian, *J. Org. Chem.* **1988**, 53, 5145.
9. J. A. Zerkowski, J. P. Mathias, G. M. Whitesides, *J. Am. Chem. Soc.* **1994**, 116, 4305.
10. P. Canbere, D. Parry, *Bull. Soc. Chim.* **1973**, 2112.

## **Chapter 6- Conclusions**

The thesis described how to design and regulate the function of synthetic receptors. The presented receptors utilize hydrogen bonding as means to recognize substrates possessing binding features similar to those of some biologically important species. The receptors were designed to respond to environmental changes that act as the stimuli to affect and modulate the molecular recognition activity. Thus, allosteric binding sites were incorporated into the receptors so that their affinity for the substrates can be controlled by the presence in solution of only the appropriate allosteric cofactor. The binding of a specific metal ion and a proton to the allosteric sites triggered conformational changes in the receptors rendering their hydrogen-bonding sites non-functional. The removal of the cofactors or, in some cases, the modulation of their properties induced the reactivation of the receptors.

Metal ions were the first example of allosteric cofactors used to control the binding of hydrogen-bonding receptors. The presence of Cu(I) ion inhibited the binding of imide and carboxylate substrates to triaminotriazine and urea receptors, respectively (Chapter 2). The complexation of the metal ion by the bipyridine ligands on the receptors led to the destruction of the active sites of the receptors. These conformational changes rendered the receptors inactive toward binding the substrates. The triazine receptor was modified to incorporate a terpyridine ligand which, along with one of the bipyridine ligands, provided a suitable chelation site for the Cu(II) ion (Chapter 3). The complexation of this diamonotriazine receptor with Cu(II) ion increased the affinity of the receptor for its imide substrates. The binding of the diamonotriazine to the imide substrates was then controlled through redox process. The switching between Cu(II) and Cu(I) switched the receptor's binding from active to inactive and vice versa. Finally, zinc

ion was used to control the binding of **34** receptor to its barbiturate substrate (Chapter 4). In this case, the chelation of the metal ion blocked the entrance of the binding pocket of the receptor without altering the hydrogen-bonding surface.

Protons were also used as negative allosteric cofactors to inhibit the binding of imide and carboxylate substrates by triaminotriazine and urea receptors, respectively (Chapter 5). The incorporation of an alkyl amine and a crown-ether into the receptors provided the allosteric sites. In the presence of an acid, the amino group was protonated inducing the formation of an intramolecular hydrogen-bonding complex between the ammonium salt and the crown ether. This complex formation destroyed the hydrogen-bonding active site of the receptor and thus prevented the recognition of the guest by its receptor.

## Appendix I- Crystallographic Experimental Details

**Compound:**  $[[2\text{-}^n\text{Bu}_2\text{N-4,6-(NHCH}_2\text{C}_5\text{H}_3\text{NC}_5\text{H}_3\text{NMe)}_2\text{-1,3,5-triazine}\text{]Cu}][\text{PF}_6]\cdot\text{H}_2\text{O}$

**Formula:**  $\text{C}_{35}\text{H}_{46}\text{CuF}_6\text{N}_{10}\text{OP}$  ( $\text{C}_{35}\text{H}_{44}\text{CuF}_6\text{N}_{10}\text{P}\cdot\text{H}_2\text{O}$ )

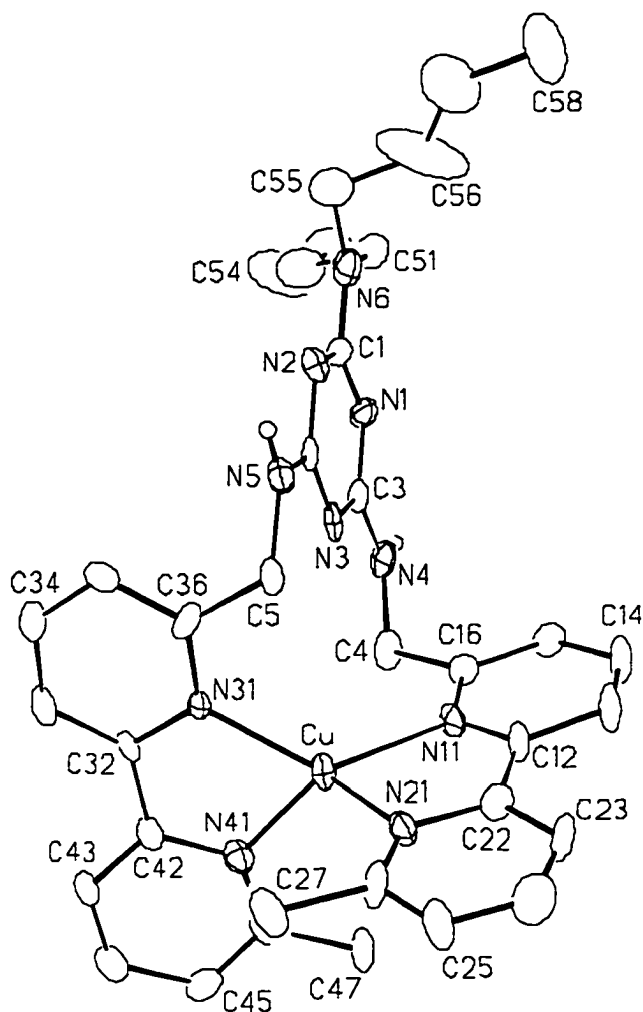


**Figure 1.** Crystal structure of  $6\cdot\text{Cu}$ . Perspective view of one of the two crystallographically-independent  $[[2\text{-}^n\text{Bu}_2\text{N-4,6-(NHCH}_2\text{C}_5\text{H}_3\text{NC}_5\text{H}_3\text{NMe)}_2\text{-1,3,5-triazine}\text{]Cu}^+$  ions showing the atom labelling scheme. Non-hydrogen atoms are represented by Gaussian ellipsoids at the 20% probability level. Hydrogen atoms bound to nitrogens N4 and N5 are shown with arbitrarily small thermal parameters; all other hydrogens are not shown.

**Table 1.** Crystallographic Experimental Details for **6•Cu**

<b>A. Crystal Data</b>	
formula	$C_{35}H_{46}CuF_6N_{10}OP$
formula weight	831.33
crystal dimensions (mm)	$0.37 \times 0.14 \times 0.02$
crystal system	triclinic
space group	<i>PI</i> (No. 2)
unit cell parameters <sup>a</sup>	
<i>a</i> (Å)	14.278 (2)
<i>b</i> (Å)	15.202 (2)
<i>c</i> (Å)	20.190 (3)
$\alpha$ (deg)	70.992 (4)
$\beta$ (deg)	78.889 (4)
$\gamma$ (deg)	69.360 (3)
<i>V</i> (Å <sup>3</sup> )	3862.5 (10)
<i>Z</i>	4
$\rho_{\text{calcd}}$ (g cm <sup>-3</sup> )	1.430
$\mu$ (mm <sup>-1</sup> )	0.679
<b>B. Data Collection and Refinement Conditions</b>	
diffractometer	Bruker P4/RA/SMART 1000 CCD <sup>b</sup>
radiation ( $\lambda$ [Å])	graphite-monochromated Mo K $\alpha$ (0.71073)
temperature (°C)	-80
scan type	$\phi$ rotations (0.3°) / $\omega$ scans (0.3°) (30 s
exposures)	
data collection $2\theta$ limit (deg)	51.50
total data collected	22324 ( $-17 \leq h \leq 17$ , $-17 \leq k \leq 18$ , $-24 \leq l \leq$
24)	
independent reflections	14674
number of observations ( <i>NO</i> )	2803 [ $F_o^2 \geq 2\sigma(F_o^2)$ ]
structure solution method	direct methods ( <i>SHELXS-86</i> <sup>c</sup> )
refinement method	full-matrix least-squares on $F^2$
( <i>SHELXL-93</i> <sup>d</sup> )	
absorption correction method	Gaussian integration (face-indexed)
range of transmission factors	0.9793–0.8336
data/restraints/parameters	14674 [ $F_o^2 \geq -3\sigma(F_o^2)$ ] / 0 / 977
goodness-of-fit ( <i>S</i> ) <sup>e</sup>	0.753 [ $F_o^2 \geq -3\sigma(F_o^2)$ ]
final <i>R</i> indices <sup>f</sup>	
<i>R</i> <sub>1</sub> [ $F_o^2 \geq 2\sigma(F_o^2)$ ]	0.0763
<i>wR</i> <sub>2</sub> [ $F_o^2 \geq -3\sigma(F_o^2)$ ]	0.1869
largest difference peak and hole	0.558 and -0.584 e Å <sup>-3</sup>

<sup>a</sup>Obtained from least-squares refinement of 2357 centered reflections.

<sup>b</sup>Programs for diffractometer operation, data collection, data reduction and absorption correction were those supplied by Bruker.

<sup>c</sup>Sheldrick, G. M. *Acta Crystallogr.* **1990**, *A46*, 467–473.

<sup>d</sup>Sheldrick, G. M. *SHELXL-93*. Program for crystal structure determination. University of Göttingen, Germany, 1993. Refinement on  $F_o^2$  for all reflections (all of these having  $F_o^2 \geq -3\sigma(F_o^2)$ ). Weighted  $R$ -factors  $wR_2$  and all goodnesses of fit  $S$  are based on  $F_o^2$ ; conventional  $R$ -factors  $R_1$  are based on  $F_o$ , with  $F_o$  set to zero for negative  $F_o^2$ . The observed criterion of  $F_o^2 > 2\sigma(F_o^2)$  is used only for calculating  $R_1$ , and is not relevant to the choice of reflections for refinement.  $R$ -factors based on  $F_o^2$  are statistically about twice as large as those based on  $F_o$ , and  $R$ -factors based on ALL data will be even larger.

<sup>e</sup> $S = [\sum w(F_o^2 - F_c^2)^2 / (n - p)]^{1/2}$  ( $n$  = number of data;  $p$  = number of parameters varied;  $w = [\sigma^2(F_o^2) + (0.0313P)^2]^{-1}$  where  $P = [\text{Max}(F_o^2, 0) + 2F_c^2]/3$ ).

<sup>f</sup> $R_1 = \sum ||F_o| - |F_c|| / \sum |F_o|$ ;  $wR_2 = [\sum w(F_o^2 - F_c^2)^2 / \sum w(F_o^4)]^{1/2}$ .

**Table 2.** Atomic Coordinates and Equivalent Isotropic Displacement Parameters*(a) [(2-<sup>n</sup>Bu<sub>2</sub>N-4,6-(NHCH<sub>2</sub>C<sub>5</sub>H<sub>3</sub>NC<sub>5</sub>H<sub>3</sub>NMe)<sub>2</sub>-1,3,5-triazine)Cu]<sup>+</sup> atoms (Molecule A)*

Atom	x	y	z	<i>U</i> <sub>eq</sub> , Å <sup>2</sup>
Cu	-0.19831(10)	-0.08231(10)	0.41094(7)	0.0520(5)*
N1	-0.4825(7)	-0.2142(8)	0.3215(5)	0.052(3)*
N2	-0.4535(7)	-0.3256(7)	0.4386(5)	0.048(3)*
N3	-0.3717(6)	-0.2044(7)	0.3920(5)	0.044(3)*
N4	-0.4051(6)	-0.0960(7)	0.2814(4)	0.048(3)*
N5	-0.3439(7)	-0.3140(7)	0.5008(5)	0.053(3)*
N6	-0.5603(8)	-0.3309(8)	0.3686(6)	0.064(3)*
N11	-0.3447(6)	0.0069(6)	0.3955(5)	0.048(3)*
N21	-0.2246(7)	-0.0237(7)	0.4918(5)	0.051(3)*
N31	-0.1339(6)	-0.2286(6)	0.4236(5)	0.045(3)*
N41	-0.0734(7)	-0.0786(8)	0.3441(4)	0.051(3)*
C1	-0.4944(9)	-0.2912(11)	0.3774(9)	0.056(4)*
C2	-0.3899(9)	-0.2804(10)	0.4406(8)	0.048(3)*
C3	-0.4188(9)	-0.1748(9)	0.3335(7)	0.042(3)*
C4	-0.3460(8)	-0.0418(9)	0.2896(5)	0.058(4)*
C5	-0.2720(8)	-0.2693(8)	0.5064(5)	0.054(3)*
C12	-0.3843(9)	0.0526(9)	0.4450(6)	0.051(3)*
C13	-0.4853(9)	0.1127(9)	0.4425(6)	0.069(4)*
C14	-0.5364(9)	0.1228(9)	0.3903(7)	0.081(4)*
C15	-0.4964(9)	0.0755(8)	0.3400(6)	0.055(4)*
C16	-0.3945(9)	0.0123(8)	0.3436(7)	0.052(3)*
C22	-0.3201(10)	0.0381(9)	0.4976(6)	0.054(3)*
C23	-0.3485(9)	0.0839(8)	0.5512(7)	0.068(4)*
C24	-0.2822(12)	0.0660(11)	0.5984(7)	0.091(5)*
C25	-0.1893(10)	0.0059(10)	0.5902(8)	0.085(5)*
C26	-0.1650(10)	-0.0385(9)	0.5383(7)	0.062(4)*
C27	-0.0631(8)	-0.1057(9)	0.5319(6)	0.091(5)*
C32	-0.0457(8)	-0.2509(9)	0.3830(6)	0.042(3)*
C33	0.0055(8)	-0.3483(10)	0.3818(6)	0.063(4)*
C34	-0.0388(10)	-0.4176(9)	0.4212(6)	0.074(4)*
C35	-0.1283(9)	-0.3950(9)	0.4594(6)	0.057(4)*
C36	-0.1748(9)	-0.2994(9)	0.4622(6)	0.049(3)*
C42	-0.0098(9)	-0.1685(10)	0.3439(6)	0.050(3)*
C43	0.0861(8)	-0.1796(9)	0.3065(6)	0.055(4)*
C44	0.1139(9)	-0.0994(11)	0.2701(6)	0.063(4)*
C45	0.0432(10)	-0.0038(9)	0.2707(6)	0.066(4)*
C46	-0.0490(9)	0.0011(10)	0.3078(6)	0.056(4)*
C47	-0.1206(8)	0.0971(8)	0.3105(7)	0.094(5)*
C51	-0.6079(10)	-0.2968(10)	0.3037(8)	0.084(5)*
C52	-0.5409(11)	-0.3313(10)	0.2452(7)	0.097(5)*
C53	-0.5938(13)	-0.2926(13)	0.1781(8)	0.129(7)*



**Table 2.** Atomic Coordinates and Displacement Parameters (continued)

Atom	x	y	z	$U_{eq}, \text{\AA}^2$
C54	-0.5426(14)	-0.3055(15)	0.1197(8)	0.190(11)*
C55	-0.5899(10)	-0.4078(10)	0.4223(7)	0.079(5)*
C56	-0.6818(18)	-0.365(2)	0.4701(10)	0.248(16)*
C57	-0.7467(17)	-0.389(2)	0.4943(17)	0.30(2)*
C58	-0.8436(11)	-0.3417(12)	0.5362(8)	0.158(7)*

(b)  $[(2\text{-}^n\text{Bu}_2\text{N-4,6-(NHCH}_2\text{C}_5\text{H}_3\text{NC}_5\text{H}_3\text{NMe)}_2\text{-1,3,5-triazine)]\text{Cu}]^+$  atoms (Molecule B)

Atom	x	y	z	$U_{eq}, \text{\AA}^2$
Cu	-0.11914(10)	-0.23090(10)	0.08886(7)	0.0484(5)*
N1	0.3049(7)	-0.3569(6)	-0.0301(6)	0.053(3)*
N2	0.2168(8)	-0.3040(7)	-0.1331(5)	0.057(3)*
N3	0.1251(6)	-0.2890(6)	-0.0223(5)	0.038(2)*
N4	0.2108(7)	-0.3470(6)	0.0750(5)	0.063(3)*
N5	0.0449(7)	-0.2407(6)	-0.1223(4)	0.051(3)*
N6	0.3888(9)	-0.3641(9)	-0.1409(7)	0.096(4)*
N11	-0.0179(7)	-0.1694(7)	0.0982(4)	0.046(3)*
N21	-0.2151(7)	-0.0894(6)	0.0786(4)	0.051(3)*
N31	-0.1078(6)	-0.3198(7)	0.0296(5)	0.039(2)*
N41	-0.1570(6)	-0.3391(7)	0.1665(6)	0.048(3)*
C1	0.3004(11)	-0.3416(9)	-0.0992(8)	0.061(4)*
C2	0.1310(10)	-0.2787(8)	-0.0909(7)	0.045(3)*
C3	0.2141(10)	-0.3303(8)	0.0056(7)	0.049(3)*
C4	0.1198(8)	-0.3186(8)	0.1176(6)	0.062(4)*
C5	-0.0503(8)	-0.2210(7)	-0.0789(5)	0.049(3)*
C12	-0.0585(9)	-0.0703(10)	0.0919(5)	0.053(4)*
C13	-0.0015(11)	-0.0130(9)	0.0886(6)	0.068(4)*
C14	0.1001(11)	-0.0588(12)	0.0951(7)	0.080(5)*
C15	0.1413(9)	-0.1571(10)	0.1034(6)	0.059(4)*
C16	0.0814(9)	-0.2133(10)	0.1053(6)	0.050(3)*
C22	-0.1693(10)	-0.0283(10)	0.0833(6)	0.053(3)*
C23	-0.2220(11)	0.0678(9)	0.0798(7)	0.083(5)*
C24	-0.3225(11)	0.1007(10)	0.0729(8)	0.113(7)*
C25	-0.3688(9)	0.0372(10)	0.0687(6)	0.073(4)*
C26	-0.3153(9)	-0.0586(10)	0.0708(6)	0.058(4)*
C27	-0.3586(8)	-0.1318(9)	0.0701(6)	0.076(4)*
C32	-0.1369(8)	-0.4028(9)	0.0694(7)	0.052(3)*
C33	-0.1433(8)	-0.4656(8)	0.0355(7)	0.060(4)*
C34	-0.1198(9)	-0.4523(10)	-0.0356(8)	0.071(4)*
C35	-0.0875(8)	-0.3723(11)	-0.0738(6)	0.060(4)*
C36	-0.0844(7)	-0.3088(8)	-0.0378(6)	0.036(3)*
C42	-0.1617(9)	-0.4113(11)	0.1446(7)	0.061(4)*
C43	-0.1841(12)	-0.4948(11)	0.1920(8)	0.110(6)*
C44	-0.2053(16)	-0.4962(16)	0.2614(9)	0.171(10)*

**Table 2.** Atomic Coordinates and Displacement Parameters (continued)

Atom	x	y	z	$U_{eq}, \text{\AA}^2$
C45	-0.2074(13)	-0.4225(12)	0.2845(8)	0.113(6)*
C46	-0.1784(9)	-0.3443(10)	0.2348(7)	0.061(4)*
C47	-0.1716(8)	-0.2598(8)	0.2555(5)	0.064(4)*
C51	0.4852(10)	-0.4030(10)	-0.1106(7)	0.086(5)*
C52	0.5359(11)	-0.3290(12)	-0.1322(10)	0.145(8)*
C53	0.6281(17)	-0.3560(14)	-0.1009(11)	0.160(9)*
C54	0.6080(14)	-0.3377(16)	-0.0348(10)	0.213(12)*
C55	0.3836(12)	-0.3748(14)	-0.2216(11)	0.160(10)*
C56	0.3800(12)	-0.2862(14)	-0.2522(12)	0.147(8)*
C57	0.3463(15)	-0.2829(14)	-0.3394(11)	0.192(10)*
C58	0.4241(13)	-0.3517(13)	-0.3629(10)	0.172(9)*

*(c) hexafluorophosphate ion atoms*

Atom	x	y	z	$U_{eq}, \text{\AA}^2$
P1	0.2620(3)	-0.5253(3)	0.2966(2)	0.0628(11)*
F11	0.2106(5)	-0.4093(5)	0.2785(3)	0.084(2)*
F12	0.3140(5)	-0.6413(4)	0.3168(3)	0.082(2)*
F13	0.1638(6)	-0.5457(6)	0.3334(5)	0.150(4)*
F14	0.2825(7)	-0.5235(5)	0.3684(4)	0.138(4)*
F15	0.3588(6)	-0.5068(6)	0.2616(6)	0.184(5)*
F16	0.2352(8)	-0.5298(6)	0.2278(4)	0.175(5)*
P2	0.3365(3)	0.0493(4)	0.1682(2)	0.0843(13)*
F21	0.3742(9)	0.0880(11)	0.0943(5)	0.243(7)*
F22	0.4004(7)	0.0874(7)	0.1982(5)	0.173(4)*
F23	0.4255(7)	-0.0460(7)	0.1721(6)	0.180(4)*
F24	0.2706(7)	0.0103(7)	0.1390(5)	0.173(4)*
F25	0.2494(8)	0.1425(9)	0.1658(8)	0.249(7)*
F26	0.3051(8)	-0.0007(10)	0.2421(5)	0.225(6)*

*(d) solvent water atoms*

Atom	x	y	z	$U_{eq}, \text{\AA}^2$
O1	-0.0453(9)	-0.2498(6)	-0.2625(4)	0.138(4)*
O2	0.1778(13)	-0.7545(10)	0.2901(7)	0.244(7)*

Anisotropically-refined atoms are marked with an asterisk (\*). The form of the anisotropic displacement parameter is:  $\exp[-2\pi^2(h^2a^{*2}U_{11} + k^2b^{*2}U_{22} + l^2c^{*2}U_{33} + 2klb^{*c^*}U_{23} + 2hla^{*c^*}U_{13} + 2hka^{*b^*}U_{12})]$ .

**Compound:**  $[[\{(2-(6\text{-Me-2-pyridyl})-6\text{-pyridyl})\text{CH}_2\text{NH})_2\text{C}=\text{O}\}_2\text{Cu}_2][\text{PF}_6]_2$

**Formula:**  $\text{C}_{50}\text{H}_{48}\text{Cu}_2\text{F}_{12}\text{N}_{12}\text{O}_2\text{P}_2$

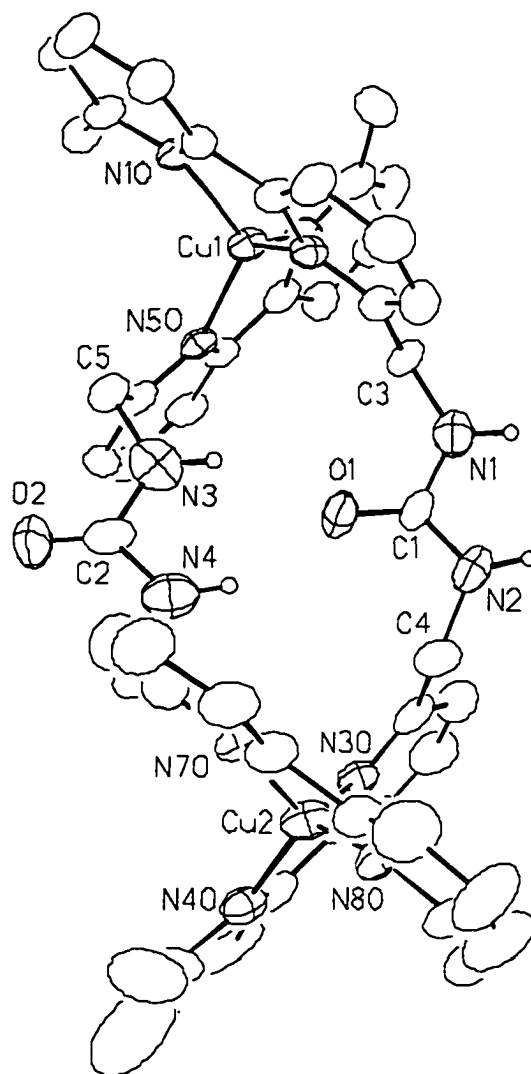


**Figure 2.** Crystal structure of  $7 \cdot \text{Cu}$ . Perspective view of the  $[[\{(2-(6\text{-Me-2-pyridyl})-6\text{-pyridyl})\text{CH}_2\text{NH})_2\text{C}=\text{O}\}_2\text{Cu}_2]^{2+}$  ion showing the atom labelling scheme. Non-hydrogen atoms are represented by Gaussian ellipsoids at the 20% probability level. The amido hydrogen atoms are shown with arbitrarily small thermal parameters; all other hydrogens are not shown.

**Table 3.** Crystallographic Experimental Details for **7•Cu**

<b>A. Crystal Data</b>	
formula	$C_{50}H_{48}Cu_2F_{12}N_{12}O_2P_2$
formula weight	1266.02
crystal dimensions (mm)	$0.23 \times 0.12 \times 0.12$
crystal system	monoclinic
space group	$C2/c$ (No. 15)
unit cell parameters <sup>a</sup>	
<i>a</i> (Å)	19.142 (2)
<i>b</i> (Å)	23.545 (2)
<i>c</i> (Å)	29.324 (3)
$\beta$ (deg)	101.428 (3)
<i>V</i> (Å <sup>3</sup> )	1000.0 (10)
<i>Z</i>	8
$\rho_{\text{calcd}}$ (g cm <sup>-3</sup> )	1.298
$\mu$ (mm <sup>-1</sup> )	0.785
<b>B. Data Collection and Refinement Conditions</b>	
diffractometer	Bruker P4/RA/SMART 1000 CCD <sup>b</sup>
radiation ( $\lambda$ [Å])	graphite-monochromated Mo K $\alpha$ (0.71073)
temperature (°C)	-80
scan type	$\phi$ rotations (0.3°) / $\omega$ scans (0.3°) (60 s
exposures)	
data collection $2\theta$ limit (deg)	52.78
total data collected	22660 ( $-23 \leq h \leq 16, -23 \leq k \leq 29, -36 \leq l \leq$
19)	
independent reflections	12186 ( $R_{\text{int}} = 0.1075$ )
number of observed reflections ( <i>NO</i> )	3116 [ $F_o^2 \geq 2\sigma(F_o^2)$ ]
structure solution method	direct methods ( <i>SHELXS-86</i> <sup>c</sup> )
refinement method	full-matrix least-squares on $F^2$
( <i>SHELXL-93</i> <sup>d</sup> )	
absorption correction method	empirical ( <i>SADABS</i> )
range of transmission factors	0.9280–0.6559
data/restraints/parameters	12186 [ $F_o^2 \geq -3\sigma(F_o^2)$ ] / 0 / 703
goodness-of-fit ( <i>S</i> ) <sup>e</sup>	0.981 [ $F_o^2 \geq -3\sigma(F_o^2)$ ]
final <i>R</i> indices <sup>f</sup>	
<i>R</i> <sub>1</sub> [ $F_o^2 \geq 2\sigma(F_o^2)$ ]	0.1388
<i>wR</i> <sub>2</sub> [ $F_o^2 \geq -3\sigma(F_o^2)$ ]	0.4355
largest difference peak and hole	1.746 and -0.568 e Å <sup>-3</sup>

<sup>a</sup>Obtained from least-squares refinement of 3791 centered reflections.

<sup>b</sup>Programs for diffractometer operation, data collection, data reduction and absorption correction were those supplied by Bruker.

<sup>c</sup>Sheldrick, G. M. *Acta Crystallogr.* **1990**, *A46*, 467–473.

<sup>d</sup>Sheldrick, G. M. *SHELXL-93*. Program for crystal structure determination. University of Göttingen, Germany, 1993. Refinement on  $F_o^2$  for all reflections (all of these having  $F_o^2 \geq -3\sigma(F_o^2)$ ). Weighted  $R$ -factors  $wR_2$  and all goodnesses of fit  $S$  are based on  $F_o^2$ ; conventional  $R$ -factors  $R_1$  are based on  $F_o$ , with  $F_o$  set to zero for negative  $F_o^2$ . The observed criterion of  $F_o^2 > 2\sigma(F_o^2)$  is used only for calculating  $R_1$ , and is not relevant to the choice of reflections for refinement.  $R$ -factors based on  $F_o^2$  are statistically about twice as large as those based on  $F_o$ , and  $R$ -factors based on ALL data will be even larger.

$$^e S = [\sum w(F_o^2 - F_c^2)^2 / (n - p)]^{1/2} \quad (n = \text{number of data; } p = \text{number of parameters varied; } w = [\sigma^2(F_o^2) + (0.20P)^2]^{-1} \text{ where } P = [\text{Max}(F_o^2, 0) + 2F_c^2] / 3).$$

$$^f R_1 = \sum ||F_o| - |F_c|| / \sum |F_o|; \quad wR_2 = [\sum w(F_o^2 - F_c^2)^2 / \sum w(F_o^4)]^{1/2}.$$

**Compound:**  $[\text{Cu}\{(\text{MeC}_5\text{H}_3\text{NC}_5\text{H}_3\text{NCH}_2\text{NH})_2\text{C}_3\text{N}_3\text{OCH}_2(\text{C}_5\text{H}_3\text{N})_2\text{C}_5\text{H}_4\text{N}\}]$   
 $[\text{PF}_6]\cdot\text{PhMe}$

**Formula:**  $\text{C}_{50}\text{H}_{44}\text{CuF}_6\text{N}_{12}\text{OP}$  ( $\text{C}_{43}\text{H}_{36}\text{CuF}_6\text{N}_{12}\text{OP}\cdot\text{C}_7\text{H}_8$ )

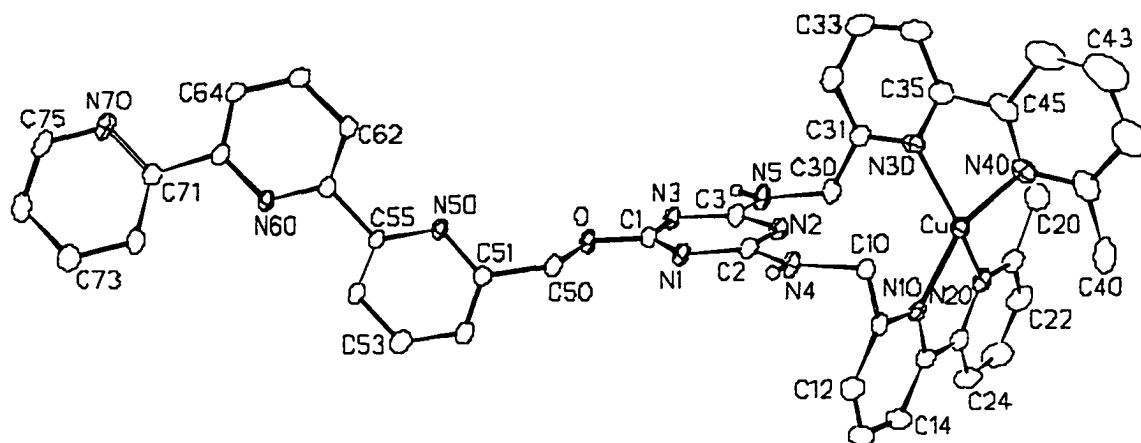


**Figure 3.** Crystal structure of  $\text{Cu}(17)^+$ . Perspective view of the  $[\text{Cu}\{(\text{MeC}_5\text{H}_3\text{NC}_5\text{H}_3\text{NCH}_2\text{NH})_2\text{C}_3\text{N}_3\text{OCH}_2(\text{C}_5\text{H}_3\text{N})_2\text{C}_5\text{H}_4\text{N}\}]^+$  ion showing the atom labelling scheme. Non-hydrogen atoms are represented by Gaussian ellipsoids at the 20% probability level. The hydrogen atoms attached to N4 and N5 are shown with arbitrarily small thermal parameters; all other hydrogens have been omitted.

**Table 4.** Crystallographic Experimental Details for Cu(17)<sup>a</sup>

<b>A. Crystal Data</b>	
formula	C <sub>50</sub> H <sub>44</sub> CuF <sub>6</sub> N <sub>12</sub> OP
formula weight	1037.48
crystal dimensions (mm)	0.33 × 0.15 × 0.10
crystal system	triclinic
space group	PI (No. 2)
unit cell parameters <sup>a</sup>	
<i>a</i> (Å)	9.9312 (12)
<i>b</i> (Å)	15.733 (2)
<i>c</i> (Å)	17.743 (2)
α (deg)	72.366 (2)
β (deg)	80.042 (3)
γ (deg)	88.735 (2)
<i>V</i> (Å <sup>3</sup> )	2600.8 (6)
<i>Z</i>	2
ρ <sub>calcd</sub> (g cm <sup>-3</sup> )	1.325
μ (mm <sup>-1</sup> )	0.521
<b>B. Data Collection and Refinement Conditions</b>	
diffractometer	Bruker PLATFORM/SMART 1000 CCD <sup>b</sup>
radiation (λ [Å])	graphite-monochromated Mo Kα (0.71073)
temperature (°C)	-80
scan type	ω scans (0.2°) (30 s exposures)
data collection 2θ limit (deg)	52.92
total data collected	13106 (-11 ≤ <i>h</i> ≤ 12, -19 ≤ <i>k</i> ≤ 19, -22 ≤ <i>l</i> ≤ 21)
independent reflections	10515
number of observed reflections ( <i>NO</i> )	4973 [ <i>F</i> <sub>o</sub> <sup>2</sup> ≥ 2σ( <i>F</i> <sub>o</sub> <sup>2</sup> )]
structure solution method	direct methods/fragment search
( <i>DIRDIF-96</i> <sup>c</sup> )	
refinement method	full-matrix least-squares on <i>F</i> <sup>2</sup>
( <i>SHELXL-93</i> <sup>d</sup> )	
absorption correction method	Gaussian integration (face-indexed)
range of transmission factors	0.9538–0.8566
data/restraints/parameters	10515 [ <i>F</i> <sub>o</sub> <sup>2</sup> ≥ -3σ( <i>F</i> <sub>o</sub> <sup>2</sup> )] / 6 <sup>e</sup> / 601
goodness-of-fit ( <i>S</i> ) <sup>f</sup>	1.000 [ <i>F</i> <sub>o</sub> <sup>2</sup> ≥ -3σ( <i>F</i> <sub>o</sub> <sup>2</sup> )]
final <i>R</i> indices <sup>g</sup>	
<i>R</i> <sub>1</sub> [ <i>F</i> <sub>o</sub> <sup>2</sup> ≥ 2σ( <i>F</i> <sub>o</sub> <sup>2</sup> )]	0.0979
<i>wR</i> <sub>2</sub> [ <i>F</i> <sub>o</sub> <sup>2</sup> ≥ -3σ( <i>F</i> <sub>o</sub> <sup>2</sup> )]	0.2995
largest difference peak and hole	1.249 and -0.787 e Å <sup>-3</sup>

<sup>a</sup>Obtained from least-squares refinement of 4023 centered reflections.

<sup>b</sup>Programs for diffractometer operation, data collection, data reduction and absorption correction were those supplied by Bruker.

<sup>c</sup>Beurskens, P. T.; Beurskens, G.; Bosman, W. P.; de Gelder, R.; Garcia Granda, S.; Gould, R. O.; Israel, R.; Smits, J. M. M. (1996). The *DIRDIF-96* program system. Crystallography Laboratory, University of Nijmegen, The Netherlands.

<sup>d</sup>Sheldrick, G. M. *SHELXL-93*. Program for crystal structure determination. University of Göttingen, Germany, 1993. Refinement on  $F_o^2$  for all reflections (all of these having  $F_o^2 \geq -3\sigma(F_o^2)$ ). Weighted  $R$ -factors  $wR_2$  and all goodnesses of fit  $S$  are based on  $F_o^2$ ; conventional  $R$ -factors  $R_1$  are based on  $F_o$ , with  $F_o$  set to zero for negative  $F_o^2$ . The observed criterion of  $F_o^2 > 2\sigma(F_o^2)$  is used only for calculating  $R_1$ , and is not relevant to the choice of reflections for refinement.  $R$ -factors based on  $F_o^2$  are statistically about twice as large as those based on  $F_o$ , and  $R$ -factors based on ALL data will be even larger.

<sup>e</sup>The methyl carbons of the solvent toluene molecules were refined in idealized positions:  $d(\text{C}_{\text{methyl}}-\text{C}_{\text{ipso}}) = 1.54 \text{ \AA}$ ;  $d(\text{C}_{\text{methyl}} \cdots \text{C}_{\text{ortho}}) = 2.54 \text{ \AA}$ . The aromatic rings of these molecules were refined as idealized regular hexagons with a C–C bond distance of 1.39 Å.

<sup>f</sup> $S = [\sum w(F_o^2 - F_c^2)^2 / (n - p)]^{1/2}$  ( $n$  = number of data;  $p$  = number of parameters varied;  $w = [\sigma^2(F_o^2) + (0.1612P)^2]^{-1}$  where  $P = [\text{Max}(F_o^2, 0) + 2F_c^2]/3$ ).

<sup>g</sup> $R_1 = \sum ||F_o| - |F_c|| / \sum |F_o|$ ;  $wR_2 = [\sum w(F_o^2 - F_c^2)^2 / \sum w(F_o^4)]^{1/2}$ .



**Table 5.** Atomic Coordinates and Equivalent Isotropic Displacement Parameters*(a) atoms of [Cu((MeC<sub>5</sub>H<sub>3</sub>NC<sub>5</sub>H<sub>3</sub>NCH<sub>2</sub>NH)<sub>2</sub>C<sub>3</sub>N<sub>3</sub>OCH<sub>2</sub>(C<sub>5</sub>H<sub>3</sub>N)<sub>2</sub>C<sub>5</sub>H<sub>4</sub>N)]<sup>+</sup>*

Atom	<i>x</i>	<i>y</i>	<i>z</i>	<i>U</i> <sub>eq</sub> , Å <sup>2</sup>
Cu	0.13261(9)	-0.34716(5)	0.23056(5)	0.0396(3)*
O	0.5833(4)	-0.6973(3)	0.4682(3)	0.0379(11)*
N1	0.4604(5)	-0.6610(3)	0.3650(3)	0.0353(13)*
N2	0.3617(6)	-0.5153(3)	0.3374(3)	0.0362(13)*
N3	0.4964(5)	-0.5637(3)	0.4405(3)	0.0364(13)*
N4	0.3303(6)	-0.6094(4)	0.2656(3)	0.0399(14)*
N5	0.3969(6)	-0.4276(3)	0.4138(3)	0.0440(15)*
N10	0.0556(5)	-0.4709(3)	0.2940(3)	0.0361(13)*
N20	-0.0251(6)	-0.3131(4)	0.3041(4)	0.0429(14)*
N30	0.3266(6)	-0.3037(3)	0.2245(4)	0.0415(14)*
N40	0.1754(7)	-0.2879(4)	0.1121(4)	0.0504(16)*
N50	0.8010(5)	-0.8497(3)	0.5071(3)	0.0341(13)*
N60	1.0629(5)	-0.9792(3)	0.5997(3)	0.0336(12)*
N70	1.3849(6)	-1.0694(4)	0.6426(4)	0.0455(15)*
C1	0.5112(7)	-0.6386(4)	0.4208(4)	0.0353(15)*
C2	0.3852(6)	-0.5942(4)	0.3235(4)	0.0336(15)*
C3	0.4189(7)	-0.5042(4)	0.3958(4)	0.0359(16)*
C10	0.2319(7)	-0.5491(4)	0.2273(4)	0.0346(15)*
C11	0.1048(7)	-0.5495(4)	0.2855(4)	0.0396(16)*
C12	0.0390(8)	-0.6299(5)	0.3329(5)	0.059(2)*
C13	-0.0739(9)	-0.6315(5)	0.3907(6)	0.074(3)*
C14	-0.1214(8)	-0.5514(5)	0.3997(6)	0.065(2)*
C15	-0.0556(7)	-0.4719(5)	0.3503(5)	0.0472(18)*
C20	0.0290(10)	-0.1560(5)	0.2460(6)	0.069(3)*
C21	-0.0560(8)	-0.2301(5)	0.3067(5)	0.0476(19)*
C22	-0.1602(9)	-0.2175(6)	0.3637(6)	0.064(2)*
C23	-0.2318(10)	-0.2880(7)	0.4171(7)	0.082(3)*
C24	-0.2037(8)	-0.3734(6)	0.4145(6)	0.068(3)*
C25	-0.0992(7)	-0.3839(5)	0.3583(5)	0.0447(18)*
C30	0.3184(8)	-0.3569(4)	0.3684(4)	0.0420(17)*
C31	0.3935(8)	-0.3126(4)	0.2855(5)	0.0470(19)*
C32	0.5247(10)	-0.2818(6)	0.2729(7)	0.077(3)*
C33	0.5928(11)	-0.2416(8)	0.1954(9)	0.102(4)*
C34	0.5251(12)	-0.2319(7)	0.1341(7)	0.094(3)*
C35	0.3896(9)	-0.2639(5)	0.1500(5)	0.060(2)*
C40	-0.0484(12)	-0.3124(7)	0.0914(6)	0.087(3)*
C41	0.0899(13)	-0.2759(6)	0.0588(5)	0.075(3)*
C42	0.1328(19)	-0.2347(9)	-0.0211(7)	0.120(5)*
C43	0.267(2)	-0.2046(11)	-0.0477(8)	0.155(7)*

**Table 5.** Atomic Coordinates and Displacement Parameters (continued)

Atom	x	y	z	$U_{eq}, \text{\AA}^2$
C44	0.3535(16)	-0.2117(9)	0.0039(7)	0.121(5)*
C45	0.3028(12)	-0.2552(6)	0.0868(5)	0.070(3)*
C50	0.6021(7)	-0.7837(4)	0.4551(4)	0.0389(16)*
C51	0.6661(7)	-0.8418(4)	0.5232(4)	0.0336(15)*
C52	0.5862(7)	-0.8854(4)	0.5951(5)	0.0464(18)*
C53	0.6464(8)	-0.9406(5)	0.6571(5)	0.0511(19)*
C54	0.7878(7)	-0.9506(4)	0.6397(4)	0.0408(17)*
C55	0.8594(6)	-0.9046(4)	0.5651(4)	0.0316(15)*
C61	1.0097(7)	-0.9176(4)	0.5446(4)	0.0345(15)*
C62	1.0857(7)	-0.8668(4)	0.4723(4)	0.0439(17)*
C63	1.2244(7)	-0.8810(5)	0.4563(4)	0.0450(17)*
C64	1.2798(7)	-0.9453(4)	0.5129(4)	0.0399(17)*
C65	1.1976(6)	-0.9942(4)	0.5832(4)	0.0352(15)*
C71	1.2490(7)	-1.0670(4)	0.6451(4)	0.0374(16)*
C72	1.1588(8)	-1.1327(5)	0.7004(4)	0.0471(18)*
C73	1.2112(9)	-1.2024(6)	0.7544(5)	0.060(2)*
C74	1.3518(9)	-1.2032(6)	0.7532(5)	0.058(2)*
C75	1.4311(8)	-1.1370(6)	0.6973(5)	0.052(2)*

*(b) hexafluorophosphate ion atoms*

Atom	x	y	z	$U_{eq}, \text{\AA}^2$
P	0.2457(2)	0.21066(15)	0.16001(13)	0.0562(6)*
F1	0.2698(6)	0.2204(4)	0.0686(3)	0.0964(19)*
F2	0.2234(7)	0.2001(4)	0.2539(3)	0.108(2)*
F3	0.3583(6)	0.2846(4)	0.1474(4)	0.105(2)*
F4	0.1328(7)	0.1352(4)	0.1769(4)	0.112(2)*
F5	0.1344(7)	0.2834(4)	0.1512(4)	0.116(2)*
F6	0.3550(7)	0.1368(4)	0.1723(4)	0.112(2)*

*(c) solvent toluene atoms*

Atom	x	y	z	$U_{eq}, \text{\AA}^2$
C10S <sup>a</sup>	0.2476(18)	-0.4895(13)	0.0256(6)	0.091(2)
C11S <sup>a</sup>	0.2635(12)	-0.4896(9)	-0.0623(6)	0.091(2)
C12S <sup>a</sup>	0.1731(12)	-0.4434(8)	-0.1106(7)	0.091(2)
C13S <sup>a</sup>	0.1876(13)	-0.4434(9)	-0.1899(7)	0.091(2)
C14S <sup>a</sup>	0.2927(15)	-0.4897(9)	-0.2209(6)	0.091(2)
C15S <sup>a</sup>	0.3831(13)	-0.5359(9)	-0.1726(7)	0.091(2)
C16S <sup>a</sup>	0.3686(12)	-0.5359(9)	-0.0933(7)	0.091(2)
C20S <sup>a</sup>	-0.277(2)	-0.0203(17)	0.1882(10)	0.158(5)
C21S <sup>a</sup>	-0.2925(16)	-0.0233(11)	0.1040(9)	0.158(5)

**Table 5.** Atomic Coordinates and Displacement Parameters (continued)

Atom	<i>x</i>	<i>y</i>	<i>z</i>	<i>U</i> <sub>eq</sub> , Å <sup>2</sup>
C22S <sup>a</sup>	-0.1807(15)	-0.0426(12)	0.0536(11)	0.158(5)
C23S <sup>a</sup>	-0.191(2)	-0.0382(13)	-0.0246(11)	0.158(5)
C24S <sup>a</sup>	-0.313(2)	-0.0144(14)	-0.0524(10)	0.158(5)
C25S <sup>a</sup>	-0.4251(19)	0.0049(15)	-0.0020(12)	0.158(5)
C26S <sup>a</sup>	-0.4147(15)	0.0005(14)	0.0762(11)	0.158(5)

Anisotropically-refined atoms are marked with an asterisk (\*). The form of the anisotropic displacement parameter is:  $\exp[-2\pi^2(h^2a^{*2}U_{11} + k^2b^{*2}U_{22} + l^2c^{*2}U_{33} + 2klb^{*c^*}U_{23} + 2hla^{*c^*}U_{13} + 2hka^{*b^*}U_{12})]$ . <sup>a</sup>Carbons of the solvent toluene molecules were refined with an occupancy of 0.5; each molecule's carbons were refined with a common isotropic displacement parameter.

**Compound:** *N,N'*-bis(2-{6-(pyridine-2-amido)pyridyl})isophthalamide

**Formula:** C<sub>30</sub>H<sub>22</sub>N<sub>8</sub>O<sub>4</sub>

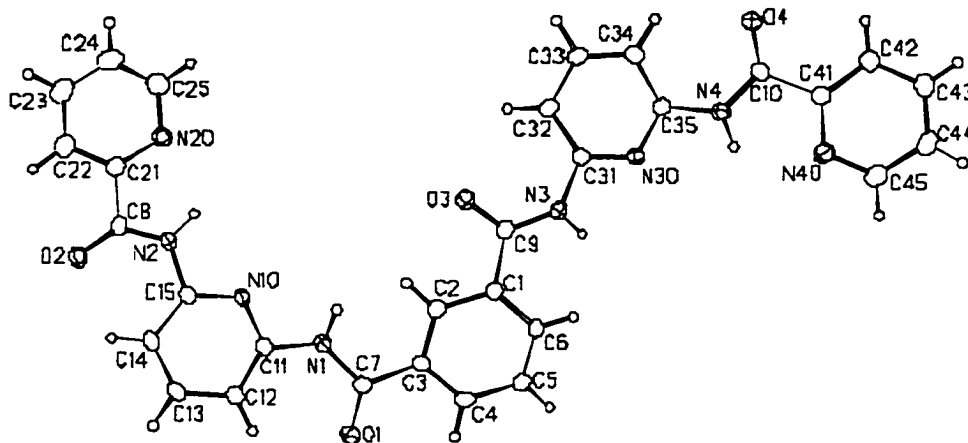


**Figure 4.** Crystal structure of receptor **28**. Perspective view of the *N,N'*-bis(2-{6-(pyridine-2-amido)pyridyl})isophthalamide molecule showing the atom labelling scheme. Non-hydrogen atoms are represented by Gaussian ellipsoids at the 20% probability level. Hydrogen atoms are shown with arbitrarily small thermal parameters.

**Table 6.** Crystallographic Experimental Details for receptor **28**

<b>A. Crystal Data</b>	
formula	$C_{30}H_{22}N_8O_4$
formula weight	558.56
crystal dimensions (mm)	$0.34 \times 0.18 \times 0.06$
crystal system	monoclinic
space group	$P2_1/c$ (No. 14)
unit cell parameters <sup>a</sup>	
$a$ (Å)	11.4591 (11)
$b$ (Å)	17.3834 (17)
$c$ (Å)	13.5351 (13)
$\beta$ (deg)	101.9892 (19)
$V$ (Å <sup>3</sup> )	2637.4 (4)
$Z$	4
$\rho_{\text{calcd}}$ (g cm <sup>-3</sup> )	1.407
$\mu$ (mm <sup>-1</sup> )	0.098
<b>B. Data Collection and Refinement Conditions</b>	
diffractometer	Bruker PLATFORM/SMART 1000 CCD <sup>b</sup>
radiation ( $\lambda$ [Å])	graphite-monochromated Mo K $\alpha$ (0.71073)
temperature (°C)	-80
scan type	$\omega$ scans (0.2°) (25 s exposures)
data collection $2\theta$ limit (deg)	52.80
total data collected	15018 ( $-14 \leq h \leq 14$ , $-21 \leq k \leq 20$ , $-16 \leq l \leq 16$ )
independent reflections	5394 ( $R_{\text{int}} = 0.1103$ )
number of observed reflections ( $NO$ )	2392 [ $F_o^2 \geq 2\sigma(F_o^2)$ ]
structure solution method	direct methods ( <i>SHELXS-86</i> <sup>c</sup> )
refinement method	full-matrix least-squares on $F^2$
( <i>SHELXL-93</i> <sup>d</sup> )	
absorption correction method	empirical ( <i>SADABS</i> )
range of transmission factors	0.9941–0.9675
data/restraints/parameters	5394 [ $F_o^2 \geq -3\sigma(F_o^2)$ ] / 0 / 379
goodness-of-fit ( $S$ ) <sup>e</sup>	1.003 [ $F_o^2 \geq -3\sigma(F_o^2)$ ]
final $R$ indices <sup>f</sup>	
$R_1$ [ $F_o^2 \geq 2\sigma(F_o^2)$ ]	0.0772
$wR_2$ [ $F_o^2 \geq -3\sigma(F_o^2)$ ]	0.2051
largest difference peak and hole	1.054 and -0.188 e Å <sup>-3</sup>

<sup>a</sup>Obtained from least-squares refinement of 2857 centered reflections.

<sup>b</sup>Programs for diffractometer operation, data collection, data reduction and absorption

correction were those supplied by Bruker.

<sup>c</sup>Sheldrick, G. M. *Acta Crystallogr.* **1990**, *A46*, 467–473.

<sup>d</sup>Sheldrick, G. M. *SHELXL-93*. Program for crystal structure determination. University of Göttingen, Germany, 1993. Refinement on  $F_o^2$  for all reflections (all of these having  $F_o^2 \geq -3\sigma(F_o^2)$ ). Weighted  $R$ -factors  $wR_2$  and all goodnesses of fit  $S$  are based on  $F_o^2$ ; conventional  $R$ -factors  $R_1$  are based on  $F_o$ , with  $F_o$  set to zero for negative  $F_o^2$ . The observed criterion of  $F_o^2 > 2\sigma(F_o^2)$  is used only for calculating  $R_1$ , and is not relevant to the choice of reflections for refinement.  $R$ -factors based on  $F_o^2$  are statistically about twice as large as those based on  $F_o$ , and  $R$ -factors based on ALL data will be even larger.

$$^eS = [\sum w(F_o^2 - F_c^2)^2 / (n - p)]^{1/2} \quad (n = \text{number of data}; p = \text{number of parameters varied}; w = [\sigma^2(F_o^2) + (0.0867P)^2]^{-1} \text{ where } P = [\text{Max}(F_o^2, 0) + 2F_c^2]/3).$$

$$^fR_1 = \sum ||F_o| - |F_c|| / \sum |F_o|; \quad wR_2 = [\sum w(F_o^2 - F_c^2)^2 / \sum w(F_o^4)]^{1/2}.$$

**Table 7. Atomic Coordinates and Equivalent Isotropic Displacement Parameters**

Atom	x	y	z	$U_{eq}, \text{\AA}^2$
O1	0.4485(2)	0.13197(19)	0.3344(2)	0.0595(9)*
O2	0.0773(3)	0.22043(18)	-0.22012(19)	0.0539(8)*
O3	-0.0451(2)	0.07994(19)	0.4399(2)	0.0594(9)*
O4	-0.4227(2)	0.05831(19)	0.8729(2)	0.0554(9)*
N1	0.2581(3)	0.1570(2)	0.2528(2)	0.0472(10)*
N2	0.0431(3)	0.1968(2)	-0.0631(2)	0.0465(9)*
N3	-0.0235(3)	0.1031(2)	0.6069(2)	0.0426(9)*
N4	-0.2306(3)	0.05172(19)	0.8497(2)	0.0437(9)*
N10	0.1613(3)	0.17334(19)	0.0907(2)	0.0405(8)*
N20	-0.1828(3)	0.2384(2)	-0.1197(3)	0.0529(10)*
N30	-0.1377(3)	0.07391(18)	0.7200(2)	0.0372(8)*
N40	-0.1444(3)	0.0529(2)	1.0450(3)	0.0545(10)*
C1	0.1455(3)	0.1197(2)	0.5275(3)	0.0372(10)*
C2	0.1831(3)	0.1232(2)	0.4361(3)	0.0388(10)*
C3	0.3005(3)	0.1412(2)	0.4333(3)	0.0401(10)*
C4	0.3807(4)	0.1550(2)	0.5237(3)	0.0469(11)*
C5	0.3444(4)	0.1506(3)	0.6144(3)	0.0519(12)*
C6	0.2275(4)	0.1337(3)	0.6162(3)	0.0480(12)*
C7	0.3449(4)	0.1435(3)	0.3366(3)	0.0441(11)*
C8	0.0109(4)	0.2191(2)	-0.1602(3)	0.0436(11)*
C9	0.0176(4)	0.0993(2)	0.5200(3)	0.0402(10)*
C10	-0.3151(4)	0.0531(2)	0.9067(3)	0.0421(10)*
C11	0.2654(3)	0.1555(2)	0.1505(3)	0.0397(10)*
C12	0.3660(4)	0.1361(2)	0.1157(3)	0.0432(10)*
C13	0.3578(4)	0.1384(3)	0.0116(3)	0.0471(11)*
C14	0.2526(4)	0.1596(2)	-0.0526(3)	0.0470(12)*
C15	0.1566(4)	0.1766(2)	-0.0090(3)	0.0416(10)*
C21	-0.1186(4)	0.2400(2)	-0.1919(3)	0.0462(11)*
C22	-0.1647(4)	0.2572(3)	-0.2917(3)	0.0580(13)*
C23	-0.2868(5)	0.2704(3)	-0.3205(4)	0.0706(15)*
C24	-0.3537(5)	0.2680(3)	-0.2473(4)	0.0757(16)*
C25	-0.2991(5)	0.2532(3)	-0.1490(4)	0.0683(14)*
C31	-0.1369(3)	0.0829(2)	0.6221(3)	0.0383(10)*
C32	-0.2378(4)	0.0756(2)	0.5461(3)	0.0450(11)*
C33	-0.3429(4)	0.0584(3)	0.5746(3)	0.0472(11)*
C34	-0.3471(4)	0.0501(3)	0.6749(3)	0.0462(11)*
C35	-0.2416(3)	0.0588(2)	0.7452(3)	0.0381(10)*
C41	-0.2634(4)	0.0482(2)	1.0177(3)	0.0420(10)*
C42	-0.3359(4)	0.0369(2)	1.0848(3)	0.0495(11)*
C43	-0.2853(5)	0.0301(3)	1.1871(3)	0.0589(13)*

**Table 7. Atomic Coordinates and Displacement Parameters (continued)**

Atom	<i>x</i>	<i>y</i>	<i>z</i>	<i>U</i> <sub>eq</sub> , Å <sup>2</sup>
C44	-0.1627(5)	0.0343(3)	1.2163(3)	0.0664(14)*
C45	-0.0966(4)	0.0458(3)	1.1429(4)	0.0672(14)*

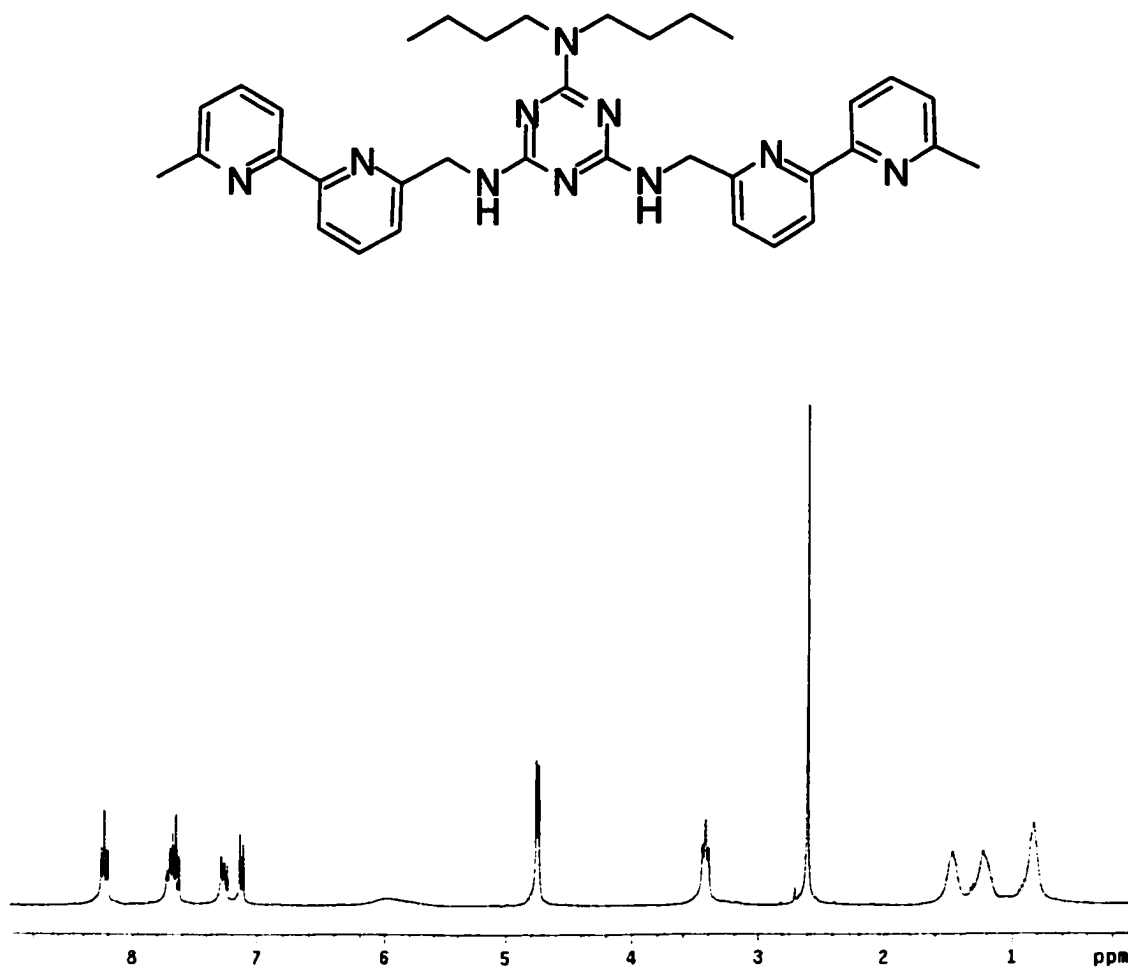
Anisotropically-refined atoms are marked with an asterisk (\*). The form of the anisotropic displacement parameter is:  $\exp[-2\pi^2(h^2a^{*2}U_{11} + k^2b^{*2}U_{22} + l^2c^{*2}U_{33} + 2klb^{*c^{*}}U_{23} + 2hla^{*c^{*}}U_{13} + 2hka^{*b^{*}}U_{12})]$ .

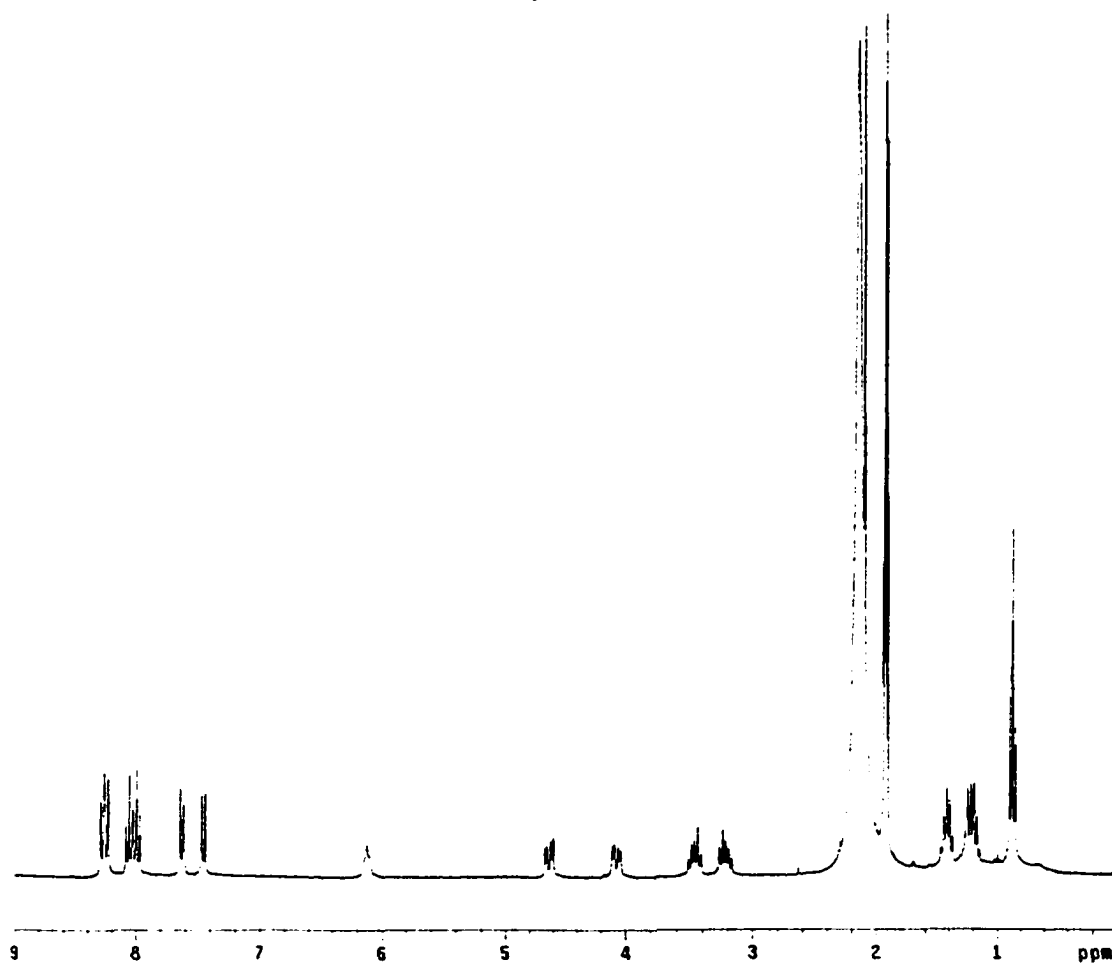
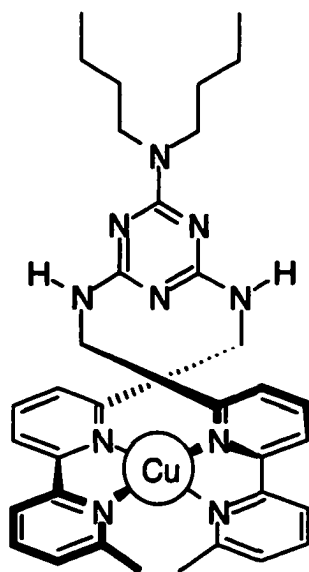


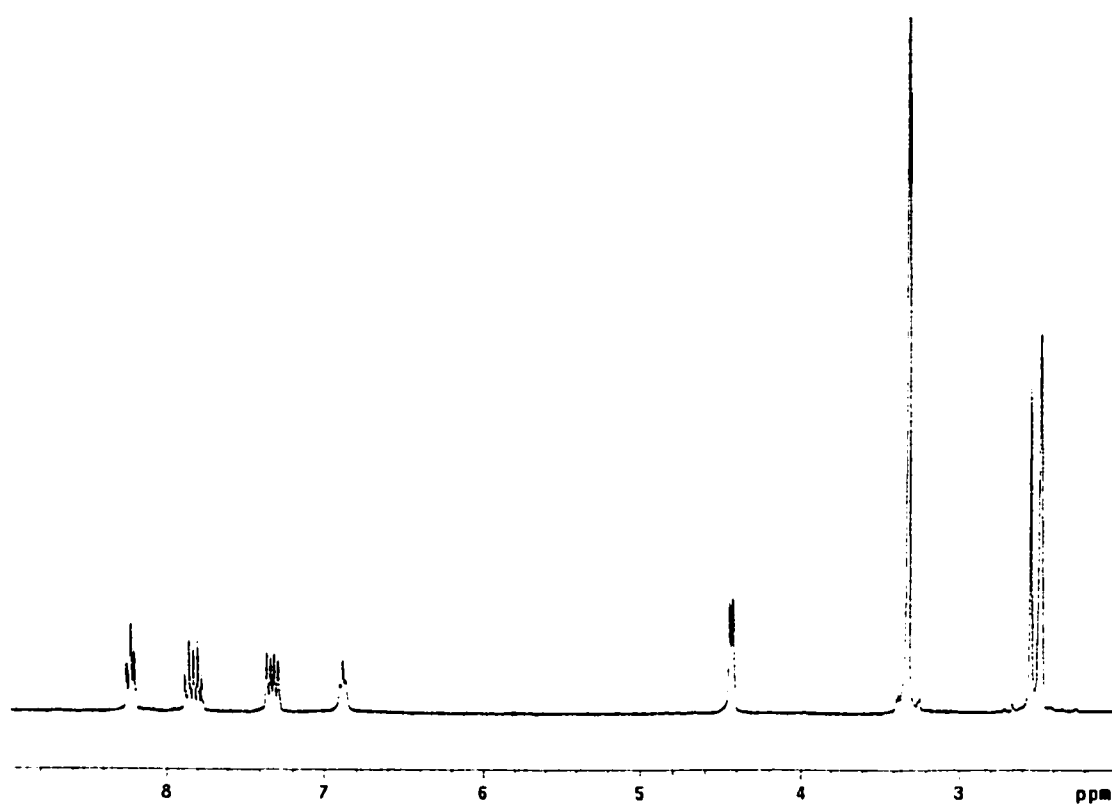
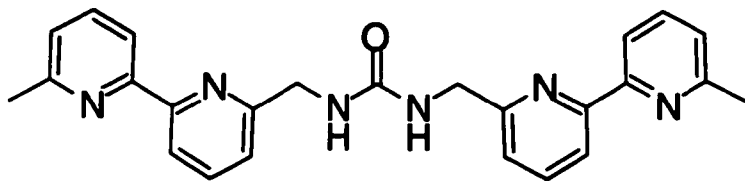
Appendix II – Selected  $^1\text{H}$  NMR Data

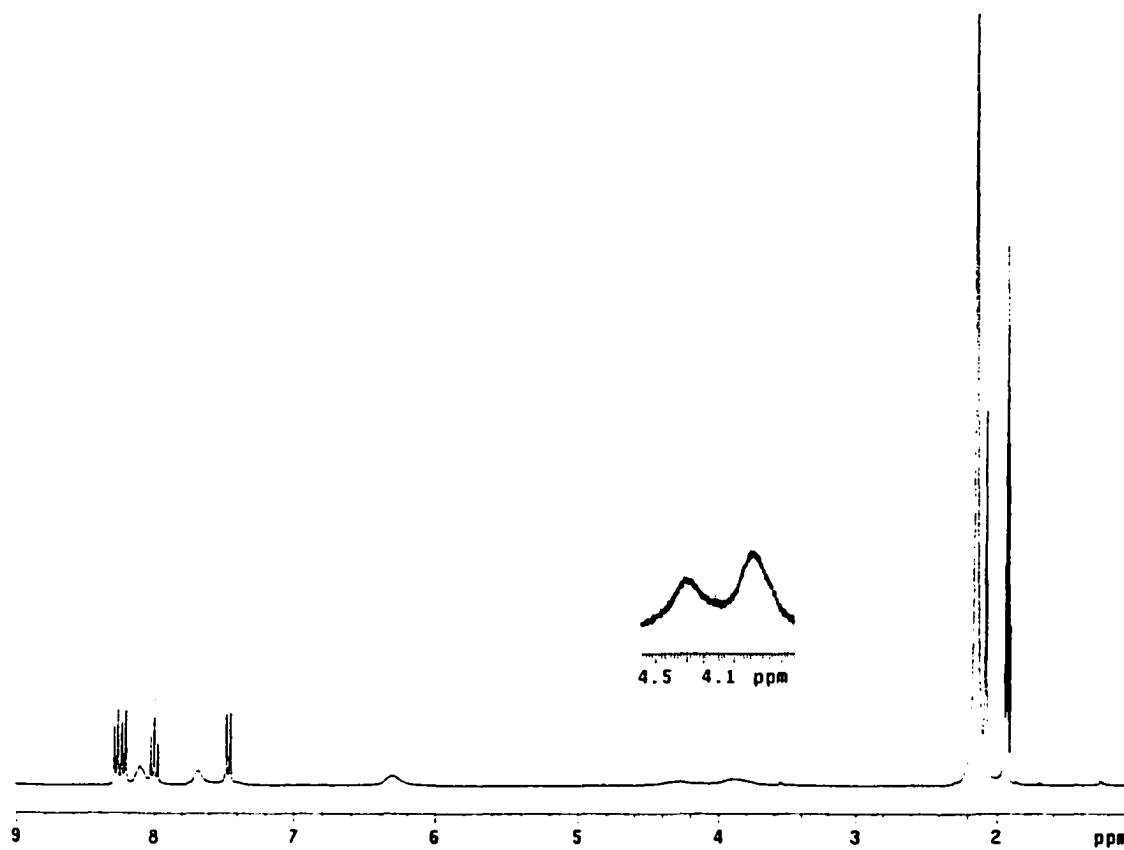
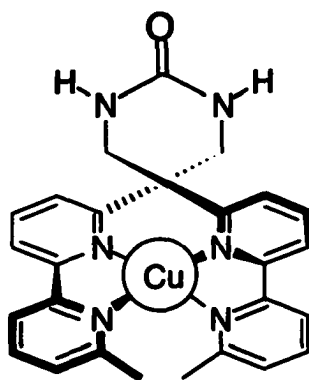
*N*<sup>2</sup>,*N*<sup>2</sup>-Dibutyl-*N*<sup>4</sup>,*N*<sup>6</sup>-bis(6'-methyl-2,2'-bipyridin-6-yl)-1,3,5-triazine-2,4,6-triamine

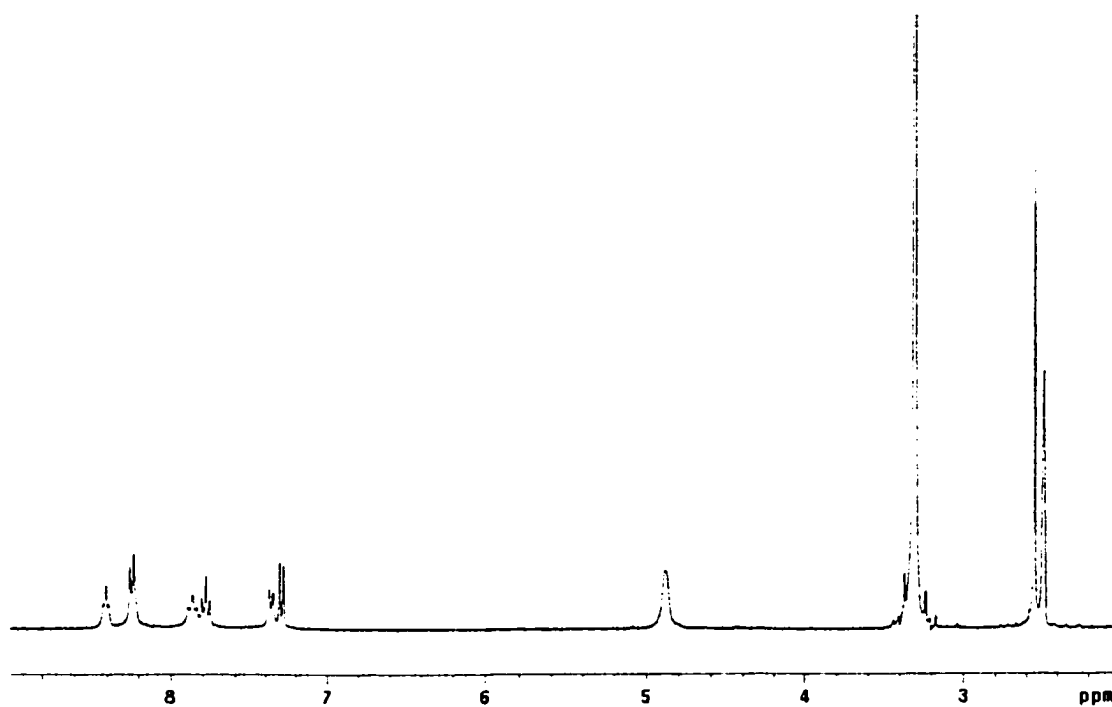
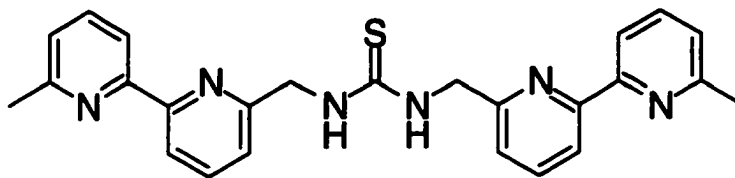
(6)

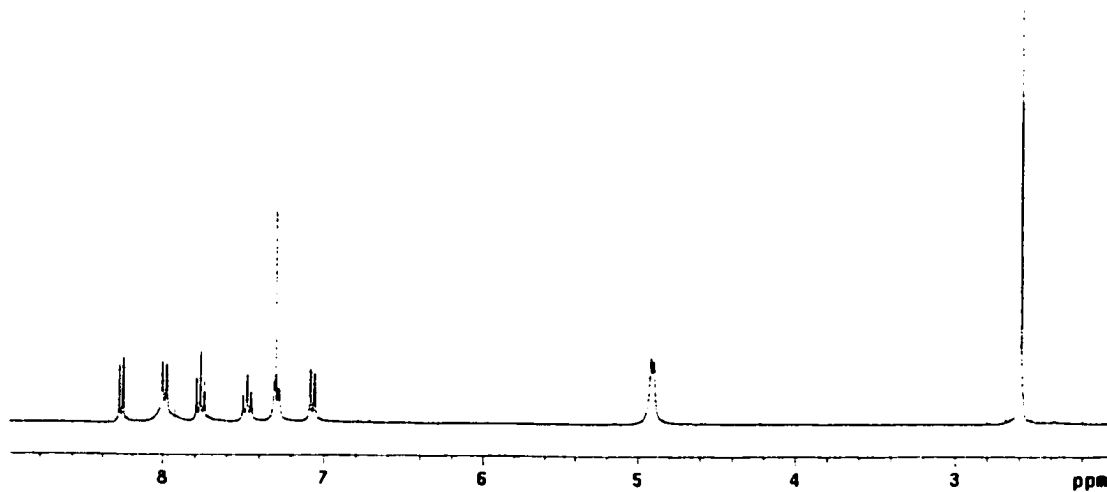
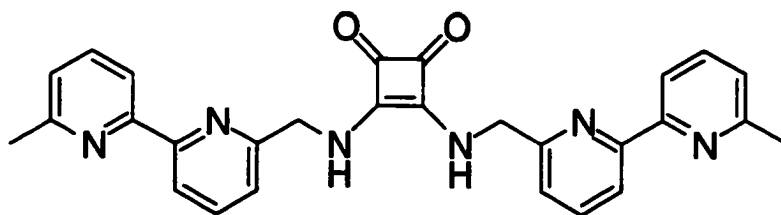


**6•Cu**

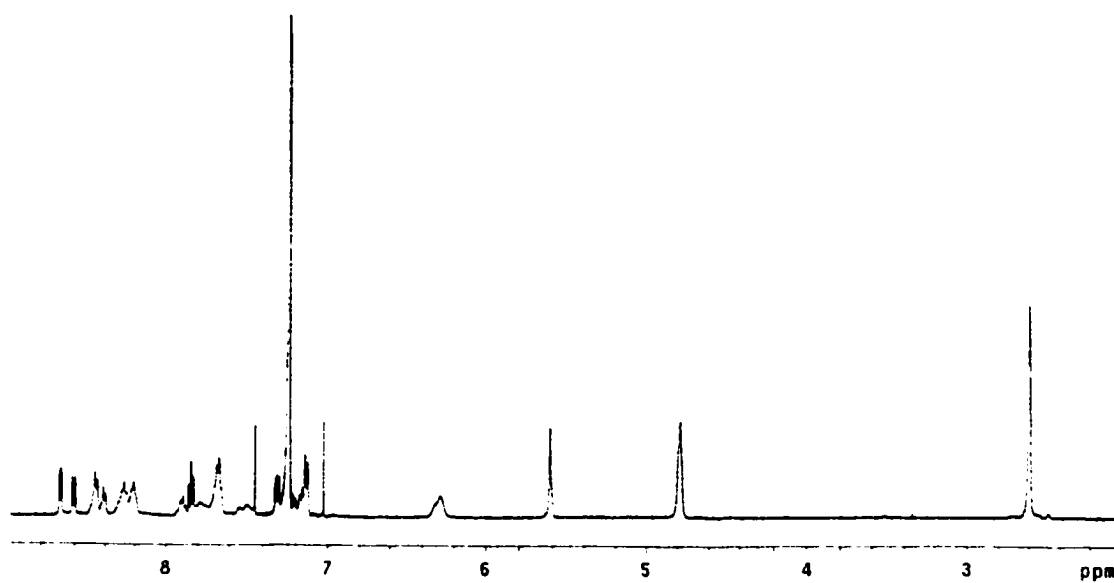
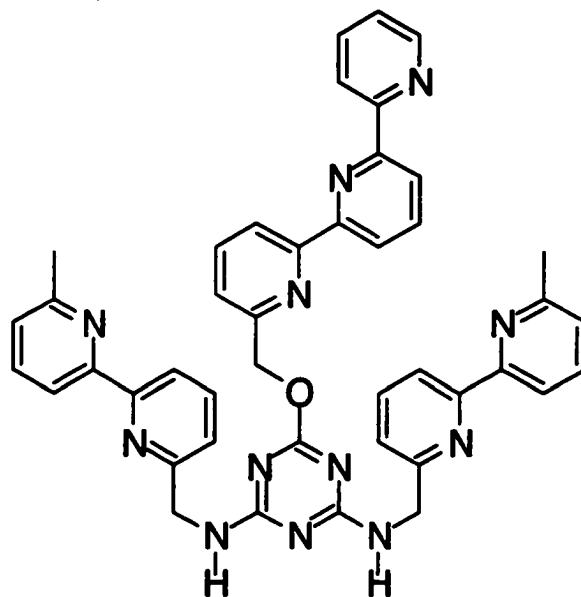
***N,N'*-Bis(6'-methyl-2,2'-bipyridin-6-yl)urea (7)**

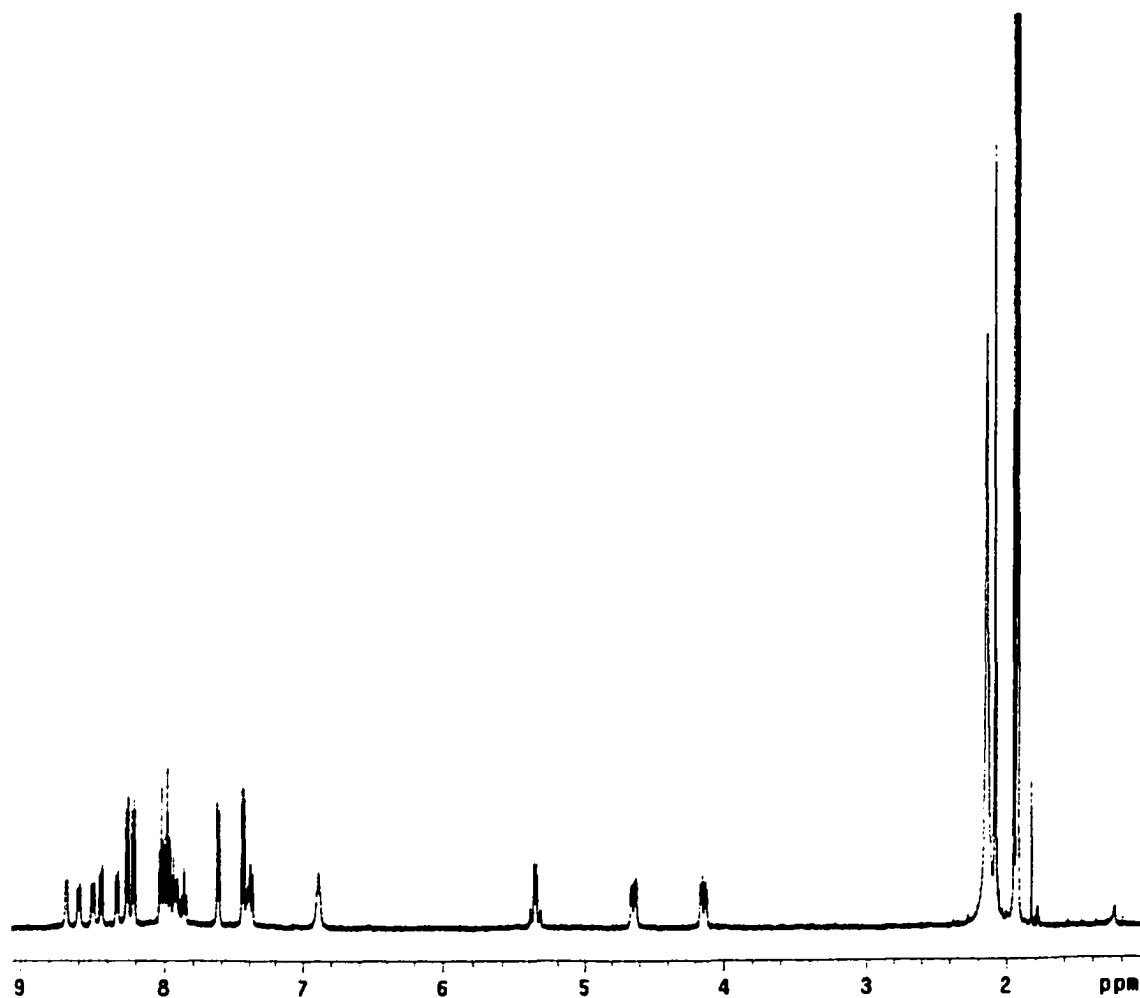
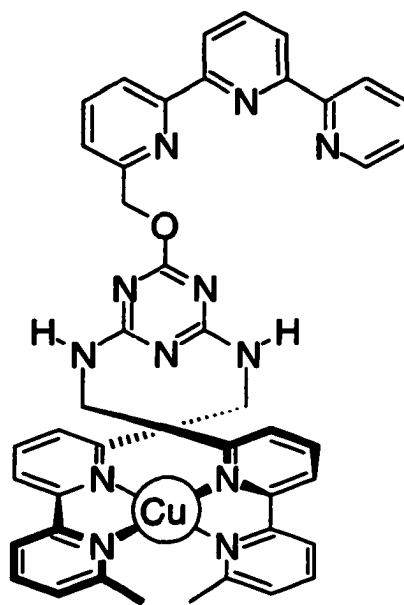
**7•Cu**

***N,N'*-Bis(6'-methyl-2,2'-bipyridin-6-yl)thiourea (10)**

**3,4-Bis[(6'-methyl-2,2'-bipyridin-6-yl)amino]cyclobut-3-ene-1,2-dione (8)**

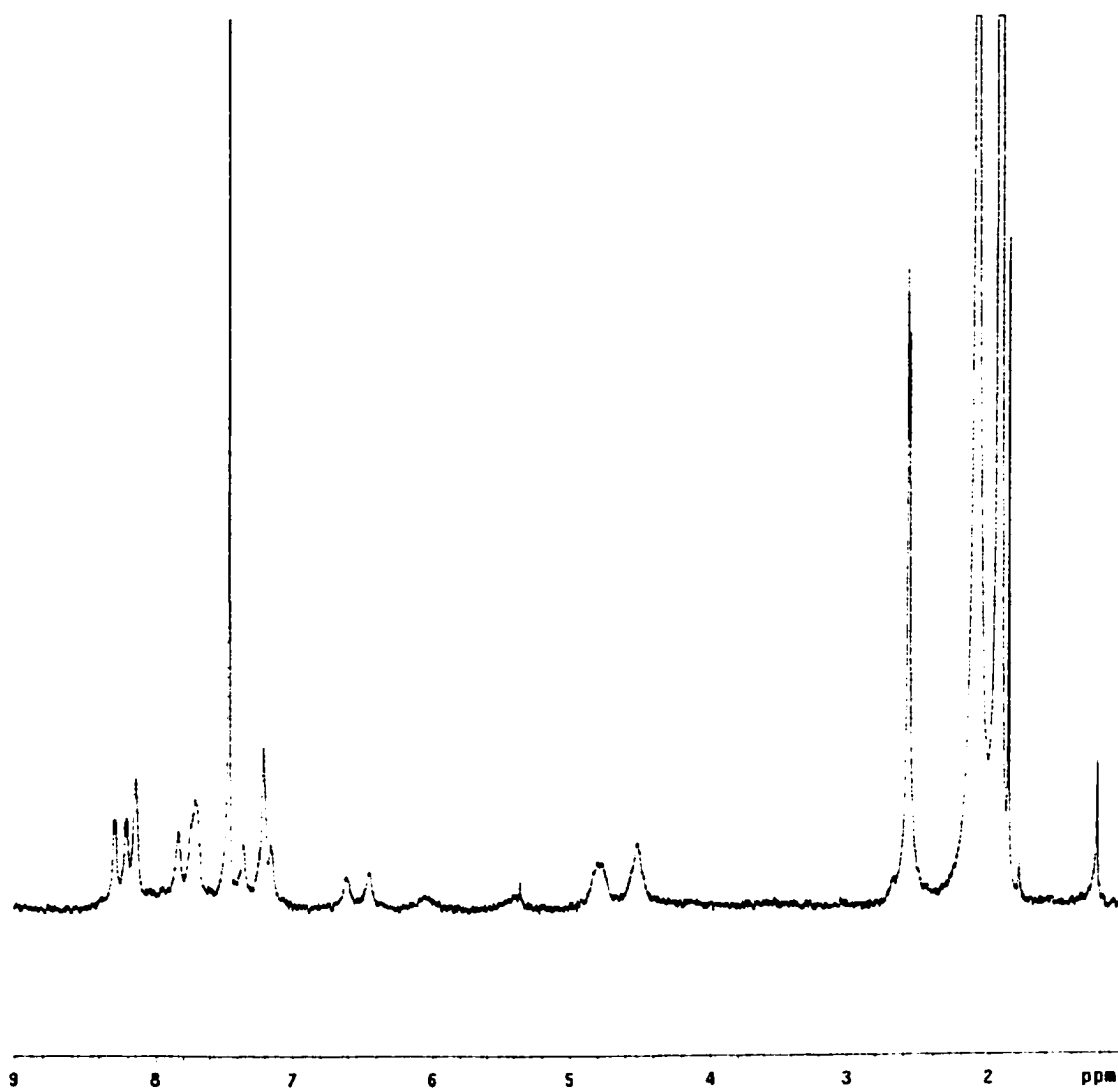
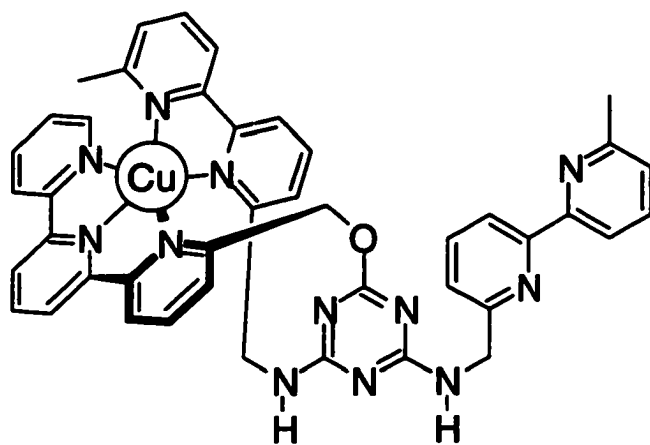
***N,N'*-Bis[(6'-methyl-2,2'-bipyridin-6-yl)methyl]-6-(2,2':6',2''-terpyridin-6-ylmethoxy)-1,3,5-triazine-2,4-diamine (17)**



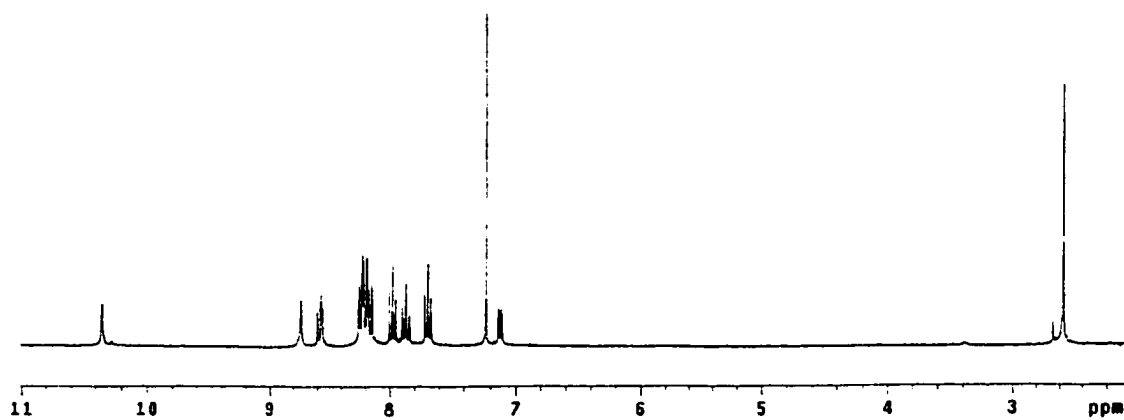
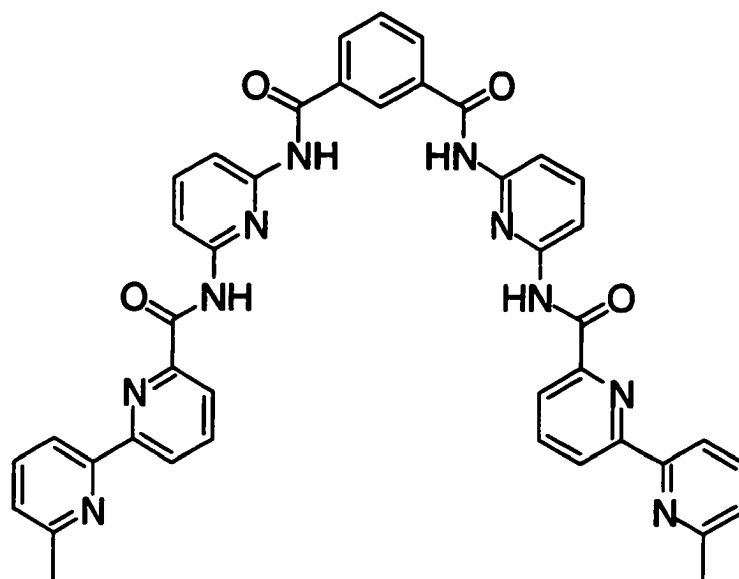
**[Cu(17)]PF<sub>6</sub>**

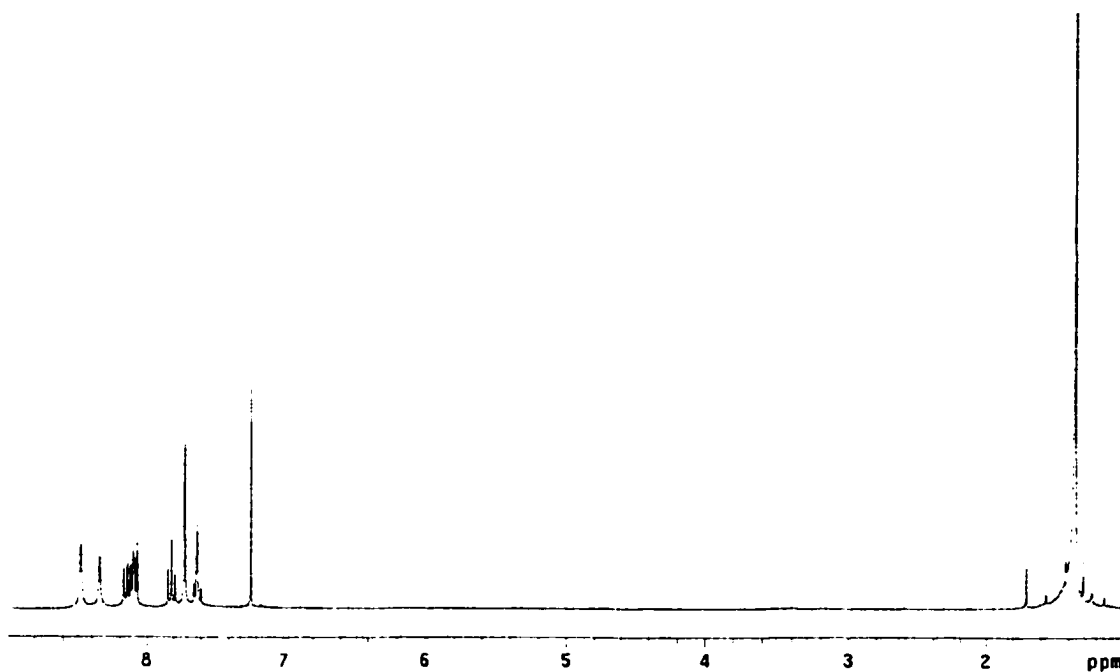
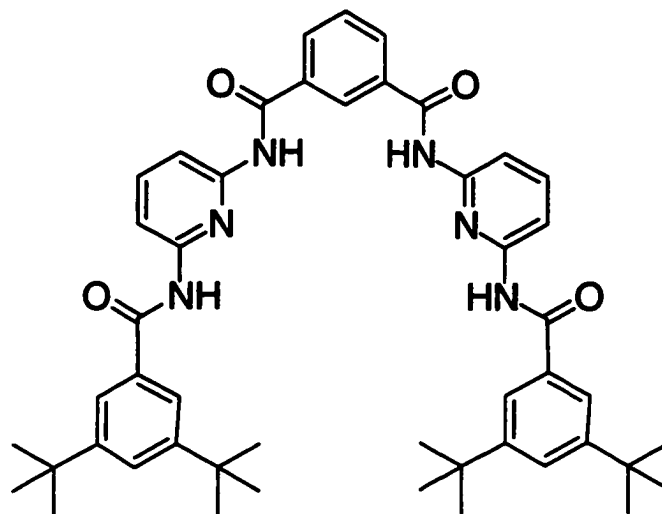


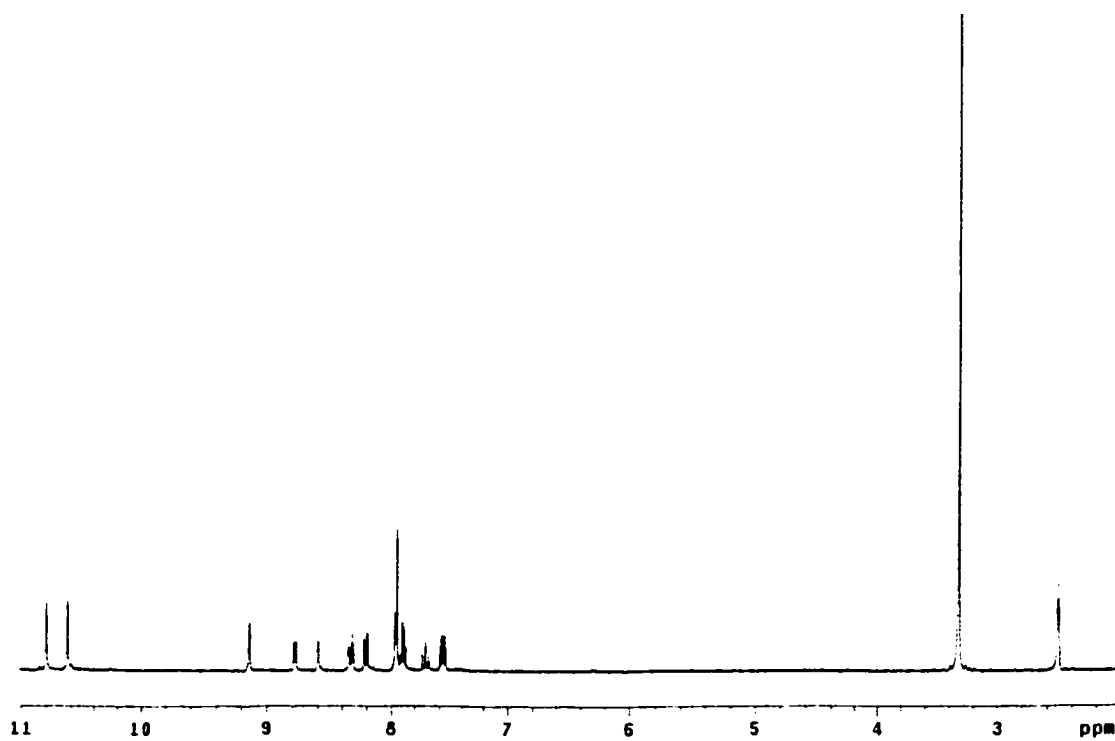
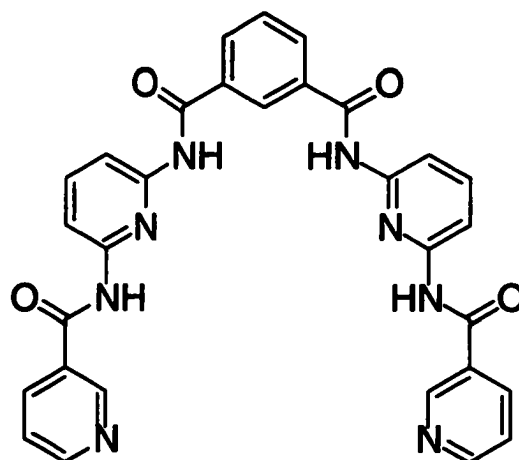
[Cu(17)](OTf)<sub>2</sub>



***N,N'*-Bis{6-[(6'-methyl-2,2'-bipyridin-6-yl)carbonyl]amino}pyridin-2-yl}isophthalamide (26)**

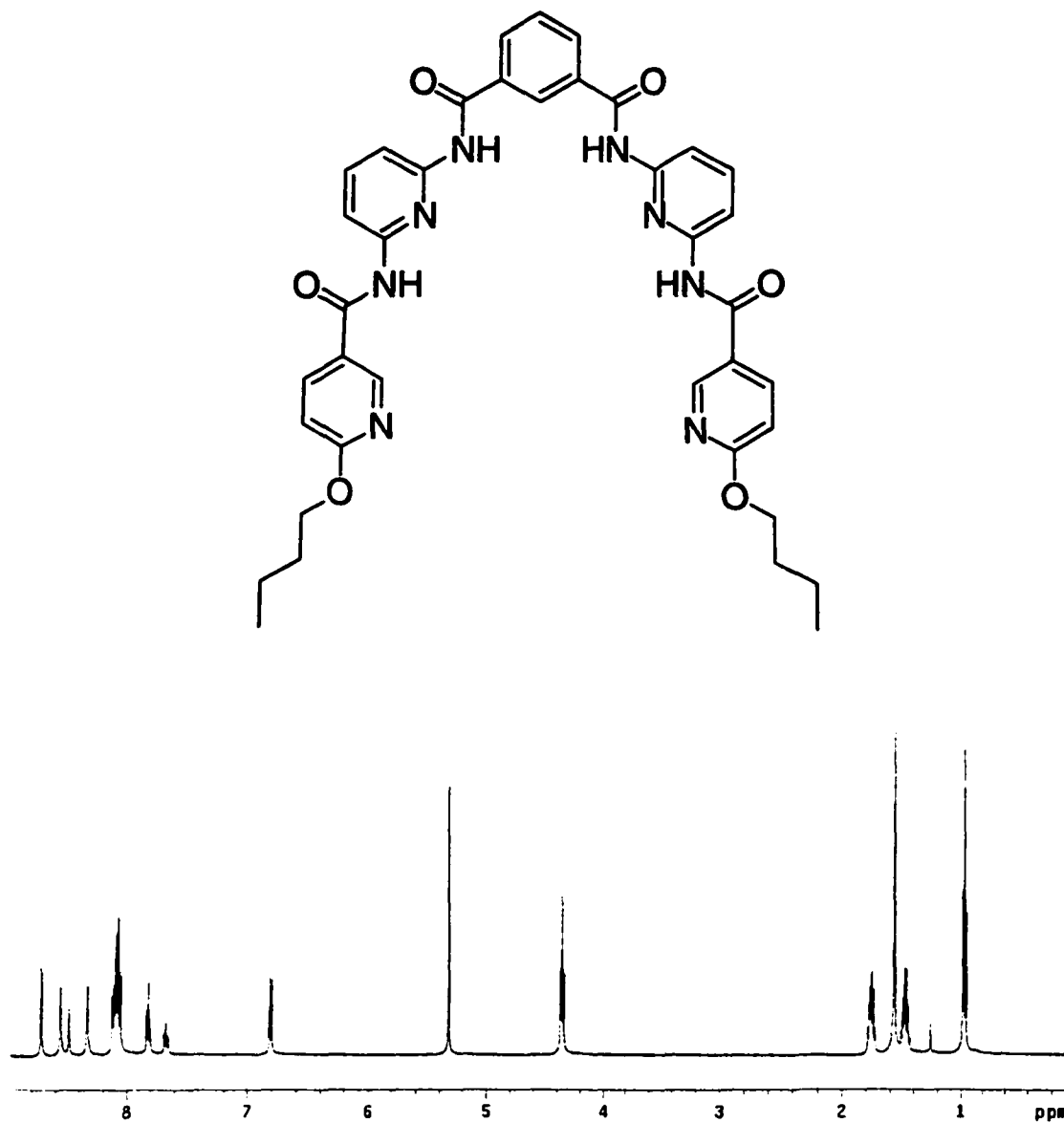


***N,N'*-Bis{6-[(3,5-di-*tert*-butylbenzoyl)amino]pyridin-2-yl}isophthalamide (27)**

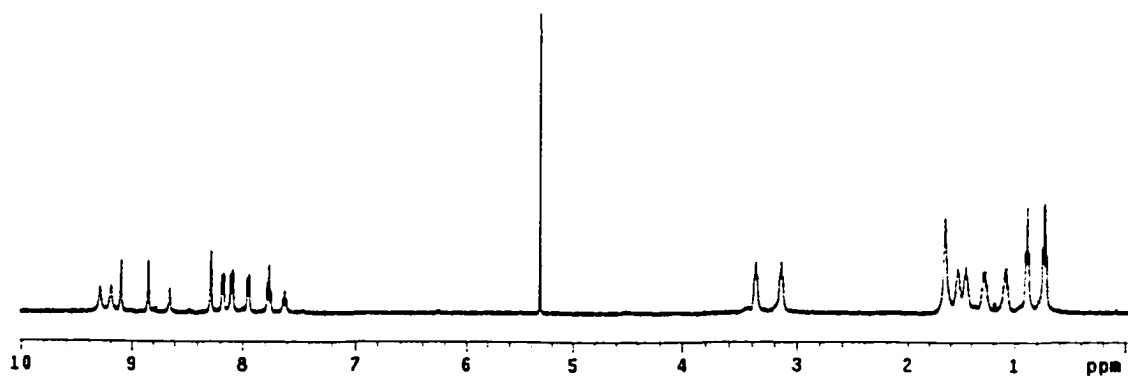
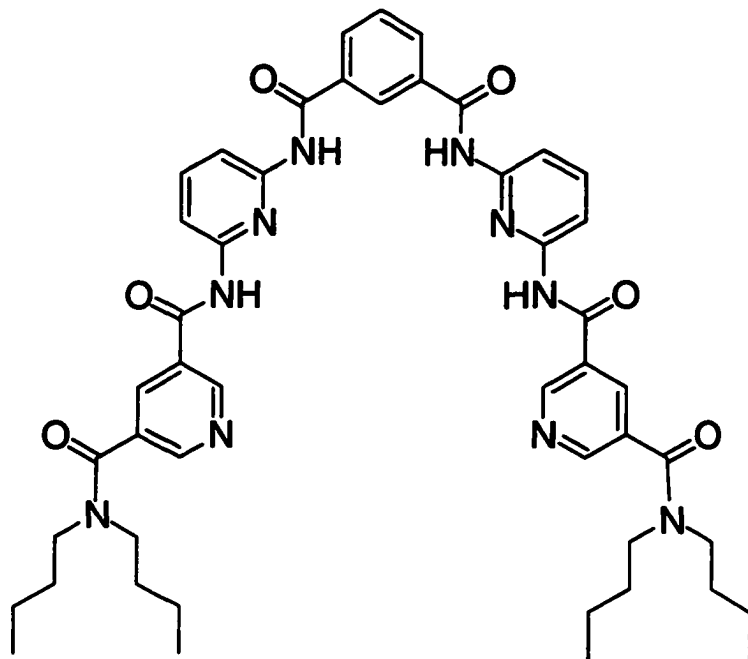
***N,N'*-Bis[6-[(pyridin-3-ylcarbonyl)amino]pyridin-2-yl]isophthalamide (29)**

***N,N'*-Bis(6-[[[(6-butoxypyridin-3-yl)carbonyl]amino]pyridin-2-yl]isophthalamide**

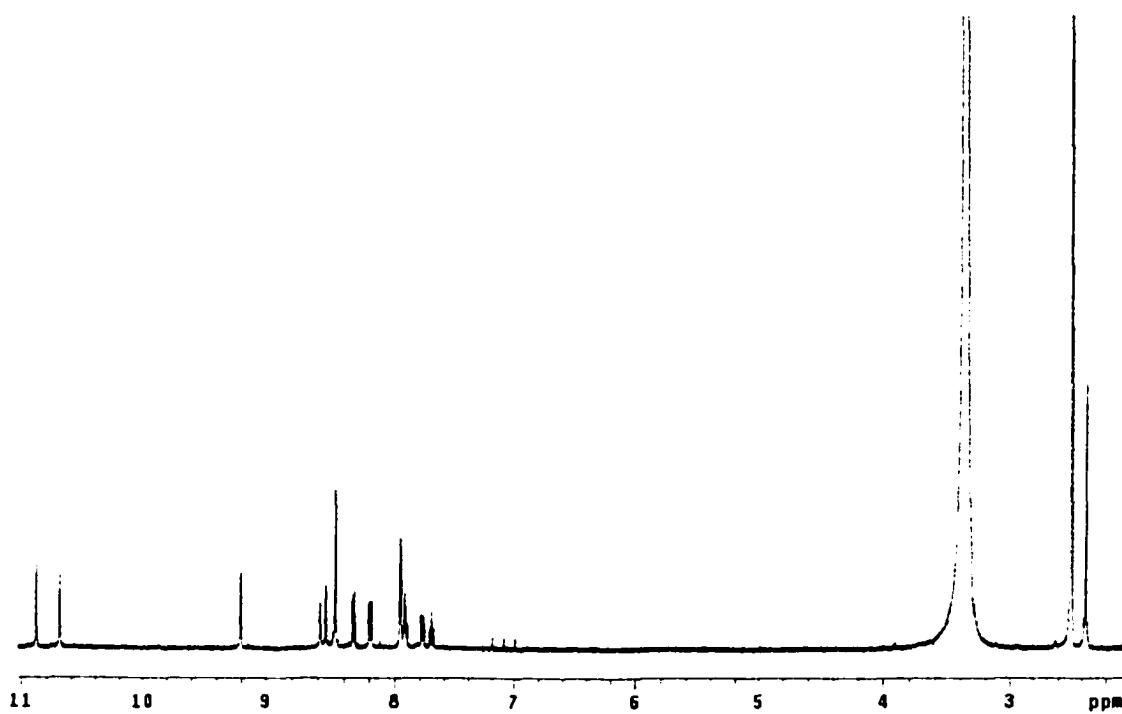
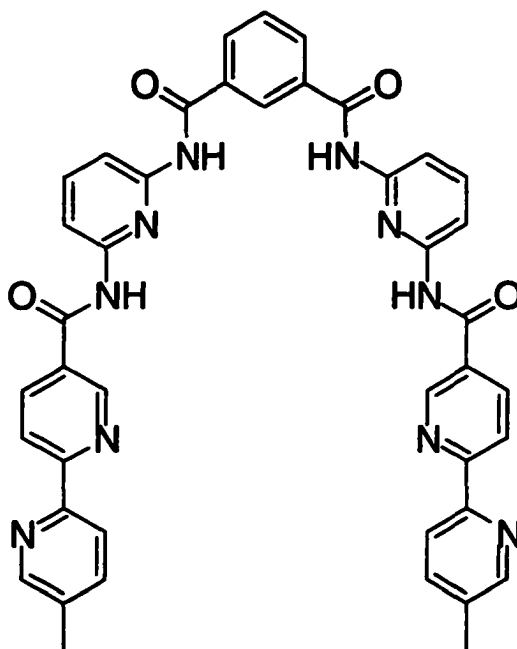
(30)



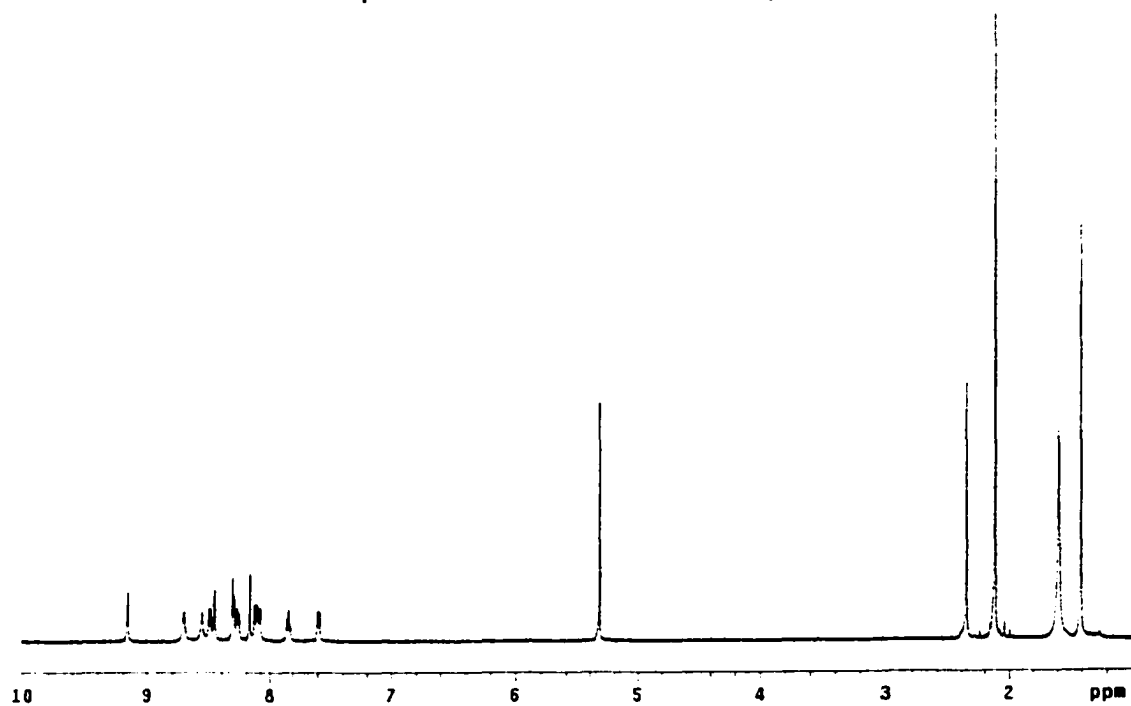
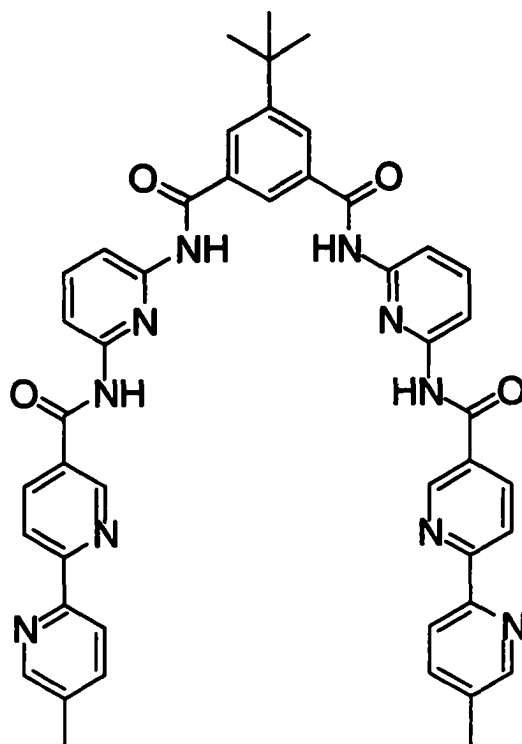
***N*-[6-({3-[[2-({5-(Dibutylaminocarbonyl)pyridin-3-yl}carbonyl)amino]pyridin-6-yl]carbonyl]benzoyl}amino)pyridin-2-yl]-*N'*-dibutylpyridine-3,5-dicarboxamide (31)**



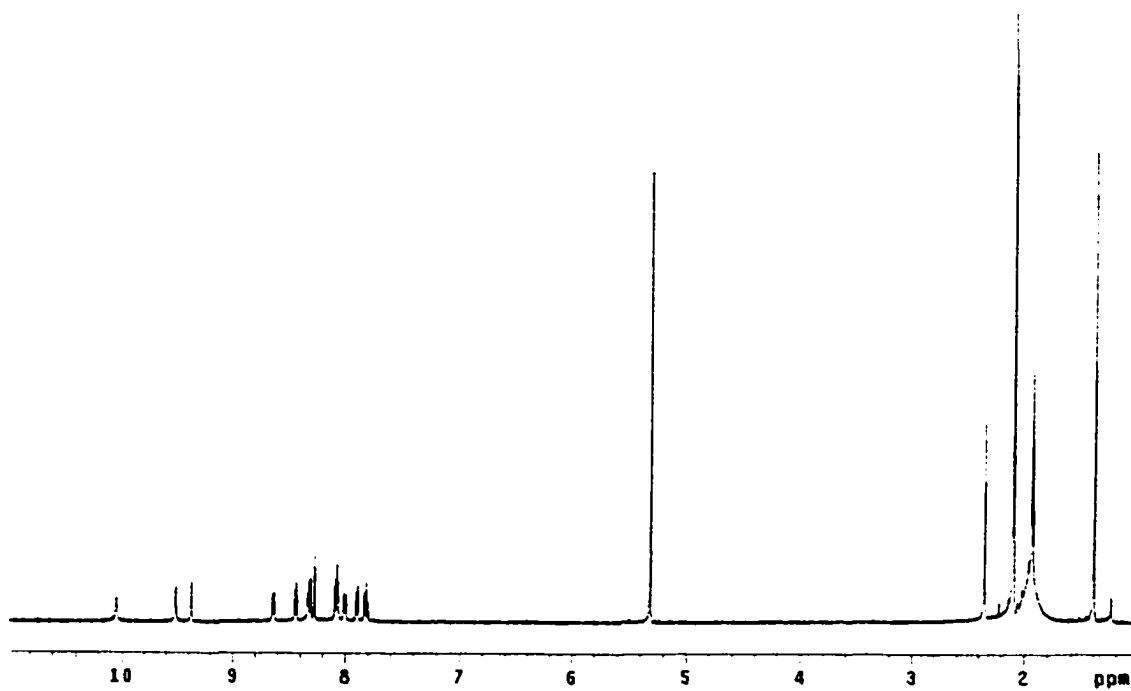
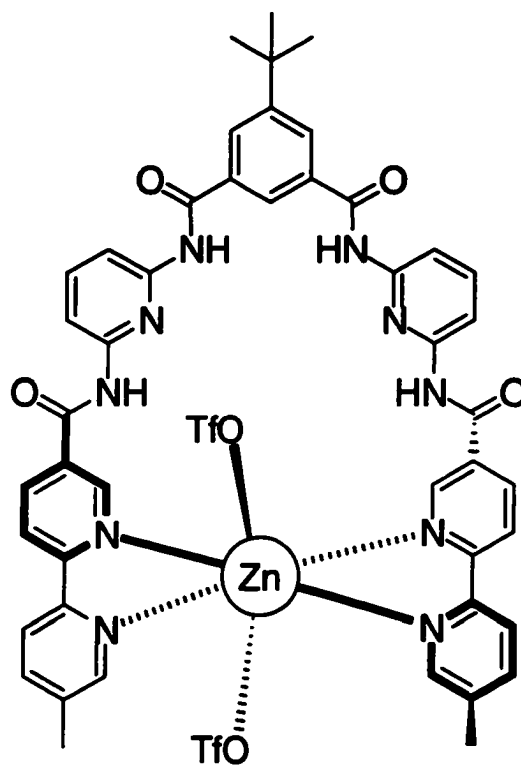
***N,N'*-Bis(6-((5'-methyl-2,2'-bipyridin-5-yl)carbonyl)aminopyridin-2-yl)isophthalamide (32)**



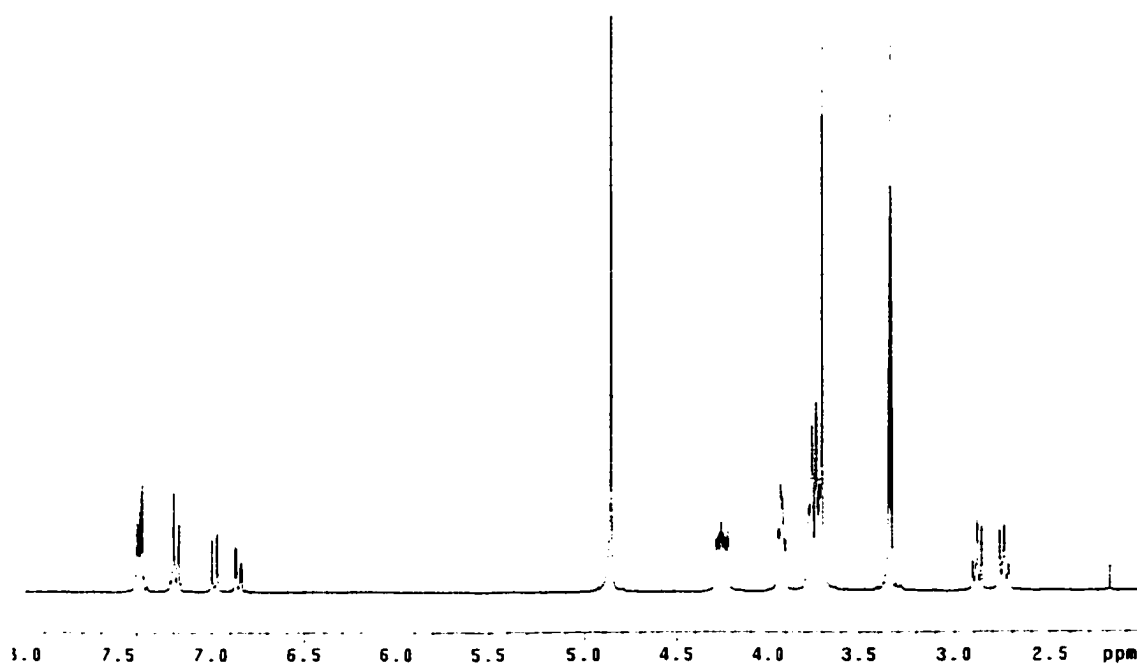
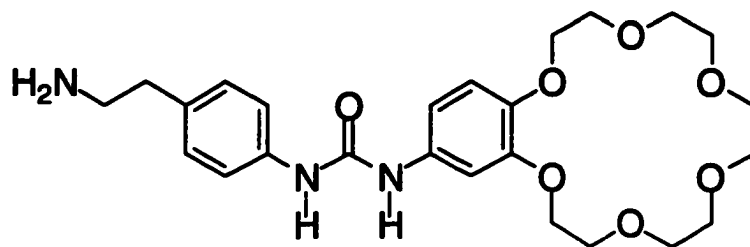
**5-tert-Butyl-*N,N'*-bis(6-[(5'-methyl-2,2'-bipyridin-5-yl)carbonyl]amino)pyridin-2-yl)isophthalamide (34)**



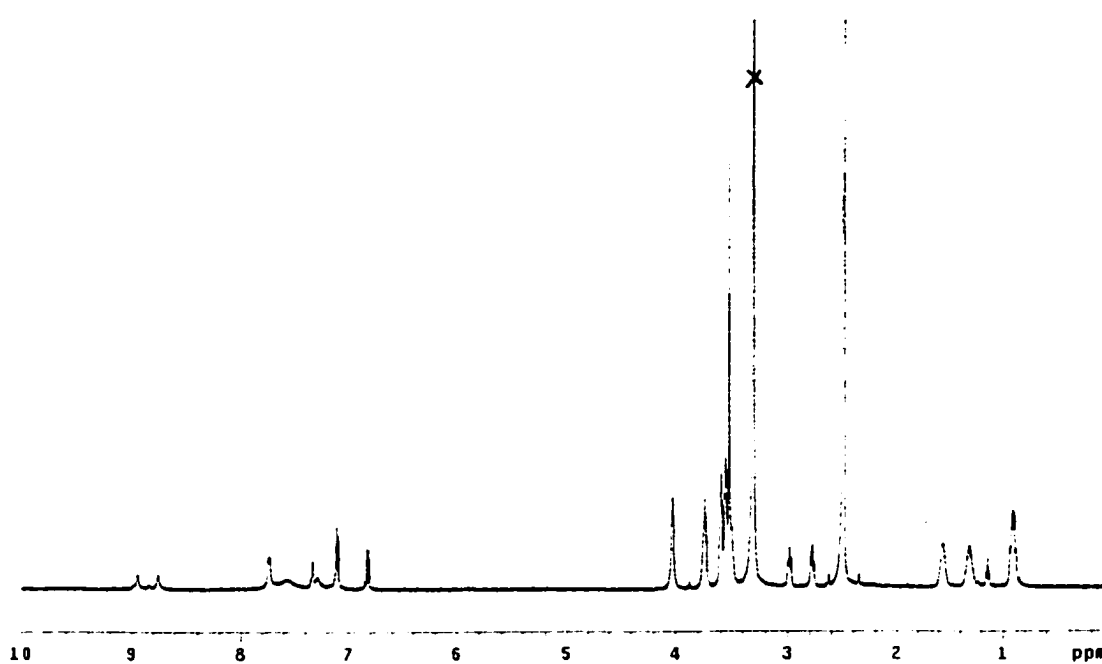
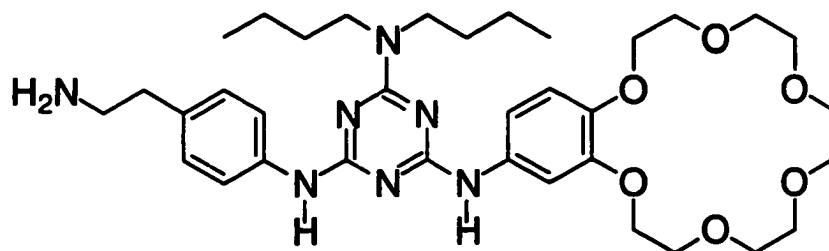


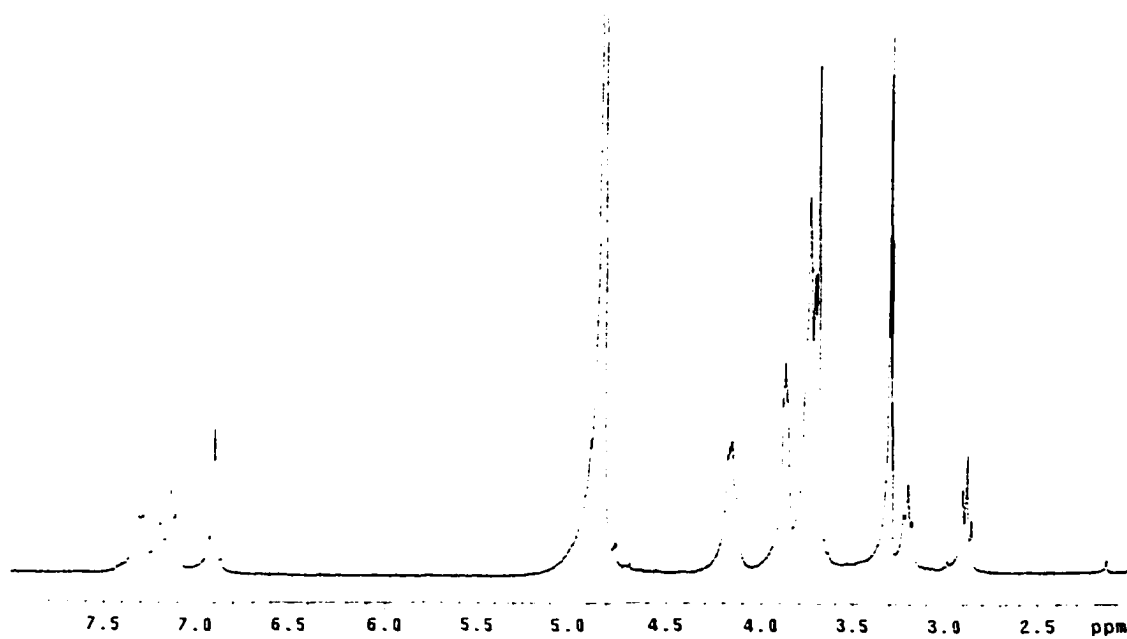
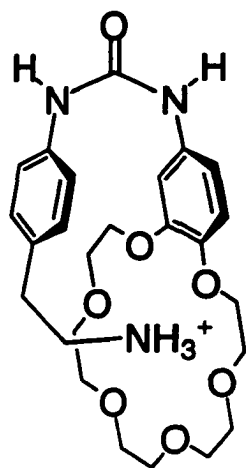
$34 \cdot \text{Zn}$ 

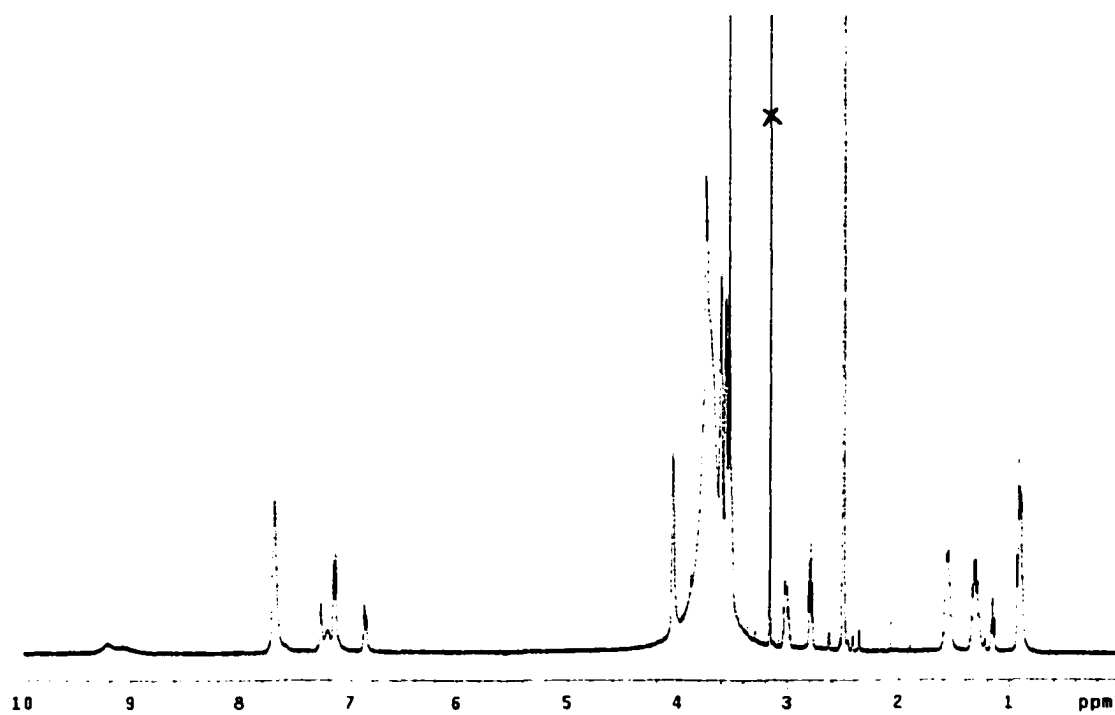
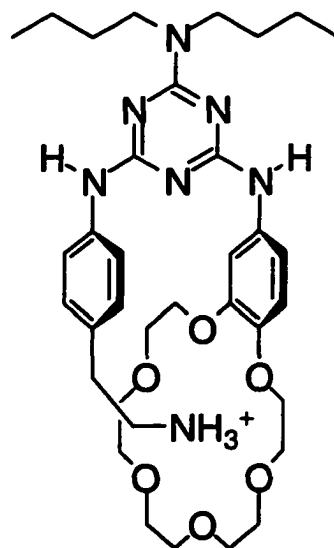
***N*-[4-(2-Aminoethyl)phenyl]-*N'*-(2,3,5,6,8,9,11,12,14,15-decahydro-1,4,7,10,13,16-benzohexaoxacyclooctadec-18-yl)urea (38)**

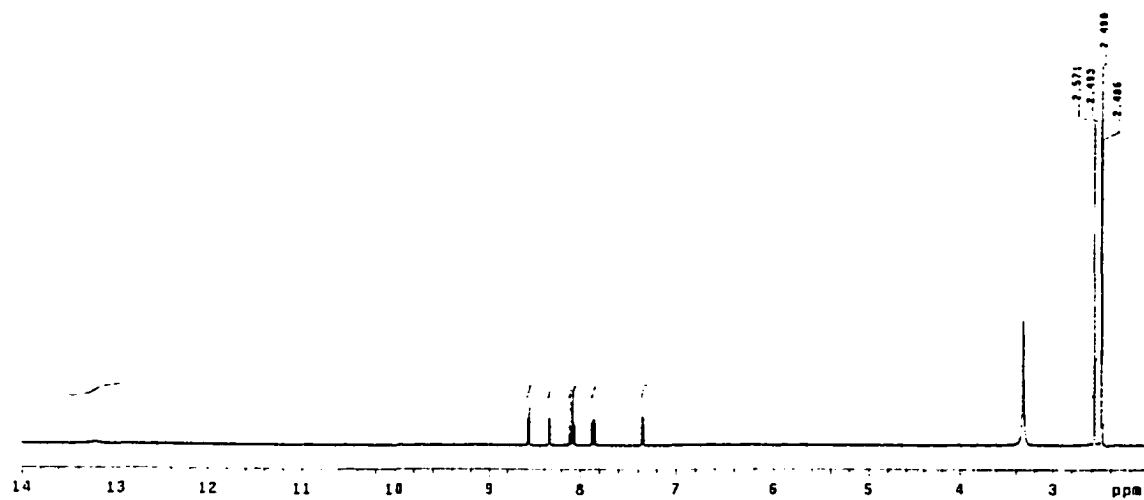
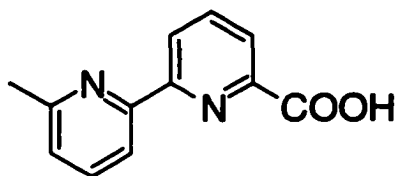


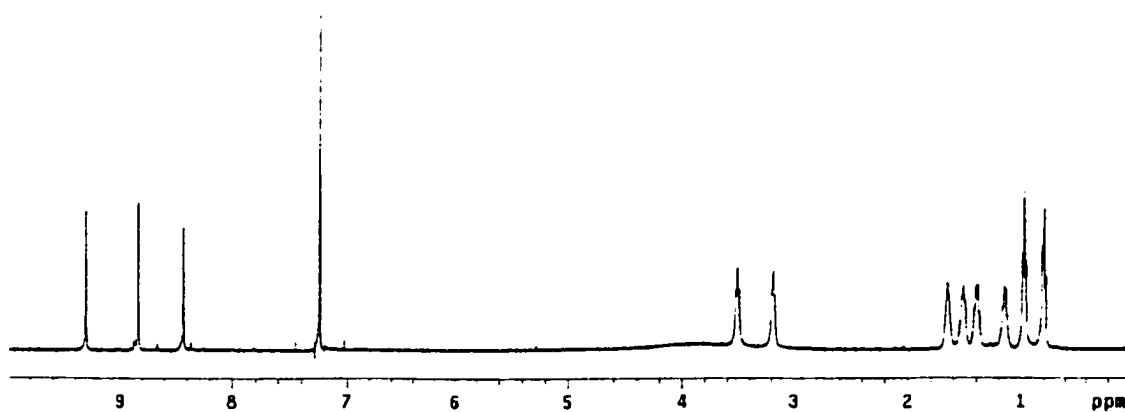
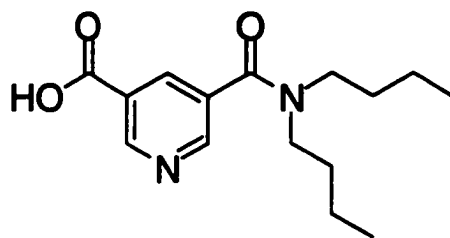
***N*<sup>4</sup>-[4-(2-Aminoethyl)phenyl]-*N*<sup>2</sup>,*N*<sup>2</sup>-dibutyl-*N*<sup>6</sup>-(2,3,5,6,8,9,11,12,14,15-decahydro-1,4,7,10,13,16-benzohexaoxacyclooctadec-18-yl)-1,3,5-triazine-2,4,6-triamine (40)**

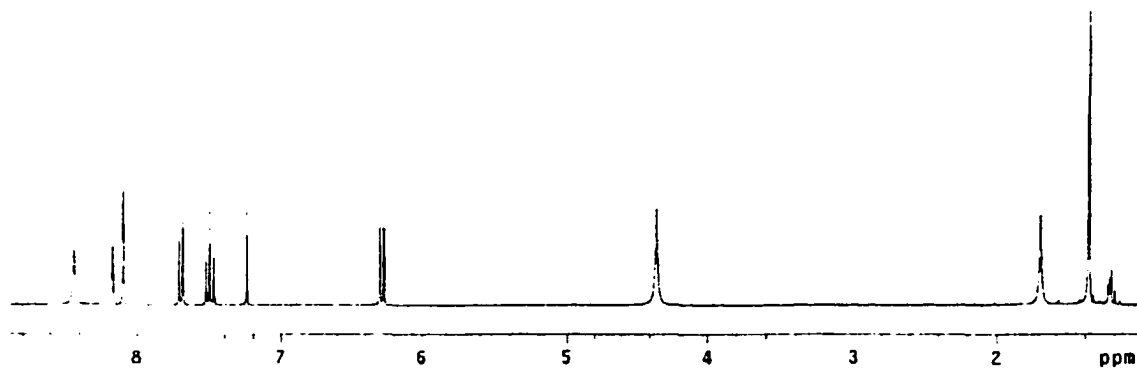
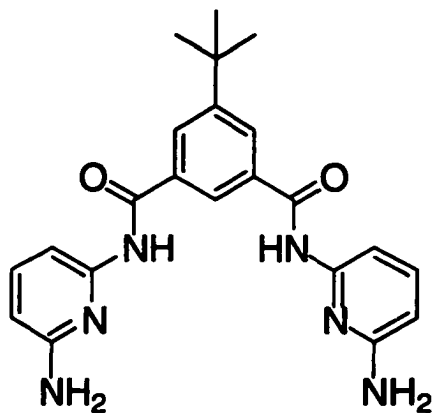


**38•HBF<sub>4</sub>**

**40•HBF<sub>4</sub>.**

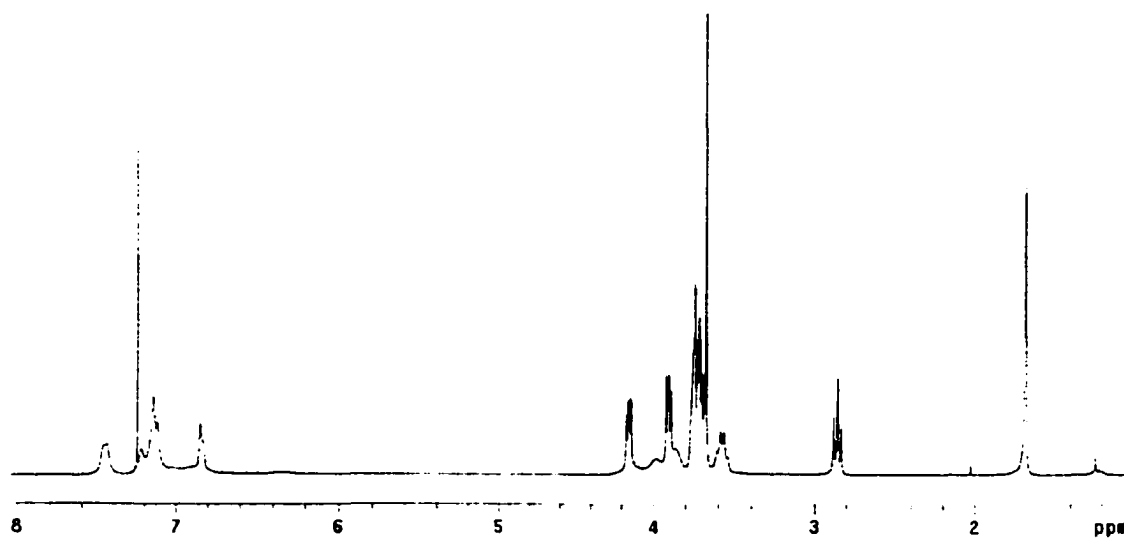
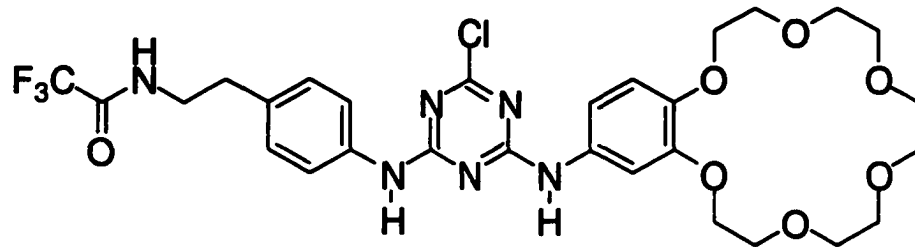
**6'-Methyl-2,2'-bipyridine-6-carboxylic acid (19)**

**5-[(Dibutylamino)carbonyl]nicotinic acid (23)**

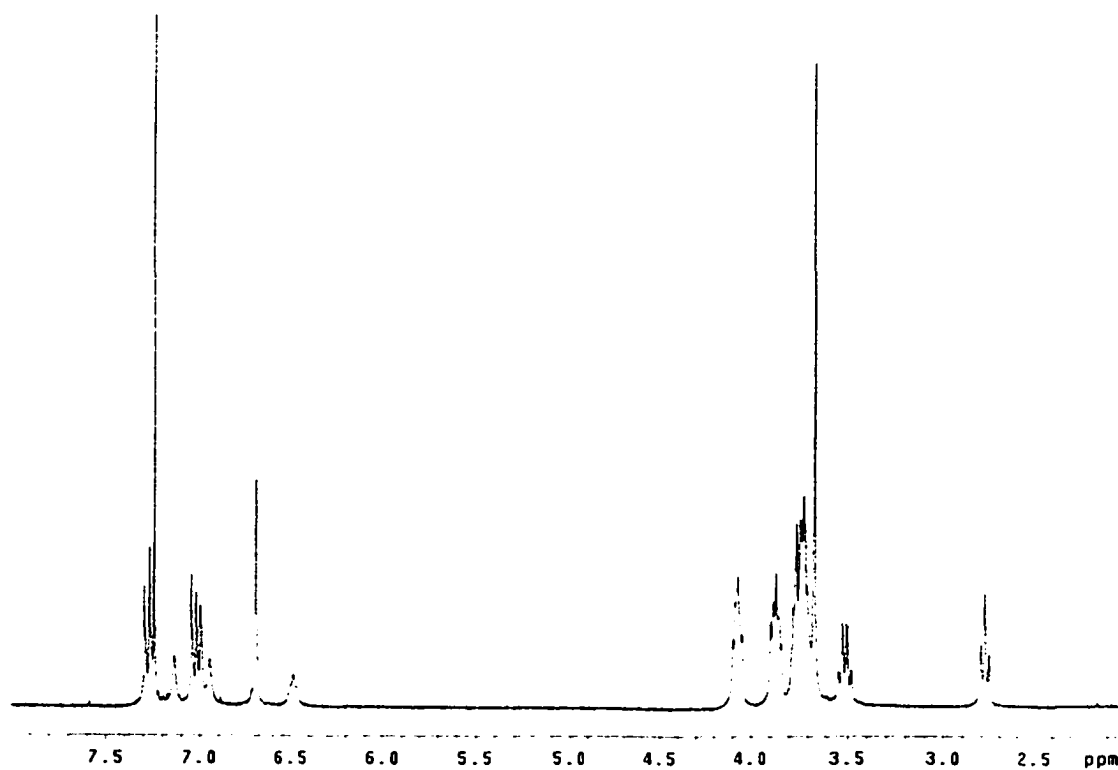
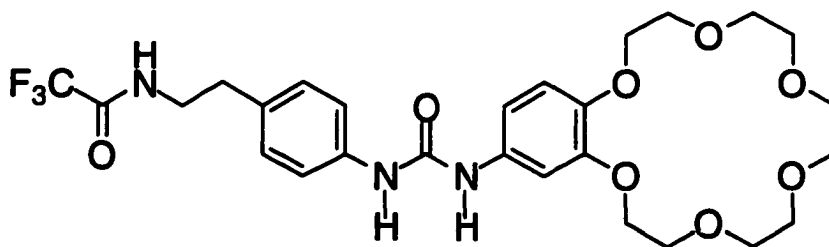
***N,N'*-Bis(6-aminopyridin-2-yl)-5-tert-butyl-isophthalamide (33)**



***N*-{2-[4-((4-Chloro-6-[(2,3,5,6,8,9,11,12,14,15-decahydro-1,4,7,10,13,16-benzohexaoxacyclooctadec-18-yl)amino]-1,3,5-triazin-2-yl)amino)phenyl]ethyl}-2,2,2-trifluoroacetamide (39)**



***N*-{2-[4-(((2,3,5,6,8,9,11,12,14,15-Decahydro-1,4,7,10,13,16-benzohexaoxacyclooctadec-18-yl)amino)carbonyl)amino]phenyl]ethyl}-2,2,2-trifluoroacetamide (37)**



***N*-butyluracil**